Changes in elastic wave velocity in a slope due to water infiltration and deformation

(斜面の水浸と変形に伴う弾性波速度の変化)

Yulong Chen
陳宇龍

Student ID 37-137170

A thesis submitted to The University of Tokyo in partial fulfillment of

the requirements for the degree of

Doctor of Philosophy

in

Civil Engineering

June, 2016

Department of Civil Engineering

The University of Tokyo

ABSTRACT

Slope failures world-wide cause many thousands of deaths each year. It is reported that over 32000 fatalities globally occurred as a result of landslides during the period 2004 to 2010. Furthermore, landslides damage infrastructure and the built environment, costing billions of pounds to repair, resulting in thousands of people being made homeless and the breakdown of basic services such as water supply and transport. The large majority of deaths from slope failures occur in countries located in rainfall and earthquake-prone regions. It is reported that 93% of those landslides were caused by heavy rainfall. Therefore, the demand for monitoring and early warning methods against landslides and slope instabilities induced by rainfall is on the rise in every country.

Current landslide early warning systems rely on monitoring slope movements by means of inclinometers or tilt sensors, in combination with soil moisture monitoring by means of dielectric moisture sensors or tensiometers, etc. A novel concept of landslide prediction by monitoring elastic wave velocity changes in soil was presented, by conducted triaxial tests on soil specimens with varying water content, and injected water into stressed soil sample. The elastic wave velocity was measured by a pair of disk type piezo-electric elements (similar to bender element), and it was found to decrease with increasing water content. More important is the acceleration in decrease of wave velocity, once failure is initiated. Therefore, the author tries to apply this finding to detect the wetting and failure process of soil slope.

Laboratory model test is regarded as the most reliable method for studying the rainfall-triggered landslide, in which the soil properties and boundary conditions can be controlled and the water content inside slope and deformation on the surface can be monitored. For the purpose of better understanding the changes in elastic wave velocity in soil slope in wetting and failure process as a result of rainfall, the author performed two types of slope model tests in the laboratory, slope angle=0° for one at

which rainfall was given at early period after which soil model was manually inclined without rainfall and 40°~50° for the other one at which artificial rainfall was continuously applied until slope failure. The changes in wave velocity with coupling effect of water content and deformation or single effect are investigated.

In the first type of test, an attempt was made to separate that two effect factors by a flat soil slope model test carried out in the laboratory. The flat slope model was exposed to rainfall at early period and then was inclined without rainfall to separately unravel the change in elastic wave velocity with increase of water content and deformation. Wave velocity is found to decrease slightly with water content and significantly with deformation. The relationship functions of normalized elastic wave velocity with either volumetric water content or tilt angle were obtained.

It was found from the other type of tests that a gradual decrease in wave velocities was followed by a rapid decrease once the failure was initiated. Wave velocity continued decreasing with an accelerated rate by the coupled effect of increasing water content and deformation that appeared to be interrelated. The effects of soil density, surface layer thickness and slope angle on elastic wave behavior were investigated during slope failure. The decrease rate of normalized elastic wave velocity with volumetric water content and tilt angle was independent of soil density, surface layer thickness and slope angle. The changes of normalized elastic wave velocity with volumetric water content and tilt angle were simulated by the relationship functions obtained from flat model tests. It showed that the simulated curves agreed well with measured data.

The wave velocity based early warning system was suggested to be installed in the bottom of slope. Such sharp decrease after a threshold about 0.92 of normalized elastic wave velocity can be useful for predicting failure initiation in actual landslide conditions.

A triaxial apparatus equipped with bender element to study the variation of elastic

wave velocities (shear wave and compression wave velocities) during drying and wetting path of SWCC was devised. The wave signal detected from model tests fails to be identified as either P-wave or S-wave.

A medium scale model test and a large scale model test were conducted to confirm the potential of applying the idea of elastic wave velocities to predict such rain induced landslides. The evolution of elastic wave velocity showed consistent observation from small scale model tests.

This finding is of practical importance with reference to real-time slope monitoring, as the actual slope movements in a slope surface can be identified by monitoring the rate of decrease of wave velocities.

Keywords: Landslide monitoring, Early warning, Wave velocity, Unsaturated soil

ACKNOWLEDGEMENT

challenges as one of the best treasures in my mind.

TABLE OF CONTENTS

List of Figures

xvii

List of Tables

CHAPTER 1

RESEARCH CURRICULUM

1.1. **INTRODUCTION**

Slope failures are frequently reported to occur. Slope failures world-wide cause many thousands of deaths each year. For example, Petley (2012) reported records of over 32000 fatalities globally that occurred as a result of landslides during the period 2004 to 2010. The annual loss caused by landslides in the United States alone is estimated to be 25 to 50 of life and $3 billion 500 million worth of damage to the infrastructure (US Geological Survey, 2004). Also in Canada, 570 people have been killed and more than 160 years of time (1840-1999) have been attributed to the landslide disaster (Evans, 2001). The death toll in less developed, densely populated areas even more high (for example Ancash, Peru, 1970, 18000 deaths; Wright, the Philippines, 20061800 death) (Mosher, 2008). Furthermore, landslides damage infrastructure and the built environment, costing billions of pounds to repair, resulting in thousands of people being made homeless and the breakdown of basic services such as water supply and transport. The large majority of deaths from slope failures occur in countries located in rainfall and earthquake-prone regions. Osanai et al. (2009) conducted s statistical study on 19035 cases of landslides between 1972 and 2007 in Japan. They reported that 93% of those landslides were caused by heavy rainfall. Therefore, the demand for monitoring and early warning methods against landslides and slope instabilities induced by rainfall is on the rise in every country.

Still, the construction of a typical landslide remediation method of the construction

support structure or soil improvement is not economically feasible. The need for more robust and economically feasible solutions, such as real-time landslide warning system is increasing. This study attempts to improve the existing landslide early warning system by applying a new technique to predict the elastic wave propagation in the landslide motion of the soil.

1.2. MOTIVATION & SIGNIFICANCE

Landslide is one of the most serious natural disasters. According to 1999 and 2012 of the 134 landslide slip records, about 63% result from the rain. Over the years, the rainfall induced landslide badly affect lots of countries, such as Japan, China, Pakistan, Brazil, Hong Kong, Italy and so on. (Brand, 1981; Wool and Hachich, 1989; Wu and Pang, 2000; Farooq et al., 2004). Landslide protection project in the world the most common includes a variety of "hard measures", including several soil maintain technology (retaining walls, barbed wire, and so on), soil amelioration using soil nailing, anchor, and other means. Because rainfall induced landslides in the air spread are usually very large (Uchimura et al., 2010), such protective measures, sometimes need to cover large areas (Fig. 1.1). As a result, these hard measures are often neither feasible nor economically feasible.

Figure 1.1: Typical landslide protection works; (a) retaining wall, (b) soil nailing

Traditional approaches to prevent rainfall-induced landslides, such as stabilization of unstable slopes by installation of retaining walls and ground anchors, has been useful. But, they are not very helpful in mitigation of small slope failures, which are less significant in scale but numerous in numbers, because of their cost of installation. In consequence of recent residential developments in hilly area, the risk of smaller landslides has been realized. There is extravagant number of slopes with potential of such failure, and it is not financially realistic to use traditional approaches for each of them. Low-cost and simple early warning system is needed to deal with such problems.

Compared to hard measures, although landslide early warning system cannot make away of landslide, it at least provide the people around with a timely reminder. If the warning is issued very early, engineers could have enough time to take necessary countermeasures to avoid the landslide itself. Even if using early warning system cannot avoid destruction of infrastructure to some extent, but to save human life is a great contribution to invest in this field.

1.3. PROBLEM STATEMENT

In order to prevent and mitigate of rainfall induced landslides, many novel approaches have been developed to serve as early warning system. For example, the rainfall record is widely used for early warning (Keefer et al., 1987; Baum and Godt, 2010; Chae and Kim, 2012; Ramesh and Vasudevan, 2012). The criteria of issuing warnings are defined based on the current rainfall intensity and/or the cumulative rainfall during a recent period of several hours in advance. However, such a sparse arrangement of rain gages cannot properly detect cloudbursts, in which extremely heavy rainfalls occur in limited areas. Besides, soil properties and slope characteristics are not taken into consideration. Displacement is another term to be monitored. Ochiai et al. (2004) reported gradual and accelerating displacement on a slope surface before failure in a

rainfall induced landslide test using strain probes. However, the exact locations of unstable soil masses often cannot be defined; and hence, the locations of the monitoring sensors cannot be decided distinctly. The rate of displacement is often used as an index to define the threshold of warning (Saito 1965, 1987; Fukuzono 1985). However, it is restricted to relatively low resolution that is insufficient for detecting the displacement of slopes in the very early stages. Uchimura et al. (2010, 2011) employs a tilt sensor in place of an extensometer to examine the relevance of measuring rotation angle on a slope surface. It is point sensor, and hence, sensitive only to deformation and moisture changes in its own vicinity. Acoustic emission monitoring is used to assess the stability of both natural and constructed slopes (e.g. Cadman and Goodman, 1967; Chichibu et al., 1989; Dixon et al., 2007, 2015a, 2015b; Nakajima et al., 1991; Rouse et al., 1991; Smith et al., 2014). Soils generate relatively low-energy acoustic emission signals that attenuate significantly over short distances, and this method is difficult for field application as well. With the objective of providing an early warning of slope instability to enable the evacuation of vulnerable people, a more flexible and effective method is preferred.

A novel concept of landslide prediction by monitoring elastic wave velocity changes in soil was presented by Irfan et al.(2013a, 2013b, 2014) and Uchimura (2010) who conducted triaxial tests on soil specimens with varying dry densities and principle stress ratio, and injected water into stressed soil sample. The elastic wave velocity was measured by a pair of disk type piezo-electric elements (similar to bender element, as shown in Figure 1.2), and it was found to decrease with increasing water content. More important is the acceleration in decrease of wave velocity, once failure is initiated (see Figures 1.3 and 1.4). Therefore, we try to apply this finding to detect the wetting and failure process of soil slope.
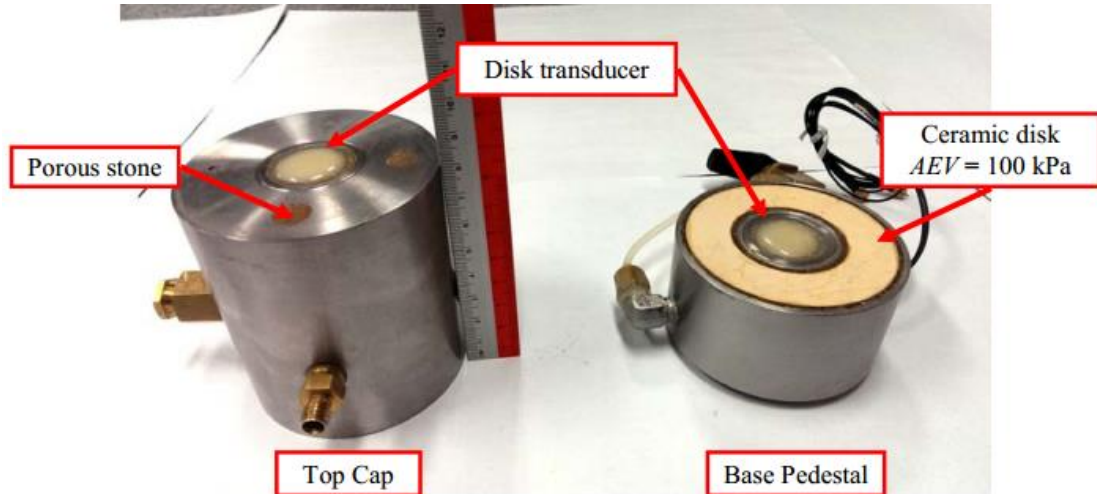
Figure 1.2: Modified pedestal and top cap of triaxial apparatus, fitted with disk type piezoelectric transducers at their respective centers.
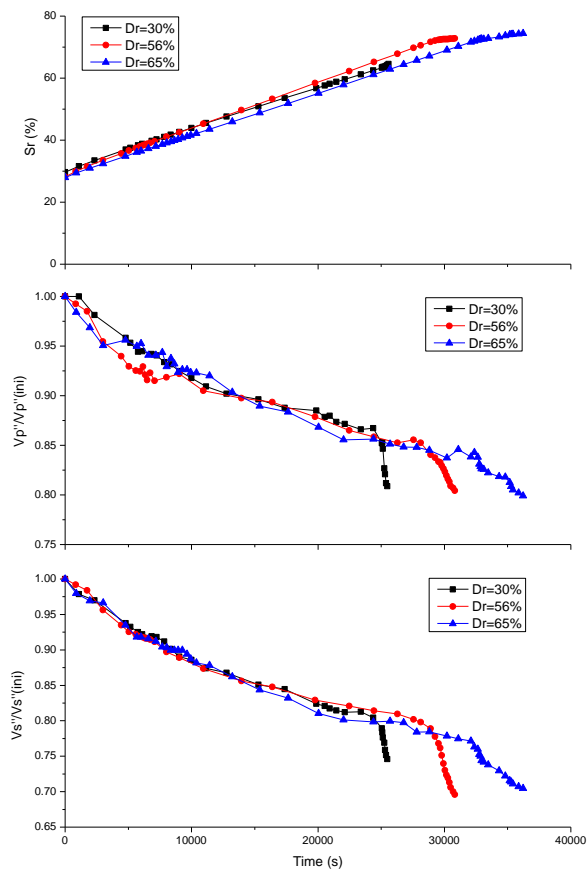
Figure 1.3: Response of elastic wave velocities (normalized corresponding to e_0=0.673, and γ_d= 1.578g/cm^3) at different specimen densities during shearing

infiltration tests; (a) Saturation ratio (*Sr*) versus time; (b) Normalized compression wave velocities (*Vp"*/*Vp"*(initial)); (c) Normalized shear wave velocities (*Vs*/*Vs*(initial)) (Irfan, 2014).
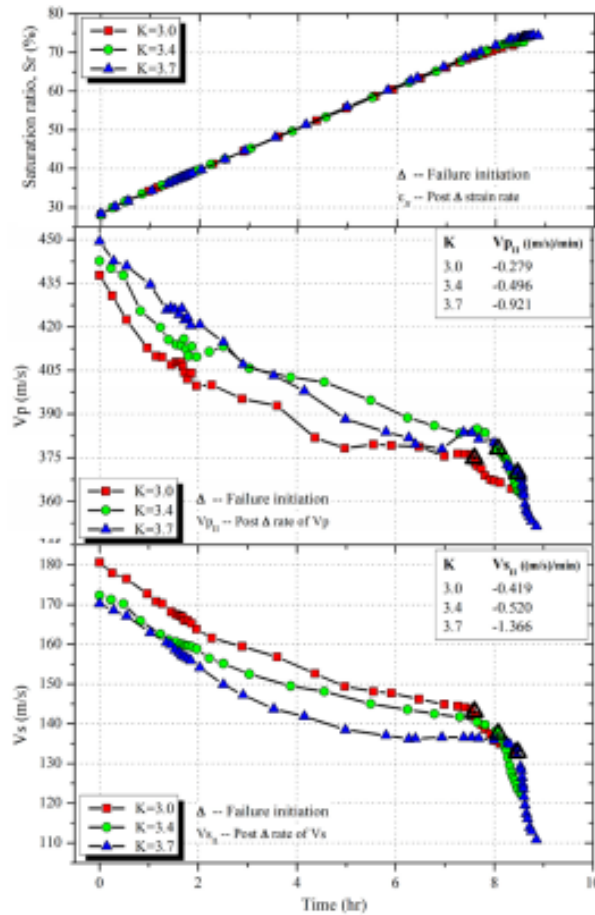
Figure 1.4: Response of elastic wave velocities at different principle stress ratios (*K*) during shearing infiltration tests; (a) Variation of saturation ratio (*Sr*) with time; (b) Compression wave velocity (*Vp*) response; (c) Shear wave velocity (*Vs*) response (Irfan, 2014) .

One elastic wave exciter and several receivers are installed on the slope surface covering large area, as shown in Figure 1.5. The wave signal is generated and transferred towards receivers with containing response of saturation state and stress state. A hollow cylindrical rod can be pushed into the slope surface by ramming until it reaches hard strata. The excitation could be created by drop hammer falling to hit

the stopper and subsequently waves are generated from the rod end and propagate at refracted path to receivers installed on the slope surface. Slope stability could be evaluated by means of elastic wave velocity detectation. Change of elastic wave velocity in soil during rainfall, can therefore be used to predict slope failures and landslides.

Laboratory model tests were conducted to explore the behavior of elastic wave velocities with soil deformations, and varying soil moisture content. Corresponding test results and related discussions shed light the potential to apply elastic wave velocity to monitor field landslide.
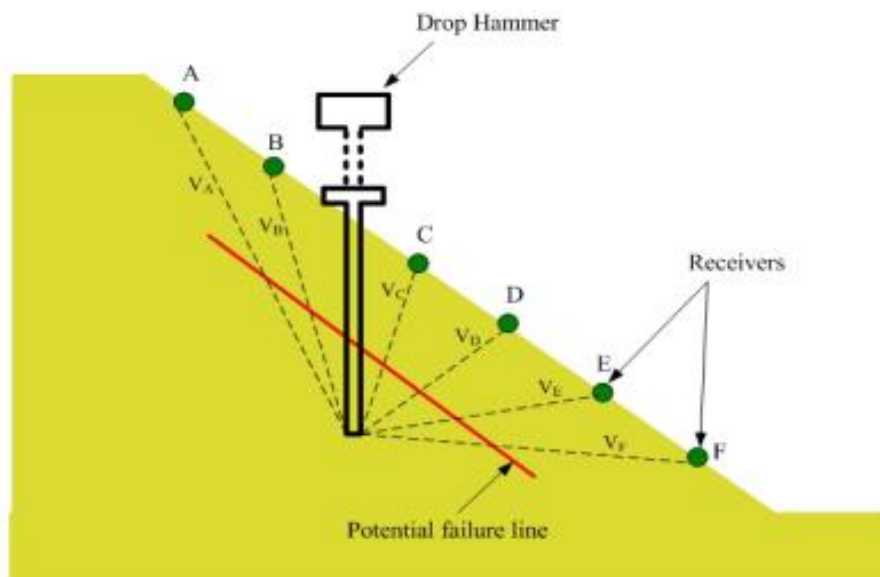
Figure 1.5: Schematic representation of wave excitation deep into soil surface (Irfan, 2014).

1.4. AIMS & OBJECTIVES

With an aim to develop ideas for the prediction of landslides by using wave propagation in soil, the change of elastic wave velocity with moisture and displacement variation is investigated by model tests. For getting fundamental

understanding of mechanism of wave velocity variation during soil wetting/drying, and slope movements, the main objectives in this research are characterizing the elastic wave velocity as a function of water content and deformation.

Many model tests were conducted to investigate the change of wave velocity under different influence factors for getting fundamental understanding of evolution of wave velocity by

exploring the influence of dry density on wave velocity during landslide;

exploring the influence of surface layer thickness on wave velocity during landslide;

exploring the influence of slope angle on wave velocity during landslide.

1.5. UNIT SYSTEM

The International System of Units (S.I.) as the modern form of the metric system and the world's most widely used system of measurement was adopted in this research. Following the usual sign and convention in soil mechanics, all mechanical variables and physical variables in soil mechanics are stipulated as positive in compression and negative as in tension.

1.6. TIME SCALE AND LOCATION OF RESEARCH

The research and all laboratory tests were conducted in Geotechnical Engineering Laboratory of The University of Tokyo located at 7-3-1 Hongo, Bunkyo-ku, Tokyo 113-8656, Japan. during October 2013-October 2016.

1.7. THESIS ORGANIZATION

1. Chapter 1 shows an introduction of research curriculum.

2. Chapter 2 provides a brief review of previous studies related to rainfall induced landslides and landslide protection approaches.

3. Chapter 3 presents the detailed description of the use of material and experimental setup employed for this study.

4. Chapter 4 describes the overall research methodology. The detailed experimental plan and step by step procedure for the performance of each type of experiment are outlined.

5. Chapter 5 presents the results of each test of flat slope test and the corresponding evolution of wave velocity are discussed.

6. Chapter 6 presents the results of each test of slope test and the corresponding evolution of wave velocity are discussed.

7. Distinguish of *Vp* and *Vs* by bender element test

8. In Chapter 8, the potential of applying the idea of elastic wave velocities to predict such rain induced landslides is discussed.

9. Chapter 9 shows conclusions and recommendations.

1.9. REFERENCES

Angeli, M.-G., Pasuto, A., & Silvano, S. (2000). A Critical Review of Landslide Monitoring Experiences. Engineering Geology, 55(3), 133-147.

Baum, L.B., Godt, J. W. (2010): Early warning of rainfall-induced shallow landslides

and debris flows in the USA, *Landslides*, 7, 259–272.

Brand, E. W. (1981). Some Thoughts on Rain-Induced Slope Failures. Proc. of 10th International Conference on Soil Mechanics and Foundation Engineering, 3, 373-376.

Cadman, J.D, and Goodman, R.E. (1967): Landslide noise, *Science*, 158(3805), 1182-1184.

Chae, B. G.and Kim, M. I. (2012): Suggestion of a method for landslide early warning using the change in the volumetric water content gradient due to rainfall infiltration, *Environmental Earth Sciences*, 66(7), 1973-1986.

Chichibu, A., Jo, K., Nakamura, M., GOTO, T. and KAMATA, M. (1989): Acoustic emission characteristics of unstable slopes, *Journal of Acoustic Emission*, 8(4), 107-112.

Dixon, N. and Spriggs, M. (2007): Quantification of slope displacement rates using acoustic emission monitoring, *Canadian Geotechnical Journal*, 44(6): 966-976.

Dixon, N., Smith, A., Spriggs, M. P., Ridley, A., Meldrum, P., and Haslam, E. (2015b): Stability monitoring of a rail slope using acoustic emission, *Proceedings of the Institution of Civil Engineers - Geotechnical Engineering*, 168(5), 373-384.

Dixon, N., Spriggs, M. P., Smith, A., Meldrum, P. and Haslam, E. (2015a): Quantification of reactivated landslide behaviour using acoustic emission monitoring, *Landslides*, 12(3), 549-560.

Evans, S. G. (2001). Landslides. A Synthesis of Geological Hazards in Canada, Geological Survey of Canada Bulletin 578, 43-79.

Farooq, K., Orense, R., & Towhata, I. (2004). Response of Unsaturated Sandy Soils under Constant Shear Stress Drained Condition. Soils and foundations, 44(2), 1-13.

FHWA. (2003). Soil Nail Walls, Geotechnical Engineering Circular No 7. Report No.

FHWAO-IF-03-017. Federal Highway Administration.

Fukuzono, T. (1985): A new method for predicting the failure time of a slope. *Proceedings of the IV International Conference and Field Workshop on Landslides*, Tokyo, 145-150.

Irfan, M. (2014). Elastic wave propagation through unsaturated soils concerning early warning of rain-induced landslides. PhD Thesis, Univeristy of Tokyo, Japan.

Irfan, M. and Uchimura, T. (2013a): Effects of soil moisture on shear and dilatational wave velocities measured in laboratory triaxial tests, *Proceedings of the 5th International Young Geotechnical Engineers' Conference*, Paris, France, 505-509.

Irfan, M., Uchimura, T. and Ghani, M.A.H. (2013b): Response of elastic wave velocities during constant shear stress drained tests on unsaturated triaxial specimens, *3rd Korea-Japan Workshop on Unsaturated Soils*, Seoul, Korea, 45-51.

Keefer, D. K., Wilson, R C., Mark, R K., Brabb, E E., Brown, W M., Ellen, S D., Harp, E L., Wieczorek, G F., Alger, C S., Zatkin, R. S. (1987): Real-time landslide warning during heavy rainfall, *Science*, 238 (4829), 921–925.

Mosher, D. C. (2008). Submarine Mass Movements in Canada: Geohazards with FarReaching Implications. Proceedings: 4th Canadian Conference on Geohazards: From Causes to Management (pp. 55-62), Quebec, Canada.

Nakajima, I., Negishi, M., Ujihira, M. and Tanabe, T. (1991) Application of the acoustic emission monitoring rod to landslide measurement. *Acoustic Emission/Microseismic Activity in Geologic Structures and Materials*: *Proceedings of the 5th Conference*, Trans Tech Publications, Du̇rnten, Switzerland, 1-15.

Ng, C. W., & Pang, Y. (2000). Influence of Stress State on Soil-Water Characteristics and Slope Stability. Journal of Geotechnical and Geoenvironmental Engineering, 126(2), 157-166.

Ochiai, H., Okada, Y., Furuya, G., Okura, Y., Matsui, T., Sammori, T., Terajima, T., Sassa, K. (2004): A fluidized landslide on a natural slope by artificial rainfall, *Landslides*, 1 (3), 211–219.

Osanai, N., Tomita, Y., Akiyama, K., Matsushita, T. (2009): Reality of cliff failure disaster, Technical Note of National Institute for Land and Infrastructure Management, 530.

Petley, D. (2012): Global patterns of loss of life from landslides, *Geology*, 40(10), 927-930.

Proceedings: The 12 th International Conference on Soil Mechanics and Foundation Engineering, Rio de Janeiro, Br, 08/13-18/89 (pp. 1639-1642.

Ramesh, M., & Vasudevan, N. (2012). The Deployment of Deep-Earth Sensor Probes for Landslide Detection. Landslides, 9(4), 457-474. doi: 10.1007/s10346-011-0300-x

Rouse, C., Styles, P. and Wilson, S.A. (1991): Microseismic emissions from flowslide-type movements in South Wales, *Engineering Geology*, 31(1), 91–110.

Saito, M. (1965): Forecasting the time of occurrence of a slope failure. *Proceedings of the 6th International Conference on Soil Mechanics and Foundation Engineering*, 2, 537–541.

Saito, M. (1987): On application of creep curves to forecast the time of slope failure-in answer to comments upon failure forecasting, *Journal of the Japan Landslide Society*, 24 (1), 30-38.

Smith. A., Dixon, N., Meldrum, P., Haslam, E. and Chambers, J. (2014) Acoustic emission monitoring of a soil slope: comparisons with continuous deformation measurements, *Geotechnique Letters*, 4(4): 255-261.

Uchimura, T. (2011). Wave Velocity in Unsaturated Slopes in Relation to Moisture

and Stability. Proceedings: Proc. of The 14th Asian Regional Conference on Soil Mechanics and Geotechnical Engineering), Hong Kong, China.

Uchimura, T., Suzuki, D., & Hongkwan, S. (2011). Combined Monitoring of Water Content and Displacement for Slope Instability. Proceedings: Proc. of 4th Japan-Korea Geotechnical Workshop (pp. 67-72), Kobe, Japan.

Uchimura, T., Towhata, I., Lan Anh, T., Fukuda, J., Bautista, C. B., Wang, L., . . . Sakai, N. (2010). Simple Monitoring Method for Precaution of Landslides Watching Tilting and Water Contents on Slopes Surface. Landslides, 7(3), 351-357. doi: 10.1007/s10346-009-0178-z

Uchimura, T., Towhata, I., Wang, L., & Qiao, J. P. (2011). Miniature Ground Inclinometer for Slope Monitoring. Proceedings: Proc. of The 14th Asian Regional Conference on Soil Mechanics and Geotechnical Engineering, ATC3 session), Hong Kong, China.

USGS. (2004). Landslide Types and Processes, Fact Sheet 2004-3072, July 2004 Retrieved 18/12/2013, from http://pubs.usgs.gov/fs/2004/3072/pdf/fs2004-3072.pdf

Wolle, C., & Hachich, W. (1989). Rain-Induced Landslides in Southeastern Brazil.

CHAPTER 2

LITERATURE REVIEW

2.1. INTRODUCTION

This chapter is to overview previous literatures related to the mechanism of rainfall-induced slope failures and elastic wave propagation in soil. The elastic wave velocity in unsaturated soils requires has been use as an indicator for evaluating the physicomechanical properties of geomaterials, including soil liquefaction and rock intactness. However, few clues are available about the prediction of landslide using elastic wave velocities in unsaturated soils. Thorough understanding of elastic wave propagation in unsaturated soils is the core of this study. Therefore, a comprehensive review of existing literature related to the response of elastic waves in unsaturated soils is presented.

2.2. RAIN-INDUCED SLOPE FAILURES

Rainfall-induced slope failures are one of the most hazardous disasters which lead to significant damage over the world. Traditional approaches to prevent rainfall-induced landslides, such as stabilization of unstable slopes by installation of retaining walls and ground anchors, has been useful. But, they are not very helpful in mitigation of small slope failures, which are less significant in scale but numerous in numbers, because of their cost of installation. In consequence of recent residential developments in hilly area, the risk of smaller landslides has been realized. There is extravagant number of slopes with potential of such failure, and it is not financially realistic to use traditional approaches for each of them. Low-cost and simple early warning system is needed to deal with such problems. A useful and cost-efficient

alternative is real-time monitoring of susceptible slope surfaces and issuing an early warning to reduce potential damages.

2.2.1   Mechanism of Rain-induced Landslides

The mechanism of rain-induced landslides has been investigated by several researchers (Brand, 1981; S. A. Anderson & Sitar, 1995; Farooq et al., 2004; Sorbino & Nicotera, 2012). Soil derives shear strength from matric suction soil. When it rains and the rainfall begins to infiltrate the ground, the moisture content of the upper soil layer rises from the surface layer. A higher water content of soil decreases the matrix suction, causing smaller shear strength of soil. When the shear strength of soil decreases to a critical value after which the equilibrium is reached, landslide is going to occur. Several researchers have found that the formation of slope failure requires the generation of positive pore water pressure (Eckersley, 1990; Johnson & Sitar, 1990; Sitar et al., 1992). Brand (1981) suggested that the typical stress ranges over which triaxial tests are usually conducted are not suitable to simulate rainfall-induced slope failures.

2.3.   ELASTIC WAVE PROPAGATION IN SOIL

Wave propagation in fluid-containing porous media has received great attention in recent years, because of its importance in geotechnical engineering for determining soil properties from the results of field or laboratory geophysical tests (Conte et al. 2009). In an infinite medium, two fundamental modes of seismic wave propagation exist: compression waves and shear waves (Kolsky 1963; White 1981; Achenbach 1991). The particle motion generated by these two types of seismic waves differs (Figure 2.1). In compression waves, also called primary waves (P-waves), the particle motion is held on a plane (polarized) parallel to the direction of propagation, whereas in shear waves, known as secondary waves (S−waves), the particle motion is perpendicular to the direction of propagation.

Elastic wave could monitor the elastic and shear stiffness and modulus of soils. Also, elastic wave could detect the stress state because the stiffness of soils is dependent on

the effective stresses (Roessler 1979). The state of effective stress for soil affects the wave velocity.
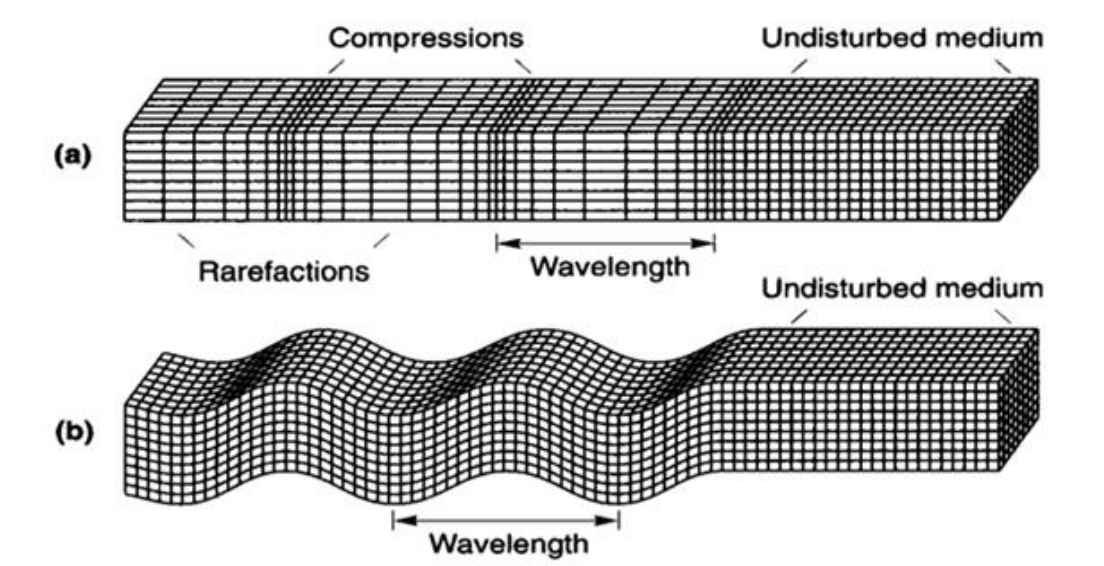
Figure 2.1: Particle motion in (a) Compression waves; (b) Shear waves (Kramer, 1996)

2.3.1   Wave Velocities

The S-wave velocity has been well recognised as an important parameter in geotechnical engineering. S-wave velocity can reflect the soil skeleton structure and is regardless of both the water content and the gas content. S-wave velocity can represent the small strain shear modulus of a soil that is a key parameter in analysis and design of various geotechnical structures. S-wave depends on the shear stiffness of soil skeleton.

The P-wave velocity is applied to describe the upper seabed sediments. P-wave velocity, on the other hand is governed by constrained compression modulus of soil, therefore it is influenced by both, the pore fluid and soil skeleton (K. H. Stokoe & Santamarina, 2000).

Wave velocity is a soil mechanical property. Extensive research efforts have been carried out to study this property, mainly through well-controlled laboratory experiments and field measurements. The in situ measurements of wave velocity result from seismic cone penetration test (SCPT) (Campanella et al. 1986), and surface waves (spectral analysis of surface waves (SASW), modal analysis of surface waves (MMASW) (Karray 2010; Karray et al. 2011).

Conventional laboratory experiments conducted to determine the wave velocity are based on resonant column (RC) (e.g., Hardin and Richart 1963; Chien and Oh 2000; Fam et al. 2002; Yang and Gu 2013), bender elements (BEs) (e.g., Dyvik and Madshus 1985; Viggiani and Atkinson 1995; Brignoli et al. 1996; Yamashita et al. 2009; Clayton 2011), and the piezoelectric ring-actuator technique (e.g., Ben Romdhan et al. 2014; Karray et al. 2015). These techniques may effectively be used to study and quantify the effects of various parameters on wave velocity.

2.3.2 Factors Influencing Elastic Wave Propagation in Soil

The equation for S-wave and P-wave velocity can write (B. O. Hardin & Richart, 1963; B. O. Hardin, 1978);

$$Vs = Cs \cdot \sqrt{F(e)} \cdot \left(\frac{\sigma'_o}{P_a} \right)^n \tag{2.3}$$

$$Vp = Cp \cdot \sqrt{F(e)} \left[\frac{\sigma'_0}{P_a} \right]^n \tag{2.4}$$

where *Vs* and *Vp* are shear and compression wave velocity, respectively. σ'_o is effective isotropic stress, C_s, C_p and n are constants reflecting soil type, grain properties and fabric. P_a represents the atmospheric pressure, and *F(e)* is the void ratio function. It can be seen that the elastic wave velocity is a function of effective stress state, void ratio, and nature of soil.

2.3.2.1 *Effective Stress State*

Some of the earliest studies on the effects of effective stress state on shear wave velocities were performed by B. O. Hardin and Richart (1963), B. Hardin and Black

(1968), and B. O. Hardin and Drnevich (1972). Results given by B. O. Hardin &
Richart (1963) is shown in Figure 2.. Similar findings for various other types of soils
were also found by other researchers (Marcuson & Wahls, 1972; Iwasaki et al., 1978;
Kokusho, 1980; T. Kim & Novak, 1981; Gu & Yang, 2013; Gu et al., 2015; Irfan,
2014; Irfan & Uchimura, 2016).
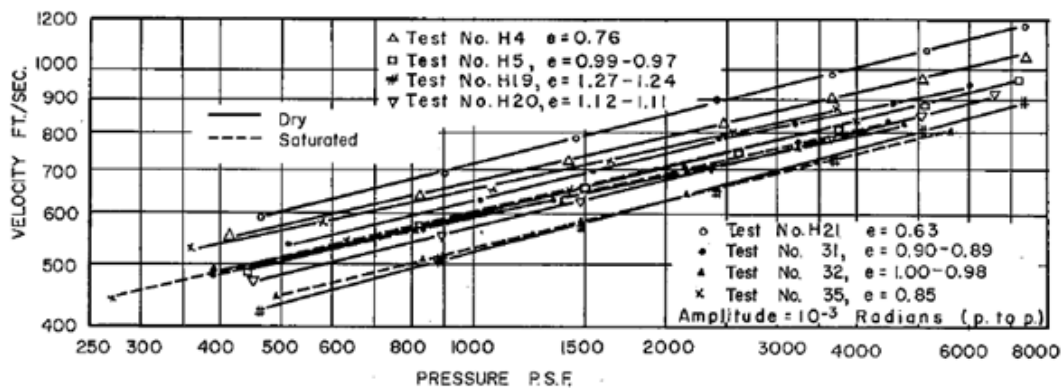
Figure 2.2: Variation of shear wave velocity with confining pressure and void ratio for
saturated and dry crushed quartz sand (B. O. Hardin & Richart, 1963).

It has been revealed that elastic wave behavior is dependent on the principle stress
directions (Roesler, 1979; K. Stokoe et al., 1991; Bellotti et al., 1996). P-wave
velocity only depends on the stress state in the direction of wave propagation, while
the S-wave velocity depends on the state of stress in the direction of not only wave
propagation but also particle vibration (Stokoe II et al., 1995; K. H. Stokoe &
Santamarina, 2000).

2.3.2.2   *Void Ratio*

Some of the earliest studies related to elastic wave propagation recognized the role of
void ratio on wave velocities (B. O. Hardin & Richart, 1963; B. Hardin & Black,
1968; Iwasaki et al., 1978). B. O. Hardin and Richart (1963) performed resonant-
column experiments and found the relationship between shear wave velocity and void
ratio, as shown in Figure 2..
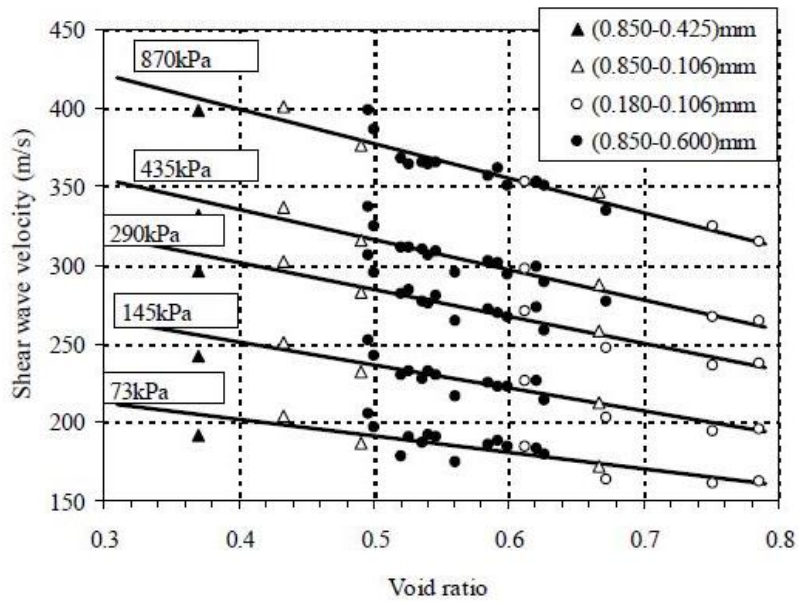
Figure 2.3: Shear wave velocity variation with void ratio for different stress states (after B. O. Hardin and Richart (1963)

Considering varying stress states as shown in Figure 2., Figure 2. shows the shear wave velocities normalized by Eq. 2.3. The normalized S-wave velocities decrease linearly with void ratio at isotropic stress level.

Triaxial compression would definitely alter the void ratio, which in turn influences the wave velocities. Void ratio function, $F(e)$, defined in Eq 2.3 and 2.4, is therefore used to normalize wave velocities to calibrate any changes in void ratio.
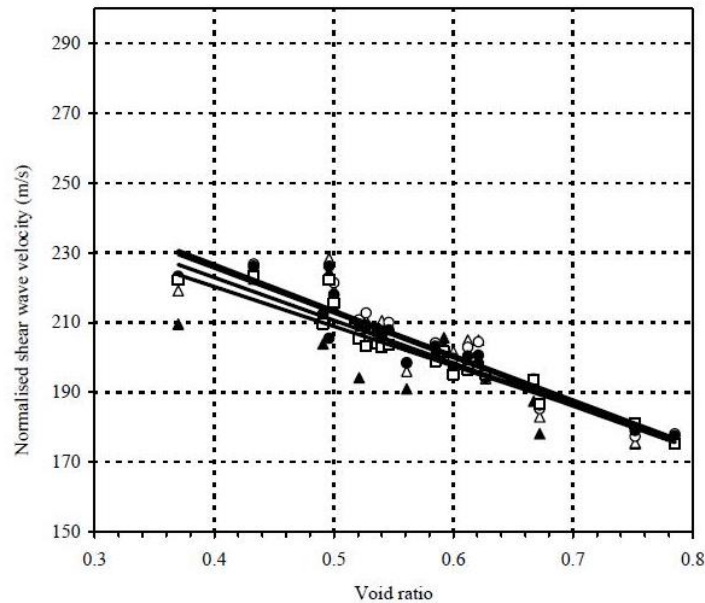
Figure 2.4: Shear wave velocity variation with void ratio. Wave velocities normalized by using Eq. 2.3 and 2.4 to cancel the effect of stress state (after B. O. Hardin and Richart, 1963)

2.3.2.3   Degree of Saturation

Kumar and Madhusudhan (2012) used bender and extender elements test to measure P-wave and S-wave velocity for a soil between the dry and fully saturated states. They found that *Vs* and *Vp* reach a maximum around the optimum value of *Sr*. Beyond the optimum *Sr*, the values of *Vs* and *Vp* decrease continuously with an increase in *Sr*. when *B* value exceeds 0.99, the value of *Vp* suddenly rises to those of the water.

Qian et al (1991) used resonant column to investigate the S-wave velocity with degree of saturation ranging from 0 to 50%. They used small strain shear modulus, *G*, to link shear wave velocity. The result shows a peak in shear modulus with degree of saturation.

Mancuso et al. (2002) studied the small strain behavior of unsaturated compacted silty sand by a resonant column combined with torsional shear cell and suction control assembly. They obtained S-shaped shear stiffness versus suction variation, as shown in Figure 2.6.
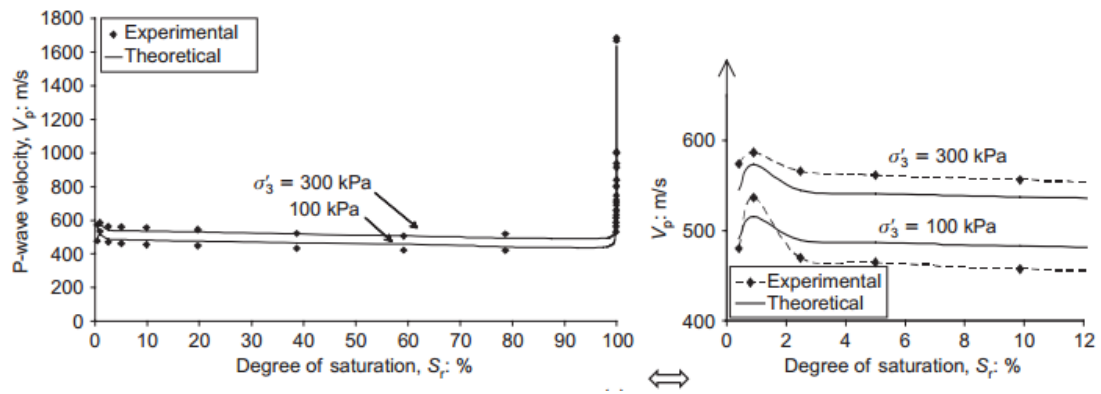
(a) P-wave
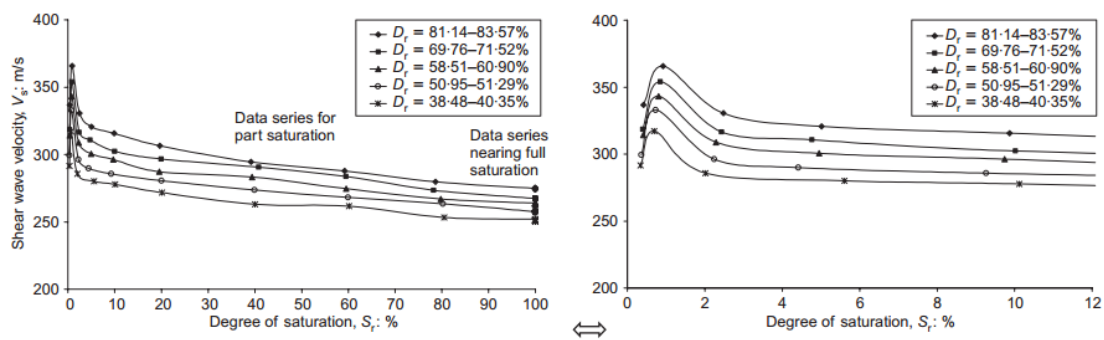
(b) S-wave

Figure 2.5: Variation of wave velocity with degree of saturation (Kumar and Madhusudhan, 2012)

Cho & Santamarina (2001) tested wave velocity on soils using bender element. They examined the change of velocity for S-wave with degree of saturation. It can be seen from Figure 2. that a continuous increase in S-wave velocity as the degree of saturation decreases.

Alramahi et al (2010) measured wave velocity on clay and silt at different degree of saturation and also found that S-wave velocity increases as the degree of saturation decreases, as shown in Figure 2.
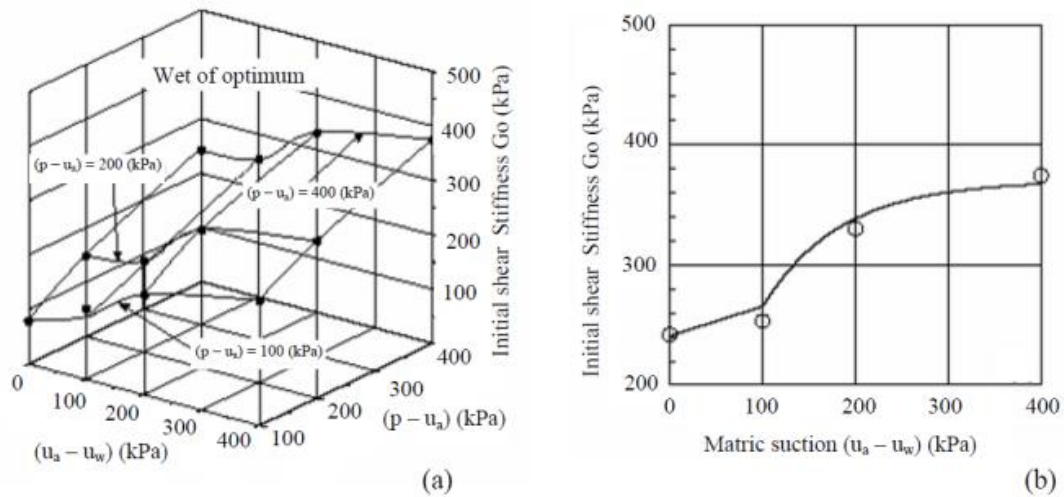
Figure 2.6: (a) Initial shear stiffness in controlled-suction resonant column tests. (b) Response of shear stiffness to suction at a mean net stress of 400 kPa. (Mancuso et al., 2002).
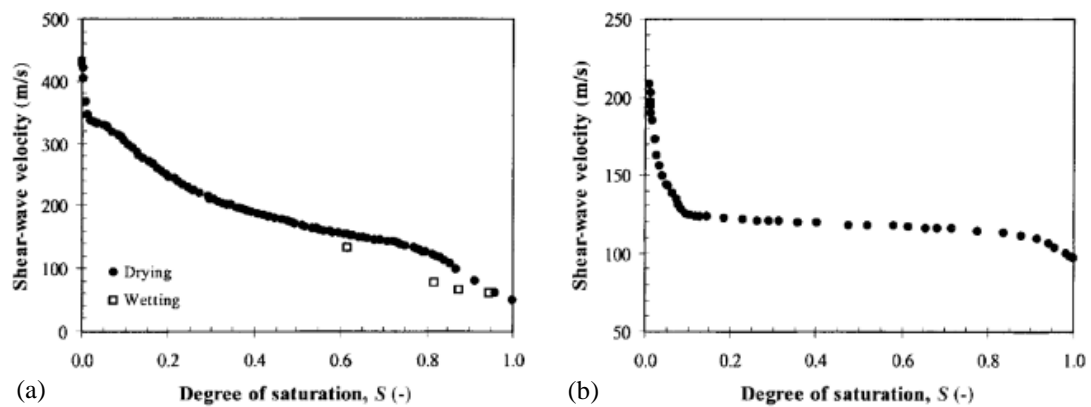
Figure 2.7: Shear wave velocity versus degree of saturation; (a) Granite Powder; (b) Sandboil sand. (Cho & Santamarina, 2001).
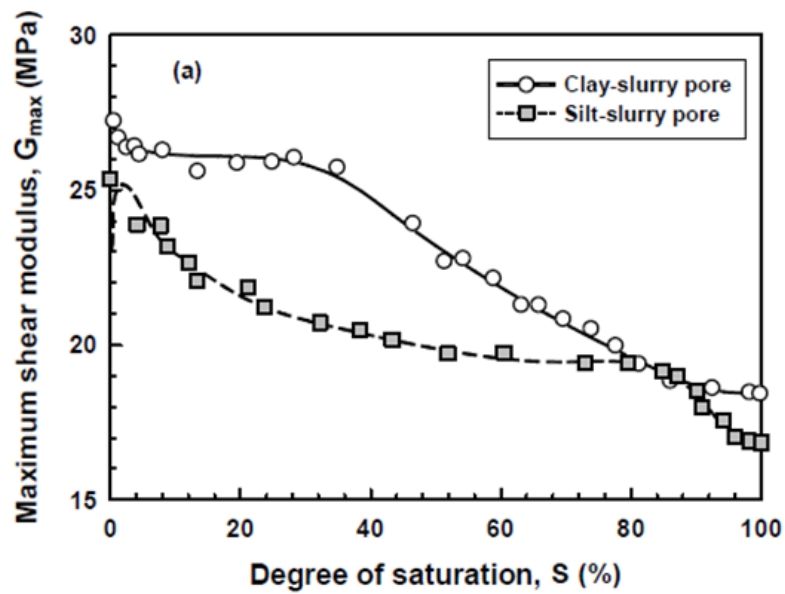
Figure 2.8: Variation of shear wave velocity (in terms of shear modulus) with degree of saturation. (Alramahi et al., 2009).

Irfan (2014) conducted bender element tests on Edosaki sand and found that both P-wave and S-wave velocities increase to a peak value at around 20% degree of saturation. Further increase in degree of saturation results in a drop in both P-wave and S-wave velocities, as shown in Figure 2.
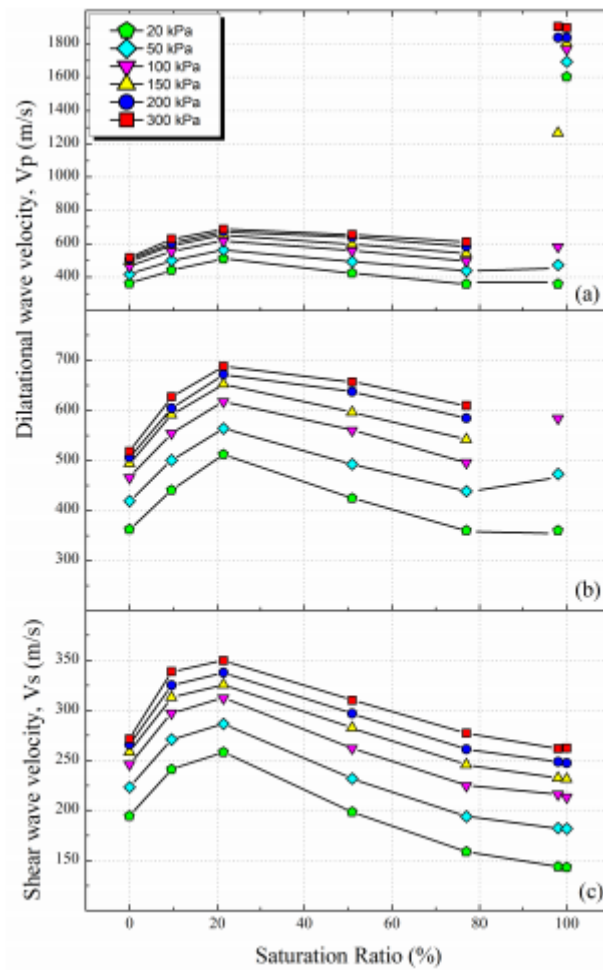
Figure 2.9: Effect of degree of saturation on wave velocities at various confining pressures. (a) P-wave (Zoomed-out), (b) P-wave (Zoomed-in), and (c) S-wave velocity

Moreover, Irfan (2014) conducted triaxial tests under constant shear stress water injection conditions, with records of Vp and Vs. As shown in Figure 2.10, a gradual decrease in wave velocities was followed by a rapid decrease once the failure was initiated.
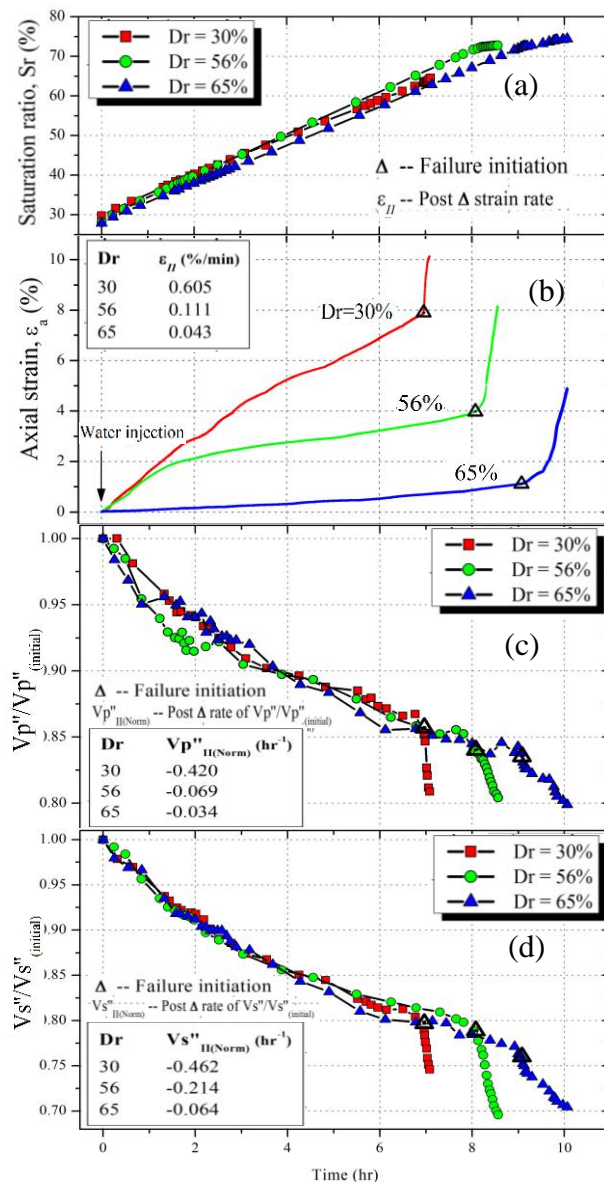
Figure 2.10: Variation of (a) saturation; (b) deformation; (c) normalized compression wave velocity, and (d) normalized shear wave velocity, with time.

2.4. SUMMARY

The fundamental and comprehensive understandings about previous main studies on landslides and elastic wave behaviors in soil are introduced in this chapter which is categorized into two fields, i.e., rainfall-induced landslides, and elastic wave propagation.

The objective of this study is to develop an elastic wave velocity based early warning system for rainfall induced landslide. Thus an extensive literature survey about the elastic wave velocity with increasing water content is also presented.

2.5. REFERENCES

Achenbach, J. (1984). *Wave Propagation in Elastic Solids*. North-Holland, New York.

Alramahi, B., Alshibli, K. A., & Fratta, D. (2009). Effect of Fine Particle Migration on the Small-Strain Stiffness of Unsaturated Soils. *Journal of Geotechnical and Geoenvironmental Engineering, 136*(4), 620-628.

Anderson, S. (1992). *The Role of Hydrologic Response and Soil Behavior in the Initiation of Rainfall-Induced Debris Flows.* PhD Thesis, Univeristy of California, Berkeley, California.

Anderson, S. A., & Sitar, N. (1991). *Influence of Stress Path on Soil Strength Parameters and Analysis of Rainfall Induced Slope Failures.* Proceedings: Symp. Eng. Geol. Geotech. Eng (pp. 21-26).

Anderson, S. A., & Sitar, N. (1995). Analysis of Rainfall-Induced Debris Flows. *Journal of Geotechnical Engineering, 121*(7), 544-552.

Au, S. (1998). Rain-Induced Slope Instability in Hong Kong. *Engineering Geology, 51*(1), 1-36.

Bellotti, R., Jamiolkowski, M., Lo Presti, D., & O'Neill, D. (1996). Anisotropy of Small Strain Stiffness in Ticino Sand. *Geotechnique, 46*(1), 115-132.

Brand, E. W. (1981). Some Thoughts on Rain-Induced Slope Failures. *Proc. of 10th International Conference on Soil Mechanics and Foundation Engineering, 3*, 373-376.

Campanella, R.G., Robertson, P.K., & Gillespie, D.G. (1986) Seismic cone penetration test. *Proceedings of In Situ '86, ASCE*, 116–130.

Cascini, L., Cuomo, S., Pastor, M., & Sorbino, G. (2009). Modeling of Rainfall-Induced Shallow Landslides of the Flow-Type. *Journal of Geotechnical and Geoenvironmental Engineering, 136*(1), 85-98.

Cho, G. C., & Santamarina, J. C. (2001). Unsaturated Particulate Materials-Particle-Level Studies. *Journal of Geotechnical and Geoenvironmental Engineering, 127*(1), 84-96.

Conte, E., Cosentini, R. M., & Troncone, A. (2009). Shear and dilatational wave velocities for unsaturated soils. *Soil Dynamics and Earthquake Engineering*, 29(6), 946-952.

Eckersley, D. (1990). Instrumented Laboratory Flowslides. *Geotechnique, 40*, 489-502.

Farooq, K., Orense, R., & Towhata, I. (2004). Response of Unsaturated Sandy Soils under Constant Shear Stress Drained Condition. *Soils and foundations, 44*(2), 1-13.

Gu X, Yang J, Huang M, et al. Bender element tests in dry and saturated sand: Signal interpretation and result comparison[J]. Soils and Foundations, 2015, 55(5): 951-962.

Gu X Q, Yang J. A discrete element analysis of elastic properties of granular materials[J]. Granular Matter, 2013, 15(2): 139-147.

Hardin, B. O. (1978). *The Nature of Stress-Strain Behavior for Soils.* Proceedings: ASCE Geotechnical Engineering Division Specialty Conference: Earthquake Engineering and Soil Dynamics (pp. 3-91), Pasadena, California.

Hardin, B. O., & Drnevich, V. P. (1972). Shear Modulus and Damping in Soils: Design Equation and Curves. *J. Soil Mech. Found. Engng. Div., ASCE 98*(7), 667-691.

Hardin, B. O., & Richart, F. E. (1963). Elastic Wave Velocities in Granular Soils. *J. Soil Mech. and Found. Div., ASCE, 89*(1), 33-65.

Iwasaki, T., Tatsuoka, F., & Takagi, Y. (1978). Shear Moduli of Sands under Cyclic Torsional Shear Loading. *Soils and Foundations, 18*(1), 39-56.

Irfan, M. (2014). *Elastic Wave Propagation through Unsaturated Soils Concerning Early Warning of Rain-induced Landslides.* PhD Thesis, Univeristy of Tokyo, Tokyo.

Irfan, M., & Uchimura, T. (2016). Modified triaxial apparatus for determination of elastic wave velocities during infiltration tests on unsaturated soils. KSCE Journal of Civil Engineering, 20(1), 197-207.

Johnson, K., & Sitar, N. (1990). Hydrologic Conditions Leading to Debris-Flow Initiation. *Canadian Geotechnical Journal, 27*(6), 789-801.

Karray, M. (2010) Shear wave velocity in geotechnical engineering. *Proceedings of the International Conference on Geotechnical Engineering*, Hammamet, 20–23 April, Tunisia.

Karray, M., Lefebvre, G., Ethier, Y., & Bigras, A. (2011) Influence of particle size on the correlation between shear wave velocity and cone tip resistance. *Canadian Geotechnical Journal*, 48(4): 599–615.

Kim, T., & Novak, M. (1981). Dynamic Properties of Some Cohesive Soils of Ontario. *Canadian Geotechnical Journal, 18*(3), 371-389.

Kokusho, T. (1980). Cyclic Triaxial Test of Dynamic Soil Properties for Wide Strain Range. *Soils and foundations, 20*(2), 45-60.

Kolsky, H. (1963). *Stress Waves in Solids* (Vol. 1098): Courier Dover Publications.

Kramer, S. L. (1996). *Geotechnical Earthquake Engineering*: Pearson Education India.

Lowe, J. (1967). Stability Analysis of Embankments. *Journal of Soil Mechanics & Foundations Div*.

Mancuso, C., Vassallo, R., & d'Onofrio, A. (2002). Small Strain Behavior of a Silty Sand in Controlled-Suction Resonant Column Torsional Shear Tests. *Canadian Geotechnical Journal, 39*(1), 22-31.

Marcuson, W. F., & Wahls, H. E. (1972). Time Effects on Dynamic Shear Modulus of Clays. *Journal of the Soil Mechanics and Foundations Division, 98*(12), 1359-1373.

Qian, X., Gray, D., & Woods, R. (1991). Resonant Column Tests on Partially Saturated Sands. *Geotechnical Testing Journal, 14*(3).

Ramesh, M., & Vasudevan, N. (2012). The Deployment of Deep-Earth Sensor Probes for Landslide Detection. *Landslides, 9*(4), 457-474. doi: 10.1007/s10346-011-0300-x

Roesler, S. K. (1979). Anisotropic Shear Modulus Due to Stress Anisotropy. *Journal of the Geotechnical Engineering Division, 105*(7), 871-880.

Sitar, N., Anderson, S., & Johnson, K. (1992). *Conditions Leading to the Initiation of Rainfall-Induced Debris Flows.* Proceedings: Geotech Eng Div Specialty Conf: Stability and Perf. of Slopes and Embankments-II. ASCE, New York (pp. 834-839).

Sorbino, G., & Nicotera, M. V. (2012). Unsaturated Soil Mechanics in Rainfall-Induced Flow Landslides. *Engineering Geology*.

Stokoe II, K., Hwang, S., Lee, J.-K., & Andrus, R. D. (1995). *Effects of Various Parameters on the Stiffness and Damping of Soils at Small to Medium Strains.* Proceedings: Pre-Failure Deformation of Geomaterials, Sapporo, Japan.

Stokoe, K., Hwang, S., & Lee, S.-H. (1991). *Characterization of Soil in Calibration Chambers with Seismic Waves.* Proceedings: 1st Int. Symposium on Calibration Chamber Testing, Potsdam, New York.

Stokoe, K. H., & Santamarina, J. (2000). Seismic-Wave-Based Testing in Geotechnical Engineering. *GeoEng 2000*, 1490-1536.

Tsukamoto, Y., Ishihara, K., Nakazawa, H., Kamada, K., & Huang, Y. (2002). Resistance of Partly Saturated Sand to Liquefaction with Reference to Longitudinal and Shear Wave Velocities. *Soils and foundations, 42*(6), 93-104.

Tsukamoto, Y., Ishihara, K., & Nosaka, Y. (1998). On the Initiation of Rainfall Induced Soil Failure. *Geotechnical Hazards*, 883-890.

Uchimura, T. (2011). *Wave Velocity in Unsaturated Slopes in Relation to Moisture and Stability*. Paper presented at the The 14th Asian Regional Conference on Soil Mechanics and Geotechnical Engineering, Hong Kong.

Vaughan, P., & Kwan, C. (1984). Weathering, Structure and in Situ Stress in Residual Soils. *Geotechnique, 34*(1), 43-59.

Hardin, B.O., and Richart, F.E. 1963. Elastic wave velocities in granular soils. Journal of Soil Mechanics and Foundation Engineering Division, ASCE, 89(1): 33–66.

Chien, L.-K., and Oh, Y.-N. 2000. Laboratory and field shear wave measurement at a reclaimed site in west Taiwan. Geotechnical Testing Journal, 23(1): 021–035.

Fam, M.A., Cascante, G., and Dusseault, M.B. 2002. Large and small strain properties of sands subjected to local void increase. Journal of Geotechnical and Geoenvironmental Engineering, ASCE, 128(12): 1018–1025.

Yang, J., and Gu, X.Q. 2013. Shear stiffness of granular material at small strains: does it depend on grain size? Géotechnique, 63(2): 165–179.

Dyvik, R., and Madshus, C. 1985. Lab measurements of Gmax using bender elements. In Proceedings of the Conference on the Advances in the Art of Testing Soil under Cyclic Conditions. ASCE Geotechnical Engineering Division, New York, pp. 186–196.

Viggiani, G., and Atkinson, J.H. 1995. Interpretation of bender element tests. Géotechnique, 45(1): 149–154.

Yamashita, S., Kawaguchi, T., Nakata, Y., Mikami, T., Fujiwara, T., and Shibuya, S. 2009. Interpretation of international parallel test on the measurement of Gmax using bender elements. Soils and Foundations, 49(4): 631–650.

Brignoli, E.G.M., Gotti, M., and Stokoe, K.H., II. 1996. Measurement of shear waves in laboratory specimens by means of piezoelectric transducers. Geotechnical Testing Journal, 19(4): 384–397.

Clayton, C.R.I. 2011. Stiffness at small strain: research and practice. Géotechnique, 61(1): 5–38.

Ben Romdhan, M., Hussien, M.N., Karray, M., Chekirad, M., and Varvara, R. 2014. The use of piezoelectric ring-actuator technique (P-RAT) in shear wave velocity measurement in granular media. In Proceedings of the 67th Canadian Geotechnical Conference, Regina, Sask., Paper no. 307.

Karray, M., Ben Romdhan, M., Hussien, M.N., and Éthier, Y. 2015. Measuring shear wave velocity of granular material using the piezoelectric ring-actuator technique (P-RAT). Canadian Geotechnical Journal, 52(9): 1302–1317.

Kumar, J., & Madhusudhan, B. N. (2012). Dynamic properties of sand from dry to fully saturated states. Geotechnique, 62(1), 45-54.

CHAPTER 3

EXPERIMENTAL SETUP

3.1. GENERAL REMARKS

Laboratory model test is regarded as the most reliable method for studying the rainfall-triggered landslide, in which the soil properties and boundary conditions can be controlled and the water content inside slope and deformation on the surface can be monitored. For the purpose of better understanding the changes in elastic wave velocity in soil slope in wetting and failure process as a result of rainfall, we performed two types of slope model tests in the laboratory, slope angle=45° for one type at which artificial rainfall was continuously applied until slope failure and slope angle=0° for the other where rainfall was given at early period after which soil model was inclined without rainfall. The changes in wave velocity with coupling effect of water content and deformation or single effect are investigated.

In all cases, sensors were carefully calibrated according to the material characteristics, giving high reliability to all measurements involved in each test.

3.2. TEST MATERIALS

Slope model tests were performed by using Edosaki Sand obtained from a natural slope in Ibaraki prefecture (Japan) and corresponds to a dusty Brown-yellowish color material classified as silty sand according with unified soil classification system (USCS) (Chaminda 2006).

Figure 3.1 shows a microscopic view of Edosaki Sand, where it can be seen that is composed about by 95% of sub-angular to sub-rounded quartz particles with attached fines particles. One possible reason for the high quartz content can be the high resistance presented by quartz to physical and chemical weathering. Additionally, angular particles suggest that soil was developed "*in situ*" or at least under low transportation process.
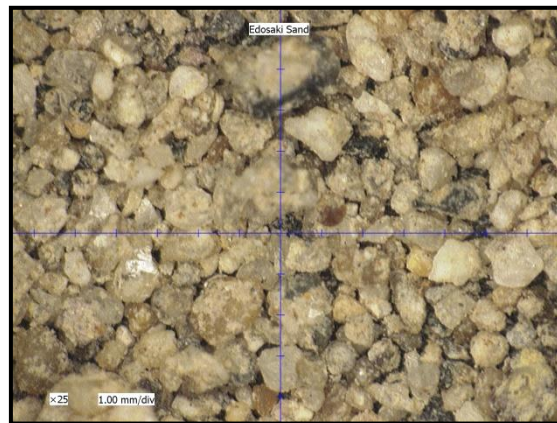
Figure 3.1: Microscopic view of Edosaki Sand (x25)

3.2.1. Material Properties

In order to obtain the physical properties of Edosaki sand, compaction and grain size distribution tests have been performed in previous studies (Garcia, 2005; Chaminda, 2006), in this study results of compaction tests were adopted and grain size distribution test was performed again by using mechani2cal sieve analysis; results showed not considerable difference with previous one, it means fines contents remain almost constant after several testing procedures. Table 3.1 summarizes the physical properties of Edosaki sand.

Table 3.1: Edosaki Sand Physical properties

Properties	Edosaki sand

Properties	Edosaki sand
Specific gravity – Gs	2.75
Mean grain size – D_{50} (mm)	0.23
Coefficient of uniformity – Cu	16.67
Coefficient of gradation – Cc	4.70
Fines content – (%)	16.40
Plastic Index	No Plastic
e_{max}	1.59
e_{min}	1.01
Max. dry unit weight – $\gamma_{d(max)}$ (kN/m3)	17.20
Saturated Conductivity Ks (cm/s)	0.005
Optimum moisture content – w_{opt} (%)	16.01

3.2.2. Grain Size Distribution

As previously mentioned, grain size distribution test was performed by using mechanical sieve method. Edosaki sand is classified as silty sand; grain size distribution curve is presented in Figure 3.2. Figure 3.3 shows the compaction characteristics of the Edosaki sand.
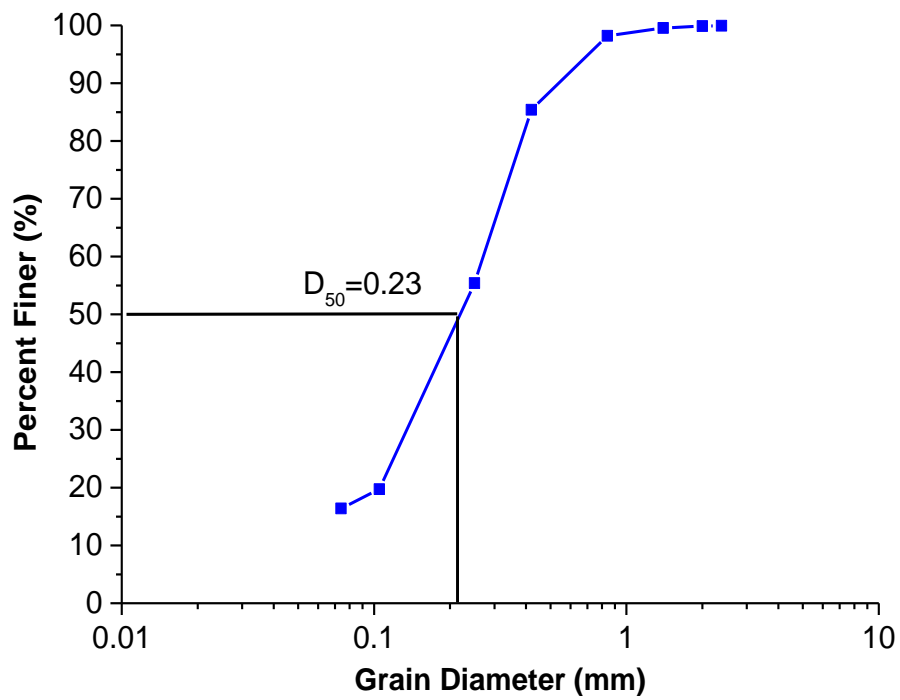
Figure 3.2: Edosaki sand grain size distribution curve.
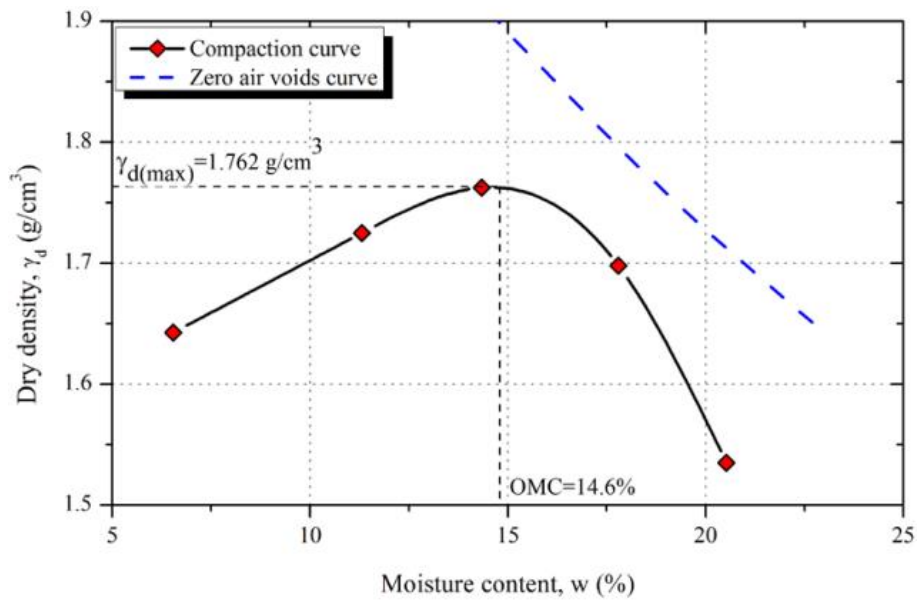
Figure 3.3: Compaction characteristics of Edosaki sand.

3.2.3. Soil Water Characteristic Curve SWCC

The soil-water characteristic curve (SWCC), is a very important concept in unsaturated soil mechanics and shows the relationship between the water content and matric suction of a soil (Orense R.P., 2003); the SWCC can be related to other properties describing the behavior of the soil, such as the unsaturated coefficient of permeability (Fredlung et al 1994) and shear strength (Vanapilli et al. 1996).

The shape of SWCC is a function of soil type; typical drying and SWCCs are illustrated in Figure 3.4. The air entry value, AEV is defined as the matric suction at which air first enters the largest pores of the soil during a drying process, (Brooks and Corey 1964). As matric suction increases from zero to the AEV, the volumetric water content, θ_w, is nearly constant. Then the water content steadily decreases to the residual water content, θ_r, as matric suction increases beyond the AEV. The residual water content is the water content at the residual state, at which water phase is discontinuous. The soil suction corresponding to the residual water content is called the residual soil suction ψ_r. The water entry value ψ_w, on the wetting SWCC, is defined as the matric suction at which the water content of the soil starts to increase significantly during the wetting process (Yang et al 2004).

Soil water characteristic curve for Edosaki Sand, has been extensively analyzed by previous researchers (i.e. Garcia, 2005; Chaminda, 2006). In order to find the best fitting parameters of the SWCC at different dry densities; several techniques and methods were used as direct measurements by using the Temp Pressure Cell Apparatus (Fredlung, 1993) and modeling by using the well-known equations from Van Genuchten (1980) and Fredlung and Xing (1994).
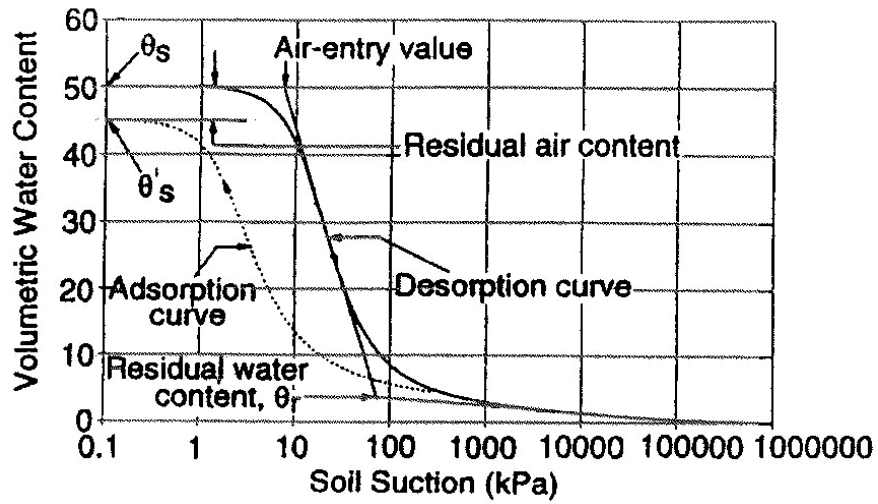
Figure 3.4: Definition of variables associated with the soil water characteristic curve
(Fredlund 1997).

Gallage and Uchimura (2010) obtained drying and wetting SWCCs for Edosaki Sand
using a Tempe pressure cell and the experimental data were fitted using the Fredlund
and Xing (1994) equation. The experimental data and the best-fit SWCC results of
Edosaki Sand for different densities are shown in Figure 3.5.
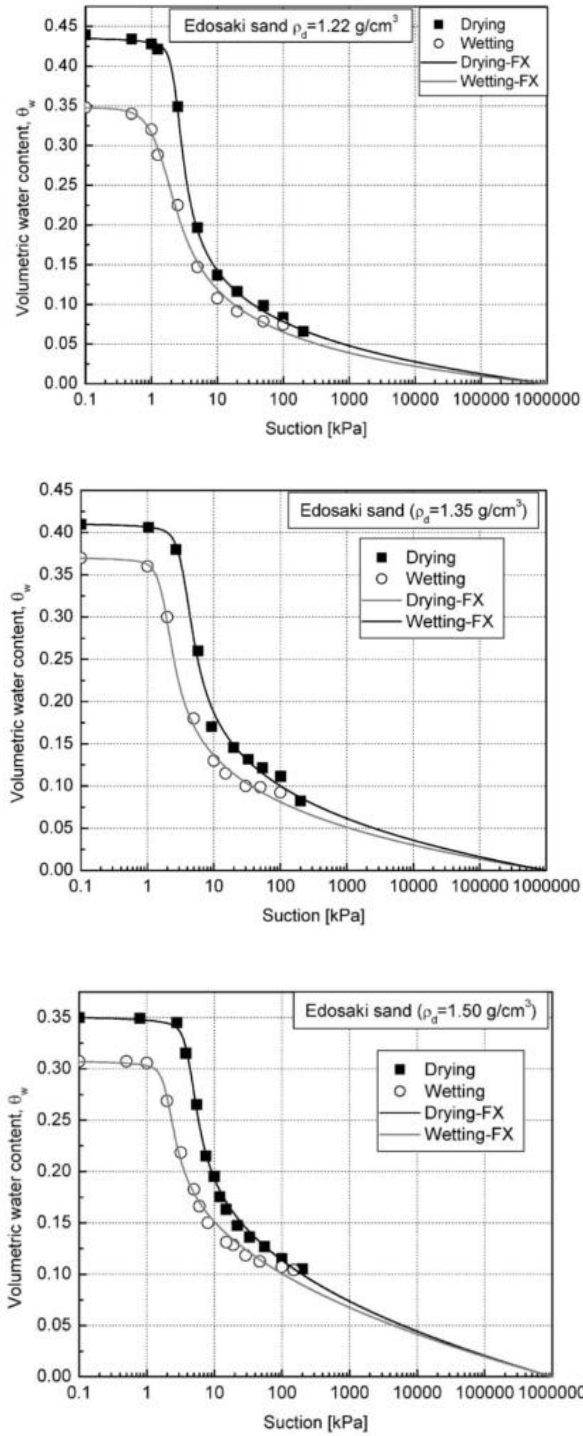
Figure 3.5: SWCC for different dry densities of Edosaki Sand measured by Gallage and Uchimura (2010).

3.3. APPARATUS

In this study, several type of equipment and apparatus were used, including moisture content, tilt angle, displacement and wave sensors, data acquisition systems and a series of wooden and acrylic containers designed according the test type. In this section, a description of the equipment is presented including the specific ones designed according the tests requirements.

3.3.1. Data Acquisition System

Two kinds of data acquisition systems are used to log the output signals from the electronic transducers. One is HOBO RX3000 and the other one is NR-500.

The HOBO RX3000 is Onset's next-generation remote data logging station that provides instant access to site-specific environmental data anywhere, anytime via the internet. The new station combines the flexibility and sensor quality of more expensive systems, an onboard LCD display, and the convenience of plug-and-play operation. Data were stored on a PC by using Digitshow software at predetermined sampling intervals. The components of whole data acquisition system for HOBO RX3000 are shown in Figure 3.6.

Figures 3.6: HOBO RX3000 data acquisition system.

NR-500 is a high performance data logger, manufactured by Keyence Corporation Ltd. It was used to realize continuous recording of wave signals with a sampling rate of 50kHz. Data acquisition was implemented using software NR-HA08 hi-speed measurement unit. Keyence NR-500 is shown in Figure 3.7.

Figure 3.7: Keyence data acquisition system.

3.3.2. ECH$_2$O Soil Moisture Content Transducers

In this study, ECH$_2$O moisture content sensors (EC-5) produced by Decagon Devices Inc. were used (Figure 3.8). Probes measure the dielectric constant of the soil in order to find its volumetric water content from 0 to 100%. Since the dielectric constant of water is much higher than that of air or soil minerals, the dielectric constant of the soil is a sensitive measure of water content. The ECH$_2$O probe has a very low power requirement and high resolution, making possible to do as many measurements as wanted (even hourly) over a long period of time (like a growing season, for example), with minimal battery usage.

Figure 3.8: ECH$_2$O moisture sensors.

3.3.2.1. Specifications

- Dimensions: ECH$_2$O-5: Length 8.5 cm, width 1.9 cm, Thickness 1.5 cm.

- Accuracy: *EC-5:* 0.003 m3/m3 all soils.

- Resolution: *EC-5*: 0.001 m3/m3 VWC in mineral soils.

- Power Requirements: EC-5: 3VDC @ 10mA.

- Operating Environment: 0 to 50 °C

- Measuring range: illustrated in Figure 3.9.
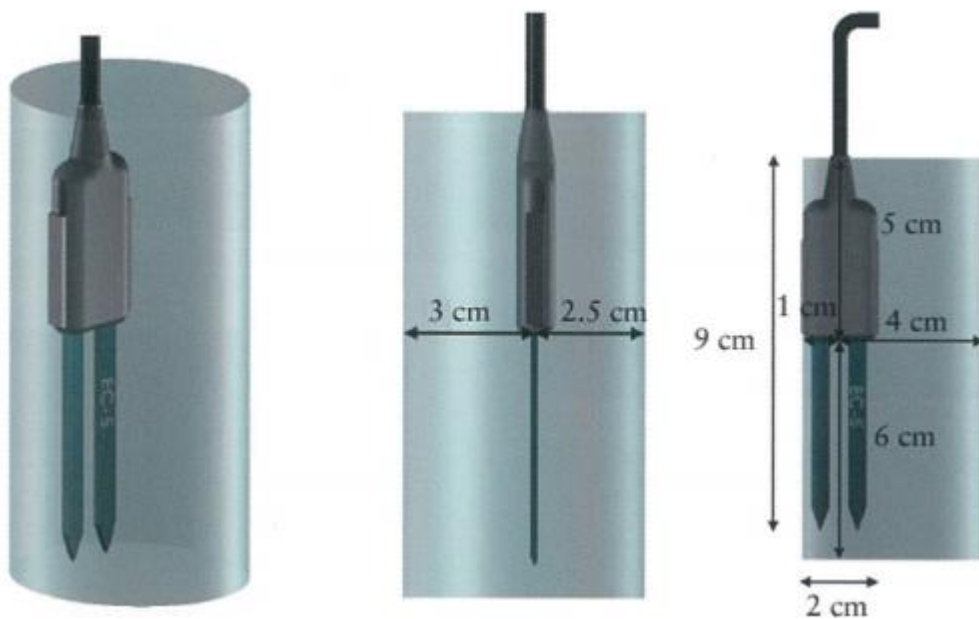
Figure 3.9: Measuring range of EC-5.

Although measurements at the soil's surface are technically a difficult task, the use of the small ECH$_2$O moisture sensor located at 2.5-7.5cm depth can be used to record the moisture content changes at the upper layer of the sand, improving the analysis with reliable measurements.

3.3.2.2. Calibration of ECH$_2$O EC-5 Soil Moisture Transducer

In order to get the maximum precision on volumetric water content measurements, sensors were calibrated by compacting Edosaki sand at dry density of 1.2g/cm^3 on a cylindrical acrylic container of 14 cm height by 8 cm radius at different moisture contents. The procedures used to obtain the calibration factor of each sensor are summarized as follows:

➢ Sample with pre-determined gravimetric water content (GWC %) is obtained by mixing the calculated amount of water with 24 hour oven dried sand.

➢ Sand is compacted at dry density of 1.2g/cm^3 on the acrylic container.

➢ Sensor is installed on the sample and voltage measure (mV) is recorded Figures 3.10 shows the procedures for the installation of the sensor on the soil container.

➢ New sample at higher gravimetric water content is prepared and the process is repeated.

➢ Volumetric water content (VWC %) is obtained by multiplying gravimetric water content (GWC %) by dry density ρ_d at which the specimen was prepared.

➢ Voltage readings (mV) are plotted against VWC (%), to obtain the linear relationship which gives the calibration factor in the form: $y = m\ X + b$. The calibration characteristics of load cell are shown in Figure 3.11. Perfect

linearity and repeatability can be observed from the load cell calibration plot. those calibration factors for moisture sensors are presented in Table 3.2.
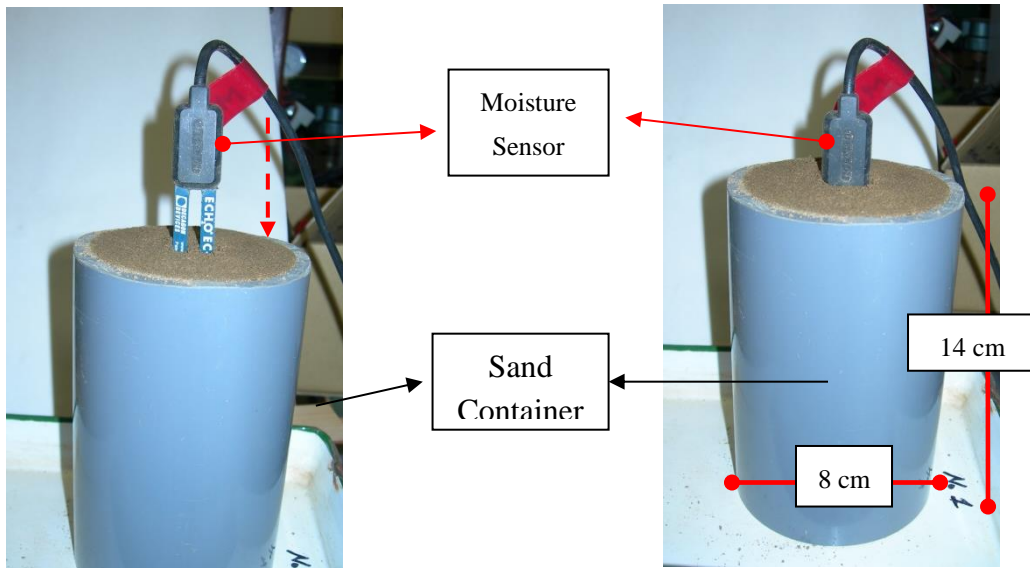
Figures 3.10: Installation of the sensor on the sand container for calibration
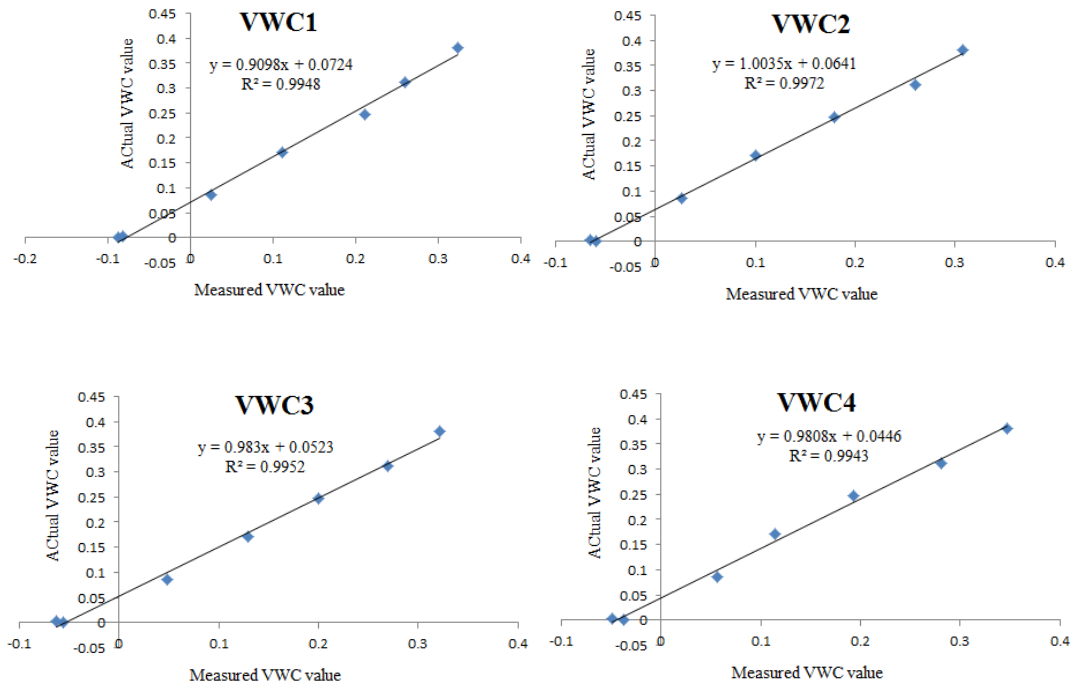
Figure 3.11: Calibration curves for moisture sensors.

Table 3.2: Calibration factors for moisture sensors

Sensor	Calibration Factor	Type
VWC1	0.9098x - 0.0724	
VWC2	1.0035x - 0.0641	
VWC3	0.983x - 0.0523	ECH_2O-EC5
VWC4	0.9808x - 0.0446	

3.3.3. Tilt Sensor

Tilt sensors (see Figure 3.12) based on Micro Electro Mechanical Systems technology were adopted to measure the tilt angles (rotations) in the unstable surface layer of slopes. Soil moisture sensors and tilt sensors were connected to a data logger (Model: HOBO RX3000) for continuous logging of data during rainfall application. It was set to log data for every 1s from all the sensors connected with this logger.
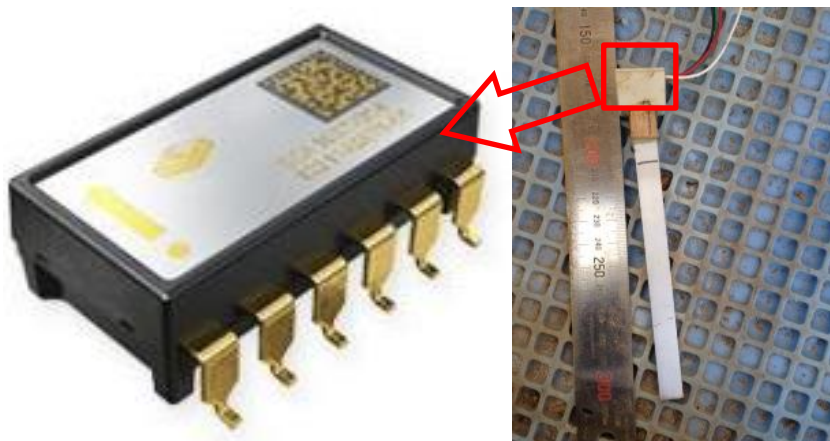
Figure 3.12: Tilt sensor based on Micro Electro Mechanical Systems technology.

3.3.4. Wave Sensor and Logger

Piezoelectric vibration sensors (Model: VS-BV201, shown in Figure 3.13) developed by NEC TOKIN Corporation were employed to record the elastic wave signals. wave sensors were connected to Keyence data logger (Model: NR-500) for continuous logging of data during rainfall application.
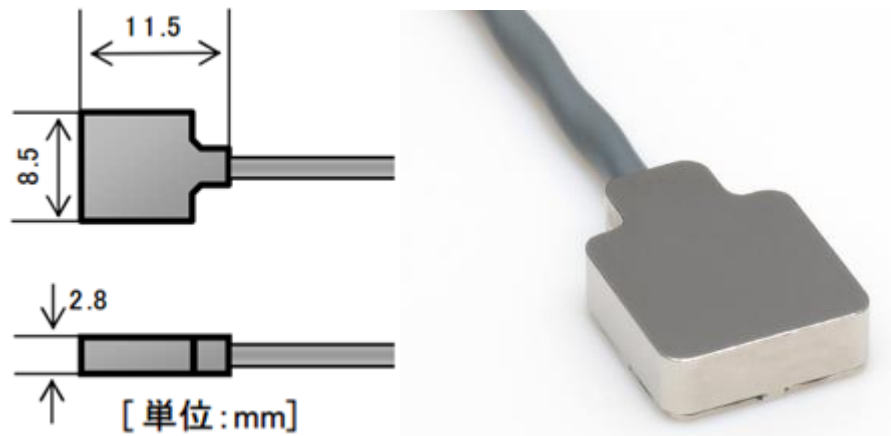
Figure 3.13: Piezoelectric vibration sensor.

3.3.5. Displacement Marker

Markers were made of tape and drawn a straight line the centerline, as shown in Figure 3.14. A tape measure was placed in the centerline of slope and markers were fixed next to the tape measure by nails as long as 2cm, as shown in Figure 3.15. Slope surface displacement was measured by markers in combination of a video camera. However, because of limitation of resolution of the video camera, small change in surface movement of slope could not be observed. Hence, video camera recorded data were not shown hereinafter.
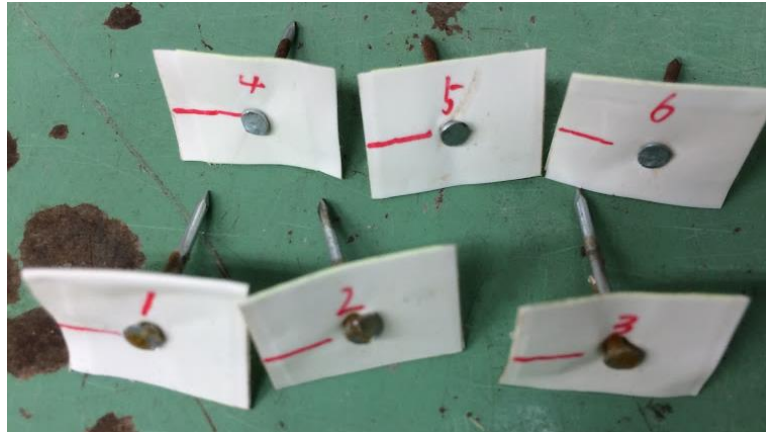
Figure 3.14: Marker acting as displacement monitor.
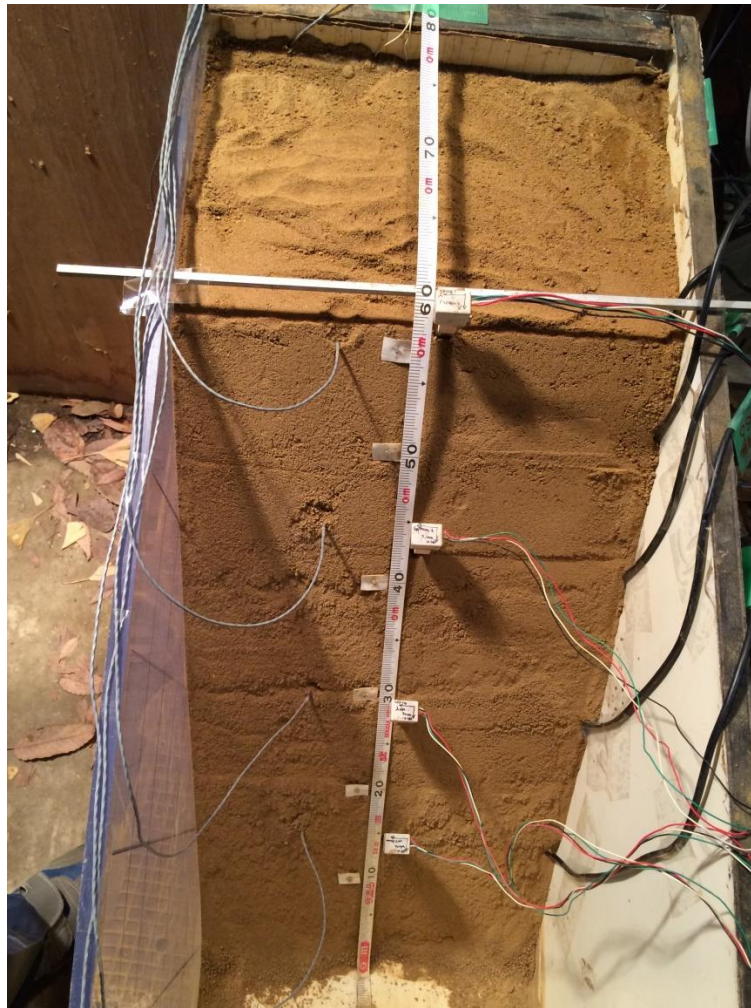
Figure 3.15: Marker and tape measure.

3.3.6. Rainfall Simulation System

The author compared several nozzle and water supply system, as shown in Figure 3.16. By careful comparison, the author finally chose square spray nozzle (SSXP) as rainfall simulator system. It was connected to a big water tank and placed 2 meter high. The rainfall intensity was controlled by adjusting an air pressure regulator (Figure 3.17). 200kPa air pressure was applied to drive water to spray out at an intensity of 100mm/h. However, irregularities in the rainfall were registered as consequence of wind disturbance or pressure variations on the water supplier.

Figure 3.18, shows the rainfall simulation system used for the experiments where the nozzle is highlighted.
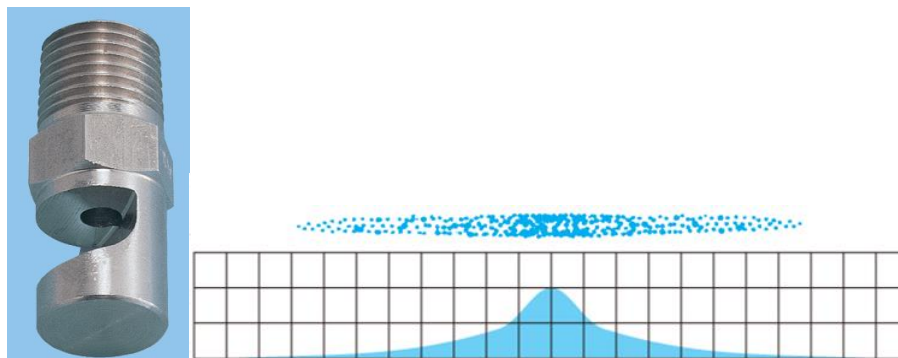
(a)Flat Fan Spray Nozzle (YYP)
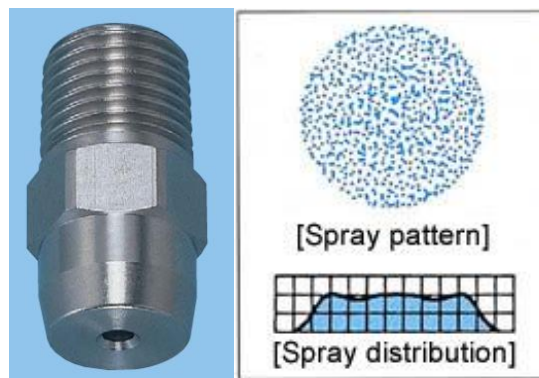
(b) Full Cone Spray Nozzle (JJXP)
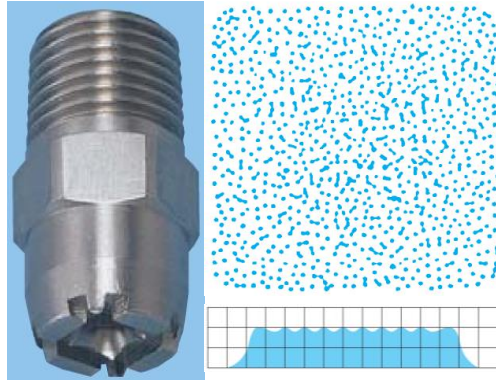
(c) Square Spray Nozzle (SSXP)

(d)Electromagnetic metering pump (EHN-C36VC4R)
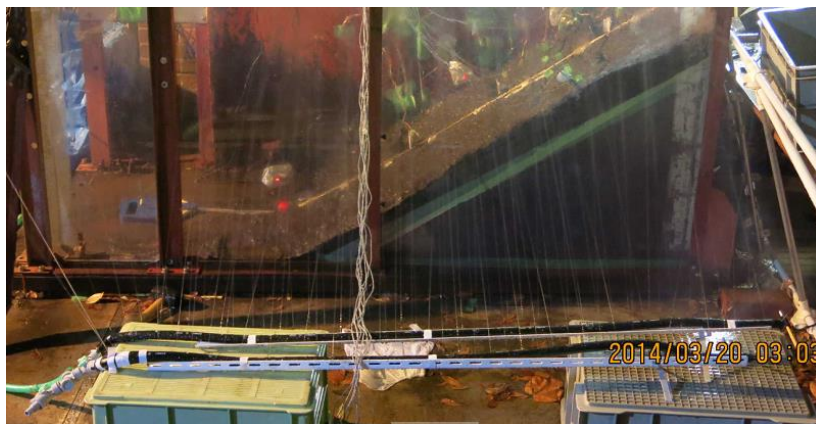
(e) Porous pipe

Figure 3.16:   Rainfall simulation system.

Figure 3.17: Air pressure regulator.

Figure 3.18: Rainfall simulation system.

3.3.7. Wave Exciter

At the beginning, the author generated the elastic wave by using a steel pile to manually hit a steel plate. This method disturbed the slope much. Besides, the wave form was different from each other. In addition, the noise from this rough assembly was rather high. Therefore, an exciter which could generate uniform wave with less noise and gentle effect on slope was needed.

Solenoid is an alternative for wave excitation. It is a coil of wire in a corkscrew shape wrapped around an iron plunger, and it is used as an electromagnet to generate magnetic field when an electric current is passed through the wire. Electric current activates the solenoid by converting electrical energy to magnetic energy, which in turn causes the plunger to move forward to strike the iron frame of solenoid. Consequently, elastic wave is created. This plunger moves backward by a return spring twined at the endpiece of plunger when removing the electric current, which is what makes it useful as switches and valves and allows it to be entirely automated.

The solenoid used in this study has dimension of 20×16×13mm and stroke of 0-5mm, as shown in Figure 3.19. It was sealed in a plastic cylinder box and buried inside slope.

Figure 3.19: Solenoid used in this study.

3.3.8. Microcontroller

Real world data rarely comes clean. Precise determination of the elastic wave velocity in soils is essential for the prediction of the slope instability. Unfortunately, raw signal inevitably comes noisy. In order to eliminate random signal noise and to extract useful information from raw signals, a microcontroller (Figure 3.20) was designed to generate repeated pulse at once electric input. Accordingly, solenoid was triggered repeatedly for each measurement and the corresponding received signals were stacked. For each reading, twenty measurements of wave were stacked.
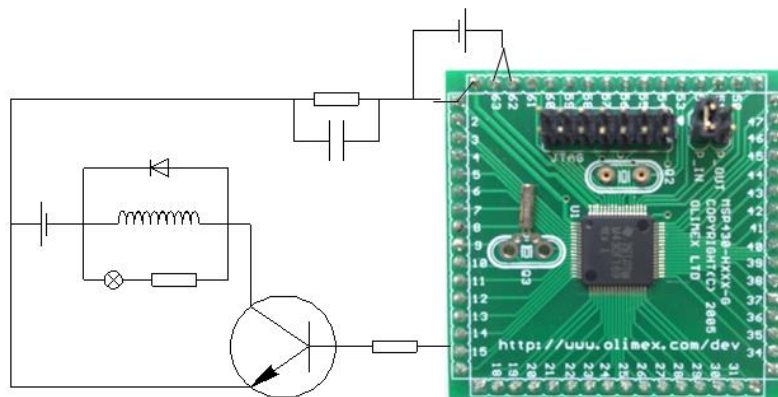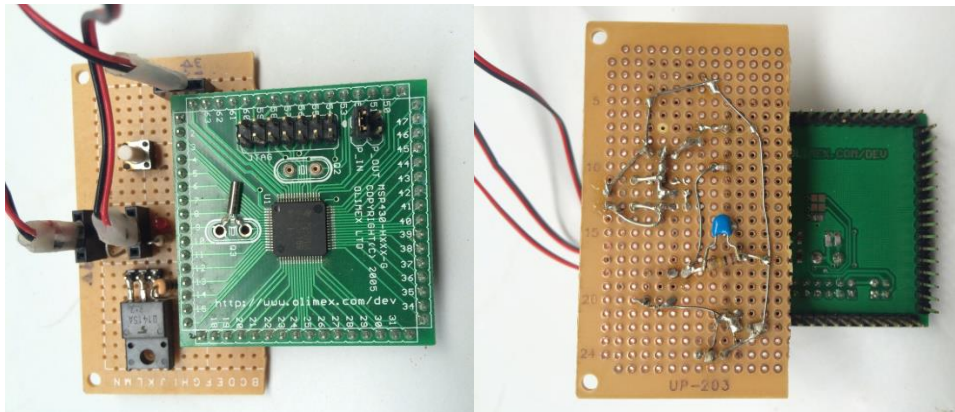
Figure 3.20: Microcontroller used in this study.

In this study 20 times stacking was used (Figure 3.21) and the program language is given as follows:

#include <msp430.h>

```c
int test_cnt = 0;

int main(void)

{

WDTCTL = WDTPW + WDTHOLD;                        // Stop WDT

 P1DIR |= BIT3;                                 // P1.3 output

TACTL = TASSEL_2 + MC_2 + TAIE;                 // SMCLK, contmode, interrupt

__bis_SR_register(LPM0_bits + GIE);             // Enter LPM0 w/ interrupt

}

// Timer_A3 Interrupt Vector (TAIV) handler

#if defined(__TI_COMPILER_VERSION__) || defined(__IAR_SYSTEMS_ICC__)

#pragma vector=TIMERA1_VECTOR

__interrupt void Timer_A(void)

#elif defined(__GNUC__)

void __attribute__ ((interrupt(TIMERA1_VECTOR))) Timer_A (void)

#else

#error Compiler not supported!

#endif

{

switch( TAIV )
```

```c
    {

    case   2: break;                          // CCR1 not used

    case   4: break;                          // CCR2 not used

    case 10:

    test_cnt++;

    if(test_cnt < 40){

    P1OUT ^= BIT3;                    // overflow

    }

    else{

    TACTL=0;

    P1OUT &= ~BIT3;

    }

    break;

    }

    }
```
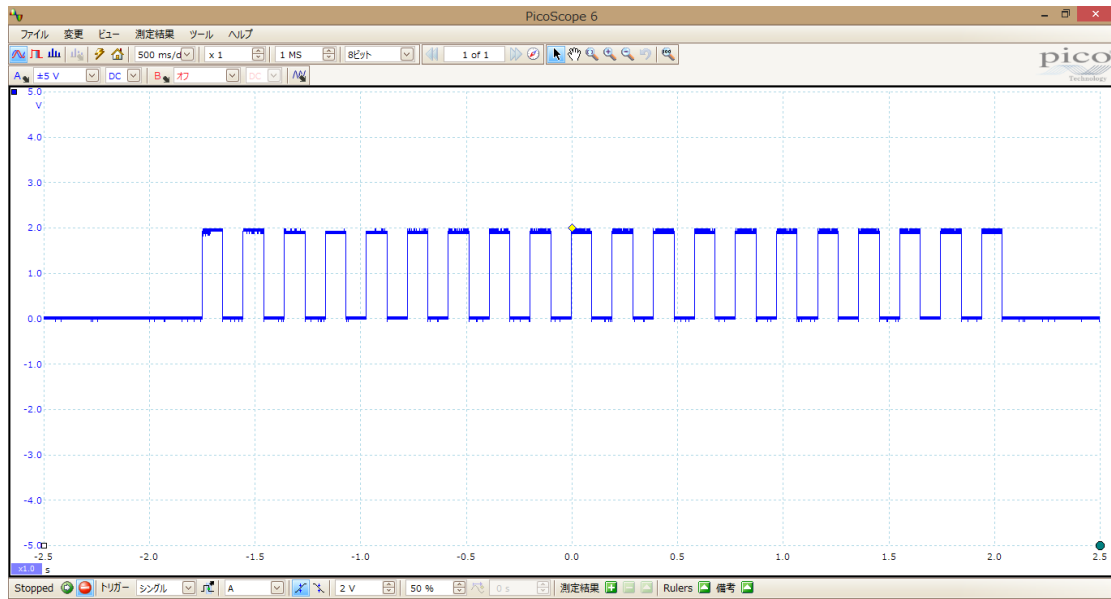
Figure 3.21: 20 times stacking realized by microcontroller.

3.3.9. Slope Tank

Two types of slope tanks were used to study the behavior of elastic wave with increase of water content and deformation.

Type 1:

This type of tank is made of wood for three walls and glass for the other one. It is not immobile. It is 80 cm long, 45 cm high and 30 cm wide. The front wall is made of transparent glass and a grid was drawn to control the volumes during setup procedures. Gaps of the wooden tanks were sealed with silicone and a mesh of 2mm was placed at each drainage hole to drain water and avoid soil loss, as shown in Figure 3.22.
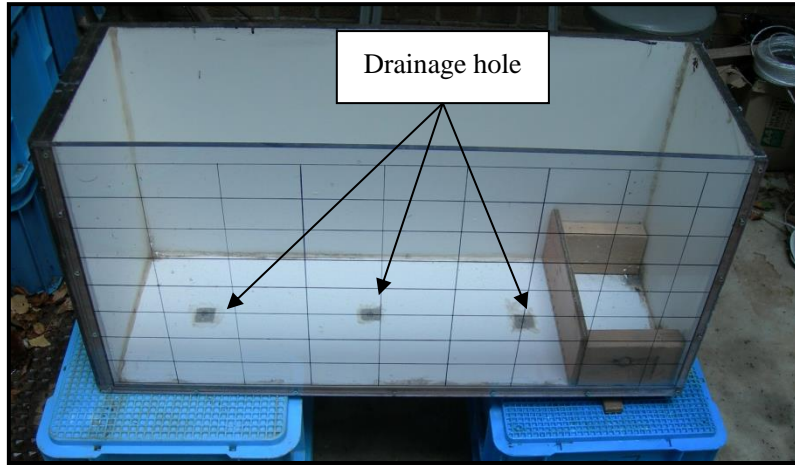
Figure 3.22: Slope tank for Type 1.

Type 2:

This type of tank is also made of wood. Its dimension is 90cm×30cm×40cm. The front and upper sides are uncovered and exposed, as shown in Figure 3.23. Gaps of the wooden tanks were sealed with silicone. The bottom plate was extended by steel frame. This tank was flexible so that it could be inclined.

Figure 3.23: Slope tank for Type 2.

3.4. SUMMARY

This chapter exhibits the experimental equipment. Details of the sensors including water content sensor, tilt sensor and wave sensor are presented. Wave exciter is introduced and microcontroller is assembled. The slope model tanks for two types of tests and rainfall system are established.

3.5. REFERENCES

American Society for Testing and Materials (2000) Annual book of ASTM standards 2000, section four, Construction, volume 04.08, *soil and rock (I): D 420-D 5779. Easton, MD, U.S.A.*

Brooks, R. H. and Corey, A. T. (1964). Hydraulic properties of porous medium, *Colorado State University (Fort Collins), Hydrology Paper 3.*

Chaminda, G. P.K, (2006). Real Time Prediction of Rain-Induced Embankment by Minimum Measurements with Back-analysis for SWCC Parameters. *PhD.Thesis, University of Tokyo*, Japan

Farooq, K. (2002). Experimental study on failure initiation in sandy slopes due to rainfall infiltration; *PhD thesis, The University of Tokyo*, Tokyo, Japan.

Fredlund, D. G. and Rahardjo, H. (1993). Soil mechanics for unsaturated soils. *Wiley Inter Science publication, John Wiley & Sons, New York.*

Fredlund, D. G. and Xing, A. (1994). Equation for the soil-water characteristic curve, *Canadian Geotechnical Journal,* 31, 521-532.

Gallage, C. P. K., Uchimura, T. (2010) Effects of dry density and grain size distribution on soil-water characteristic curves of sandy soils. *Soils and Foundations*, 50(1): 161-172.

Garcia, E. (2005). Function of permeable geosynthetics in artificial unsaturated embankments subjected to rainfall infiltration, *M.Eng.Thesis, University of Tokyo*, Japan.

Orense, R. P. (2003). *Geotechnical Hazards: Nature, Assessment and Mitigation*. The University of the Philippines Press, E. de los Santos St., U. P. Campus, Philippines.

Van Genuchten, M. T. (1980). A closed-form equation for predicting the hydraulic conductivity of unsaturated soils, *Soil Science Society of America Journal*. 44,. 892-898.

Vanapilli, S.K, Fedlund, D.G, Pufahl, D.E and Cliffton, A.W. (1996) Model of prediction of shear strength with respect to the soil suction. Canadian Geotechnical Journal, 33: 379-392

Yang, H, Rahardjo H, Leong, E and Fredlund D.G. (2004) Factors affecting the frying and wetting soil water characteristic curves of sandy soils. *Canadian Geotechnical Journal*, 41: 908-920.

CHAPTER 4

METHODOLOGY

4.1. EXPERIMENTAL PROGRAM

Laboratory model test is regarded as the most reliable method for studying the rainfall-triggered landslide, in which the soil properties and boundary conditions can be controlled and the water content inside slope and deformation on the surface can be monitored. For the purpose of better understanding the changes in elastic wave velocity in soil slope in wetting and failure process as a result of rainfall, two model test series performed as part of this research are summarized below;

(1) Flat model test (Figure 4.1)

A slope with an angle of 45° and a long crest was constructed. Two stages of test scheme were applied. At the 1st stage, rainfall was continuously applied for 2, 4, 6, 8, and 10min. At the 2nd stage, rainfall was stopped. Then, the author manually inclined the slope slowly. Wave signal was recorded during both test stages. This was to separately investigate the change in elastic wave velocity with increase of water content and deformation.

(1) Convential model test (Figure 4.2)

This type of tests was conventional model tests on rainfall induced landslides at which artificial rainfall was continuously applied until slope failure.

For this type model tests, conditions of slope angle=30°, 45°, 50°, and dry density=1.2,

1.3, 1.4 g/cm^3 (Dc=68.1%, 73.8%, and 79.5%, respectively), and failure plane thickness=5, 10, 15 cm are considered. Wave velocity was measure during the progress of landslides. In this type model test, the resulting change of wave velocity is coupled by increasing water content and deformation that appear to be interrelated. Therefore, more attempts should be made to separate the two influence factors.
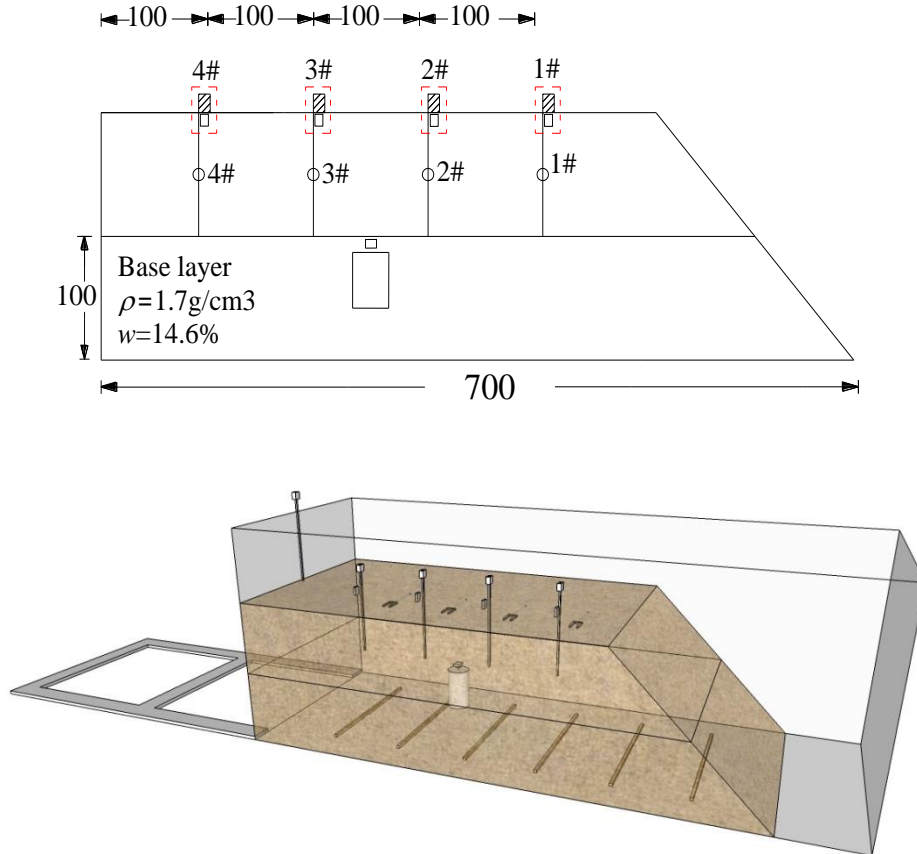
Figure 4.1: model for Type 1.
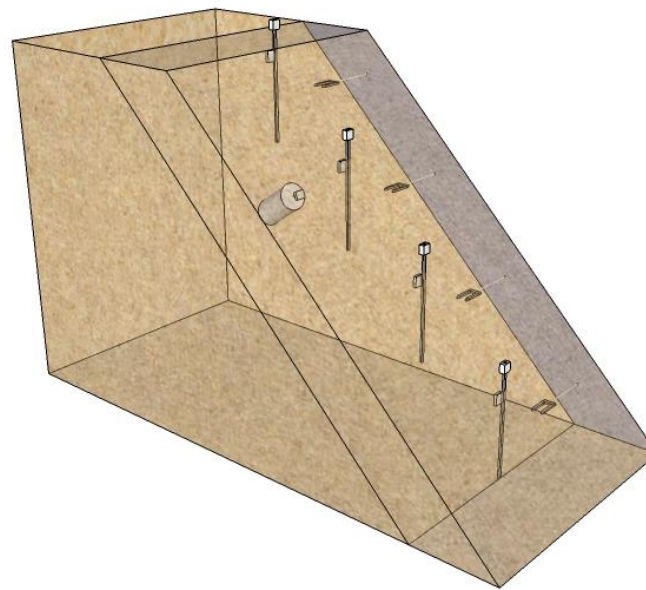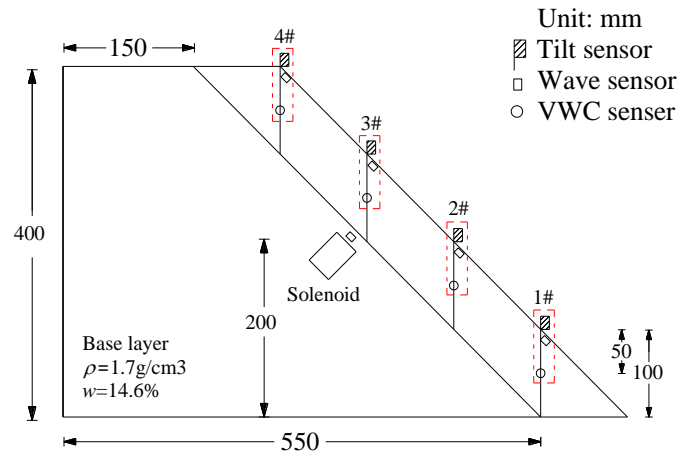
Figure 4.2: model for Type 2.

4.2. EXPERIMENTAL PROCEDURES

In this study, failure mechanism is analyzed by soil slope models under rainfall. The first type of slope model tests was conducted with changing parameters as slope angle, dry density and thickness. Slopes were instrumented with tilt and moisture content and wave sensors. Additionally, one digital video camera was placed in front of the model to trace the sequence of the deformation process. One camera was placed in front of the transparent side wall to capture the wetting front. The second type of

slope model tests was conducted with changing only thickness. Slopes were instrumented with tilt and moisture content and wave sensors. Table 4.1 summarizes characteristics of experiments. Erosion between the side wall and slope soil occurred in 4 of 15 cases.

Table 4.1: Slope model tests program.

Type 1				
Case No.	Rainfall duration (min)	Slope angle(°)	Thickness(cm)	Density(g/cm^3)
1-45-5-0	0			
1-45-5-4	4			
1-45-5-6	6		5	
1-45-5-8	8			
1-45-5-10	10			
1-45-10-0	0	45		1.3(Dc=73.8%)
1-45-10-4	4			
1-45-10-6	6		10	
1-45-10-8	8			
1-45-10-10	10			
1-45-15-0	0		15	
1-45-15-4	4			

Case No.	Slope angle(°)	Thickness(cm)	Density(g/cm^3)
1-45-15-6	6		
1-45-15-8	8		
1-45-15-10	10		
Type 2			
Case No.	Slope angle(°)	Thickness(cm)	Density(g/cm^3)
2-45-5-1.2 (erosion)			1.2(Dc=68.1%)
2-45-5-1.3(erosion)		5	1.3(Dc=73.8%)
2-45-5-1.4			1.4(Dc=79.5%)
2-45-10-1.2			1.2
2-45-10-1.3(erosion)	45	10	1.3
2-45-10-1.4(erosion)			1.4
2-45-15-1.2			1.2
2-45-15-1.3		15	1.3
2-45-15-1.4			1.4
2-40-10-1.2			1.2
2-40-10-1.3	40		1.3
2-40-10-1.4		10	1.4
2-50-10-1.2	50		1.2

2-50-10-1.3			1.3
2-50-10-1.4			1.4

The procedures involved on the preparation of the slope model for Type 1 are described as follows:

As shown in Figure 4.3, several wooden strips at first were fixed at the bottom of tank to increase the friction between soil and the tank to prevent failure occurring from the bottom interface.

Similar to Type 2, the base layer was constructed at dry density of $1.7g/cm^3$. Edosaki sand was mixed with water to achieve the optimum water content of 14.6%. A certain weight of sand was weighted for each layer. Then it was poured into the tank and a plate was fixed aside the sand with angle of 45°. Sand was compacted using a 10kg weight all over the sand surface to attain the target height. The solenoid was installed at the middle of base layer, as shown in Figure 4.4. Subsequently, a wave sensor was placed next to it.

Subsequent surface sand was poured and compacted to dry density reached $1.3g/cm^3$ until reaching the final thickness. Between the compaction of layers, the surfaces of the compacted layers were scratched in order to provide a reasonable bond between the layers.

Once the slope is completed, tilt, moisture content and wave sensors are installed at the specific locations as shown in Figure 4.5.

Note that one tilt sensor was attached to the wall of tank to serve as a reference, as shown in Figure 4.6. The deformation of slope surface is defined as the difference between the angles obtained from the sensor in the slope and that from the reference sensor.

The full view of experimental setup for Type 1 is shown in Figure 4.7.

Figure 4.3: Wooden strips fixed at the bottom of tank to increase the friction between soil and the tank to prevent failure occurring from the bottom interface.

Figure 4.4: Installation of solenoid in the middle of base layer.

Figure 4.5: Installation of sensors s after slope completion.

Figures 4.6: Reference tilt sensor attached to the wall.
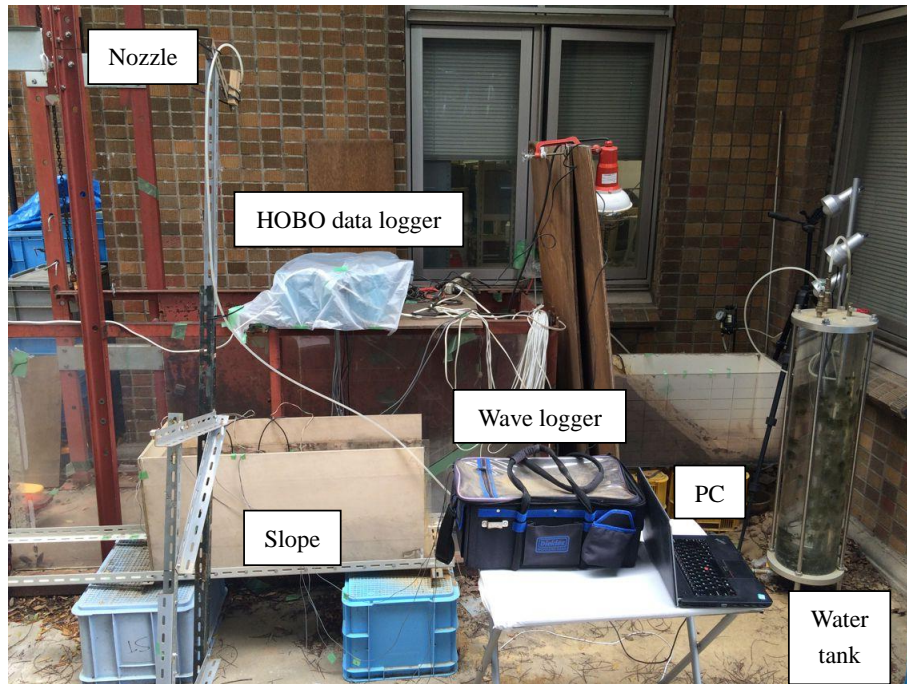
Figure 4.7: Full view of experimental setup for type 1.

The procedures involved on the preparation of the slope model for Type 2 are described as follows:

At first, the base layer should be constructed. Edosaki sand was mixed with water to achieve the optimum water content of 14.6%. A certain weight of sand was weighted for each layer. Then it was poured into the tank in eight layers and a plate was fixed aside the sand with a certain angle according to the designed inclination. Sand was compacted using a 10kg weight all over the sand surface to attain the target height of 5cm (see Figure 4.8) so that the dry density was 1.7g/cm^3.

Between the compaction of layers, the surfaces of the compacted layers were scratched in order to provide a reasonable bond between the layers.

Once 20cm height was completed, the solenoid was installed at the shallow surface and perpendicular to the surface and a wave sensor was placed next to it, as shown in Figure 4.9.

Subsequent layers were compacted until whole slope model is achieved, reaching the

final height of 40cm (see Figure 4.10).

Figure 4.8: Tamping of base layer soil.

Figure 4.9: Installation of solenoid and wave sensor.

Figure 4.10: Completion of base layer.

After completing base layer, we started to build surface layer. Surface layer was relatively loose and its initial water content is 5%. A certain weight of sand was weighted for each layer. Then it was poured into the tank in eight layers and a plate was fixed aside the sand with a certain angle according to the designed inclination. Sand was compacted to attain the target height of 5cm (see Figure 4.11) so that the desired dry density was made. Between the compaction of layers, the surfaces of the compacted layers were scratched in order to provide a reasonable bond between the layers. The completed slope is shown in Figure 4.12.

Once the slope is completed, tilt, moisture content and wave sensors are installed at the specific locations as shown in Figures 4.13.

Figure 4.11: Construction of surface layer.

Figure 4.12: Completed slope.

Figure 4.13: Installation of sensors s after slope completion.

The full view of experimental setup for Type 2 is shown in Figure 4.14.
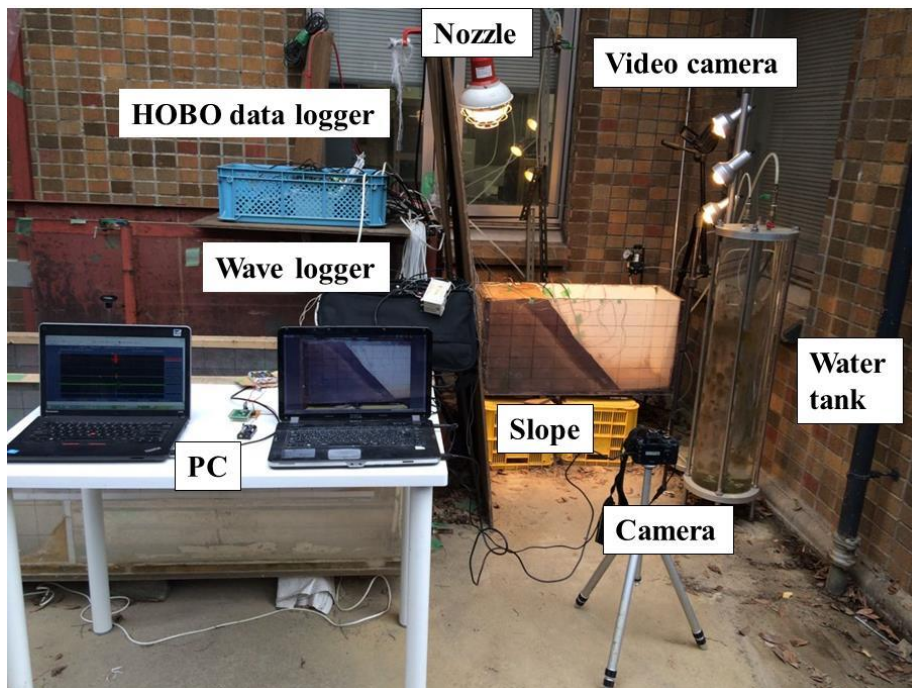
Figure 4.14: Full view of experimental setup for Type 2.

4.3. DATA TREATMENT

4.3.1. Calibration of Water Content Sensor

In order to get the maximum precision on volumetric water content measurements, sensors were calibrated by compacting Edosaki sand at a certain dry density on a cylindrical acrylic container of 14 cm height by 8 cm radius at different moisture contents. Those calibration factors for moisture sensors are presented in Table 4.2.

Table 4.2: Calibration factors for moisture sensors.

Sensor	Calibration Factor	Type
VWC1	0.9098x - 0.0724	
VWC2	1.0035x - 0.0641	
VWC3	0.983x - 0.0523	
VWC4	0.9808x - 0.0446	ECH_2O-EC5

4.3.2. Conversion Of Data From Tilt Sensor

Tilt sensors recorded data in value of voltage. The voltage is conversed to angle by the following equation:

$$\theta = \operatorname{asin}((v\text{-}2.5)/4) \tag{4.1}$$

Where, θ is the tilt angle in unit of rad and v is the voltage value.

4.3.3. Stacking Wave Data by Matlab Analysis

Because of the huge amount of data from the wave receivers, it is quite time-consuming to deal with such big data to obtain the first arrival point of each

received signal. A program based on Matlab was developed.
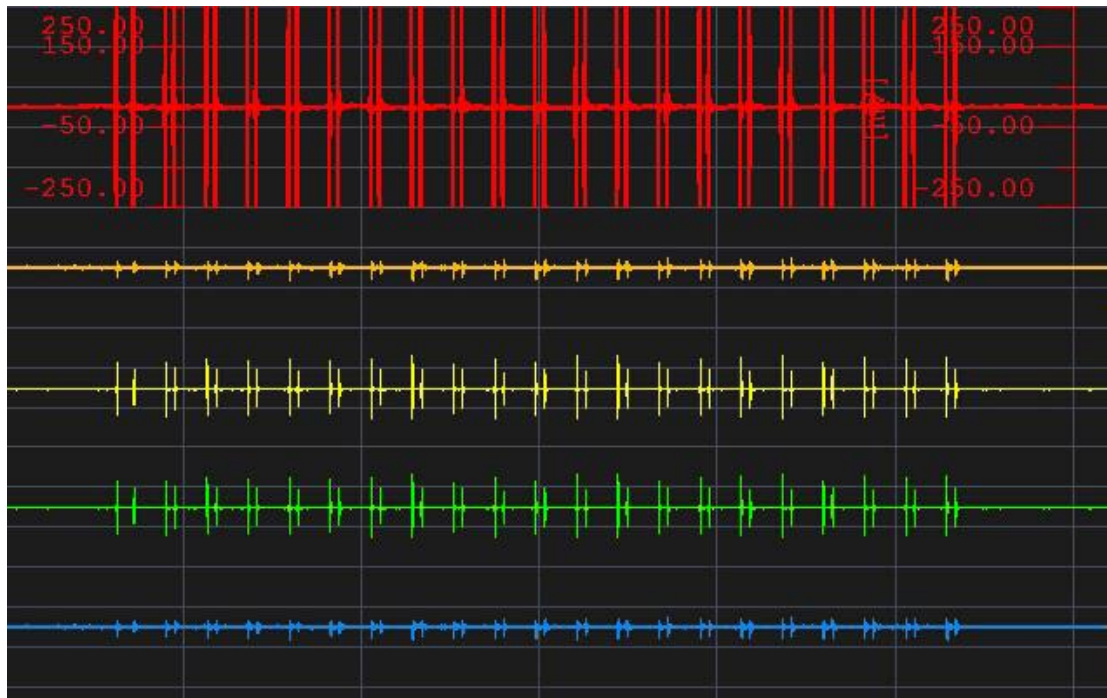
(b)zoom out
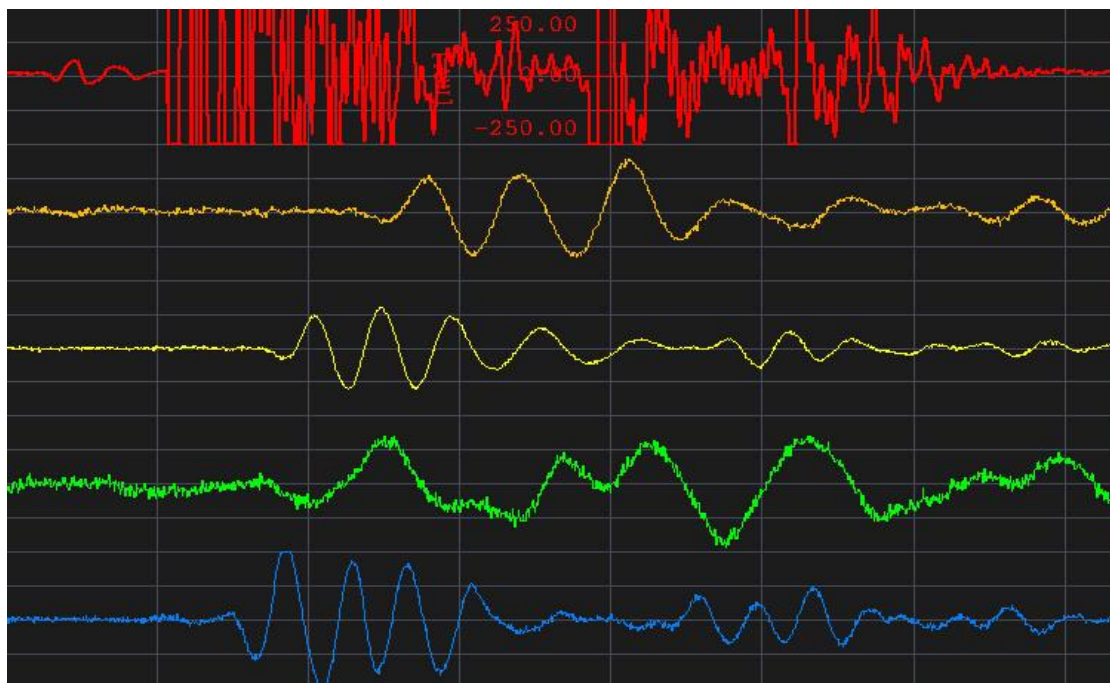
(b)zoom in

Figure 4.15: Recorded wave signal for one excitation event.

As shown in the Figure 4.15, the data of the red curve depicted in the figure is from the receiver installed near to the source, and the data for other curves are from the receiver on the surface of a slope. Because of the influence of noise, it is very difficult to distinguish the first arrival point from these curves, especially for those curses about the data received by the receivers on the surface.

To minimum the influence caused by noise on the first arrival point of each curse, the stacking wave signal from 20 similar signals for each curve is used as the wave signal to determine the first arrival point of the curse.

Considering the impact of random noises, an input file containing the value of the first arrival point and the last point of 20 signals from the red curve have to be prepared for the program. When inputting this file into the program, the stacking wave signal for other curves can be obtained automatically by this program.

Here is the Matlab code:

```
for shijianii=1:size(data,1)

data(shijianii,6)=shijianii*50;

end

%define the path of target txt file.

path='C:\Users\Administrator\Desktop\11.txt';

X11=load(path);

s=0;

maxweishu=0;

for i=1:size(X11,1)/2
```

```
if maxweishu<(X11(2*i)-X11(2*i-1)+1)

maxweishu=(X11(2*i)-X11(2*i-1)+1);

end

end

for i=1:maxweishu

sumbiaomian1(i,1)=0.0;

averagebiaomian1(i,1)=0.0;

sumbiaomian2(i,1)=0.0;

averagebiaomian2(i,1)=0.0;

end

for i=1:size(X11,1)/2

for j=1:(X11(2*i)-X11(2*i-1)+1)

j1=j;

j1=s+j1;

newdatatime(j1,1)=data(X11(2*i-1)-1+j,6);

newdata1(j1,1)=data(X11(2*i-1)-1+j,3);

newdatabiaomian1(j1,1)=data(X11(2*i-1)-1+j,4);

newdatabiaomian2(j1,1)=data(X11(2*i-1)-1+j,5);

sumbiaomian1(j,1)=sumbiaomian1(j,1)+newdatabiaomian1(j1,1);
```

sumbiaomian2(j,1)=sumbiaomian2(j,1)+newdatabiaomian2(j1,1);

end

s=s+(X11(2*i)-X11(2*i-1)+1);

end

for i=1:size(sumbiaomian1,1)

averagebiaomian1(i,1)=sumbiaomian1(i,1)/(size(X11,1)/2);

averagebiaomian2(i,1)=sumbiaomian2(i,1)/(size(X11,1)/2);

end

%%%%%%%%%%%%%%%%%%%%%%%%%%%%

xlswrite('C:\Users\Administrator\Desktop\111.xlsx',newdatatime(:,1),1,'A1')

xlswrite('C:\Users\Administrator\Desktop\111.xlsx',newdata1(:,1),1,'B1')

xlswrite('C:\Users\Administrator\Desktop\111.xlsx',newdatabiaomian1(:,1),1,'C1')

xlswrite('C:\Users\Administrator\Desktop\111.xlsx',newdatabiaomian2(:,1),1,'D1')

xlswrite('C:\Users\Administrator\Desktop\111.xlsx',sumbiaomian1(:,1),1,'E1')

xlswrite('C:\Users\Administrator\Desktop\111.xlsx',averagebiaomian1(:,1),1,'F1')

xlswrite('C:\Users\Administrator\Desktop\111.xlsx',sumbiaomian2(:,1),1,'G1')

xlswrite('C:\Users\Administrator\Desktop\111.xlsx',averagebiaomian2(:,1),1,'H1')

Figure 4.16 gives an example of stacked wave signal. It can be seen that the noise contained in the original wave signal is reduced so that the first arrival point of the

wave could be easily determined.
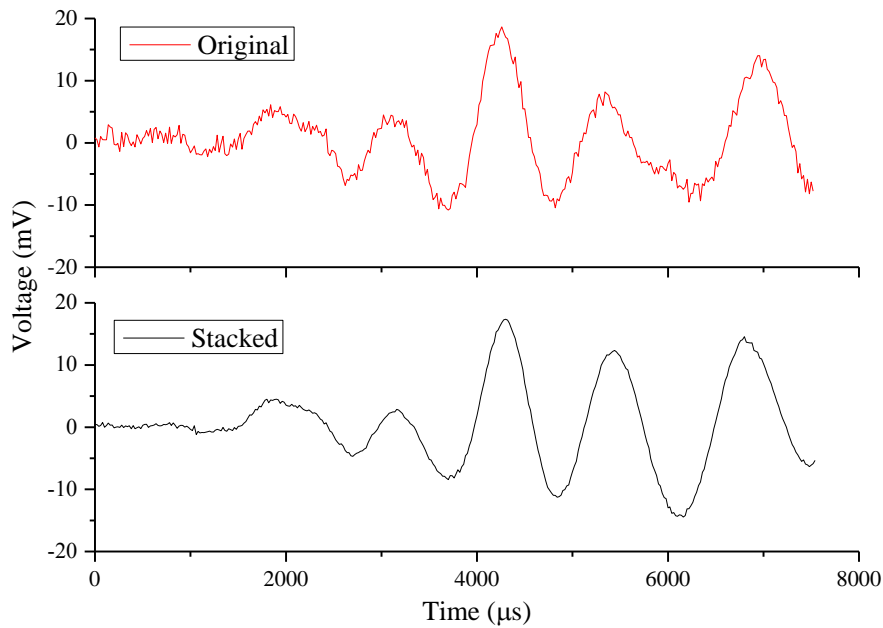
Figure 4.16: Stacked wave signal.

4.4. BOUNDARY FRICTION EFFECT

The model for both Type 1 and Type 2 tests was 30 cm wide. The friction angle was 55 ° and 14 ° for the interface between base layer and surface layer and model wall and soil, respectively. The friction force exists on the model boundary. The effect of deformation should be studied in advance. A new model was established with width of 35 cm, see Figure 4.17. One plate was placed in the middle to divide the inner space to two cells. This plate was flexible to adjust the width of the left and right cells. It was elevated by chain block and hold by a long frame to keep balance.

Figure 4.17: Model set up for study of boundary friction effect.

Figure 4.18 shows the failure of 15 and 20 cm-wide cells. It shows that 15 and 20 cm-wide cells failed at the same inclination of 45 °. Figure 4.19 shows the failure of 10 and 25 cm-wide cells. It shows that 10 and 25 cm-wide cells failed at the inclination of 55 ° and 43 °, respectively. Figure 4.20 shows the failure of 5 and 30 cm-wide cells. It shows that 5 and 30 cm-wide cells failed at the inclination of 68 ° and 42 °, respectively. Figure 4.21 summarizes the failure inclination for cells with different widths. It shows that the boundary friction effect is ignorable when width is larger than 15 cm.

Figure 4.18: Failure of 15 and 20 cm-wide cells.

Figure 4.19: Failure of 10 and 25 cm-wide cells.

Figure 4.20: Failure of 5 and 30 cm-wide cells.
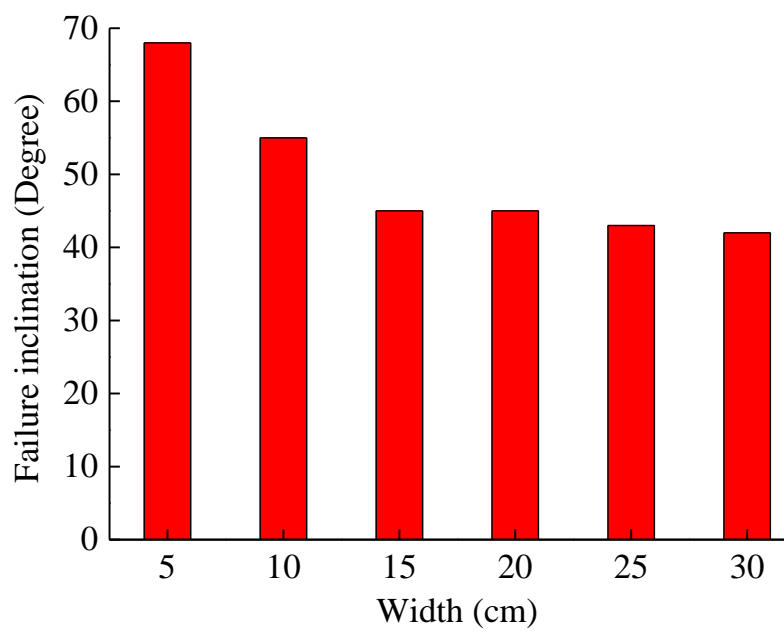
Figure 4.21: Failure inclination for cells with different widths.

4.5. SUMMARY

The overall experimental program designed to achieve the objectives of this research was presented. Details of experimental procedures were discussed in detail. A detailed discussion on the stacking of elastic wave velocities and the determination of travel time is presented. The boundary friction effect is ignorable when width is larger than 15 cm.

CHAPTER 5

INVESTIGATION OF WAVE PROPAGATION THROUGH SLOPE SURFACE LAYER AS A FUNCTION OF WATER CONTENT AND SHEAR DEFORMATION

5.1. GENERAL REMARKS

In chapter 5, we investigated the wave velocity evolution during slope failure. The resulting change of wave velocity is coupled by increasing water content and deformation that appear to be interrelated. Therefore, more attempts should be made to separate the two influence factors.

5.2. TEST CONDITIONS

This chapter covers flat model studies exploring the behavior of wave velocities with soil moisture and deformation in terms of tilt angle. Flat model tests with different failure plane thickness and rainfall duration were conducted and wave velocities were determined during tests. Rainfall was given at the first stage and stopped for the second stage. In the second stage, the slope model was inclined manually. The following sections explain the test results and corresponding discussions of these tests. Test conditions and other important parameters of each test are summarized in Table 5.1. Similar to previous section, wave velocities was normalized with the corresponding initial values from the onset of rainfall.

Table 5.1: Test conditions in Type 1 tests.

Type 1				
Case No.	Rainfall duration (min)	Slope angle(°)	Thickness(cm)	Density
1-45-5-0	0			
1-45-5-4	4			
1-45-5-6	6		5	
1-45-5-8	8			
1-45-5-10	10			
1-45-10-0	0			
1-45-10-4	4			
1-45-10-6	6	45	10	1.3 g/cm^3 Dc=73.8%
1-45-10-8	8			
1-45-10-10	10			
1-45-15-0	0			
1-45-15-4	4			
1-45-15-6	6		15	
1-45-15-8	8			
1-45-15-10	10			

5.3. TEST RESULTS

Figure 5.1 and Figure 5.2 respectively show the variations in volumetric water content and tilt angle for soil slope with thicknesses of 5cm for surface layer under different rainfall durations during the rainfall and inclination. The tilt angle shown for T1~T4 is defined as the difference between the data from tilt sensors T1~T4 installed in the

slope surface layer and T5 fixed on the model wall.

Variations in volumetric water content and tilt angle under different rainfall durations during the rainfall and inclination is shown in Figure 5.3 and Figure 5.4 for soil slope with thicknesses of 10cm for surface layer.

Figure 5.5 and Figure 5.6 respectively show the variations in volumetric water content and tilt angle for soil slope with surface layer thicknesses of 15cm under different rainfall durations during the rainfall and inclination.
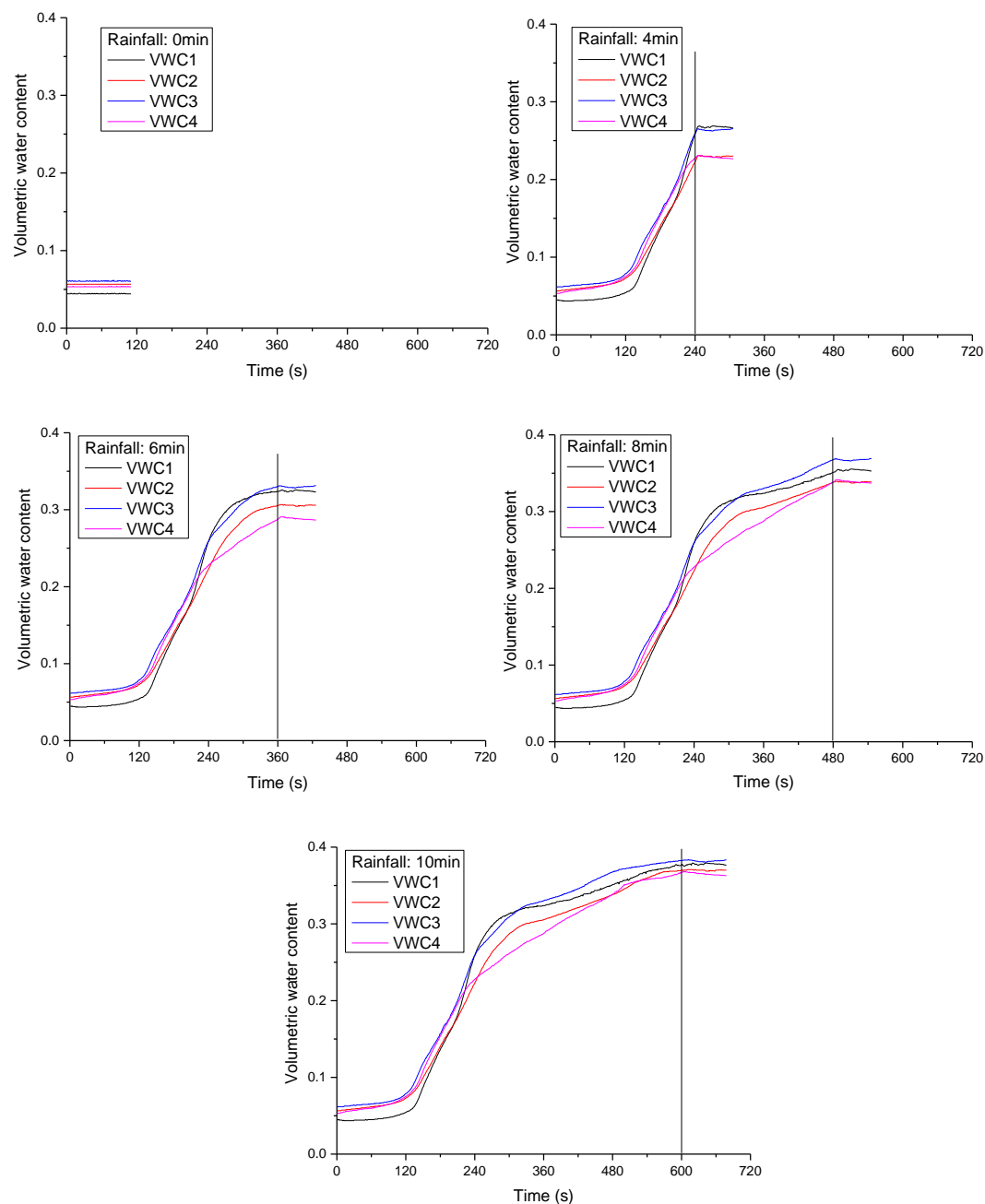
Figure 5.1: Variation in the volumetric water content for soil slope with thicknesses of 5cm for surface layer under different rainfall durations during the rainfall and inclination.
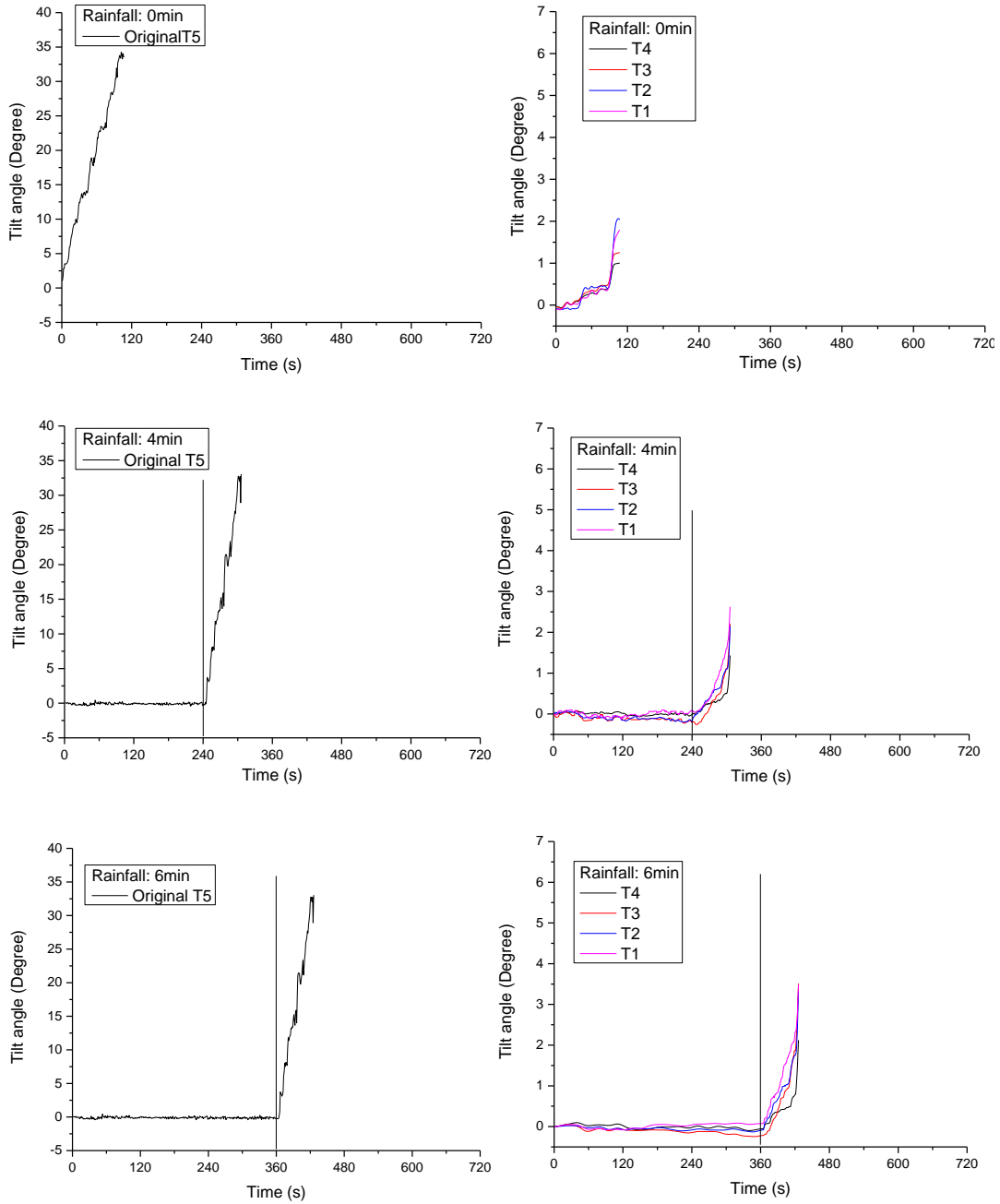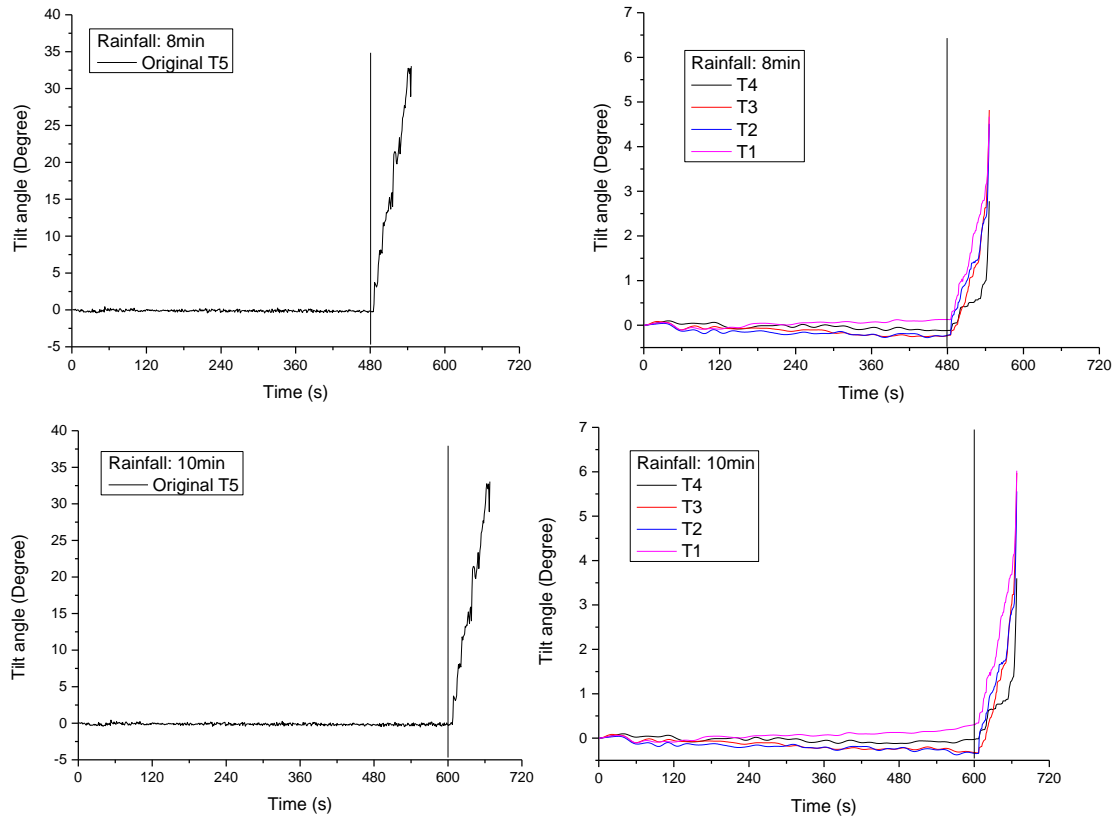
Figure 5.2: Variation in the tilt angle for soil slope with thicknesses of 5cm for surface layer under different rainfall durations during the rainfall and inclination.
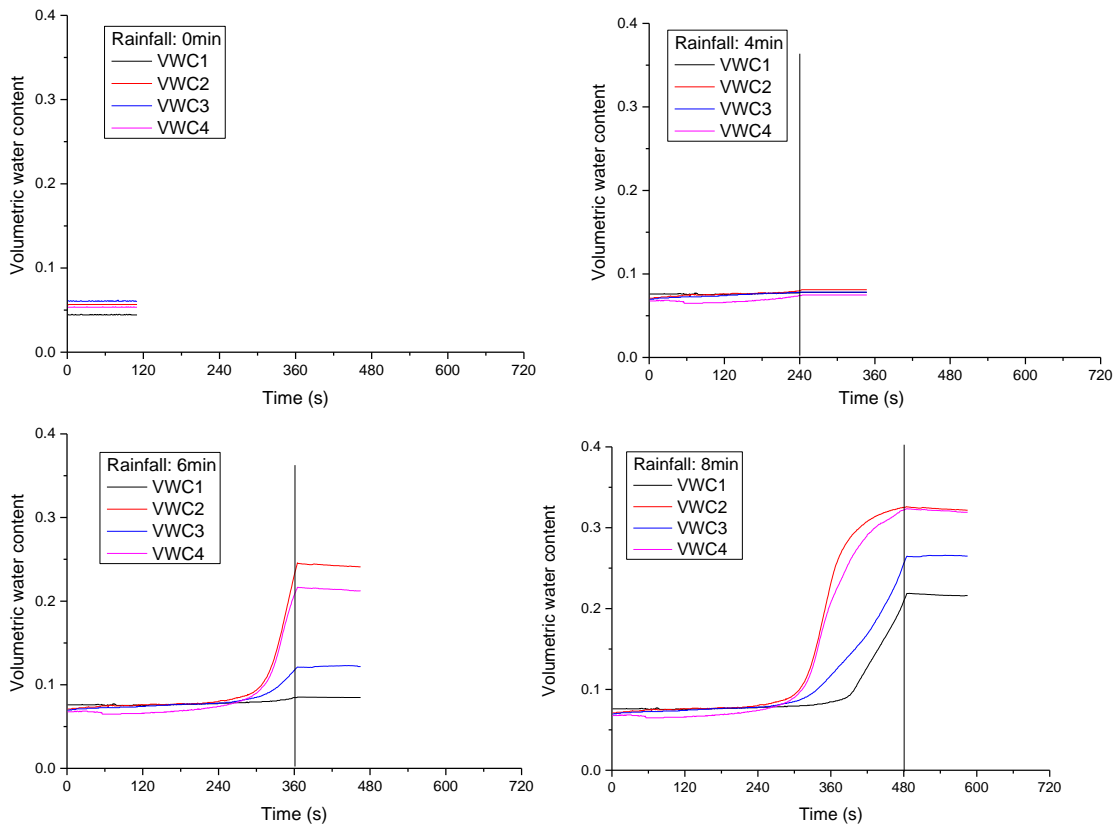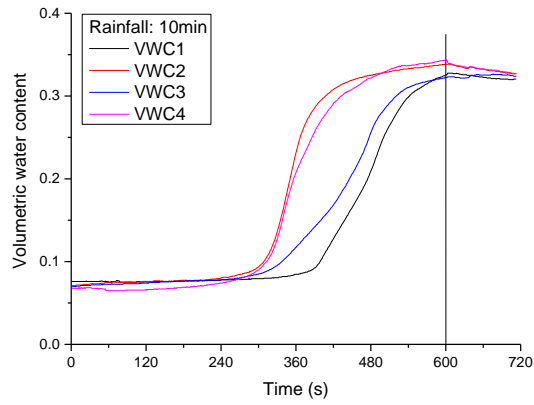
Figure 5.3: Variation in the volumetric water content for soil slope with thicknesses of 10cm for surface layer under different rainfall durations during the rainfall and inclination.
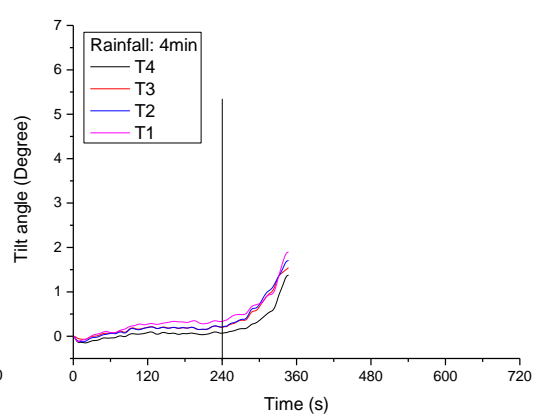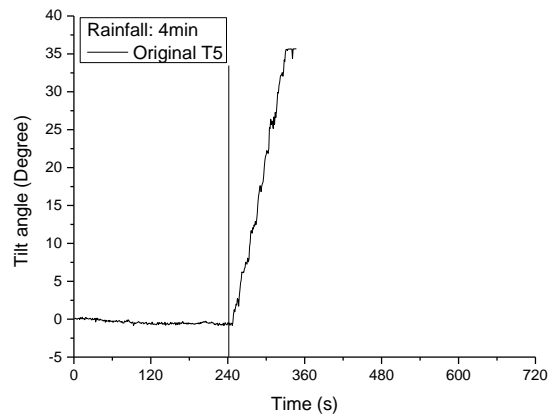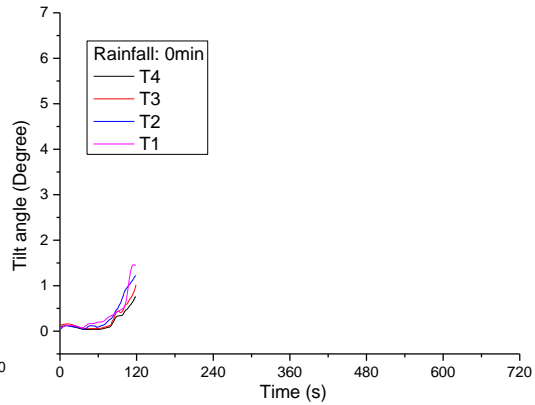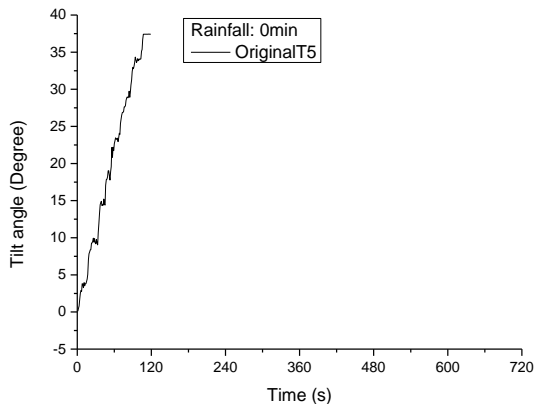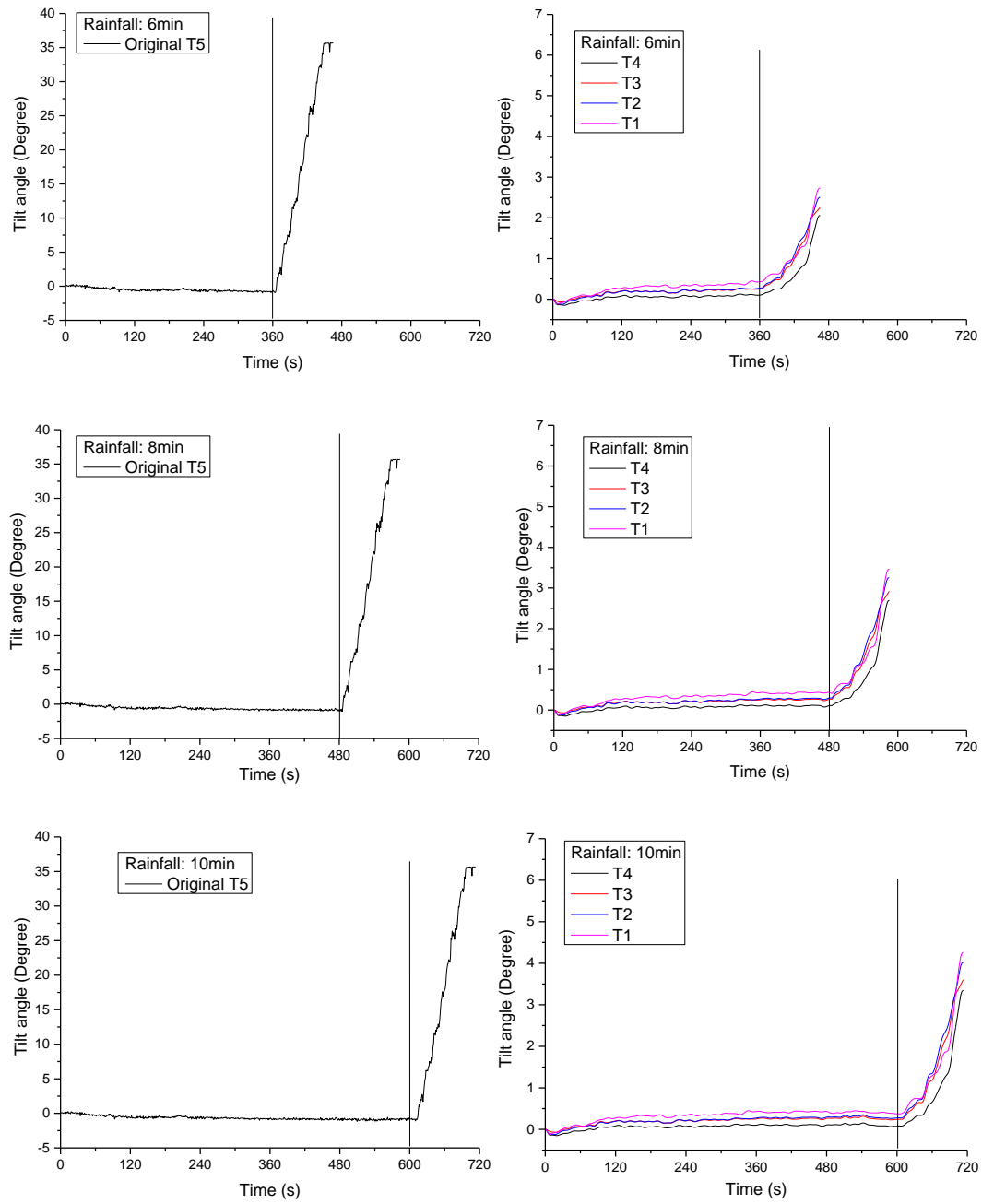
Figure 5.4: Variation in the tilt angle for soil slope with thicknesses of 10cm for surface layer under different rainfall durations during the rainfall and inclination.
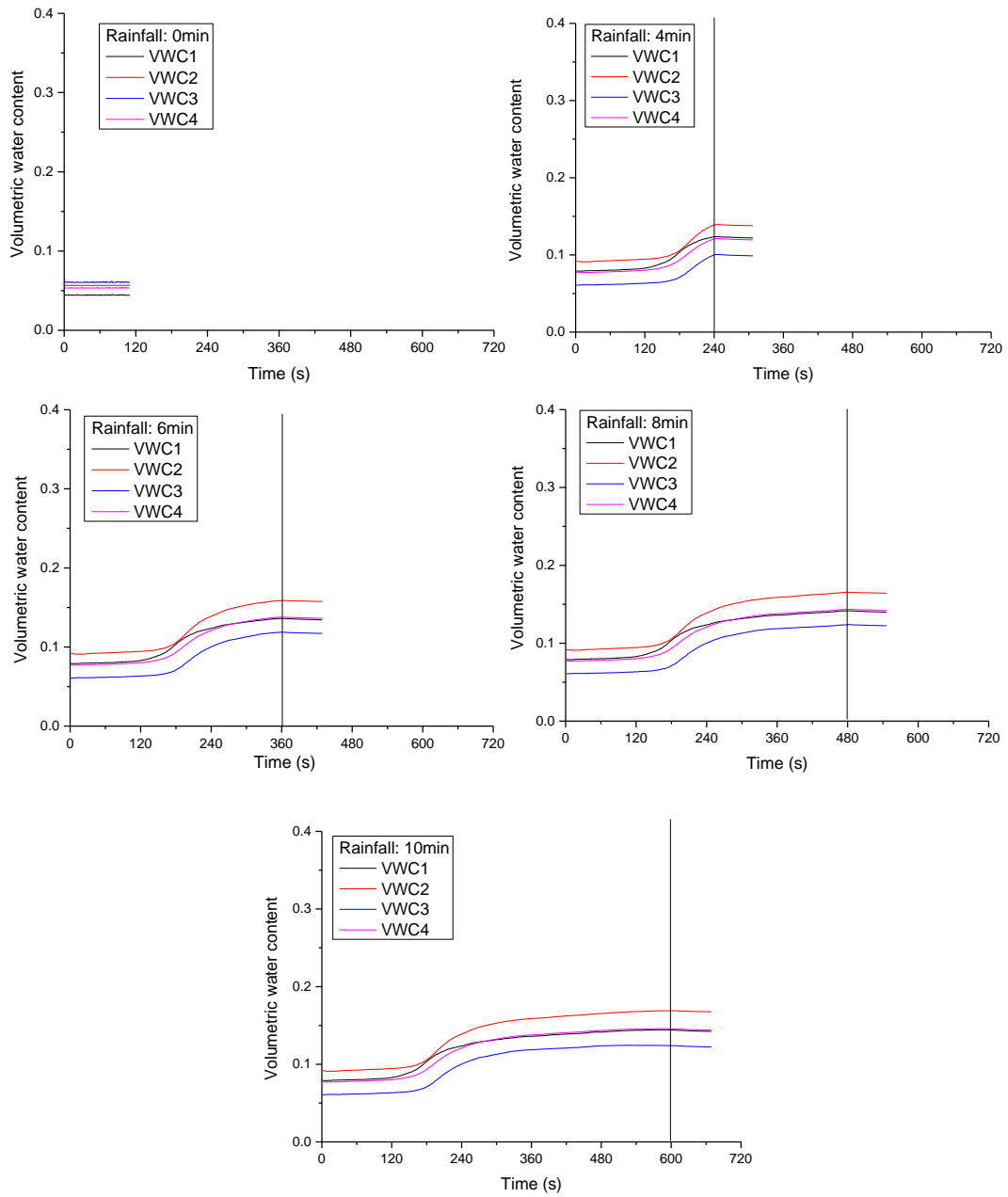
Figure 5.5: Variation in the volumetric water content for soil slope with thicknesses of
15cm for surface layer under different rainfall durations during the rainfall and
inclination.
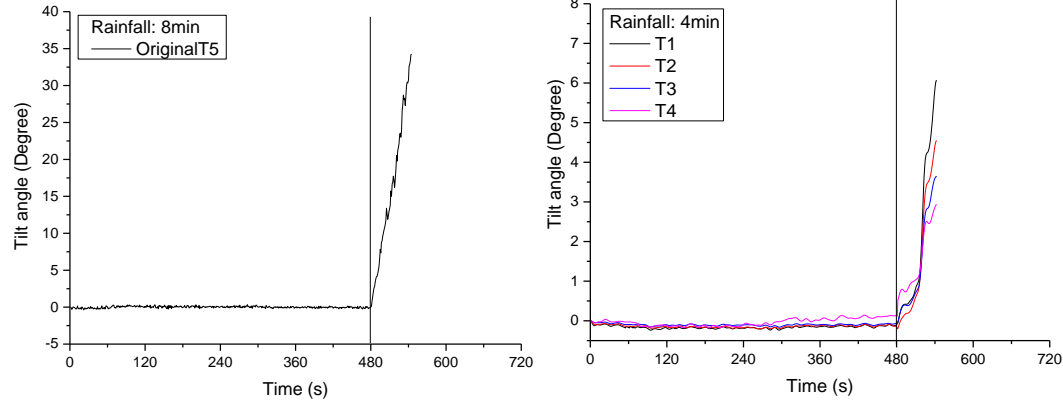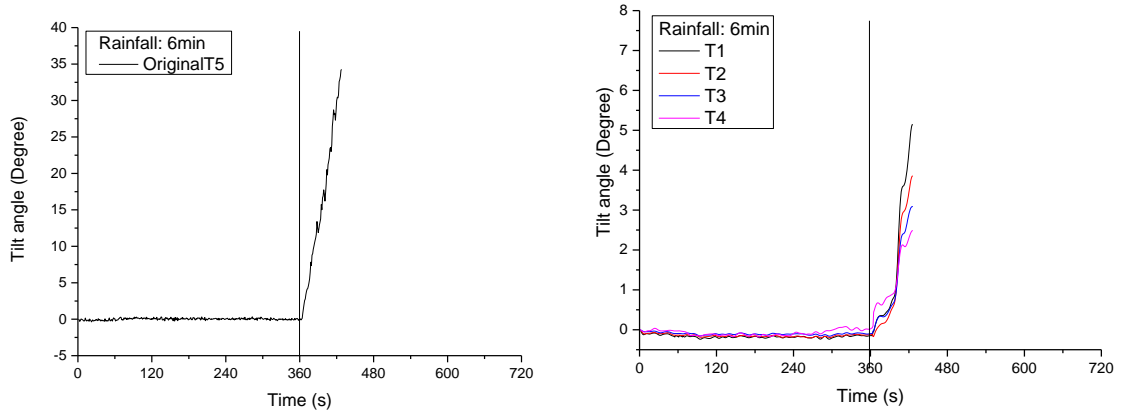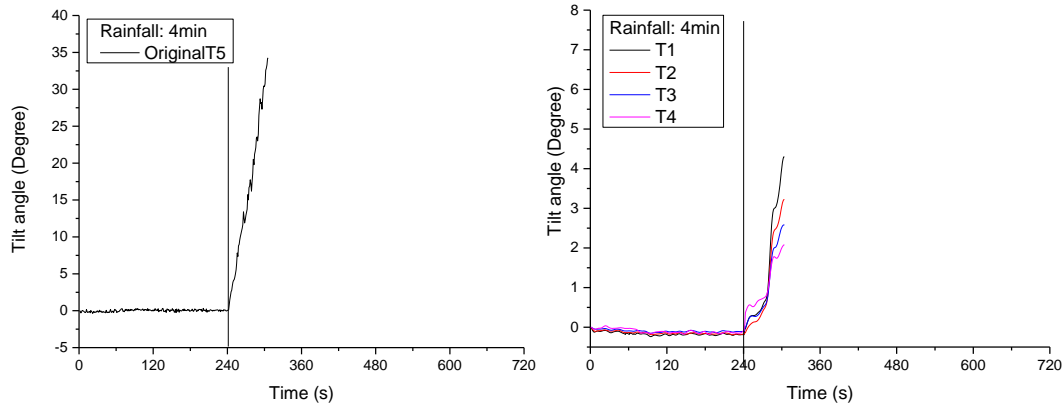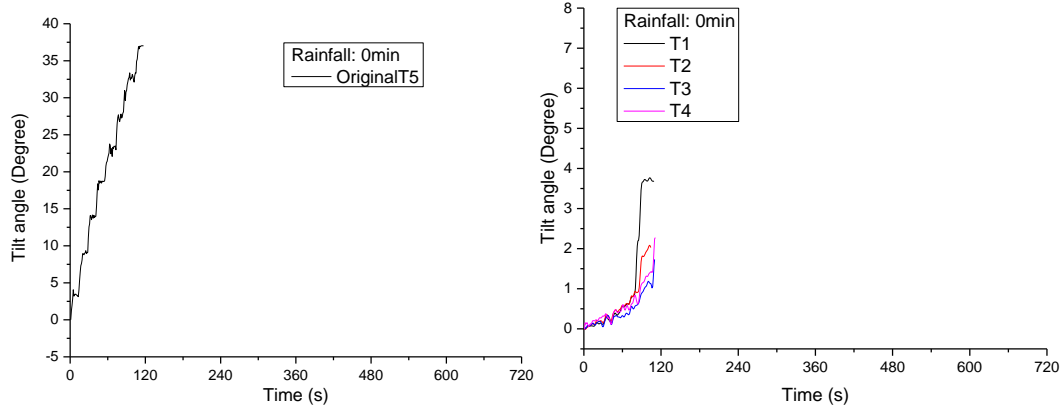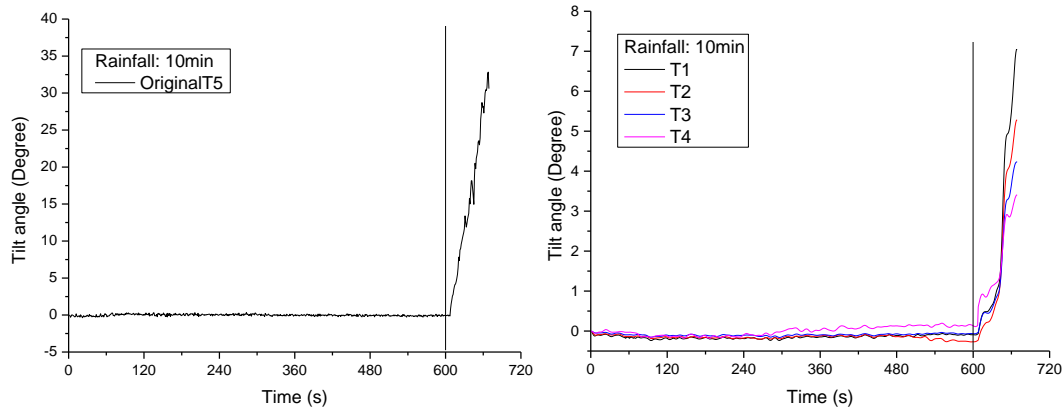
Figure 5.6: Variation in the tilt angle for soil slope with thicknesses of 15cm for surface layer under different rainfall durations during the rainfall and inclination.

From Figure 5.1 and Figure 5.3 and Figure 5.5, one can see that the volumetric water content at the different locations in the flat slope exhibited initial steady state as it takes time for water to infiltrate into the location of VWC sensors. Subsequently, volumetric water content at the different locations was increased as the rainfall progressed. After rainfall was stopped, the volumetric water content was nearly constant. Similarly, as shown in Figure 5.2 and Figure 5.4 and Figure 5.6, during rainfall, only very small tilt angle change was observed. The maximum tilt angle just resulting from rainfall under all cases was 0.4 degree. This value was used as the criteria deformation value for definition of slope failure. As tilt angle exceeded 0.4 degree, we assume that it is caused by failure initiation.

Then, the tilt angle increased when the slope model started to be inclined. Hence, the author can assume that the change of elastic wave velocity is only caused by increase of water content in the rainfall stage and deformation in the inclination stage.

Figure 5.7 to Figure 5.9 show the change of elastic wave velocity with elapsed time for slope with surface layer thickness of 5cm, 10cm and 15cm, respectively. It can be seen that the elastic wave velocity kept decreasing with elapsed time. More specially, the elastic wave velocity decreased gradually with volumetric water content in the rainfall stage, and sharply with deformation in the inclination stage. The decrease in elastic wave velocity became more significant as the rainfall duration was longer. This

was because the longer rainfall duration caused higher water content which made the soil softer so that the deformation increased. Under the condition of the longest rainfall (10min), the elastic wave velocity decreased by 10% as the volumetric water content increased from the initial condition to nearly saturation condition. The additional large decrease was caused by deformation.
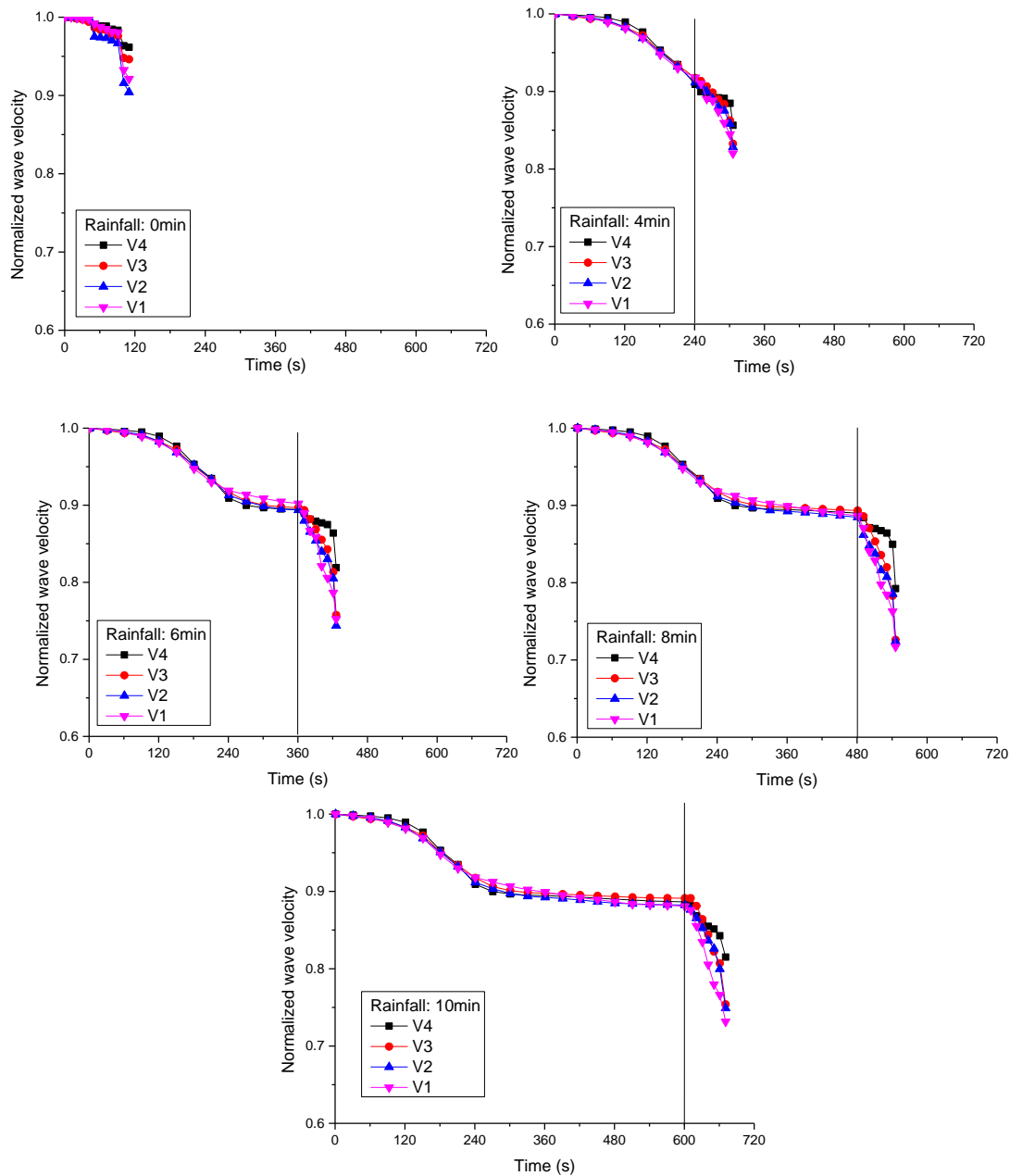

Figure 5.7: Change of elastic wave velocity with elapsed time during the rainfall and inclination for flat slope with thicknesses of 5cm for surface layer under different rainfall durations.

5-11
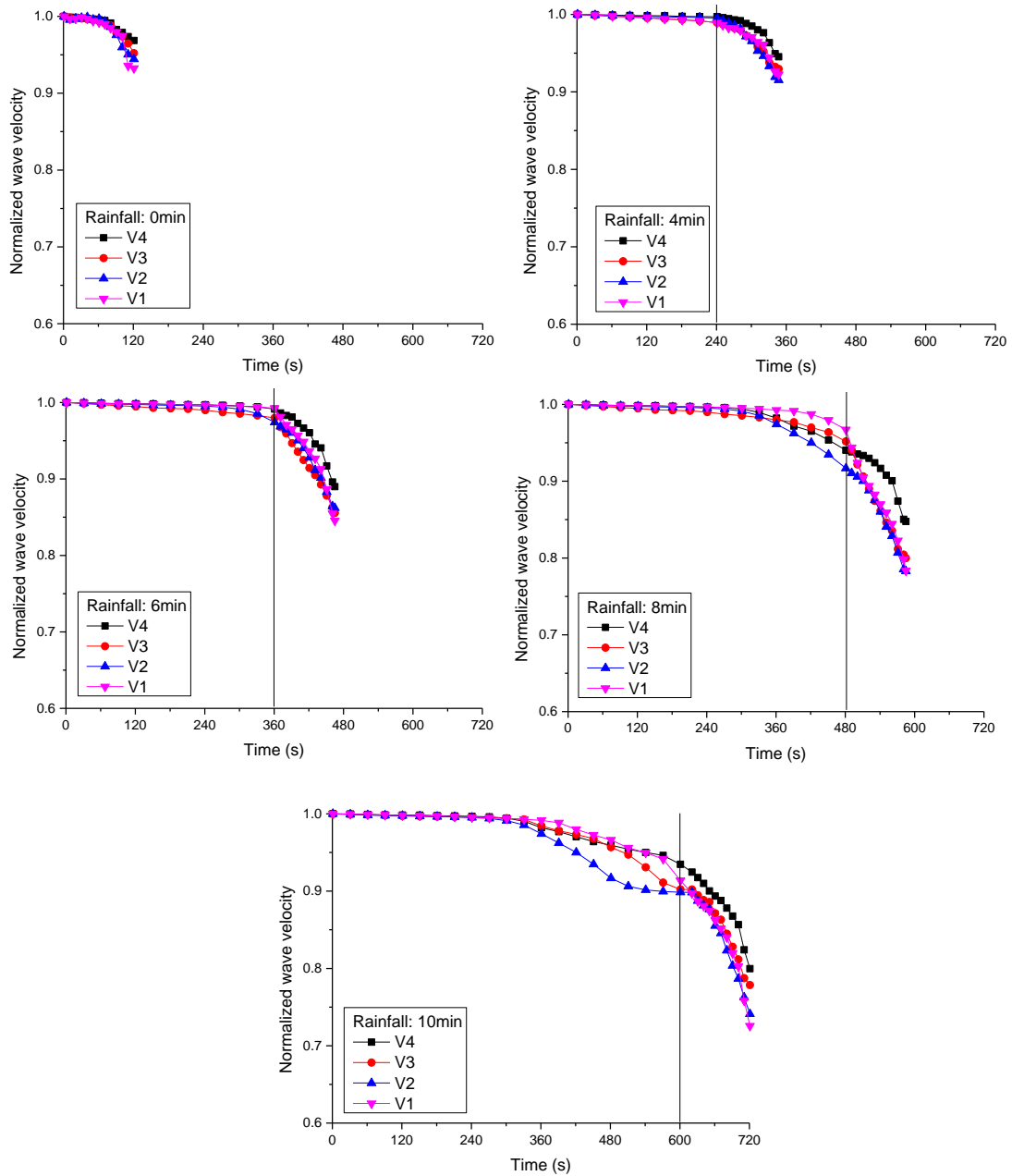
Figure 5.8: Change of elastic wave velocity with elapsed time during the rainfall and inclination for flat slope with thicknesses of 10cm for surface layer under different rainfall durations.
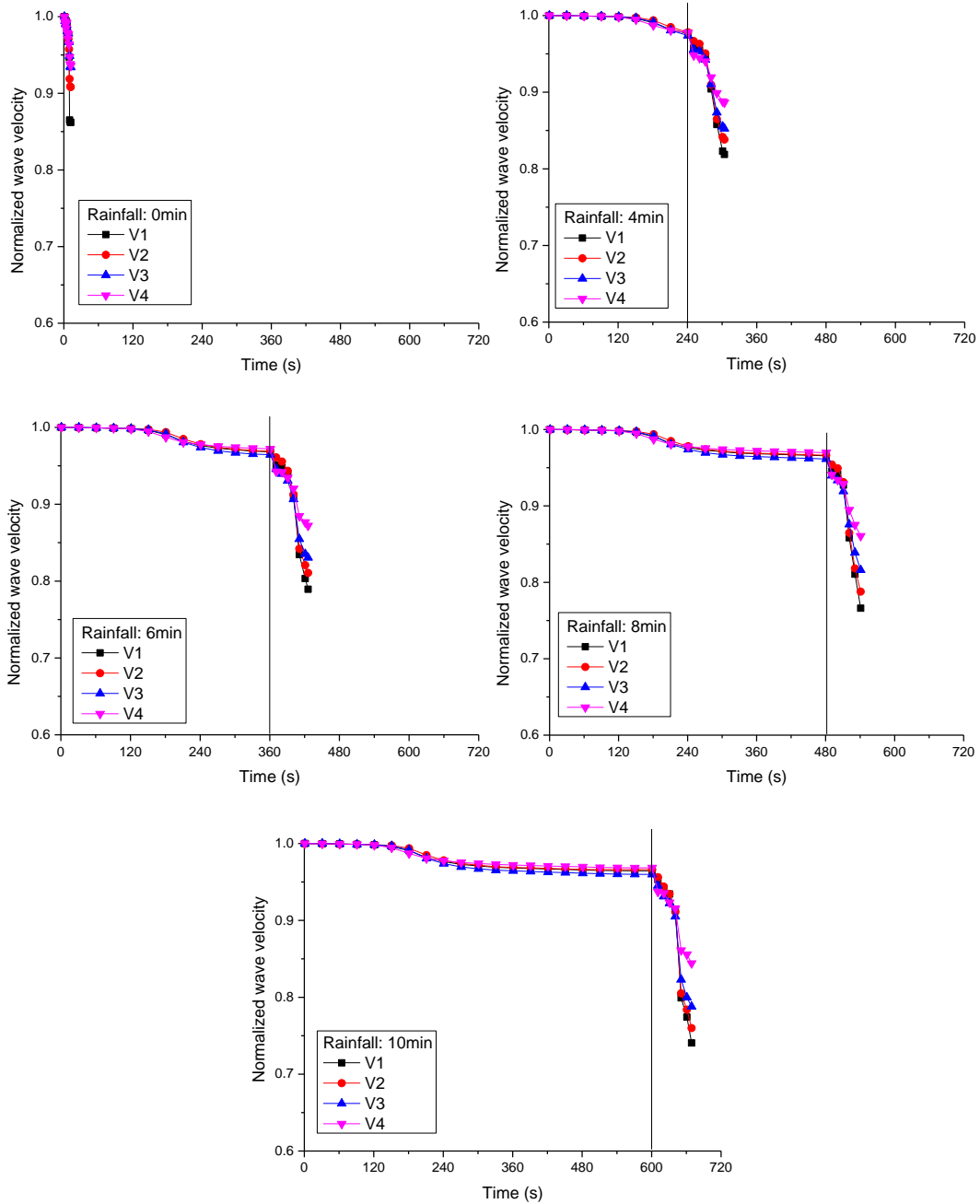
Figure 5.9: Change of elastic wave velocity with elapsed time during the rainfall and inclination for flat slope with thicknesses of 15cm for surface layer under different rainfall durations.

Figure 5.10 to Figure 5.12 show the change of elastic wave velocity with volumetric water content and tilt angle under different rainfall durations for slope with surface layer thickness of 5cm, 10cm and 15cm, respectively. It can be seen that as the volumetric water content increased, the normalized wave velocity decreased gradually

during rainfall stage, followed by a sharp decrease during inclination stage with negligible change in water content. As the volumetric water content increased to nearly saturation condition, just 10% decrease in elastic wave velocity was observed. The additionally larger decrease in elastic wave velocity was caused by deformation.

Also, it can be seen that the normalized wave velocity kept decreasing initially with no change in tilt angle. This decrease resulted from the increase of volumetric water content. As the slope began to be inclined, the normalized wave velocity decreased at larger rate.
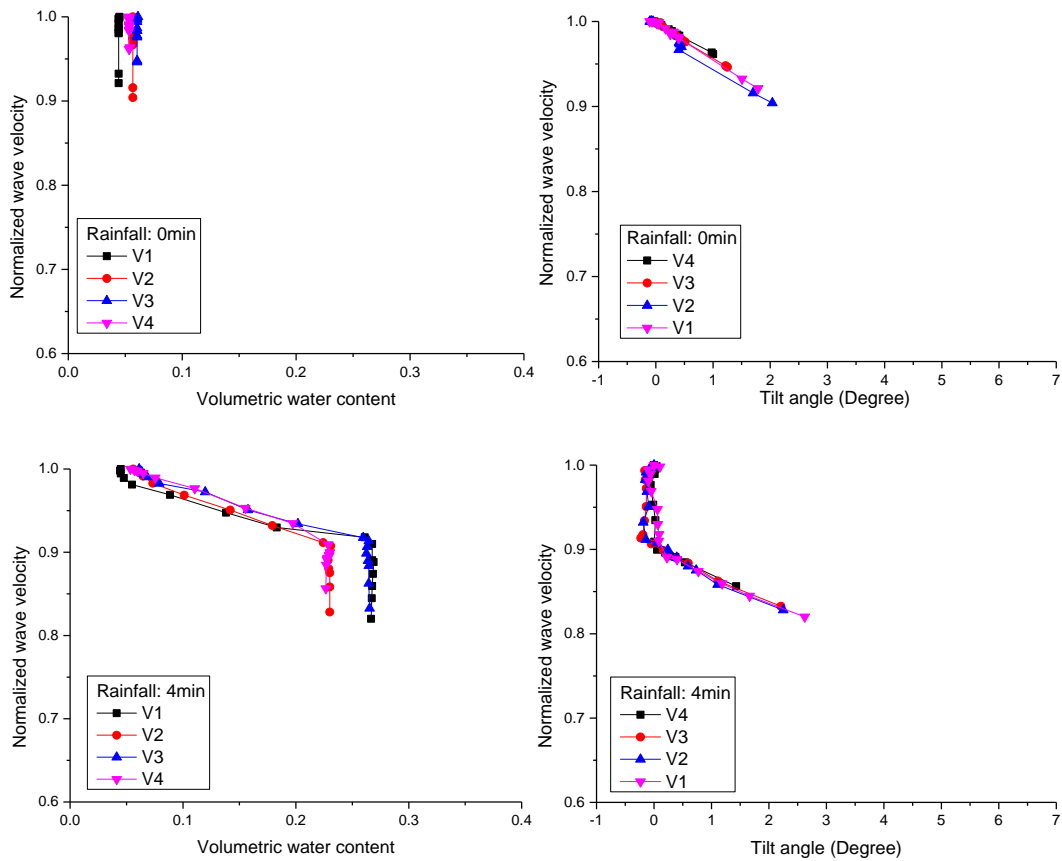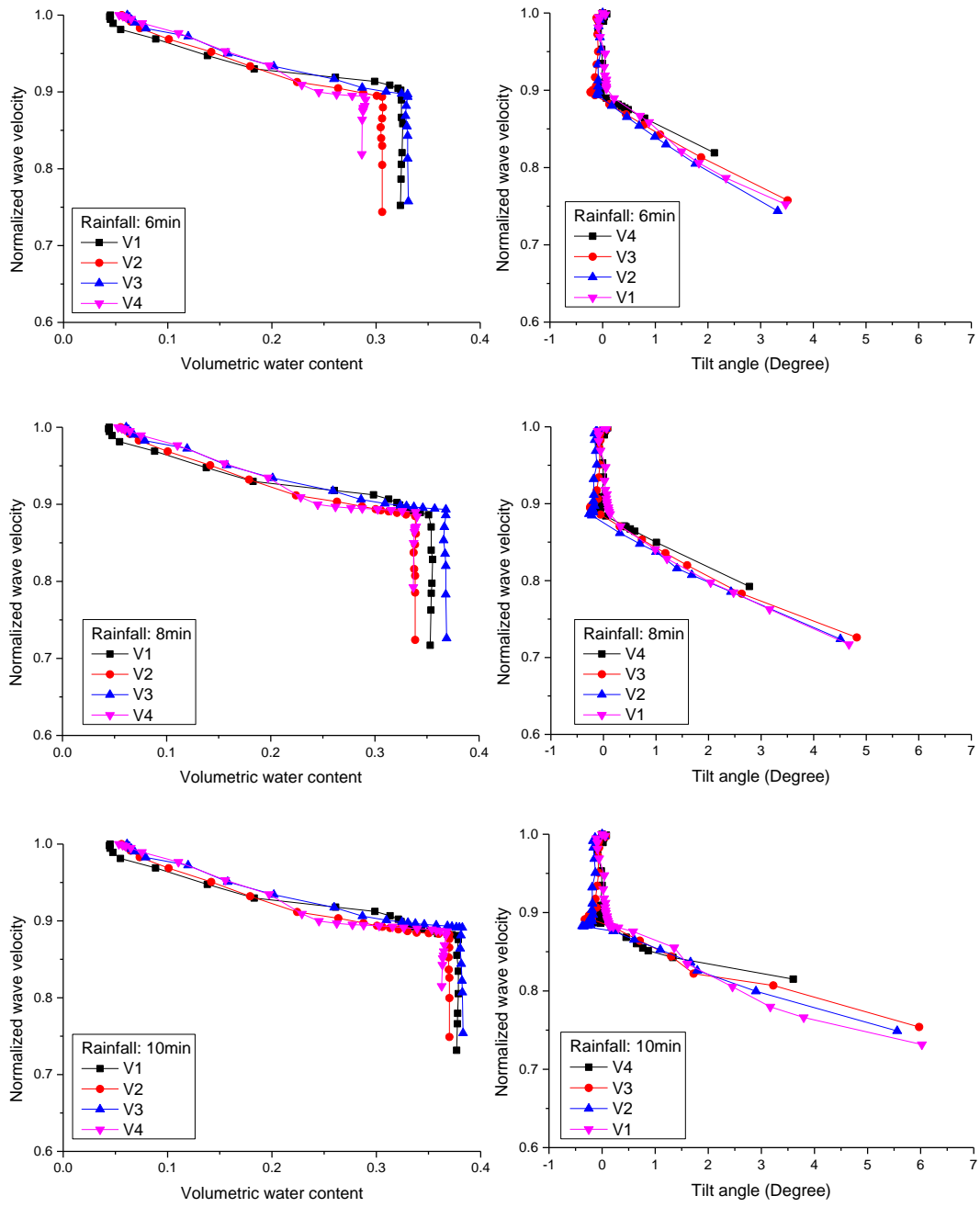
Figure 5.10: Change of elastic wave velocity with volumetric water content and tilt angle during the rainfall and inclination for flat slope with thicknesses of 5cm for surface layer under different rainfall durations.
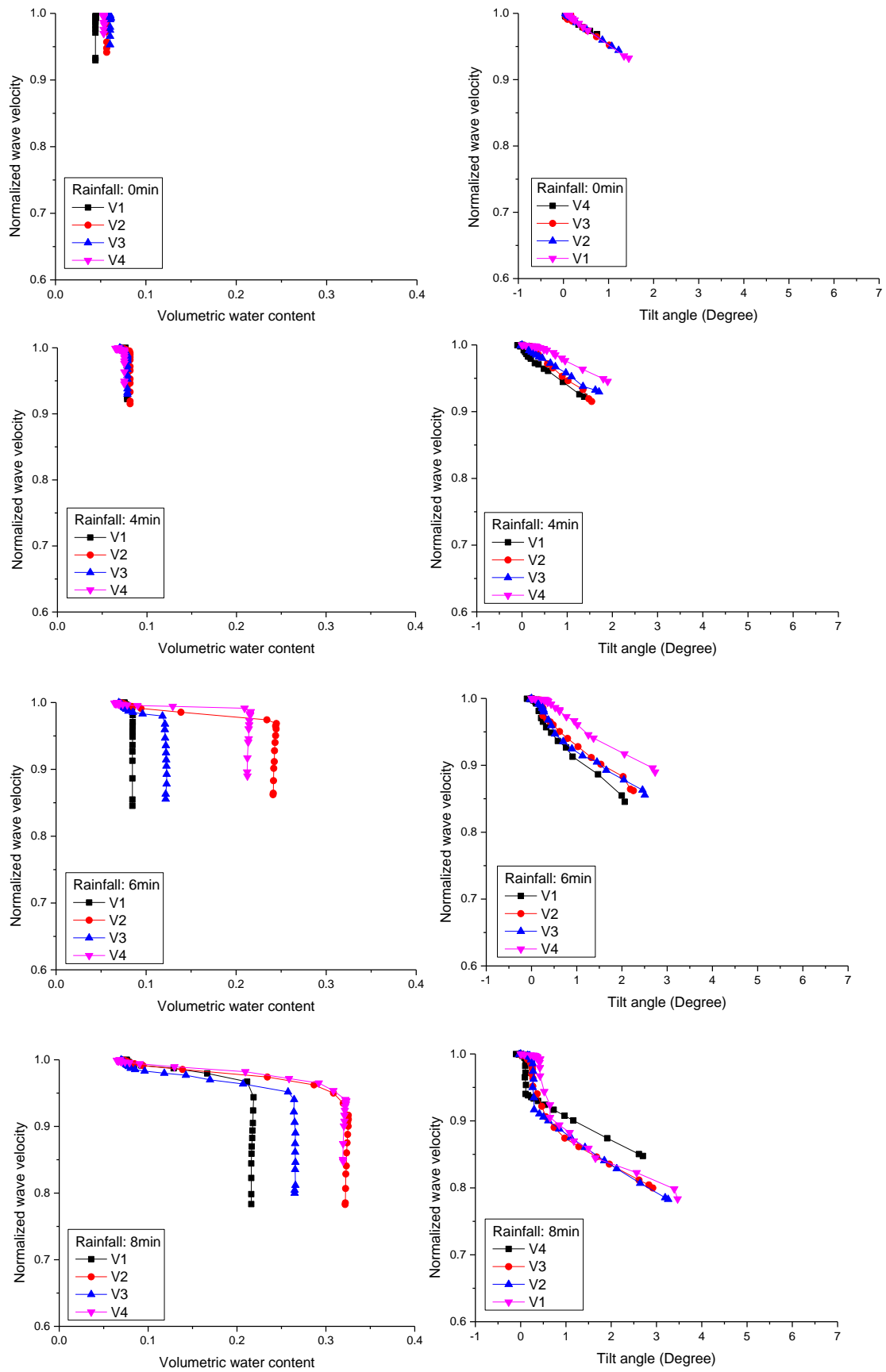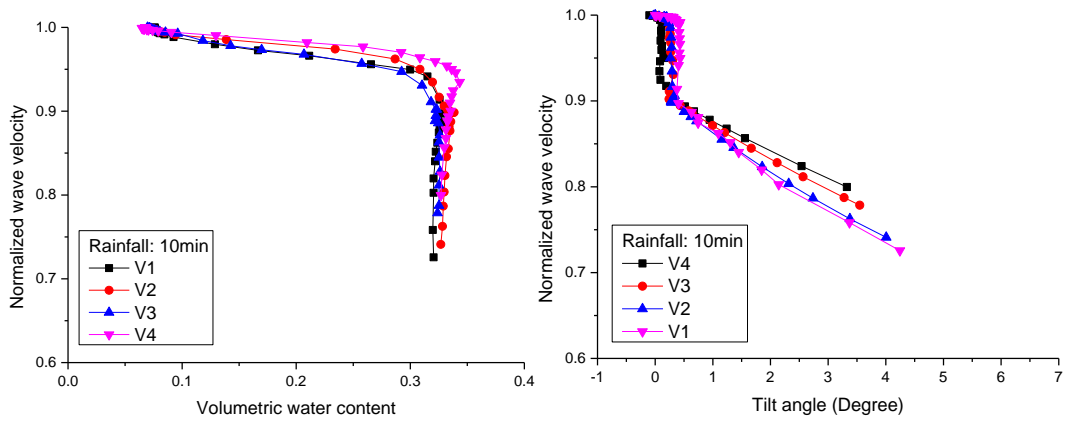
Figure 5.11: Change of elastic wave velocity with volumetric water content and tilt angle during the rainfall and inclination for flat slope with thicknesses of 10cm for surface layer under different rainfall durations.
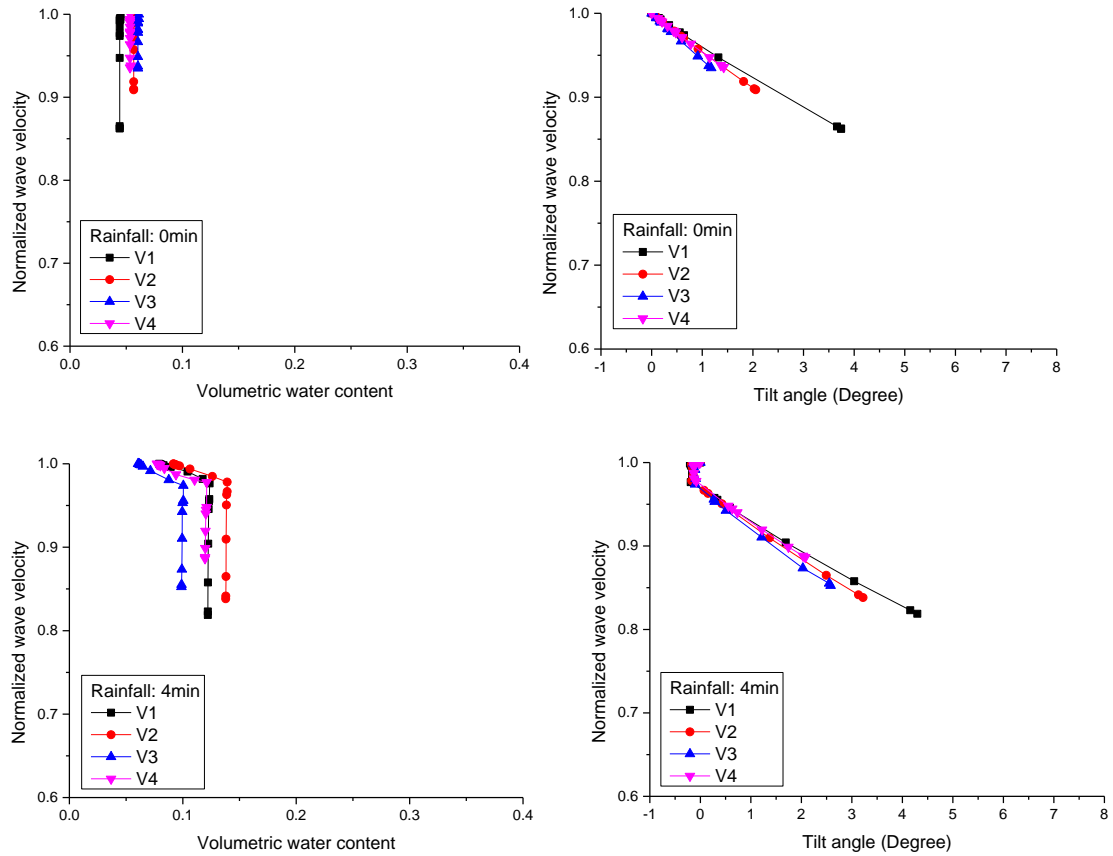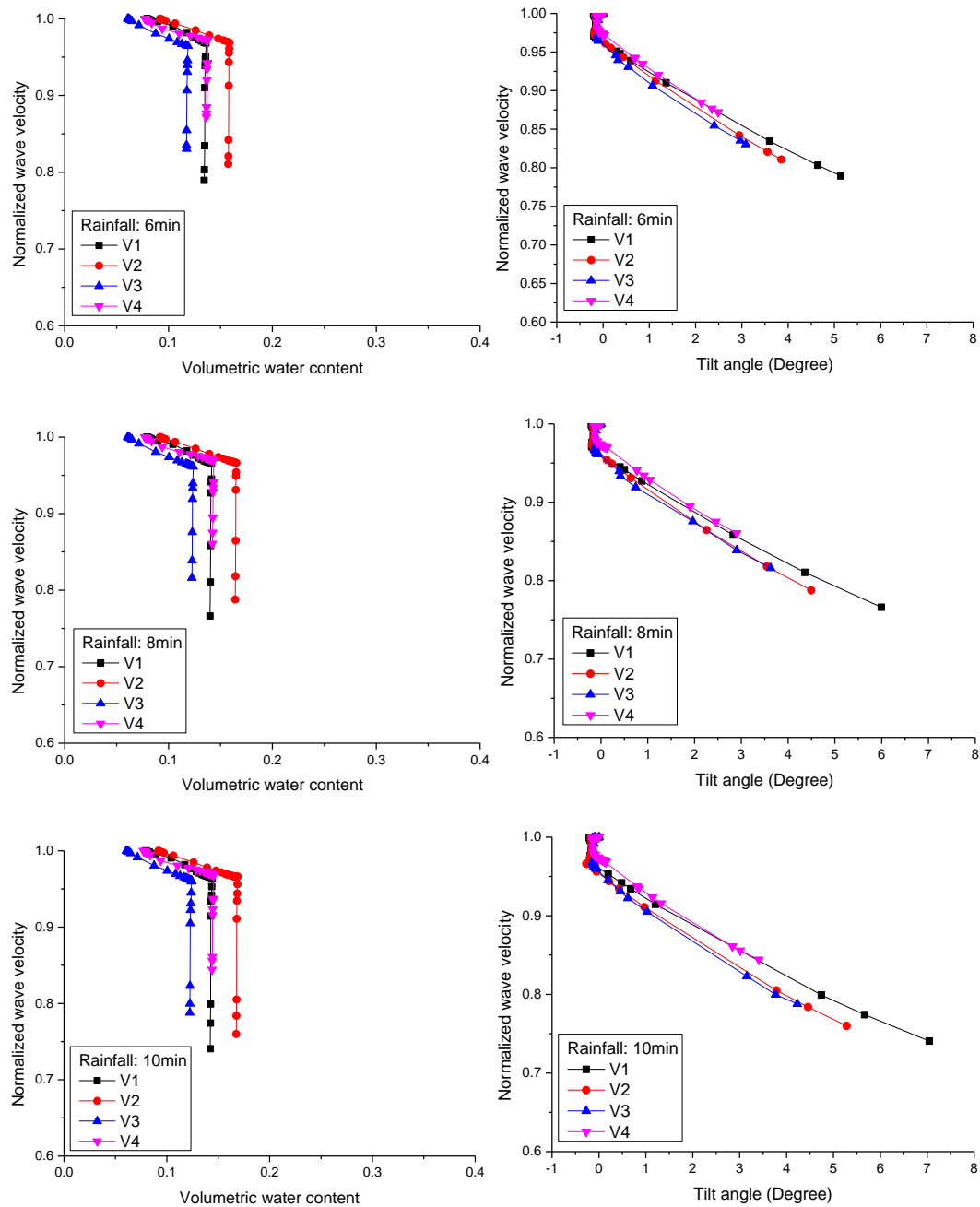
Figure 5.12: Change of elastic wave velocity with volumetric water content and tilt angle during the rainfall and inclination for flat slope with thicknesses of 15cm for surface layer under different rainfall durations.

The determination of elastic wave velocity depends on both of volumetric water content and tilt angle. Figure 5.13 to 5.15 shows the relationship between normalized elastic wave velocity against volumetric water content and tilt angle under different rainfall durations for slope with different surface layer thicknesses by means of a

three-dimensional plot. Tilt angle was found to have more significant effect on elastic wave velocity than volumetric water content.
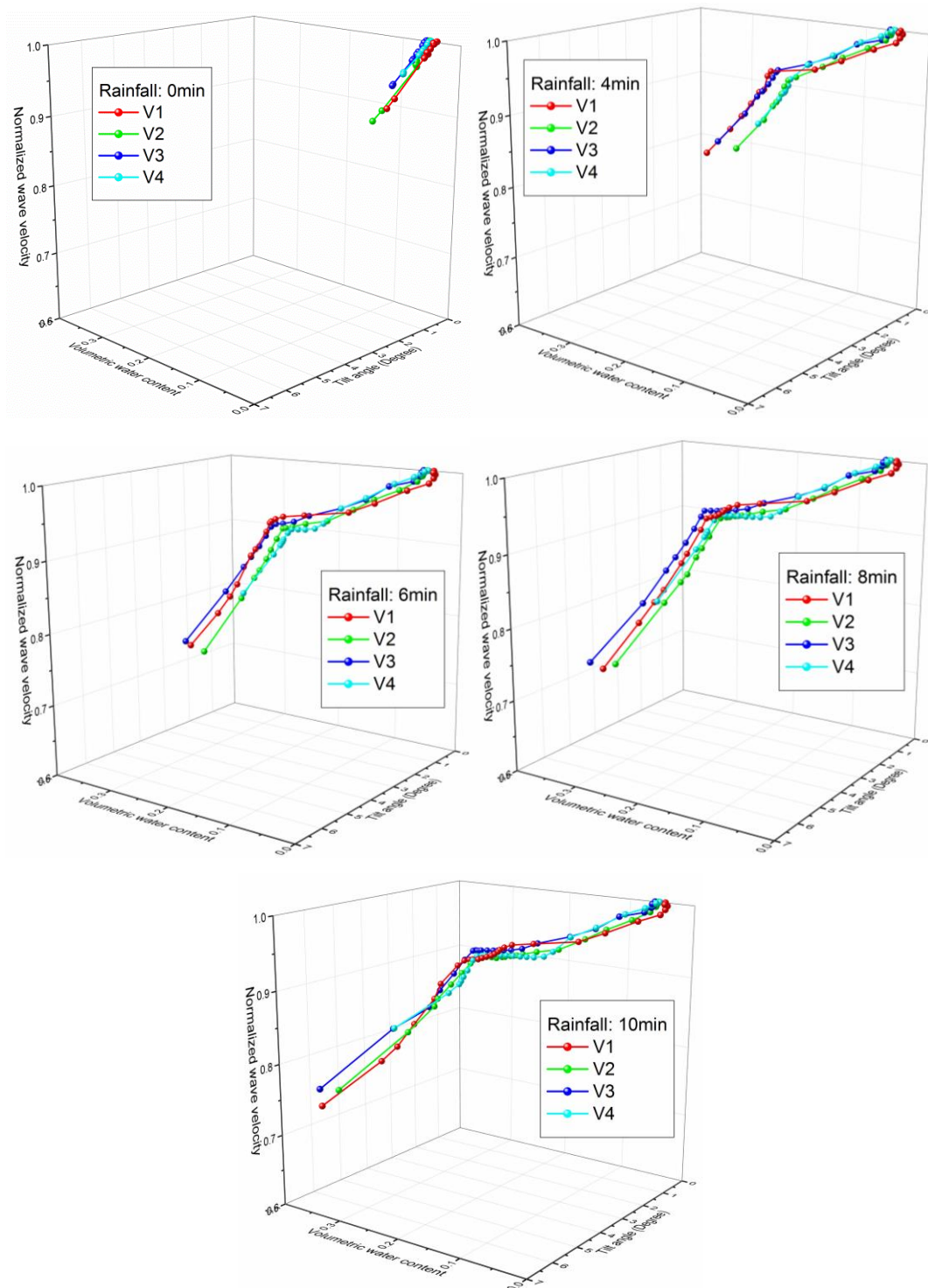

Figure 5.13: Relationship between normalized elastic wave velocity against volumetric water content and tilt angle under different rainfall durations for slope with

surface layer thickness of 5cm.
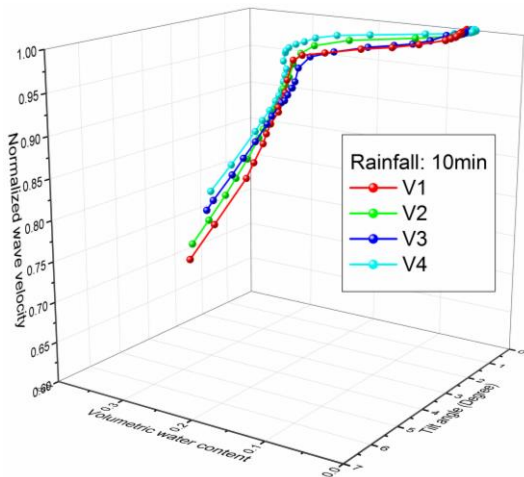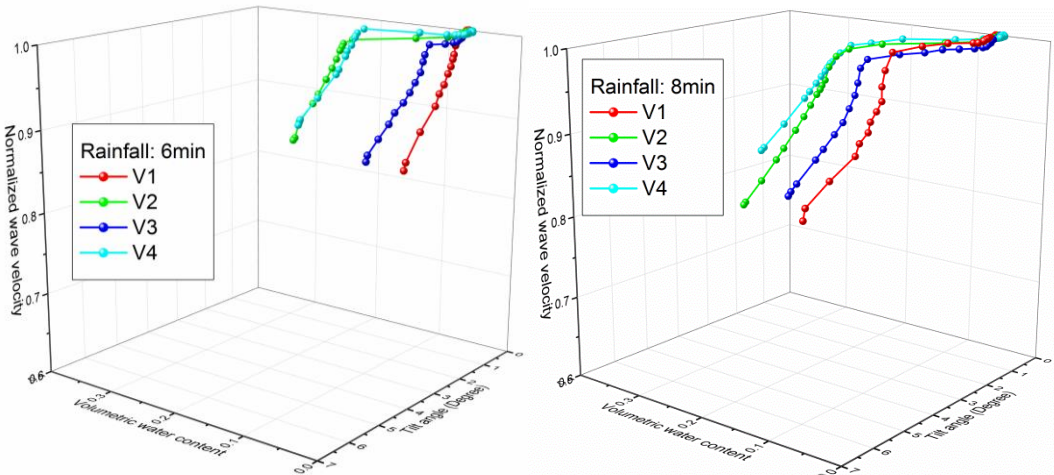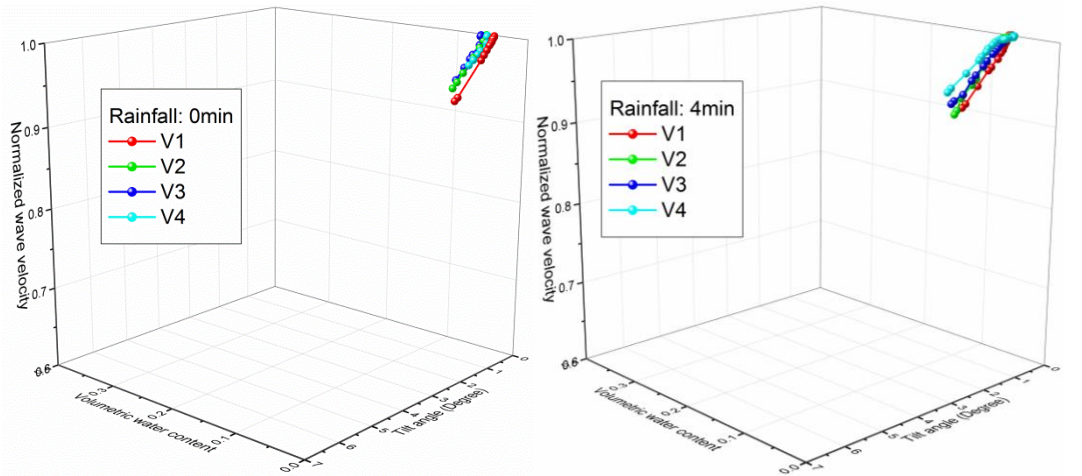
Figure 5.14: Relationship between normalized elastic wave velocity against volumetric water content and tilt angle under different rainfall durations for slope with surface layer thickness of 10cm.
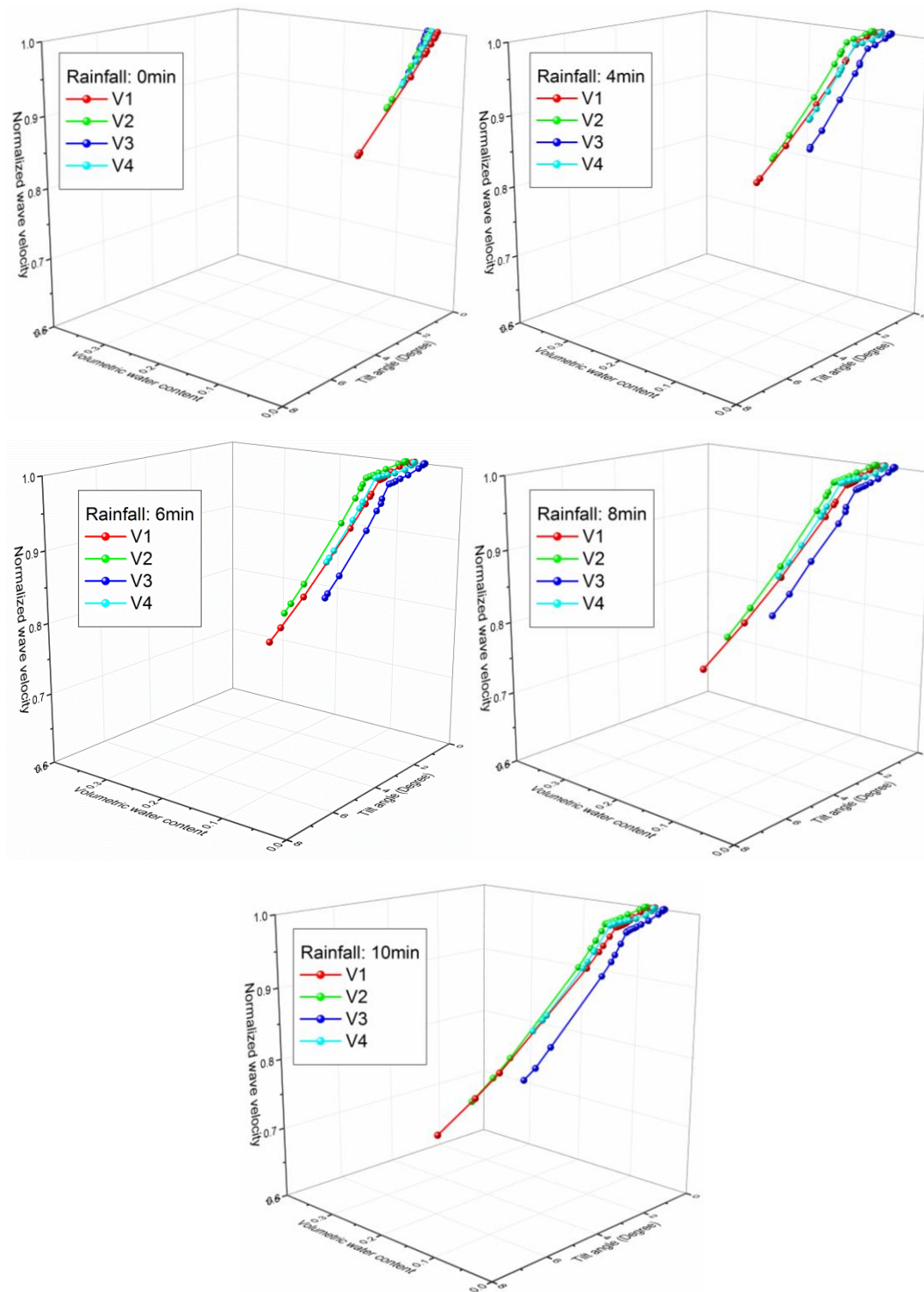

Figure 5.15: Relationship between normalized elastic wave velocity against

volumetric water content and tilt angle under different rainfall durations for slope with surface layer thickness of 15cm.

As shown in Figure 5.10 to Figure 5.15, the deformation increased with the thickness of surface layer for a given duration of rainfall. Besides, the sensor closer to the slope crest exhibited larger deformation. This finding is consistent with the observation made by Chuang (2014), who bonded and inclined the granular matter to simulate the deformation of slope (Figure 5.16). Due to the larger deformation with thicker surface layer and position closer to the slope crest, the elastic wave velocity was found to be reduced more.


Figure 5.16: deformational of slope using discrete element method (Chuang 2014).
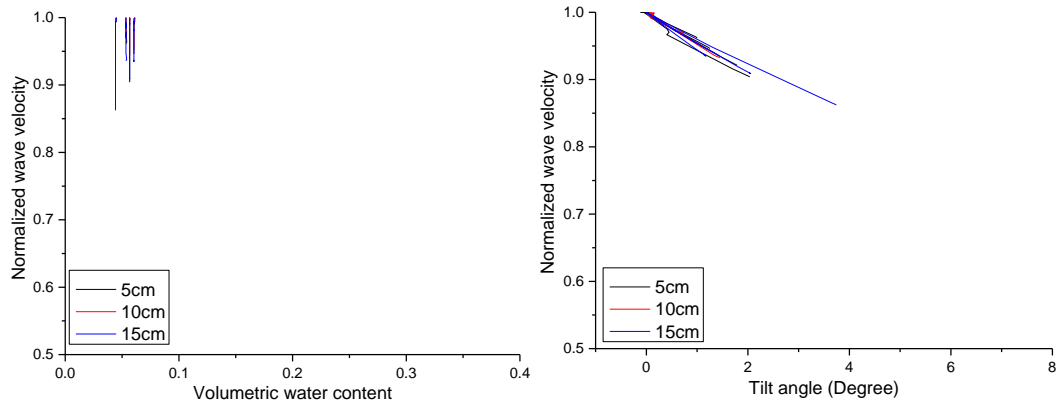
(a) Rainfall: 0min
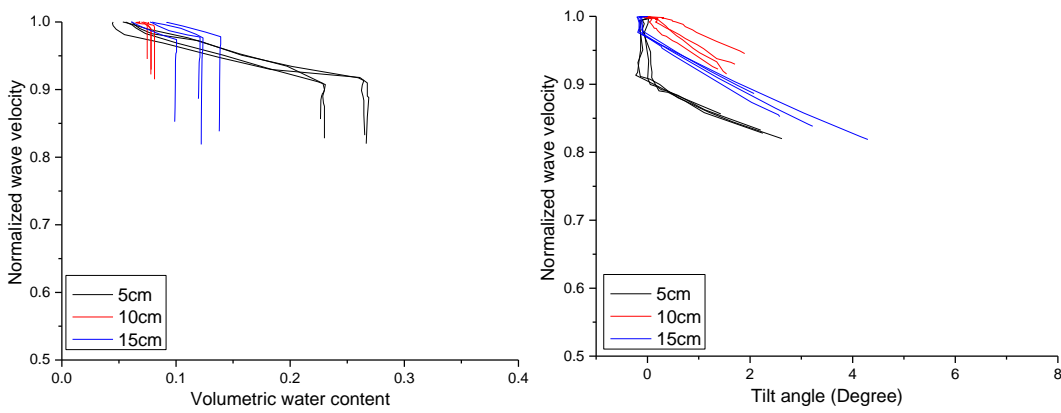
(b) Rainfall: 4min
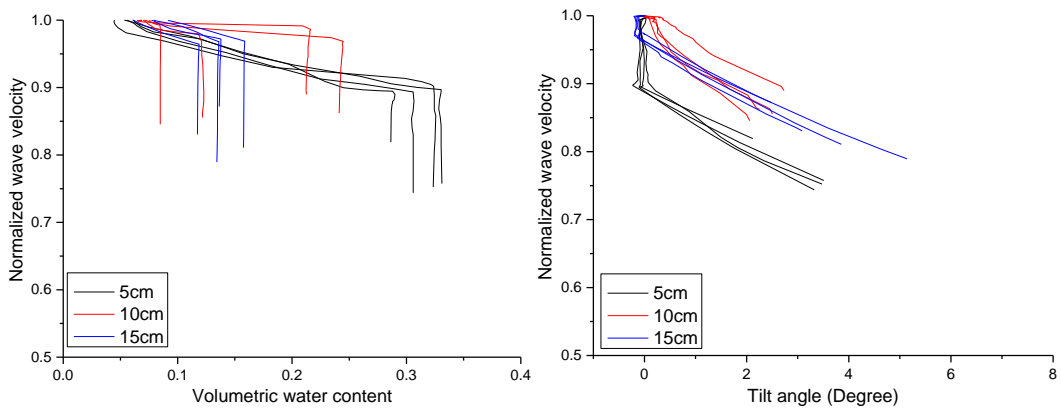
(c) Rainfall: 6min
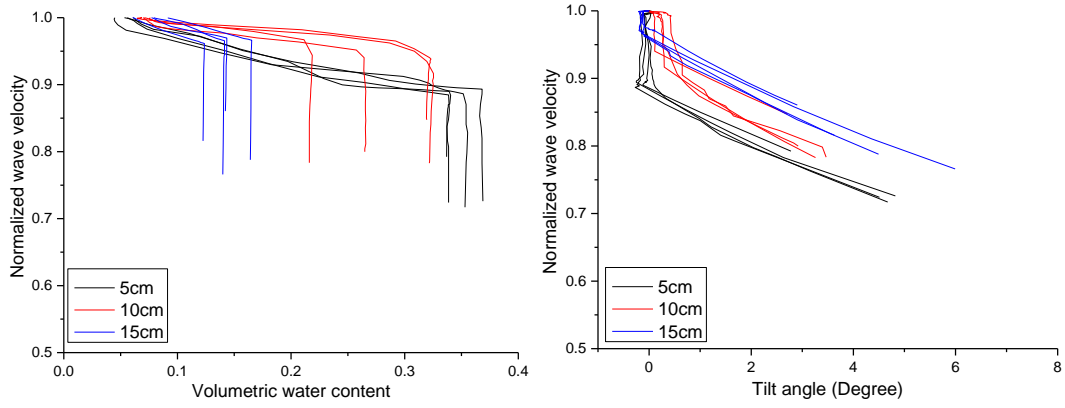
(d) Rainfall: 8min
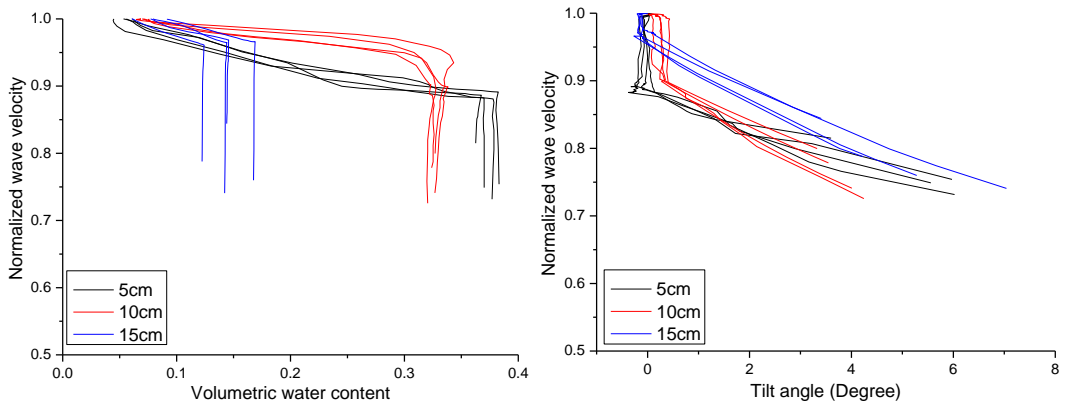
(e) Rainfall: 10min

Figure 5.17: Change of elastic wave velocity with volumetric water content and tilt angle during the rainfall and inclination for flat slope with different surface layer thicknesses under the same rainfall duration.

From Figure 5.17, it can be seen that as the surface layer thickness increased, the decrease rate of normalized wave velocity with volumetric water content became smaller. Moreover, the decrease rate of normalized wave velocity with tilt angle was found to be the same.

5.4. INTERPRETATION OF RESULTS

Shear waves (S-waves) and primary waves (P-waves) are function of G_0 and M_0,

which can be calculated as follows:

$$V_s = \sqrt{G_0/\rho} \tag{1}$$

$$V_p = \sqrt{M_0/\rho} \tag{2}$$

Where V_s and V_p are the S-wave and the P-wave velocities in the soil, respectively. ρ is the density of the soil. G_0 and M_0 are shear modulus and constrained modulus respectively.

An increase in water content causes the outside menisci to be pushed outward, which decrease both the matric suction and the effective stress in soil. As a result, a continuous decrease in the both shear modulus and constrained modulus with increasing water content was observed. Besides, density of soil increases with absorbed water. Therefore, the S-wave and the P-wave velocities decrease with increasing water content.

A stiffness degradation curve (Figure 5.18) shows that the stiffness modulus is reduced as the strain increases. This explanation was illustrated using the normalised stiffness degradation curve by comparing with the ground response from geotechnical construction and the measurement accuracy from laboratory investigation (Atkinson and Sallfors, 1991; Mair, 1993). The deformation accumulation can change the wave propagation path that creates the heterogeneity in soil. The soil structure involving void structure and distribution and water meniscus which governs the matric suction is changed by the deformation. Therefore, the wave velocity decreases with deformation.
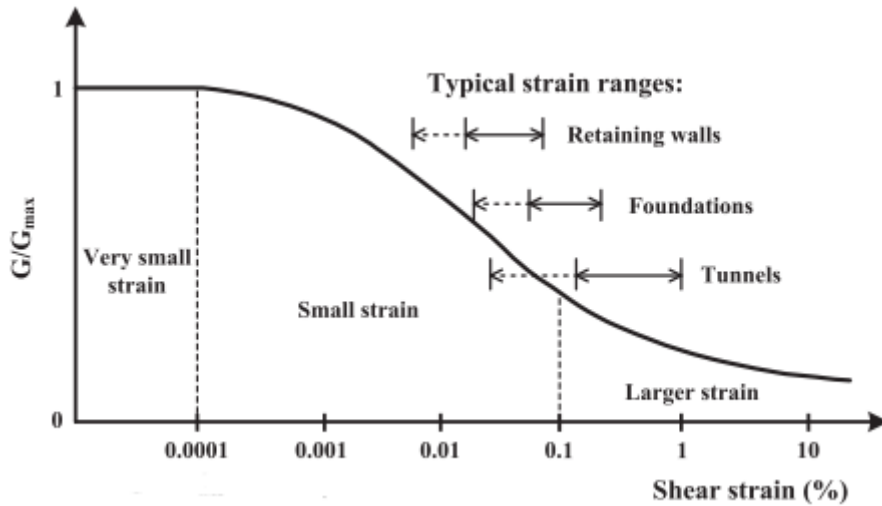
Figure 5.18: Normalized stiffness degradation curve (Likitlersuang, et al., 2013).

It should be noted that as shown in curves of normalized wave velocity versus tilt angle, the decrease rate of normalized wave velocity with tilt angle, i.e., (Δ normalized wave velocity/Δ tilt angle), is nearly the same regardless of the volumetric water content and failure plane thickness. In other words, the decrease rate of normalized wave velocity with tilt angle is independent of volumetric water content and failure plane thickness. This finding could be used to monitor the excavation slope stability where only deformation is needed to be considered. Excavation induced landslides are often encountered during engineering operations(Erginal et al. 2008), particularly in places where hydrogeological conditions are conducive to slope failures (Zaruba and Mencl, 1982). Several incidents of slope movements caused by excavation operations have been documented from around the world, for example from coal basins in south Wales (Bentley and Siddle 1996), Slovakia (Malgot and Mahr 1979; Klukanová and Rapant 1999), north Bohemia (Zaruba and Mencl 1982) and Bulgaria (Rybář 1971).

All data from cases are plotted to correlate the normalized wave velocity with volumetric water content and tilt angle. It shows that the data follow linear relationship well. It can be used to predict the wave velocity using volumetric water content and tilt angle.

$y = -0.3905x + 1.0197$
$R^2 = 0.9497$
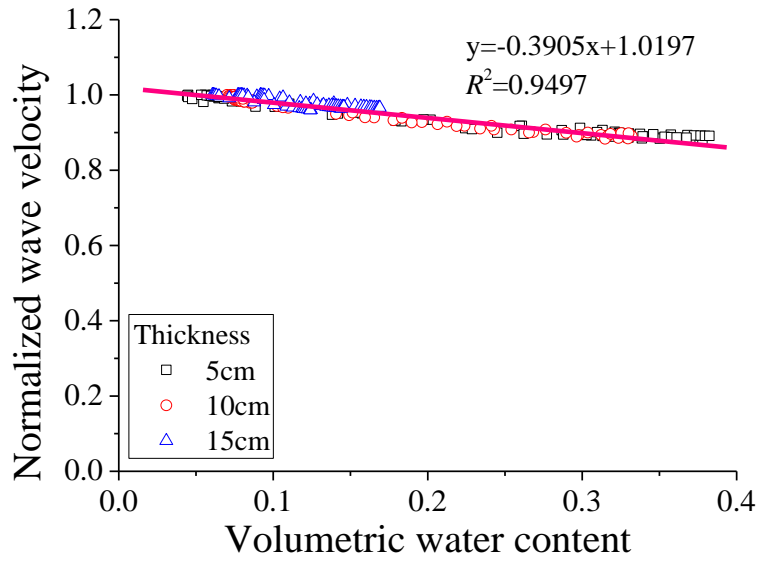
(a)normalized wave velocity~ volumetric water content

$y = -0.0282x + 1$
$R^2 = 0.9374$
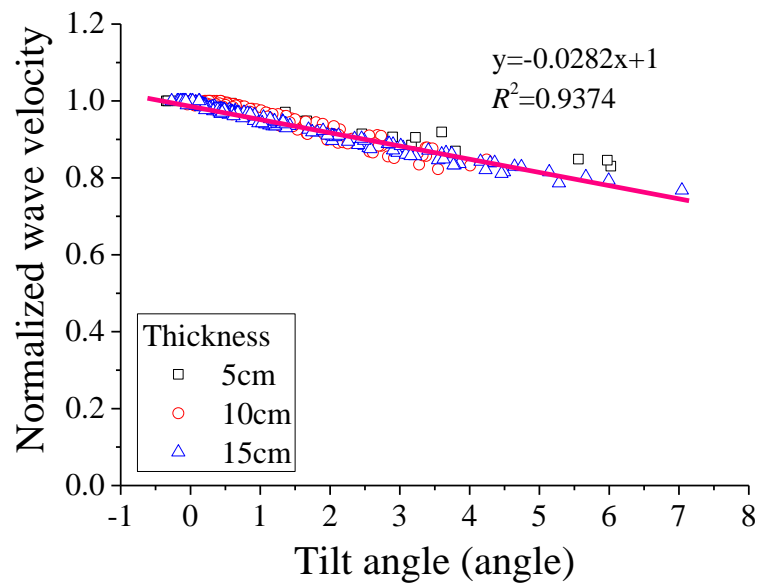
(b)normalized wave velocity~tilt angle

Figure 5.19: Relationship between normalized wave velocity and volumetric water content and tilt angle.

5.5. SUMMARY

This chapter summarizes test results and discussions related to the individual influences of water content and shear deformation on elastic wave propagation by means of flat model tests. In the study, the influence of water content on elastic wave velocity was separately investigated with no shear deformation conditions. Similarly, the influence of shear deformation on elastic wave velocity was investigated at the constant water content condition. The influence of water content was found to be limited. At most 10% decrease in normalized wave velocity was caused by increase of water content in the range of dry condition to saturated condition.

Whereas, the influence of deformation was much more significant compared to water content. The decrease rate of normalized wave velocity with tilt angle is independent of volumetric water content and failure plane thickness. This finding could be used to monitor the excavation slope stability.

0.4 Degree of tilt angle is defined as deformation criteria.

The relationship functions of normalized elastic wave velocity with either volumetric water content or tilt angle were obtained.

5.5. REFERENCE

Chuang, T.F. (2014). A study on the deformational mechanism of slate slopes using discrete element method. *Matser Thesis, National University of Kaohsiung*, Taiwan.

Likitlersuang, S., Teachavorasinskun, S., Surarak, C., Oh, E., & Balasubramaniam, A. (2013). Small strain stiffness and stiffness degradation curve of Bangkok Clays. *Soils and Foundations*, 53(4), 498-509.

Atkinson, J.H., Sallfors, G. (1991). Experimental determination of soil properties. In:

Proceedings of the 10th ECSMFE, Florence, 3,915–955.

Mair, R.J. (1993). Unwin memorial lecture 1992. Developments in geotechnical engineering research: application to tunnels and deep excavation. *Proceedings of the ICE —Civil Engineering*, 97 (1), 27–41.

Erginal, A. E., Türkeş, M., Ertek, T. A., Baba, A., & Bayrakdar, C. (2008). Geomorphological investigation of the excavation‐induced dündar landslide, Bursa—Turkey. *Geografiska Annaler: Series A, Physical Geography*, 90(2), 109-123.

Zaruba, Q., & Mencl, V. (2014). Landslides and their control (Vol. 31). Elsevier.

Bentley, S. P., & Siddle, H. J. (1996). Landslide research in the South Wales coalfield. *Engineering Geology*, 43(1), 65-80.

Rybář, J. (1971). Tektonisch beeinflusste Hangdeformationen in Braunkohlenbecken. *Rock mechanics*, 3(3), 139-158.

Malgot, J. and Mahr, T. (1979). Report on the engineering-geological mapping of slope movements in the environs of the village of Podhradie. *Geofond. Bratislava*. Manuscript: 1–15.

Klukanová, A., & Rapant, S. (1999). Impact of mining activities upon the environment of the Slovak Republic: two case studies. *Journal of Geochemical Exploration*, 66(1), 299-305.

CHAPTER 6

USE OF WAVE VELOCITY FOR SLOPE FAILURE
PREDICTION

6.1. INTRODUCTION

Rainfall-induced slope instability constitutes a major threat to both lives and property throughout the mountainous area. It is one of the most destructive natural disasters (Sharma & Nakagawa, 2010). Early warning systems can be economically used in large spatial extent, for which, however, correct representation of physical processes in mathematical terms was required. Uchimura (2011) noted that variation of elastic wave velocity in soil during rainfall could be used to predict slope failures and landslides. A new idea to watch slope movements by monitoring elastic wave velocity in soil slope is presented in this paper.

6.2. TEST CONDITIONS

This chapter covers flat model studies exploring the behavior of wave velocities to predict slope failure. Model tests with different surface layer thicknesses, dry densities and slope angles were conducted and wave velocities were determined during tests. Rainfall was given until slope failed. This series of experiments was thus designed to reproduce the actual mechanism of rain-induced landslides. During the experiments elastic wave velocities were determined at regular intervals, to study the behavior of wave velocities during rainfall-induced slope failures. Unfortunately, erosion between

the wall and slope soil occurred for 4 cases. In the further discussion, the data with erosion will be ignored.

The following sections explain the test results and corresponding discussions of these tests. Test conditions and other important parameters of each test are summarized in Table 6.1. Wave velocities were normalized with respect to their initial values.

Table 6.1: Test conditions in Type 2 tests.

Type 2			
Case No.	Slope angle(°)	Thickness(cm)	Density(g/cm3)
2-45-5-1.2	45	5	1.2
2-45-5-1.3			1.3
2-45-5-1.4			1.4
2-45-10-1.2		10	1.2
2-45-10-1.3			1.3
2-45-10-1.4			1.4
2-45-15-1.2		15	1.2
2-45-15-1.3			1.3
2-45-15-1.4			1.4
2-40-10-1.2	40	10	1.2
2-40-10-1.3			1.3
2-40-10-1.4			1.4
2-50-10-1.2	50		1.2
2-50-10-1.3			1.3
2-50-10-1.4			1.4

6.3. RESULTS

6.3.1. Evolution of Elastic Wave Velocity

Figure 6.1 shows the time series data of volumetric water content, tilt angle and normalized wave velocity with different surface layer thicknesses, dry densities and slope angles.

The lower part of the slope became saturated first forming a water table below the toe area of the slope. Wetting front progressed downward toward the impermeable base. Upon reaching the base soil layer which was highly compacted featured with low permeability, water accumulated and a water table formed, specifically in the lower half of the slope, as shown in Figure 6.2. The water table continued to rise upward and on reaching the VWC sensor locations, the water content accelerated to increase. It seemed that this failure was initiated by the decrease in the shear strength of the slope due to the loss of soil suction. The deformation seemed to be progressive with the rise of water table. A lateral through-going crack was formed at the crest of the slope before large-scale deformation occurs because of an increase in the weight of the surface soil and a decrease in strength at the slip surface due to increased water content. Tilt angle started to increase first slowly and then at a rapid rate.

As the rainfall progressed, the water content and tilt angle at the different locations in the slope increased, causing a decrease in elastic wave velocity. The elastic wave velocity decreased gradually under rainfall. The gradual decrease in elastic wave velocity may be attributed to the increase of water content where tilt angle was not changed. This gentle decrease continued until the tilt angle started to increase. Once tilt angle started to increase, the wave velocity decreased at a larger rate. The normalized elastic wave velocity where it accelerated to decrease was in the range of 0.887 and 0.992, which could be used as a threshold for early warning. A warning should be issued at the normalized elastic wave velocity at the normalized elastic wave velocity less than about 0.9.
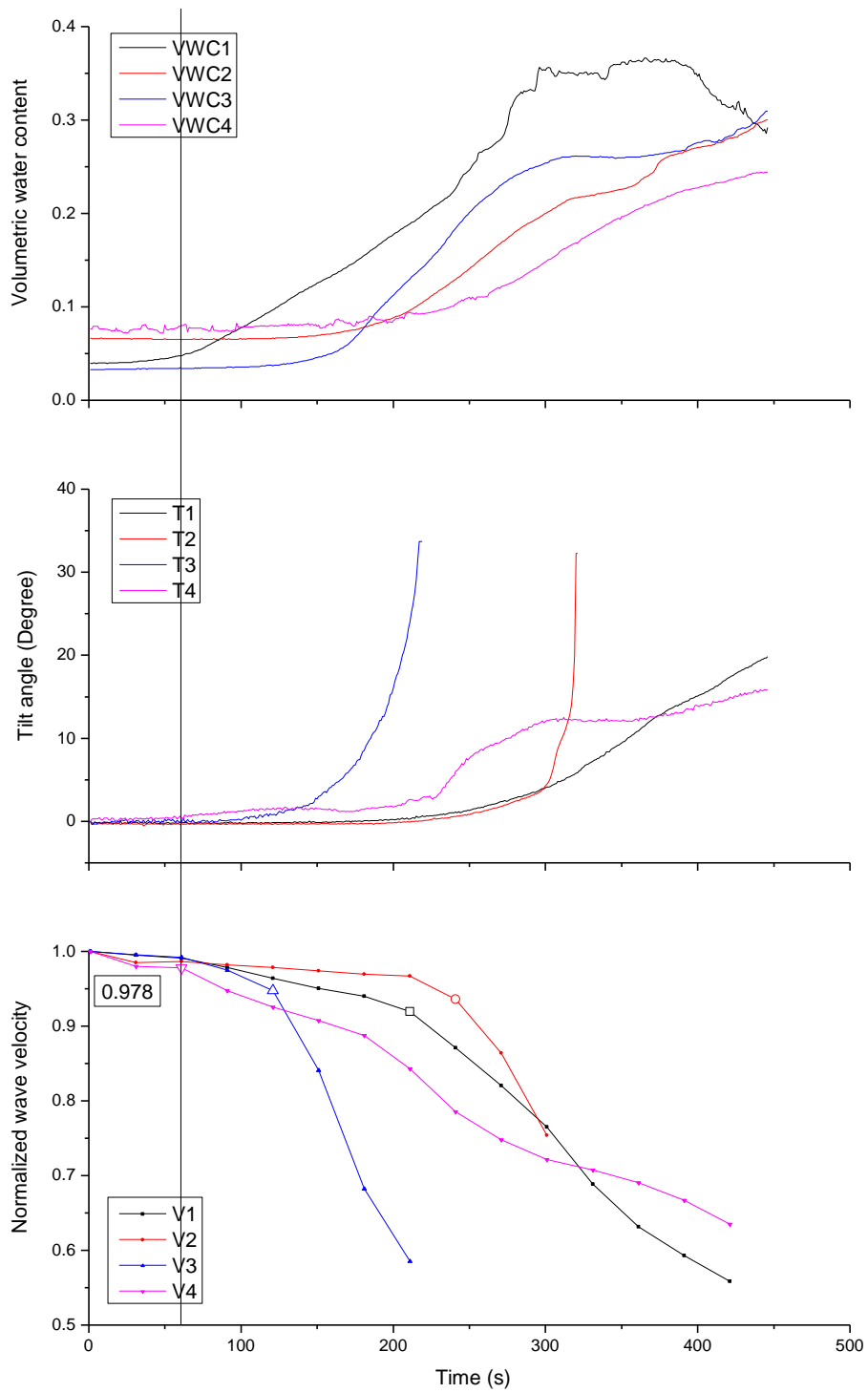
(a)2-45-5-1.2 (erosion)

Figure 6.1: Time series data of volumetric water content, tilt angle and normalized wave velocity during tests under different conditions.
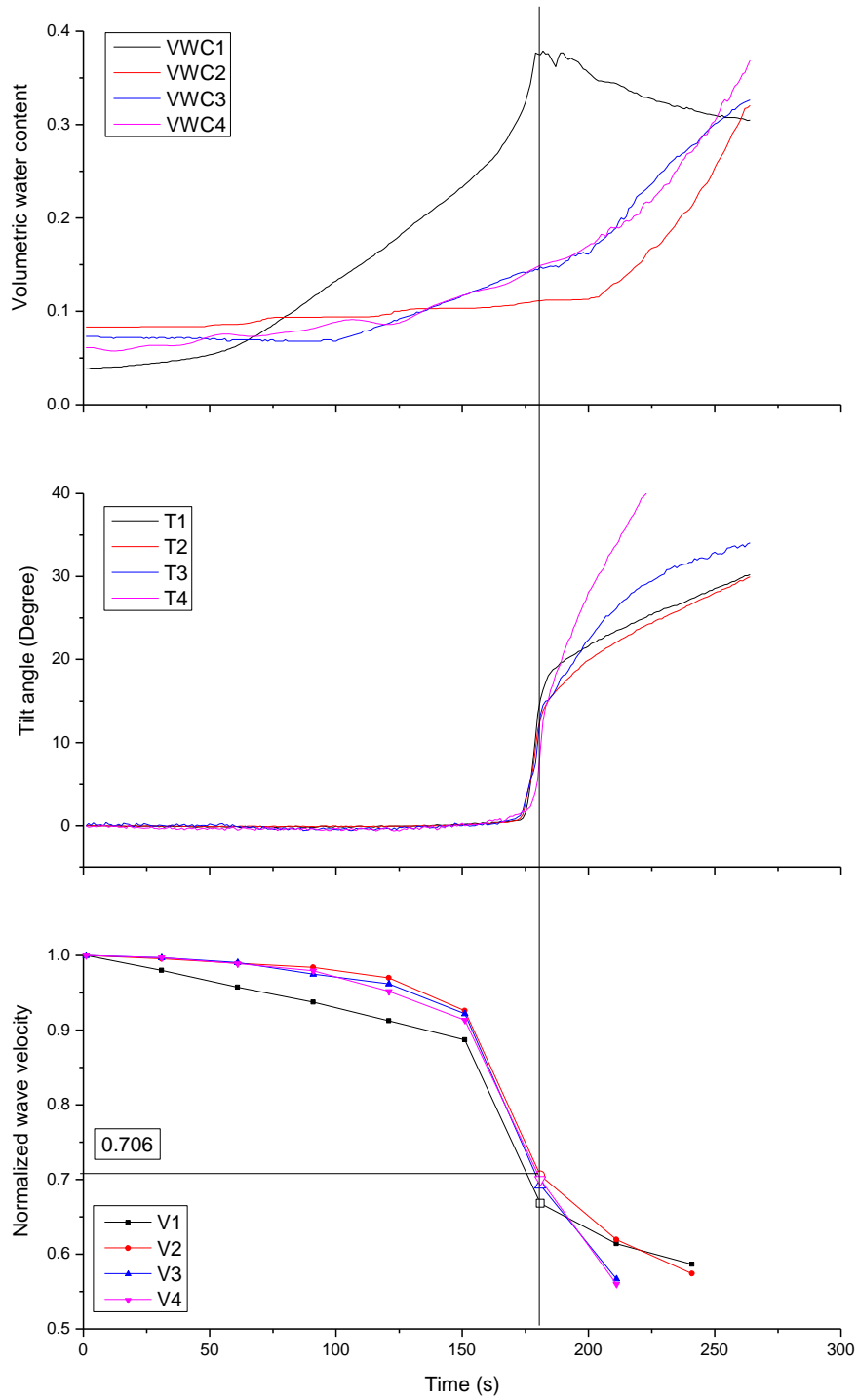
(b)2-45-5-1.3(erosion)

Figure 6.1 (continued): Time series data of volumetric water content, tilt angle and normalized wave velocity during tests under different conditions.
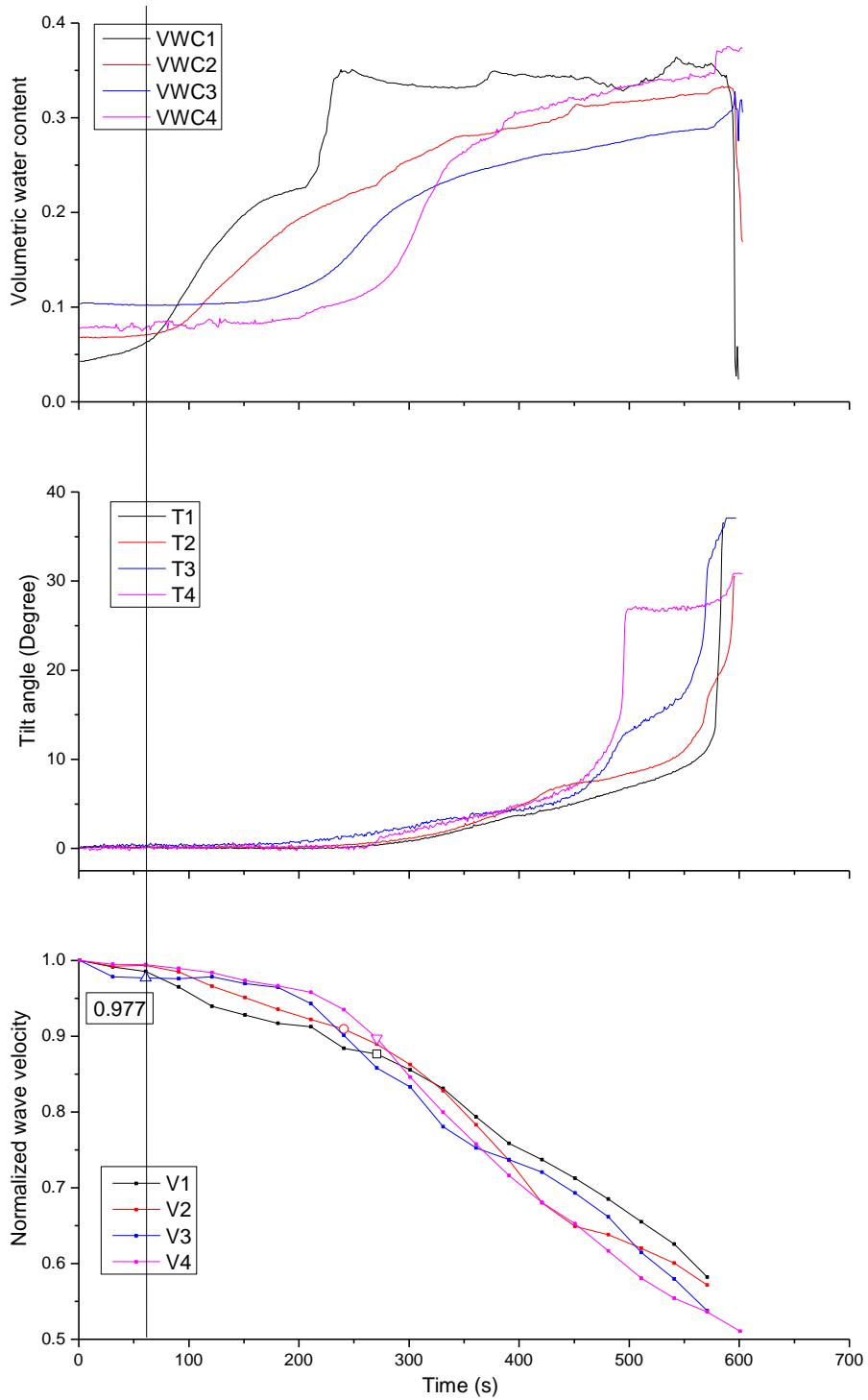
(c)2-45-5-1.4

Figure 6.1 (continued): Time series data of volumetric water content, tilt angle and

normalized wave velocity during tests under different conditions.
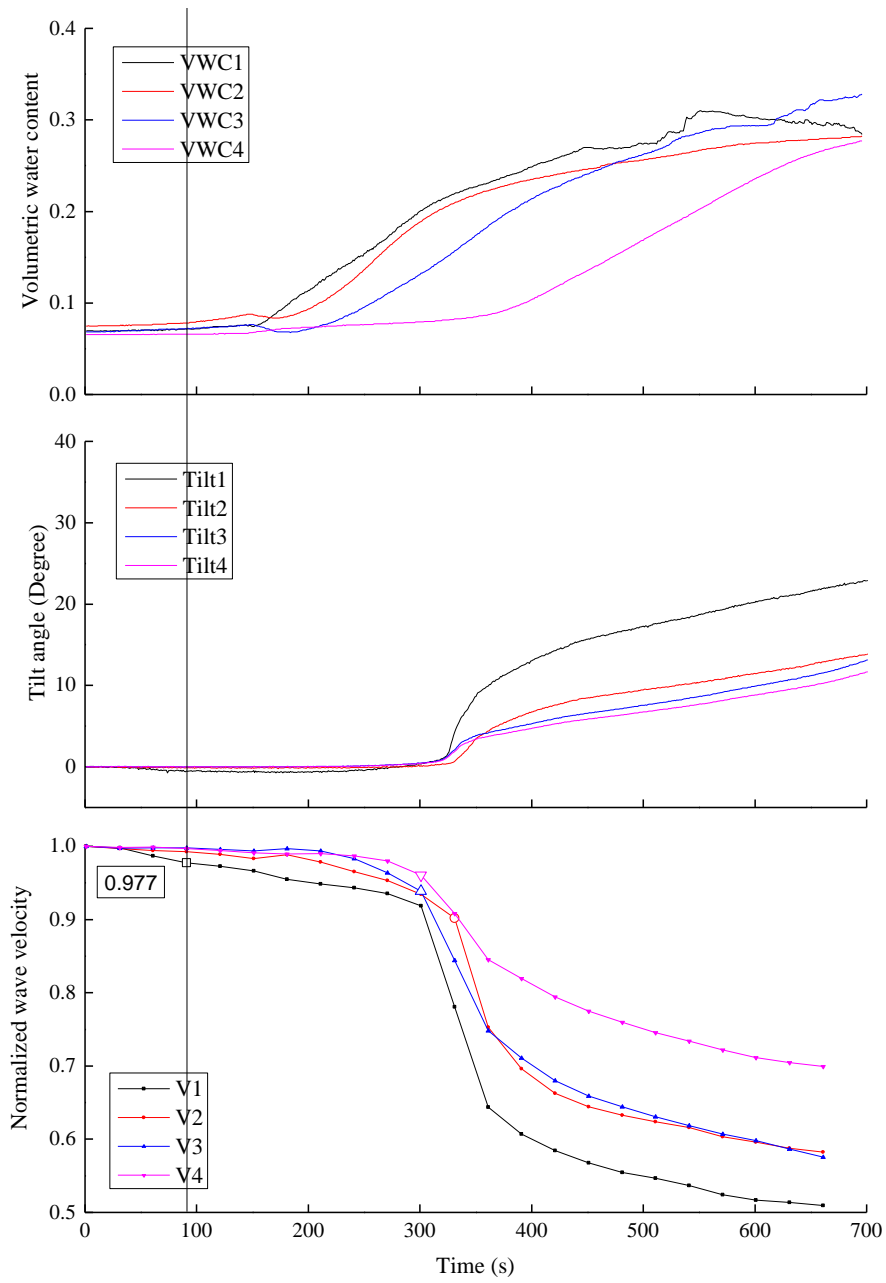
(d)2-45-10-1.2

Figure 6.1 (continued): Time series data of volumetric water content, tilt angle and
normalized wave velocity during tests under different conditions.
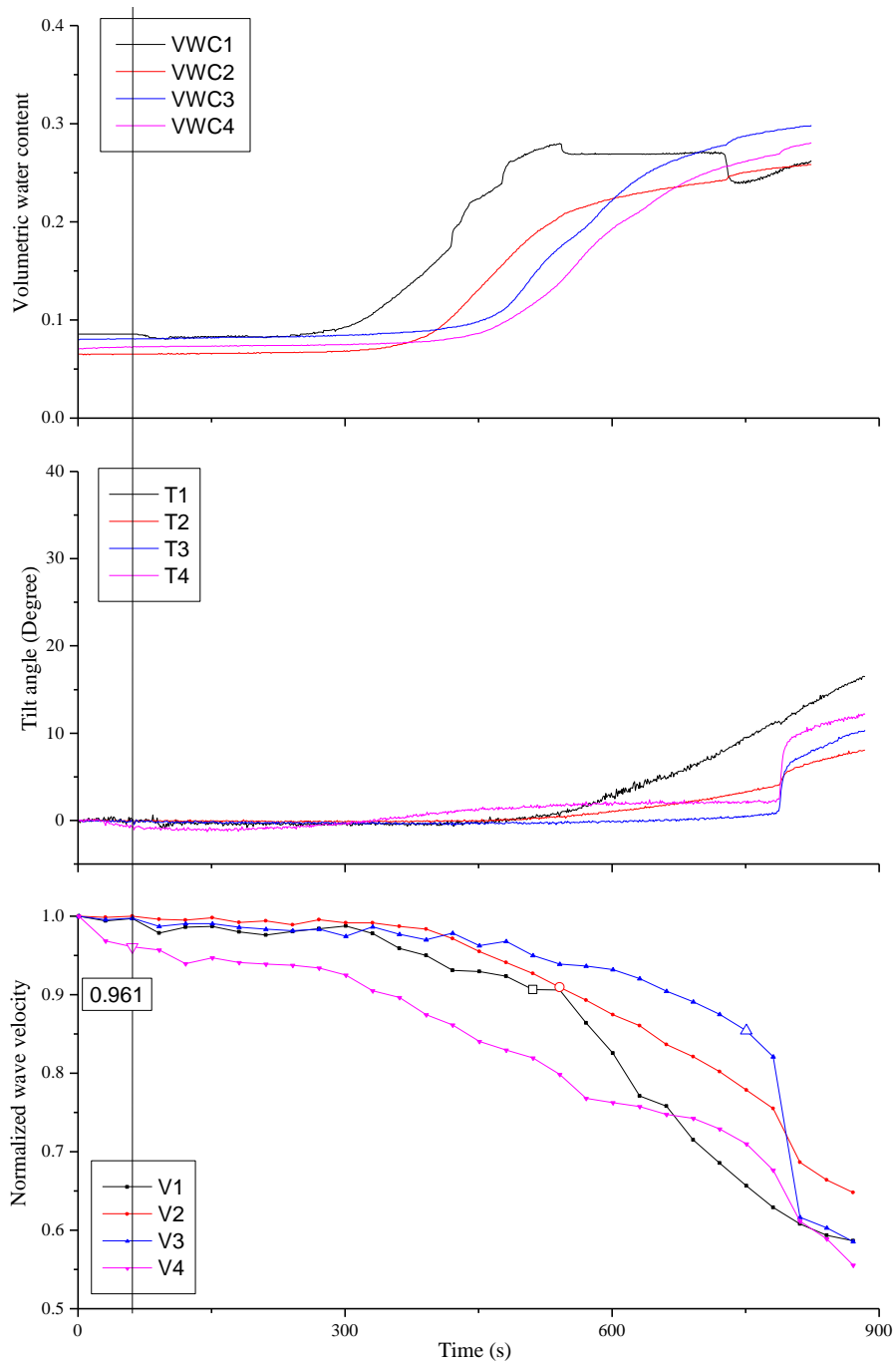
(e)2-45-10-1.3(erosion)

Figure 6.1 (continued): Time series data of volumetric water content, tilt angle and normalized wave velocity during tests under different conditions.
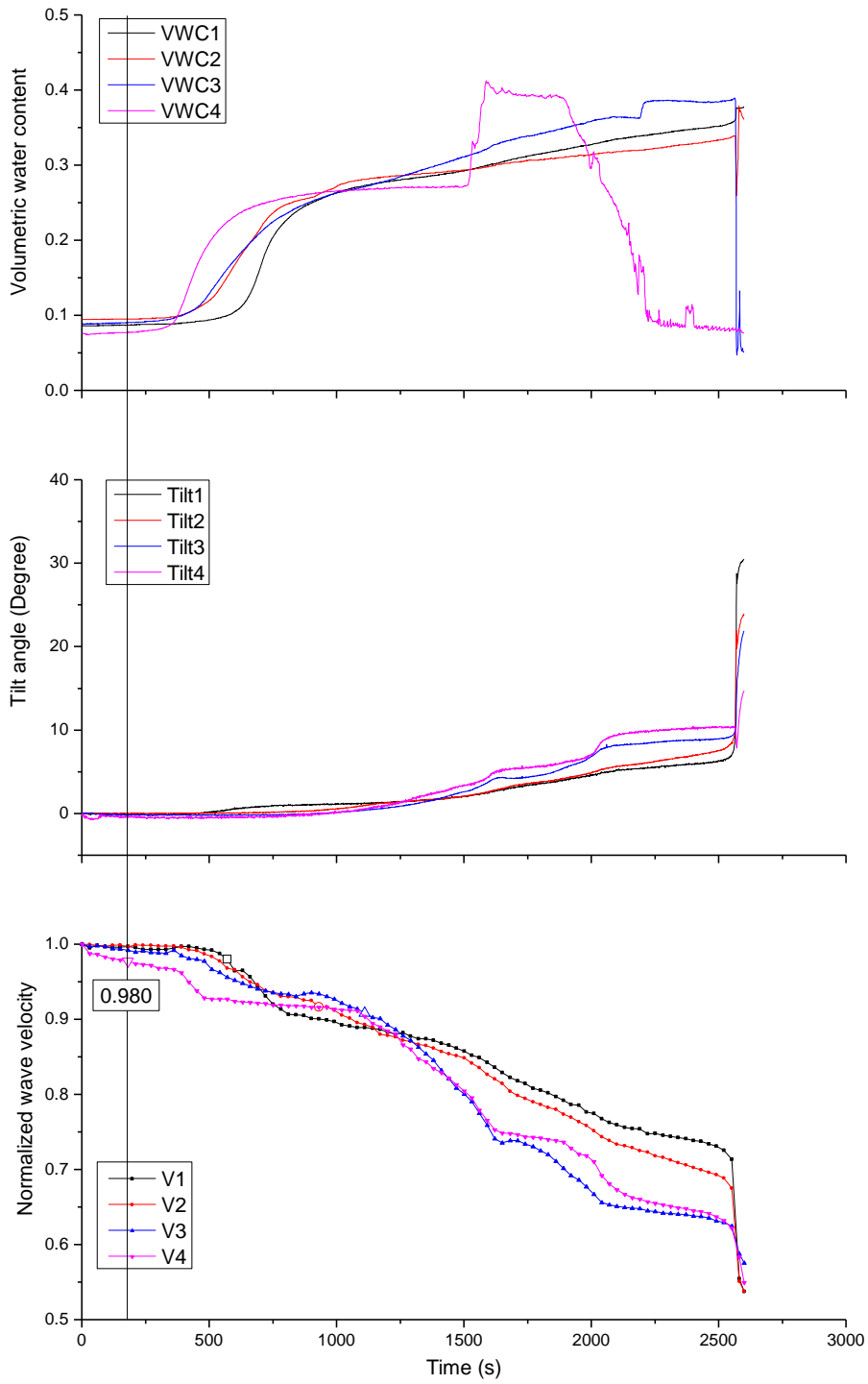
(f)2-45-10-1.4(erosion)

Figure 6.1 (continued): Time series data of volumetric water content, tilt angle and normalized wave velocity during tests under different conditions.
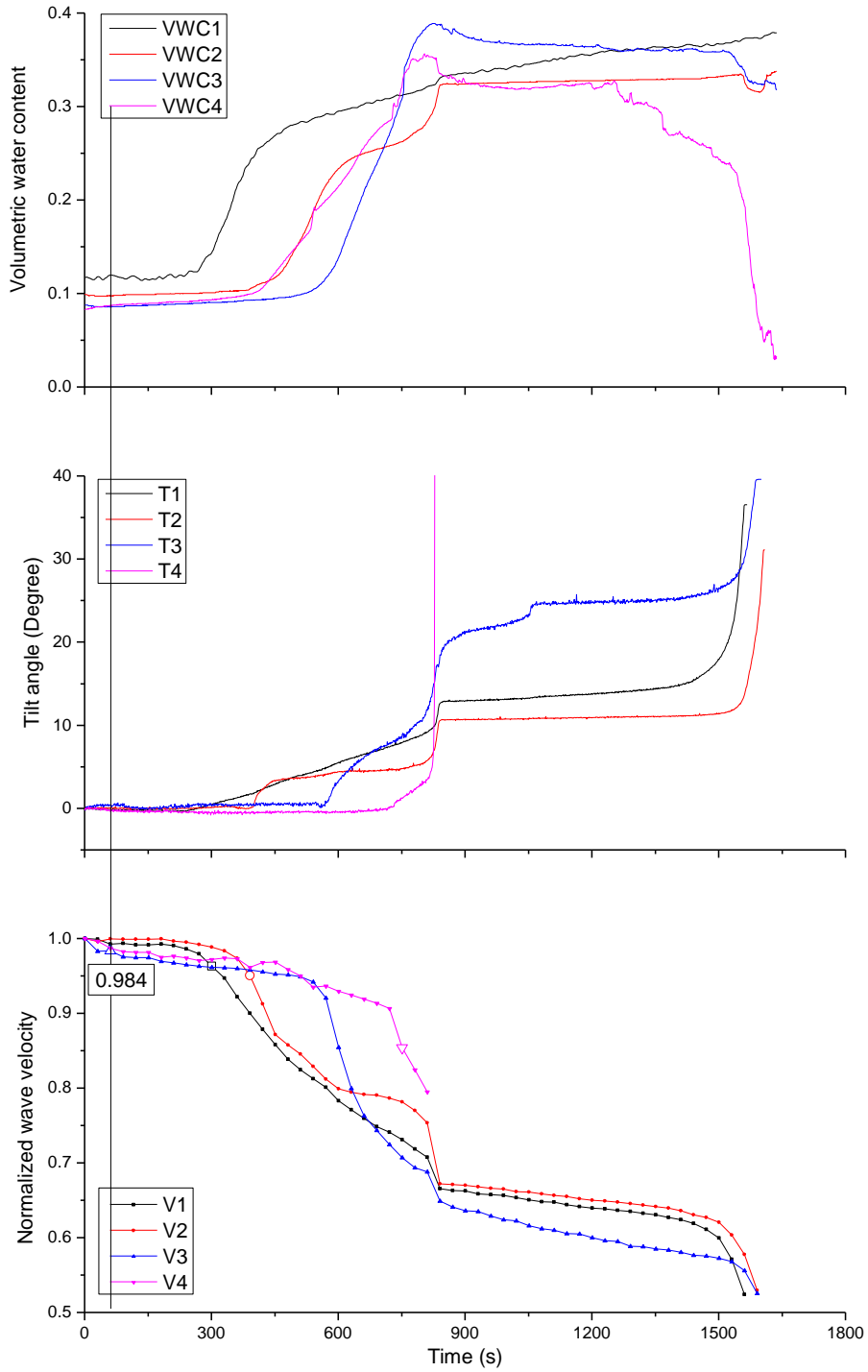
(g) 2-45-15-1.2

Figure 6.1 (continued): Time series data of volumetric water content, tilt angle and normalized wave velocity during tests under different conditions.
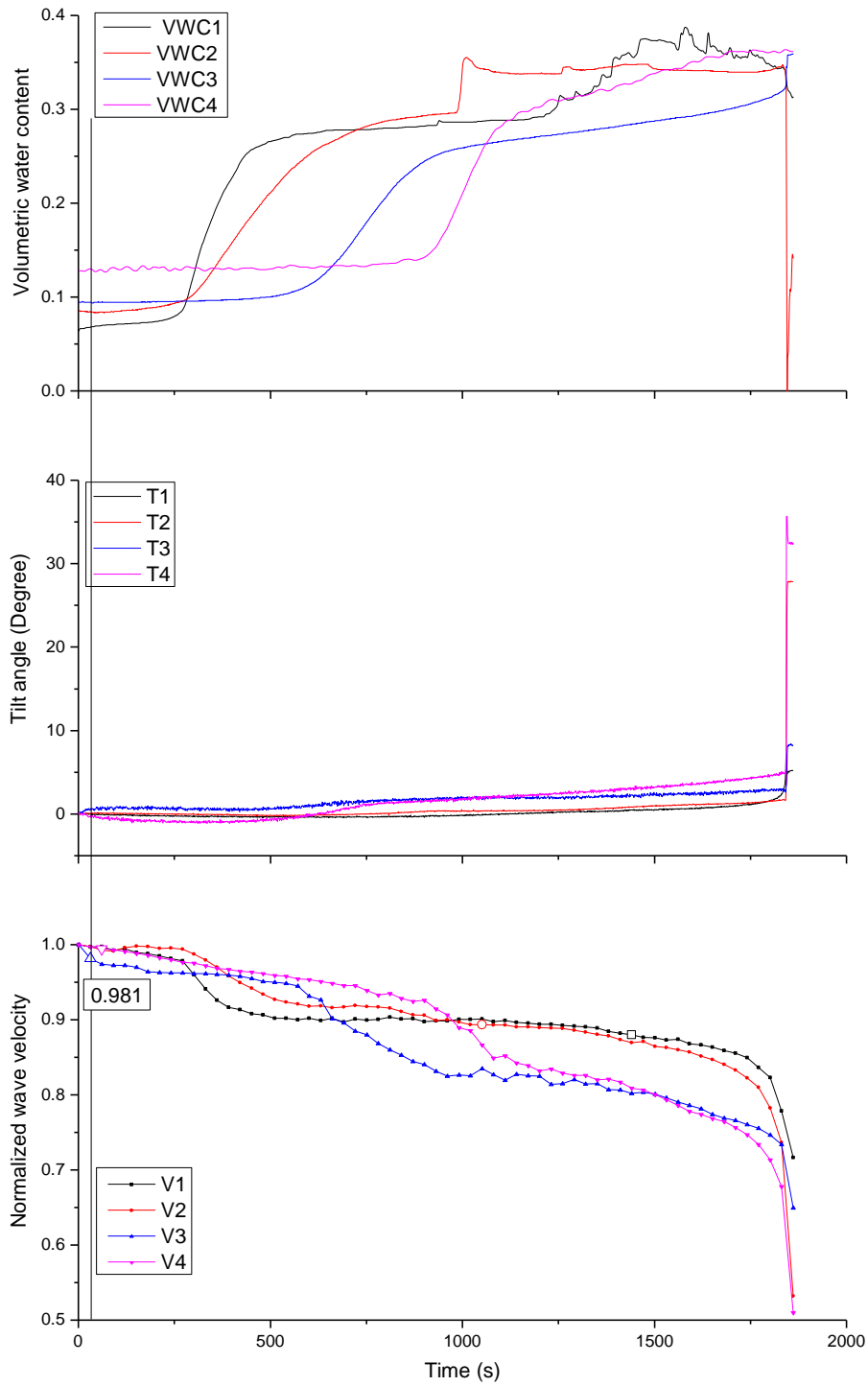
(h) 2-45-15-1.3

Figure 6.1 (continued): Time series data of volumetric water content, tilt angle and normalized wave velocity during tests under different conditions.
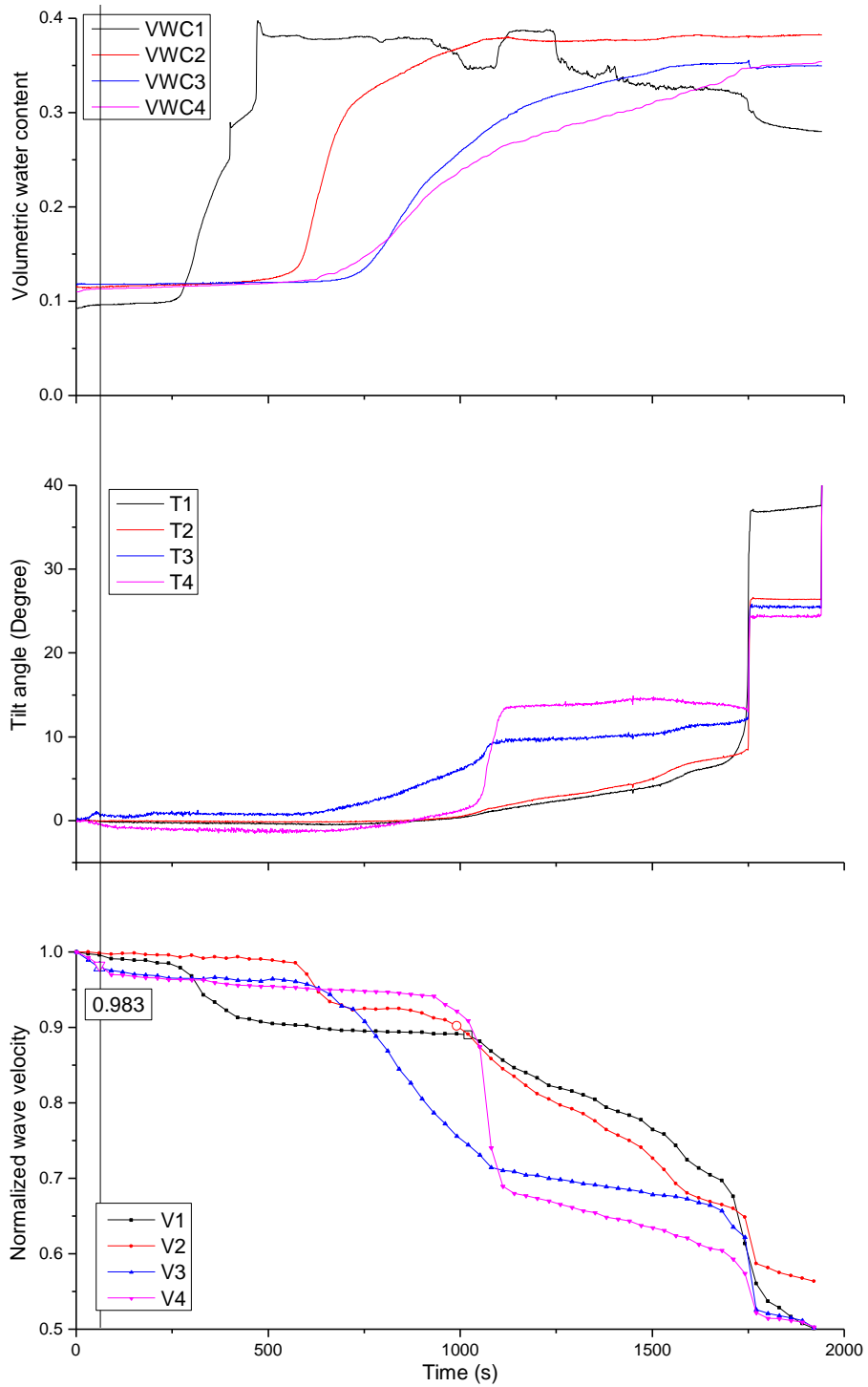
(i) 2-45-15-1.4

Figure 6.1 (continued): Time series data of volumetric water content, tilt angle and normalized wave velocity during tests under different conditions.
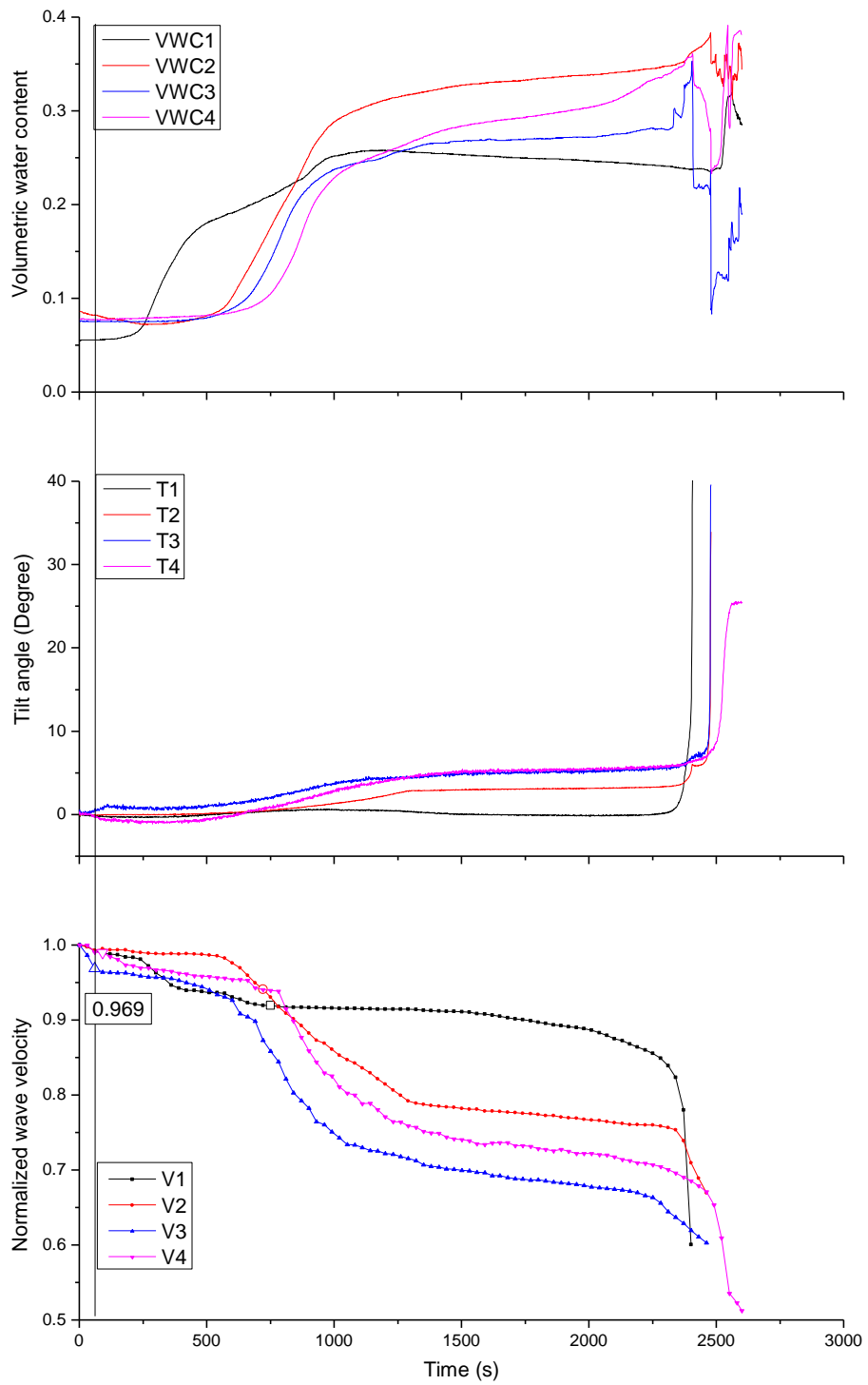
(j) 2-40-10-1.2

Figure 6.1 (continued): Time series data of volumetric water content, tilt angle and normalized wave velocity during tests under different conditions.
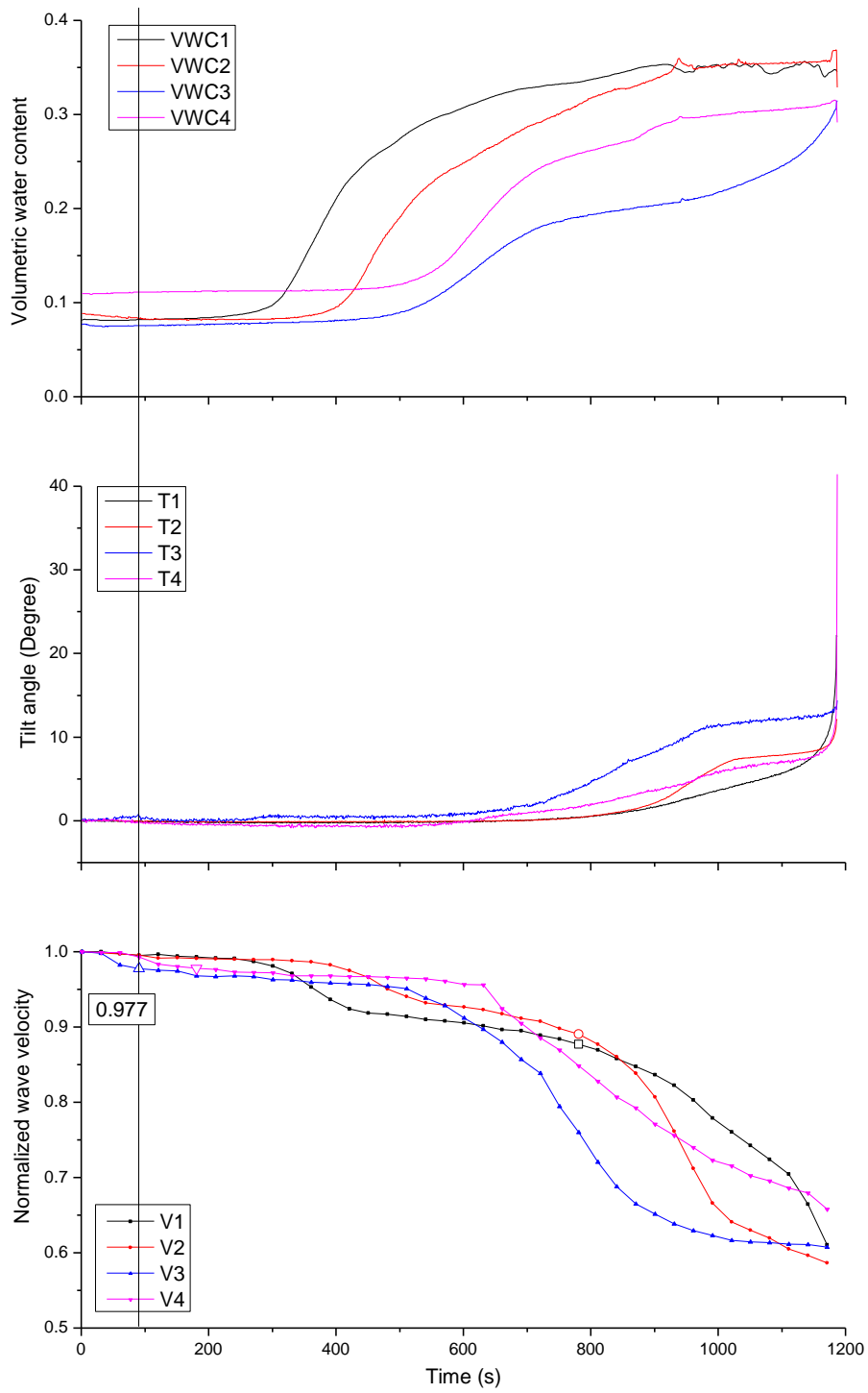
(k) 2-40-10-1.3

Figure 6.1 (continued): Time series data of volumetric water content, tilt angle and normalized wave velocity during tests under different conditions.
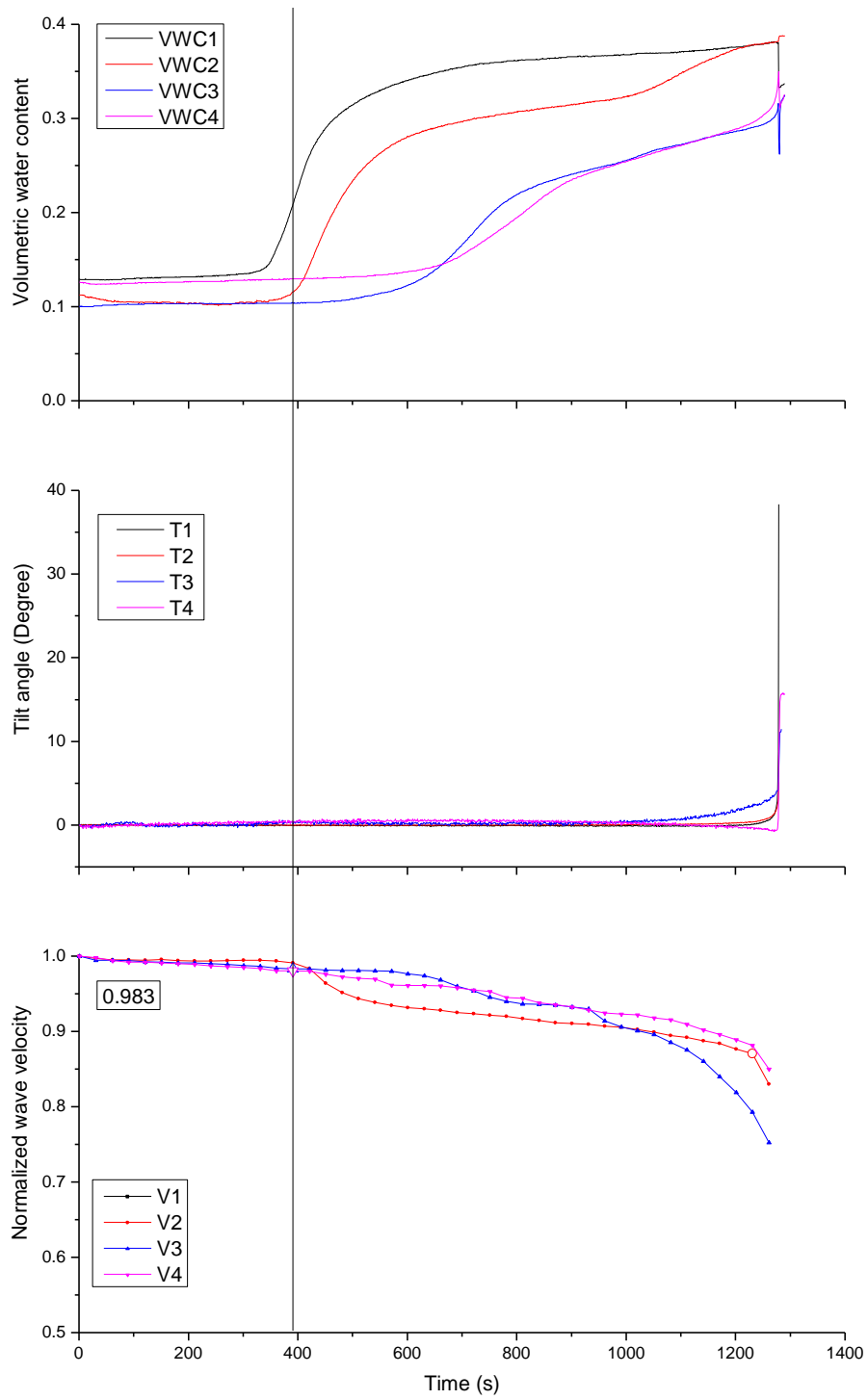
(l) 2-40-10-1.4

Figure 6.1 (continued): Time series data of volumetric water content, tilt angle and normalized wave velocity during tests under different conditions.
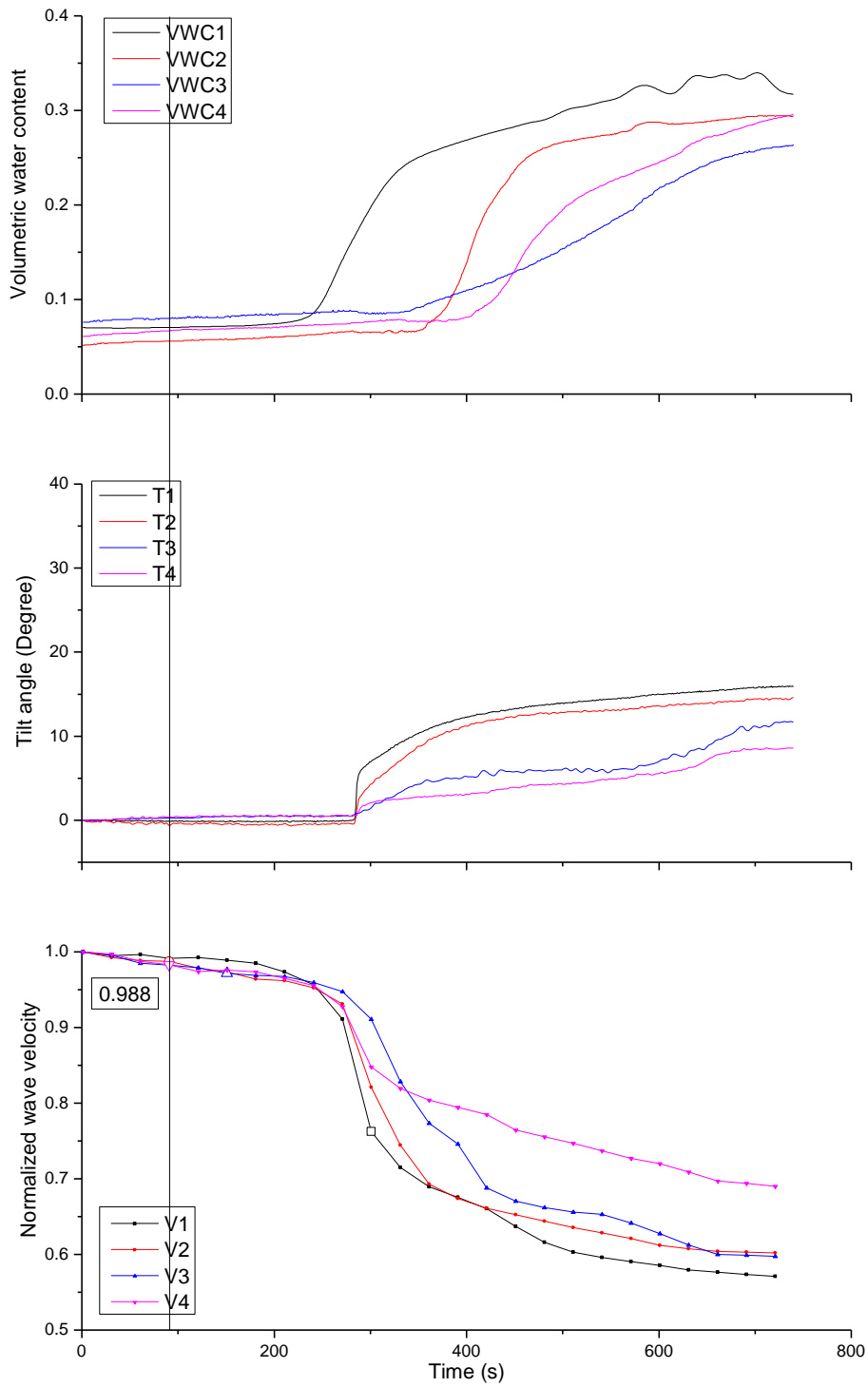
(m) 2-50-10-1.2

Figure 6.1 (continued): Time series data of volumetric water content, tilt angle and

normalized wave velocity during tests under different conditions.
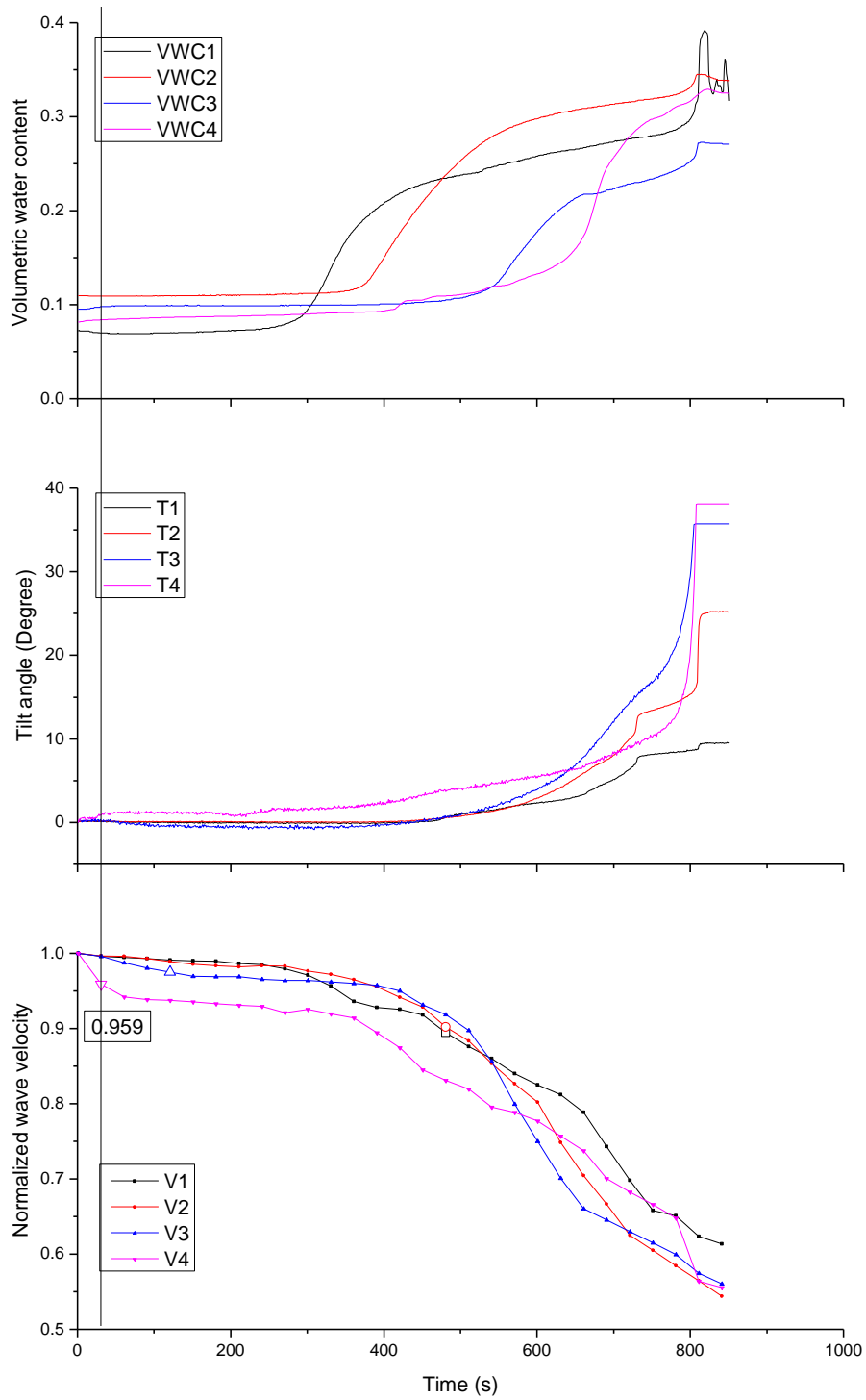
(n) 2-50-10-1.3

Figure 6.1 (continued): Time series data of volumetric water content, tilt angle and normalized wave velocity during tests under different conditions.
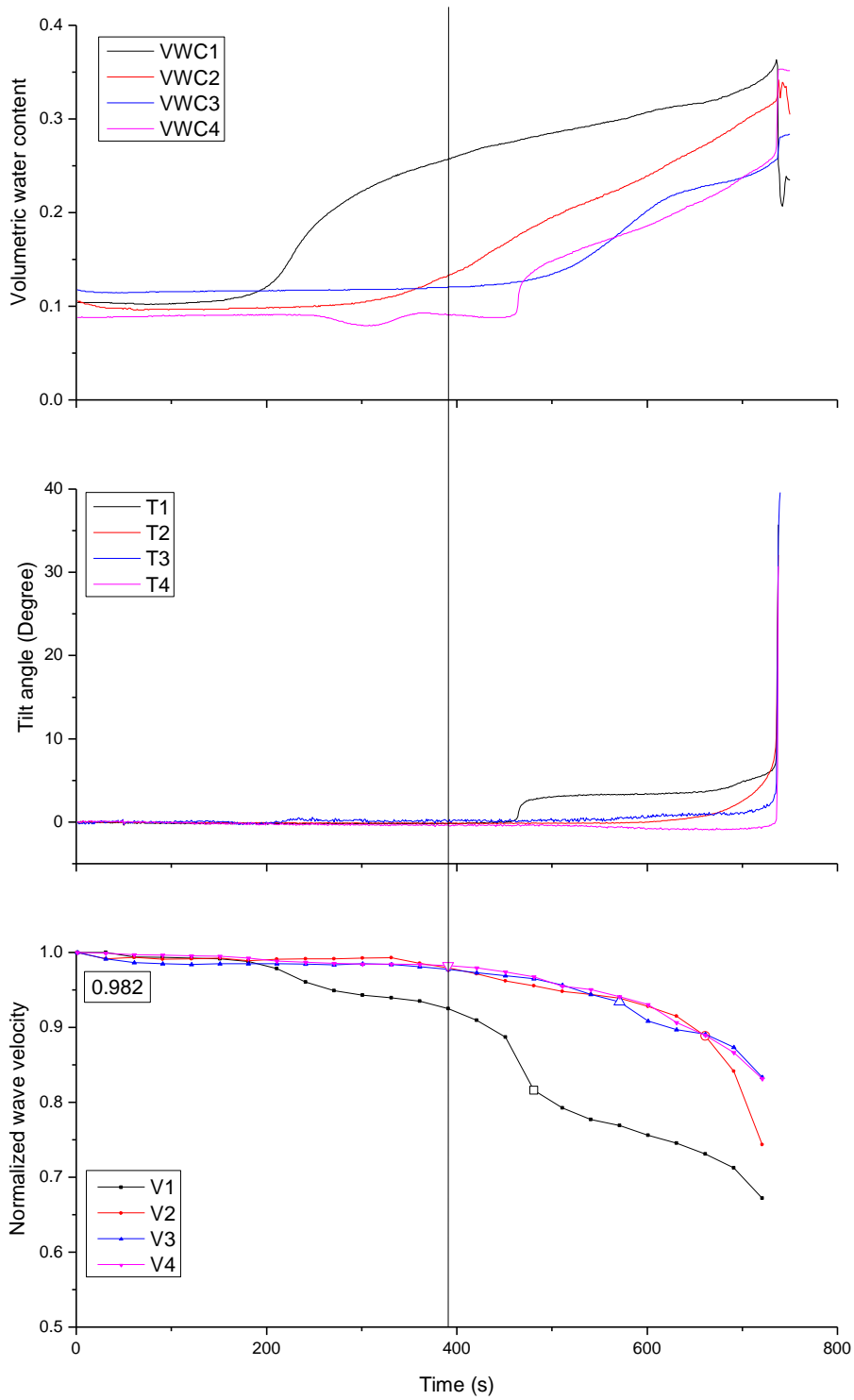
(o) 2-50-10-1.4

Figure 6.1 (continued): Time series data of volumetric water content, tilt angle and normalized wave velocity during tests under different conditions.

(a)2-45-5-1.2 (90s)
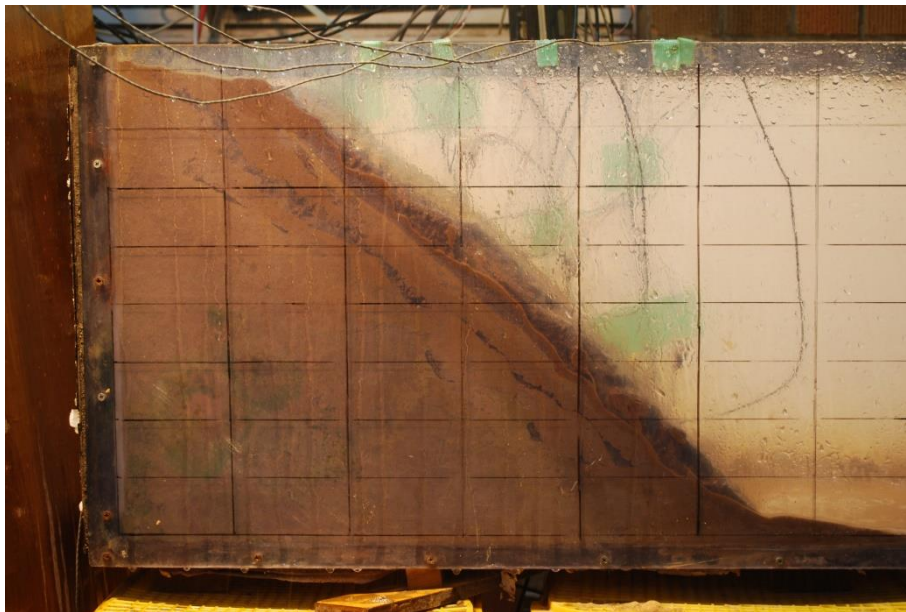
(b)2-45-5-1.3 (90s)

Figure 6.2: Wetting front during rainfall during tests under different conditions.
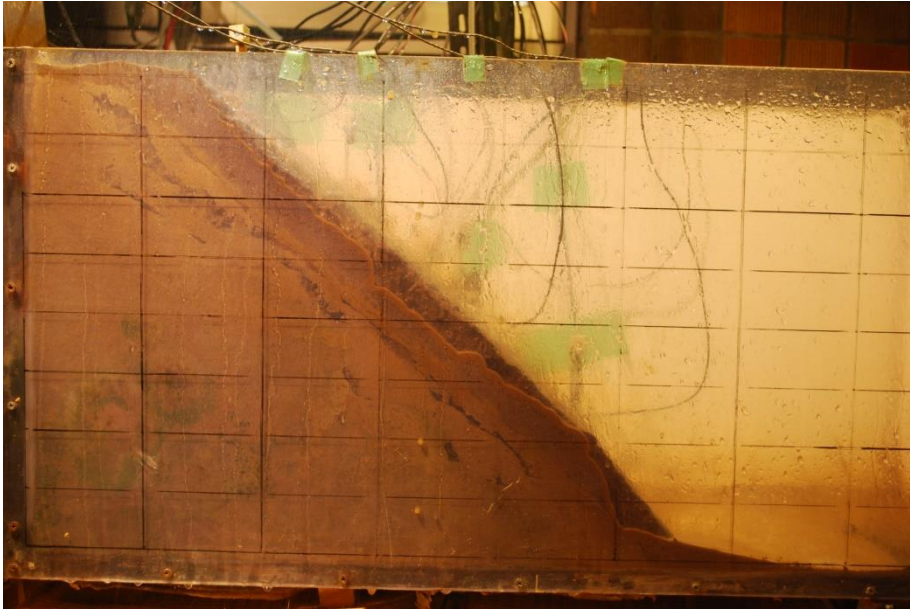
(c)2-45-5-1.4(120s)
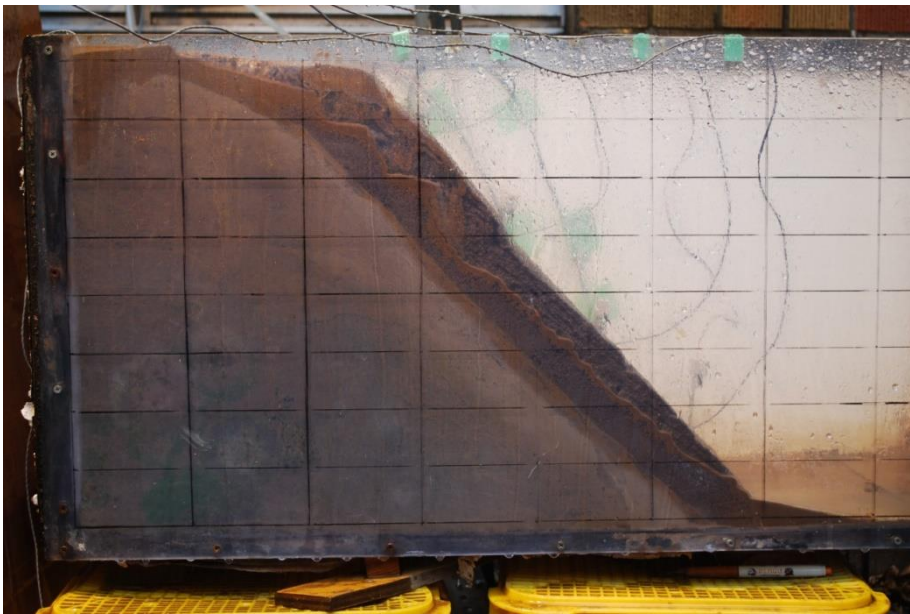
(d)2-45-10-1.2(390s)

Figure 6.2 (continued): Wetting front during rainfall during tests under different conditions.

(e)2-45-10-1.3(390s)
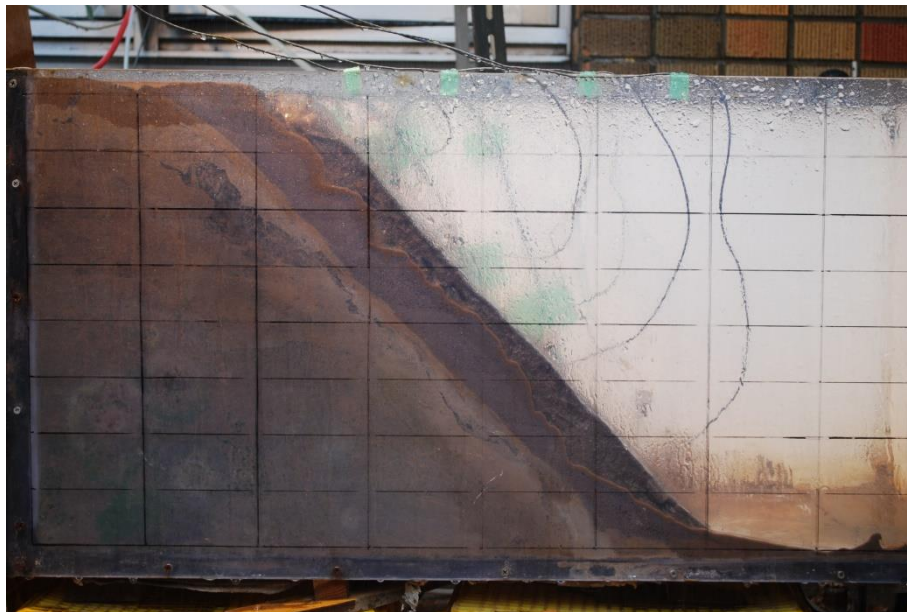
(f)2-45-10-1.4(330s)

Figure 6.2 (continued): Wetting front during rainfall during tests under different conditions.
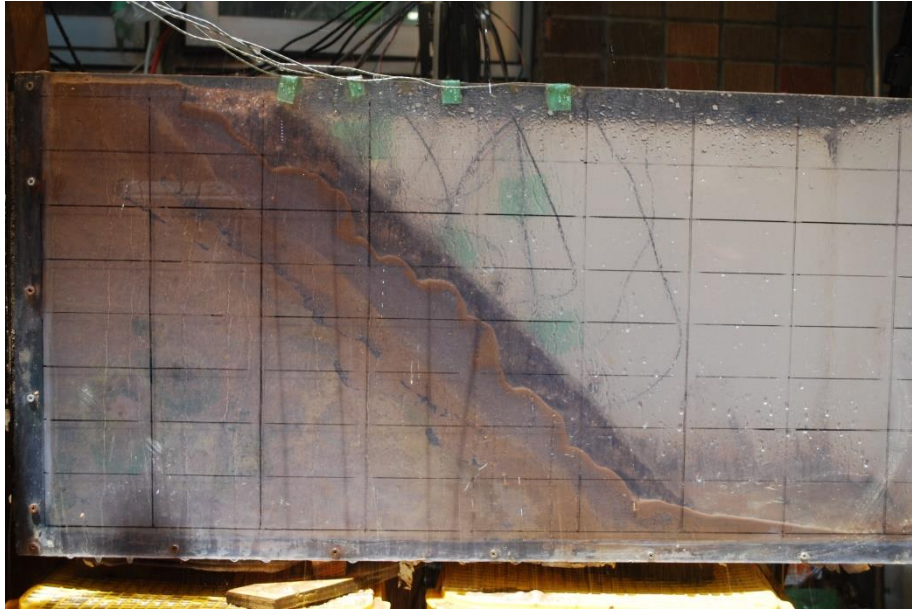
(g) 2-45-15-1.2(120s)
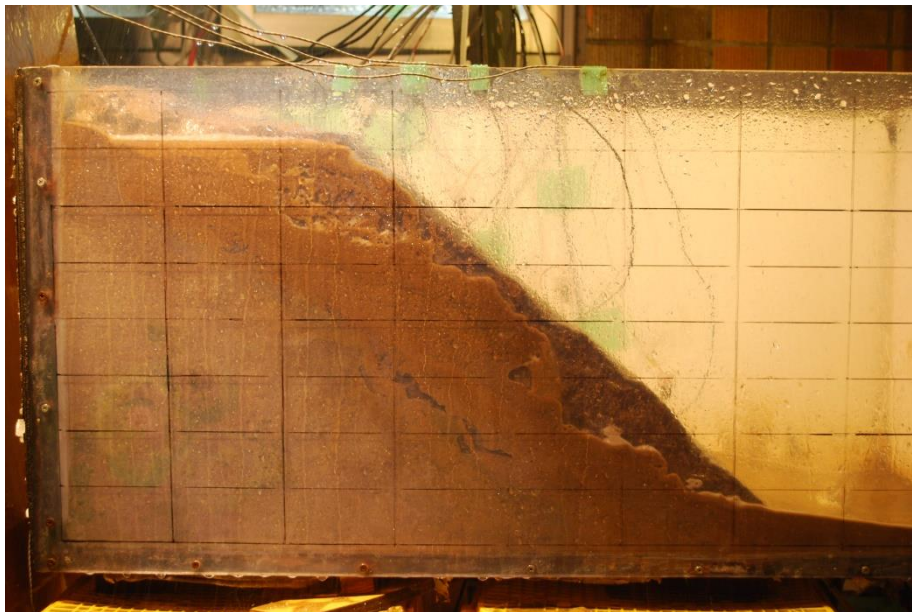
(h) 2-45-15-1.3(1560s)

Figure 6.2 (continued): Wetting front during rainfall during tests under different conditions.
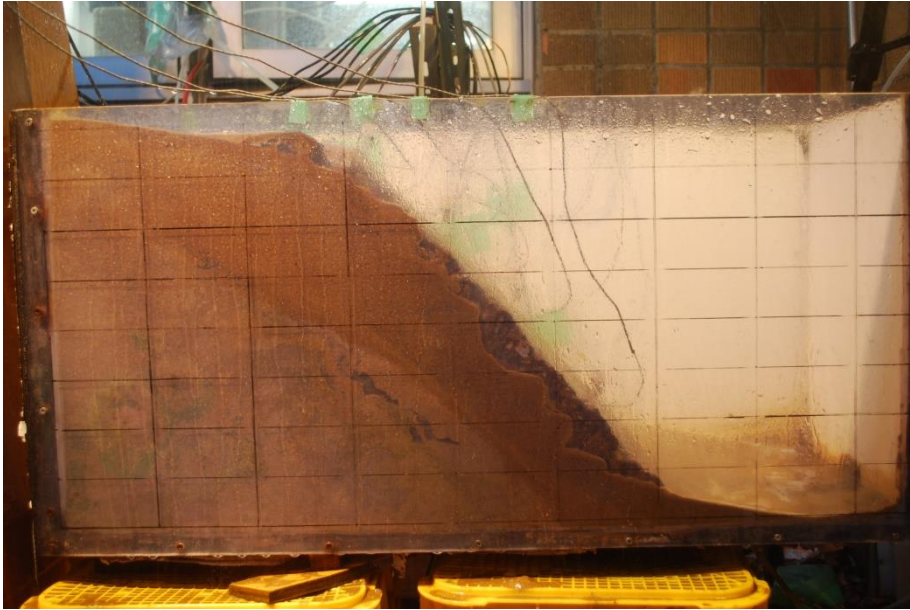
(i) 2-45-15-1.4(1050s)

(j) 2-40-10-1.2(2250s)

Figure 6.2 (continued): Wetting front during rainfall during tests under different conditions.

(k) 2-40-10-1.3(840s)

(l) 2-40-10-1.4(840s)

Figure 6.2 (continued): Wetting front during rainfall during tests under different conditions.

(m) 2-50-10-1.2(330s)

(n) 2-50-10-1.3(510s)

Figure 6.2 (continued): Wetting front during rainfall during tests under different conditions.

(o) 2-50-10-1.4(480s)

Figure 6.2 (continued): Wetting front during rainfall during tests under different conditions.

Figure 6.3 shows the change of elastic wave velocity with volumetric water content and tilt angle with different surface layer thicknesses, dry densities and slope angles. It can be seen that both volumetric water content and tilt angle can decrease the elastic wave velocity. As the volumetric water content increased, the normalized wave velocity decreased gradually, followed by a sharp decrease resulting from an increase in tilt angle.

Also, it can be seen that the normalized wave velocity kept decreasing initially with no change in tilt angle. This decrease resulted from the increase of volumetric water content. As the tilt angle began to rise, the normalized wave velocity decreased at larger rate.
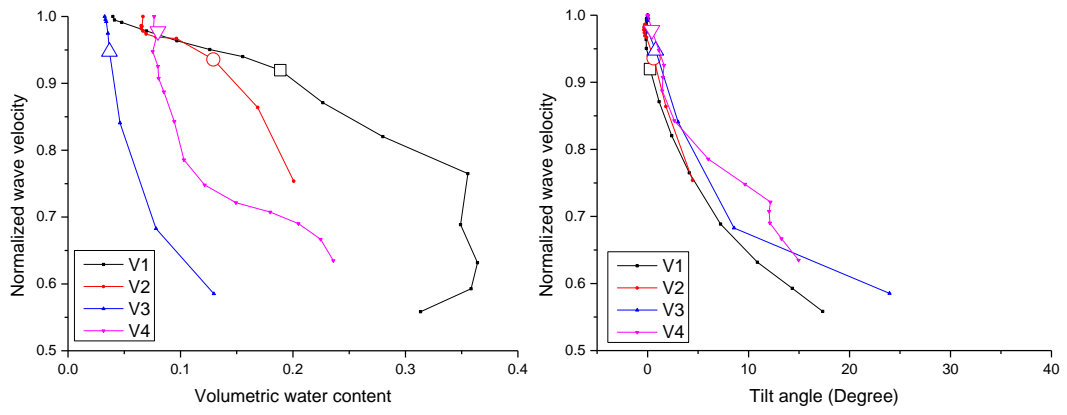
(a)2-45-5-1.2
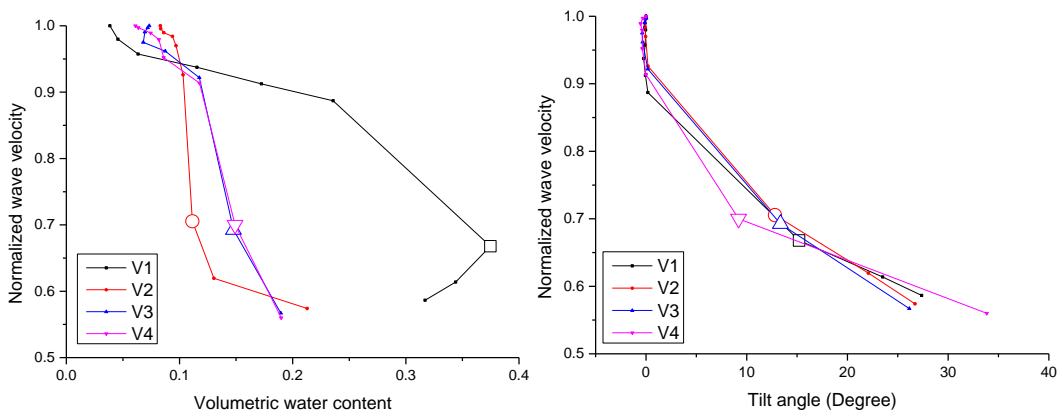
(b)2-45-5-1.3
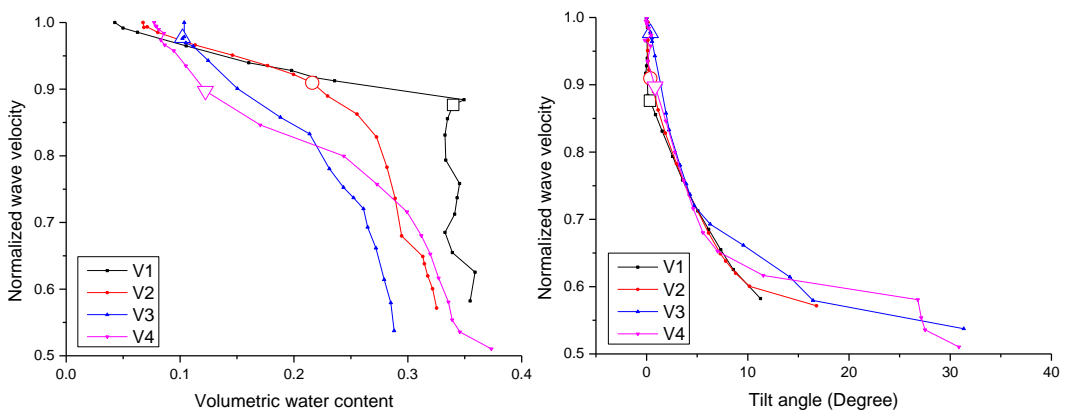
(c)2-45-5-1.4

Figure 6.3: Change of elastic wave velocity with volumetric water content and tilt angle during tests under different conditions.
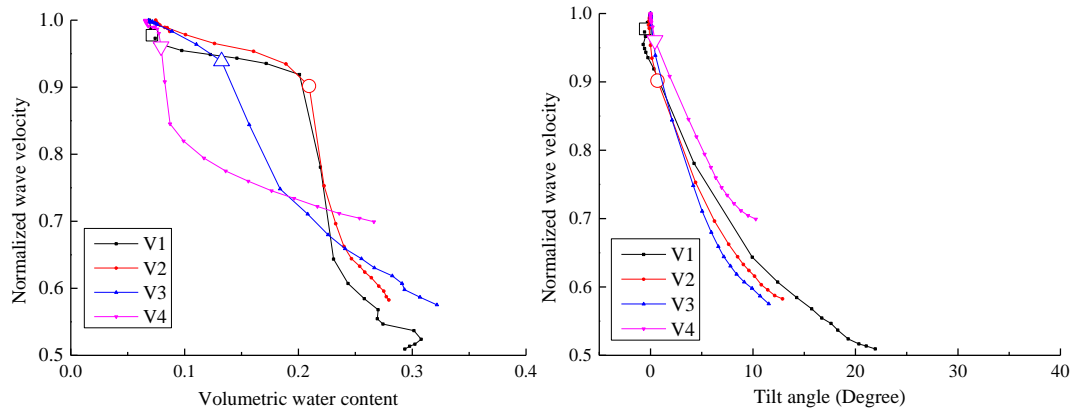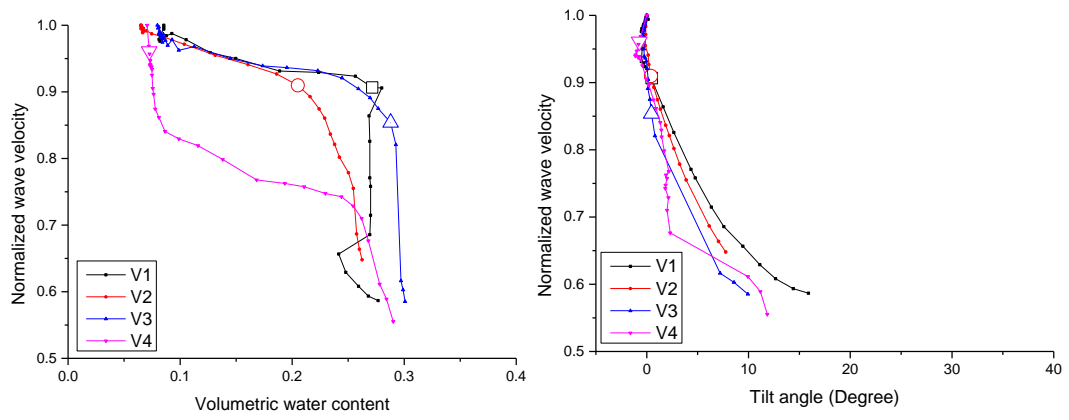
(d)2-45-10-1.2

(e)2-45-10-1.3
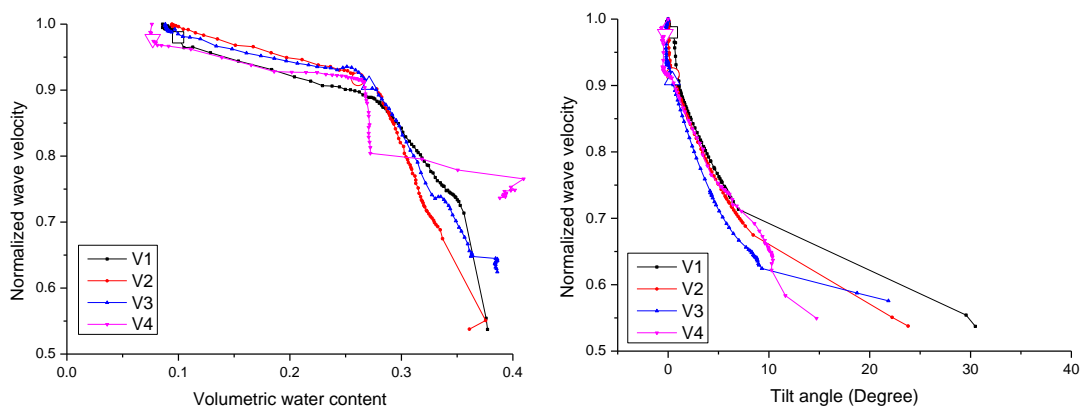
(f)2-45-10-1.4

Figure 6.3 (continued): Change of elastic wave velocity with volumetric water content and tilt angle during tests under different conditions.
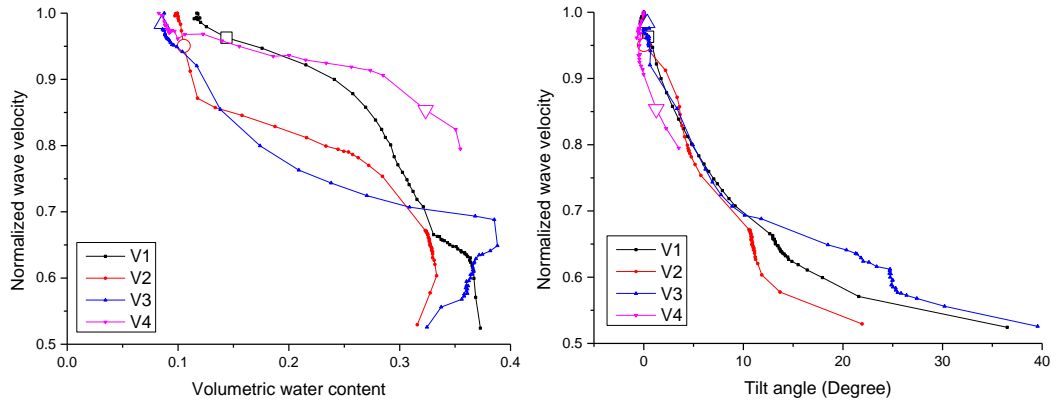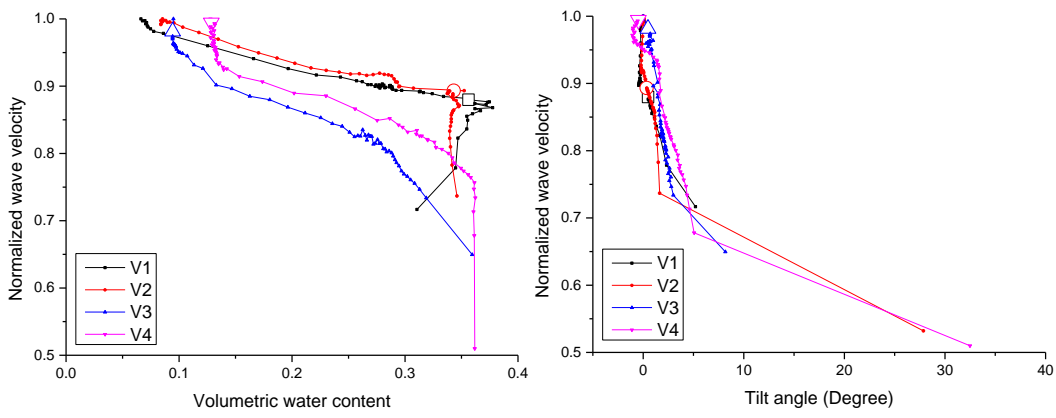
(g) 2-45-15-1.2

(h) 2-45-15-1.3
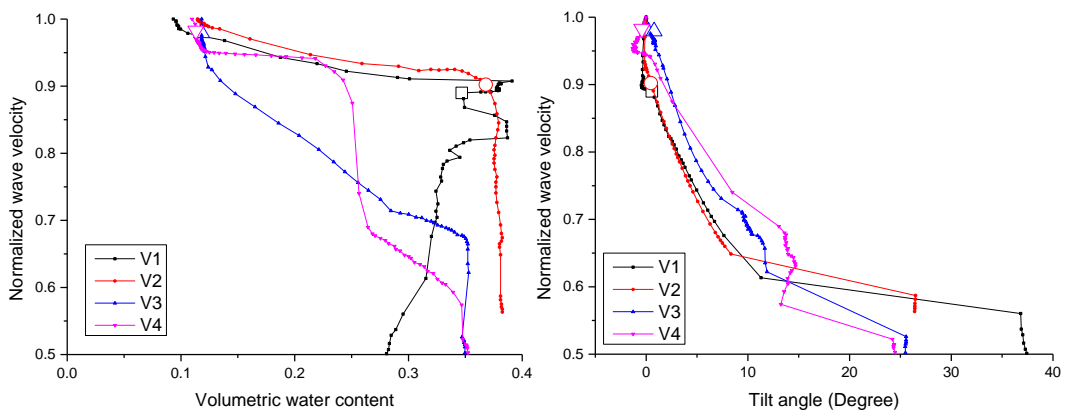
(i) 2-45-15-1.4

Figure 6.3(continued): Change of elastic wave velocity with volumetric water content and tilt angle during tests under different conditions.
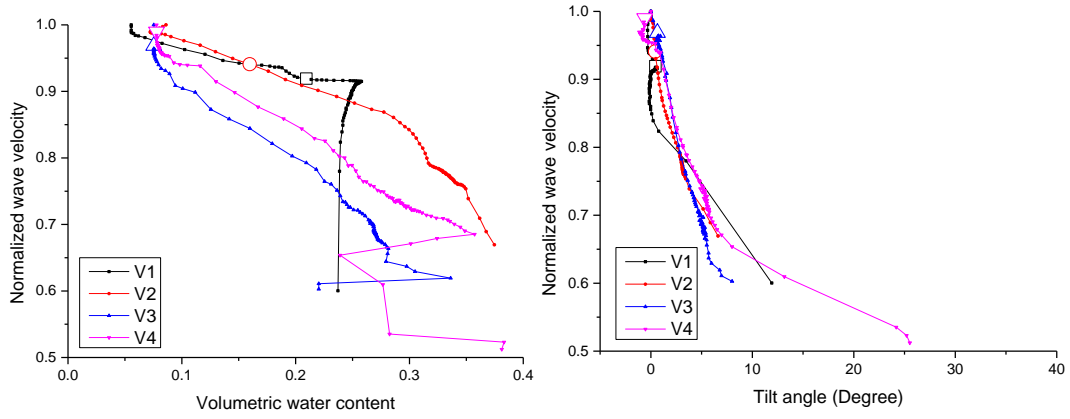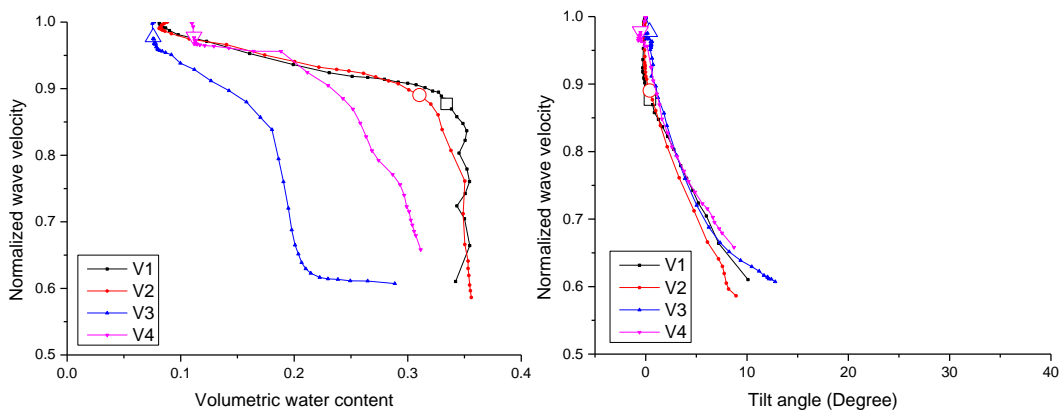
(j) 2-40-10-1.2

(k) 2-40-10-1.3
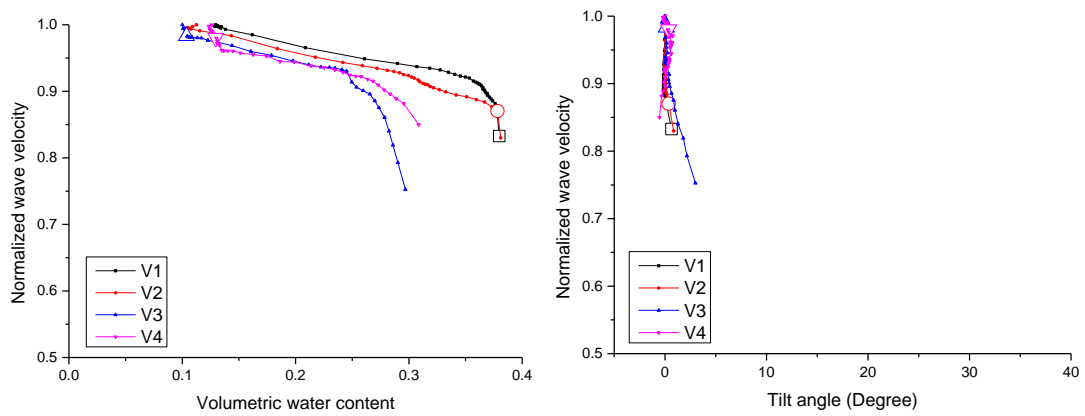

(l) 2-40-10-1.4

Figure 6.3(continued): Change of elastic wave velocity with volumetric water content and tilt angle during tests under different conditions.
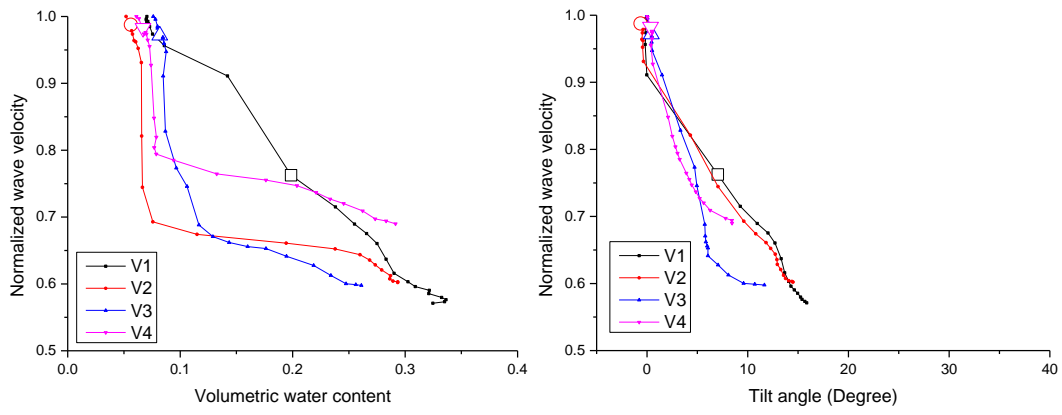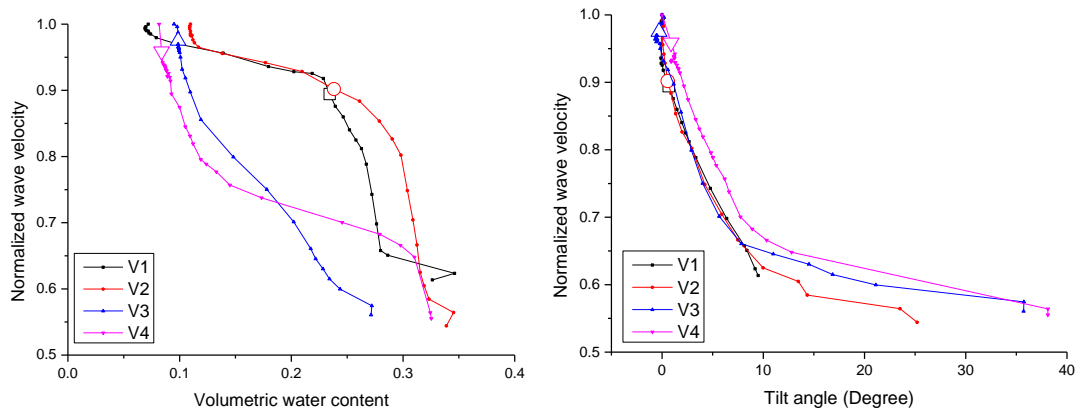
(m) 2-50-10-1.2


(n) 2-50-10-1.3
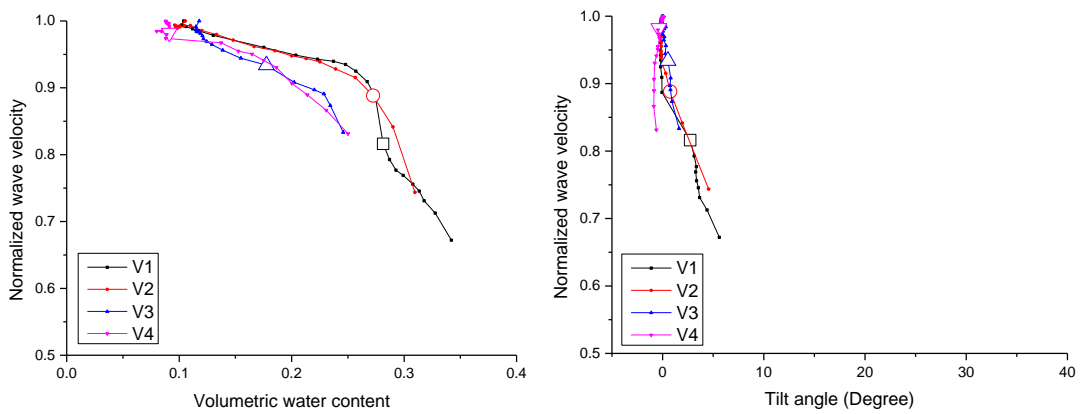
(o) 2-50-10-1.4

Figure 6.3(continued): Change of elastic wave velocity with volumetric water content and tilt angle during tests under different conditions.

Figure 6.4 shows the relationship between normalized elastic wave velocity against volumetric water content and tilt angle by means of a three-dimensional plot. A gradual decrease in wave velocities was followed by a rapid decrease once the failure was initiated. Wave velocity continued decreasing with an accelerated rate by the coupled effect of increasing water content and deformation that appeared to be interrelated.
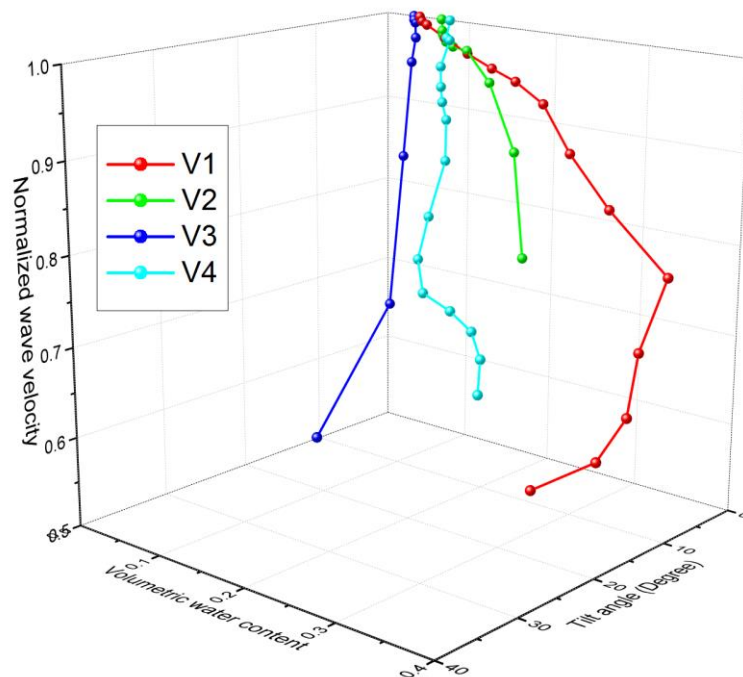
(a)2-45-5-1.2

Figure 6.4: Relationship between normalized elastic wave velocity against volumetric water content and tilt angle, presented through a 3-D plot
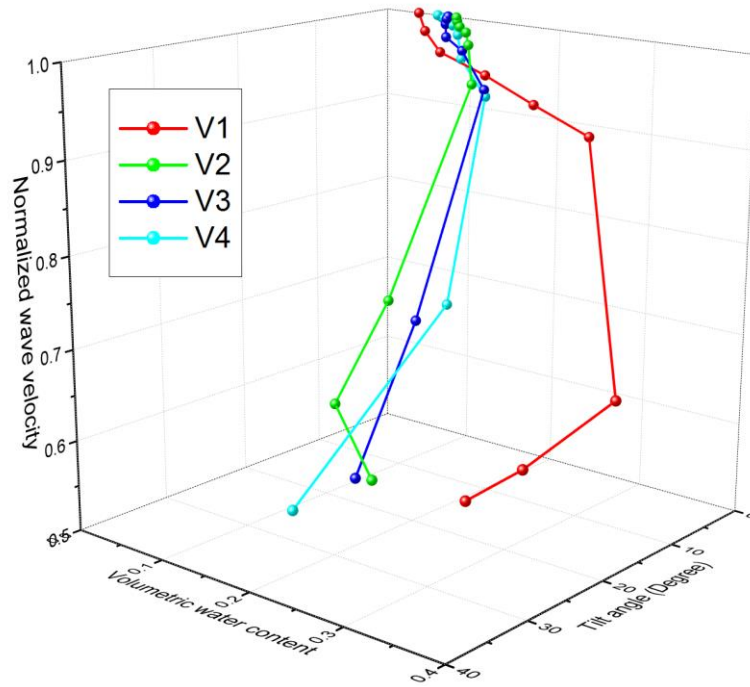
(b)2-45-5-1.3
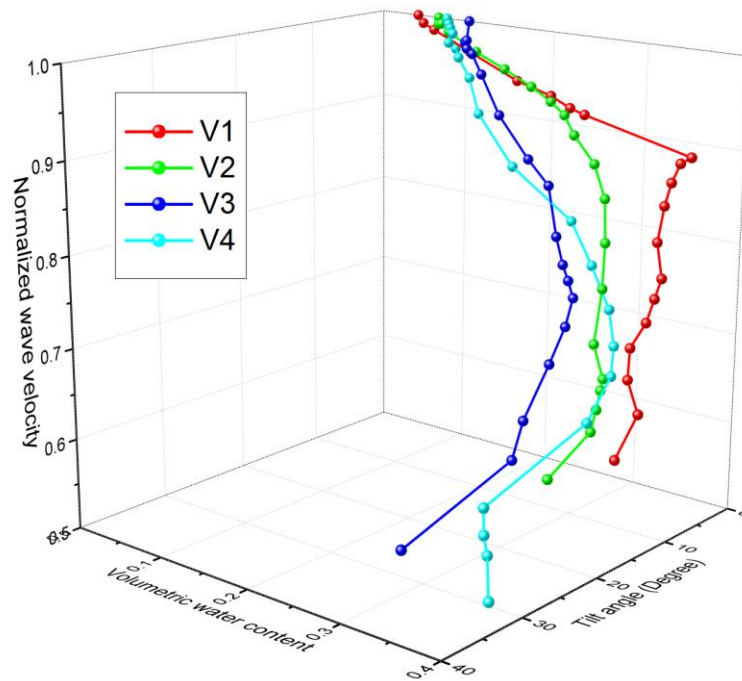
(c)2-45-5-1.4

Figure 6.4 (continued): Relationship between normalized elastic wave velocity against volumetric water content and tilt angle, presented through a 3-D plot
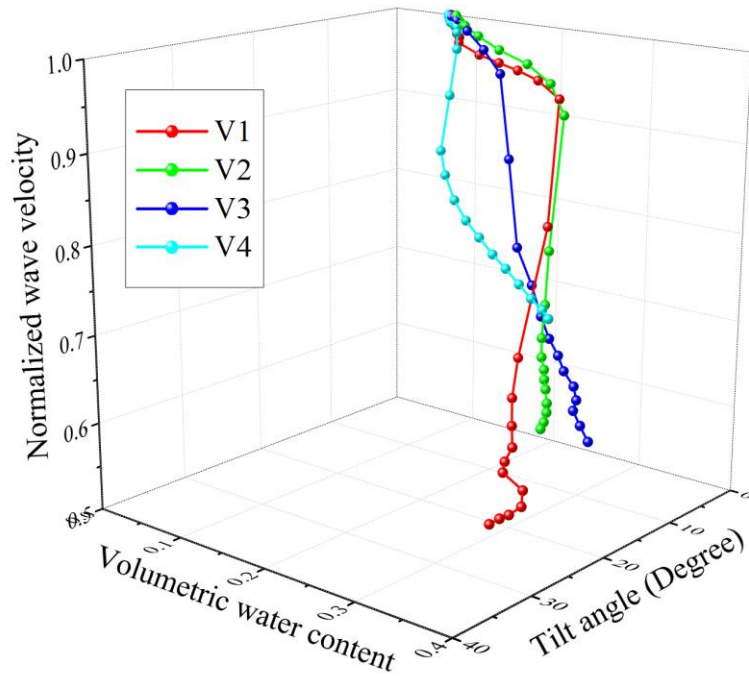
(d)2-45-10-1.2
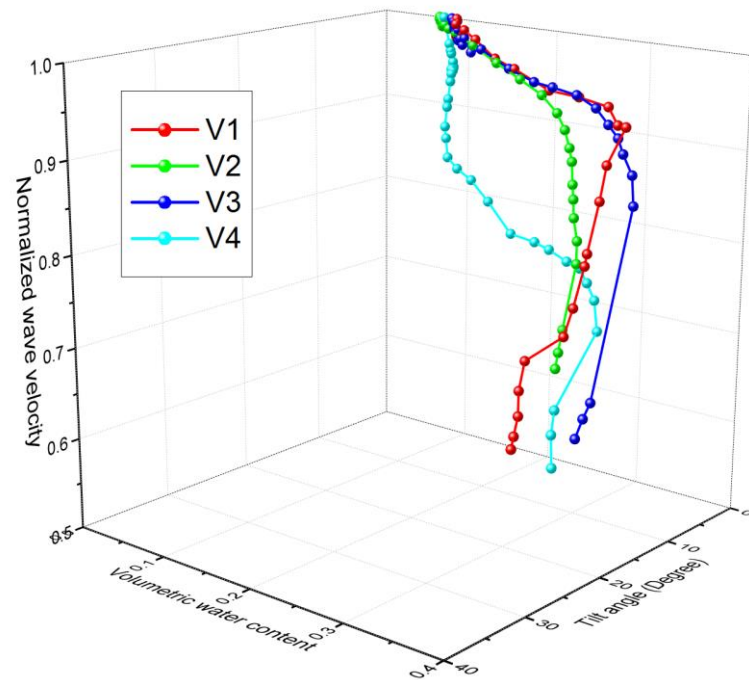
(e)2-45-10-1.3

Figure 6.4 (continued): Relationship between normalized elastic wave velocity against volumetric water content and tilt angle, presented through a 3-D plot
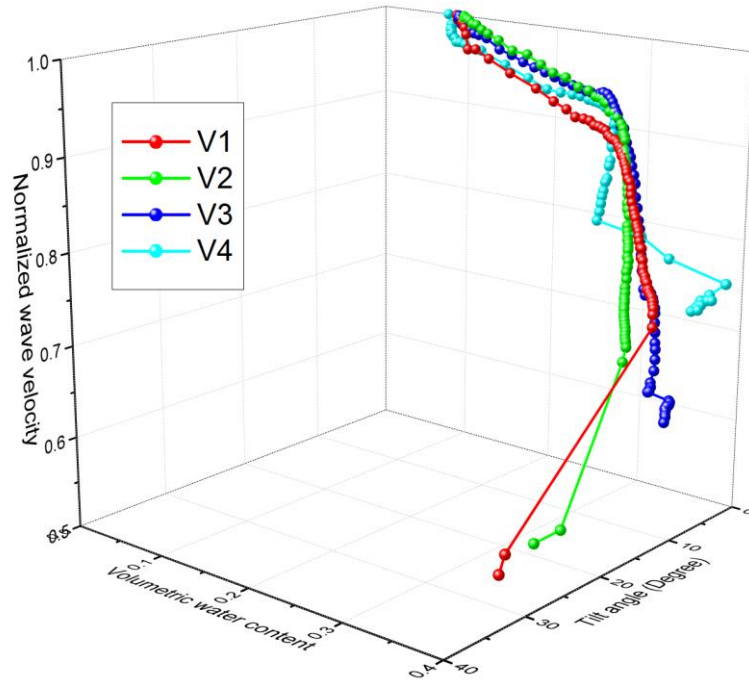
(f)2-45-10-1.4
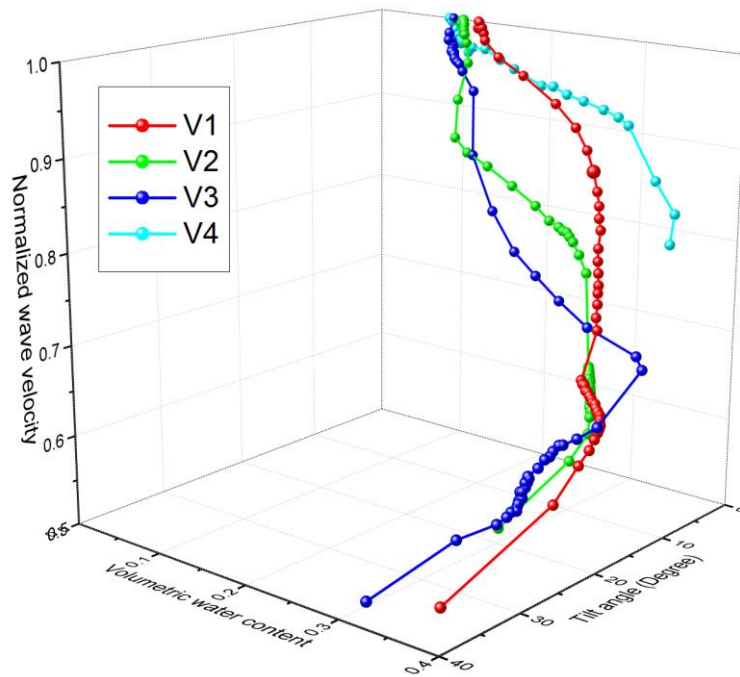
(g) 2-45-15-1.2

Figure 6.4 (continued): Relationship between normalized elastic wave velocity against volumetric water content and tilt angle, presented through a 3-D plot
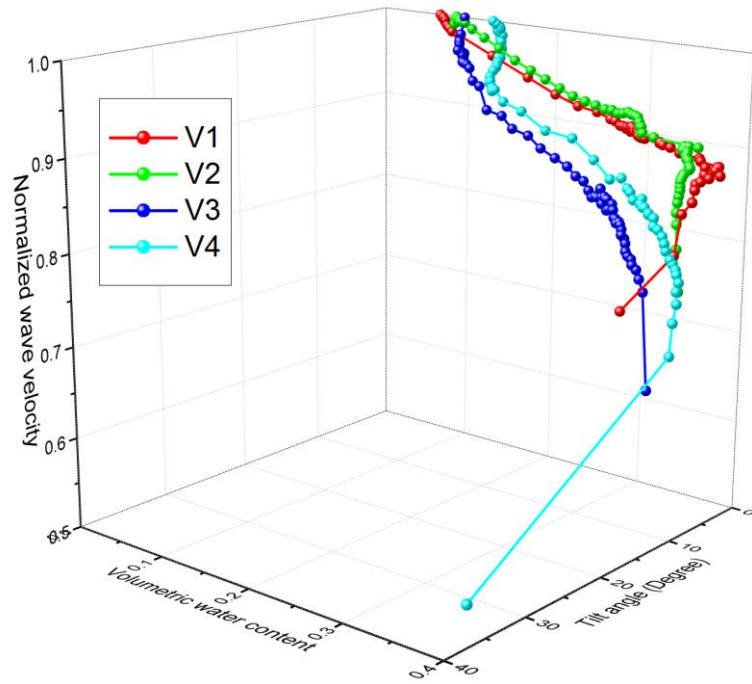
(h) 2-45-15-1.3
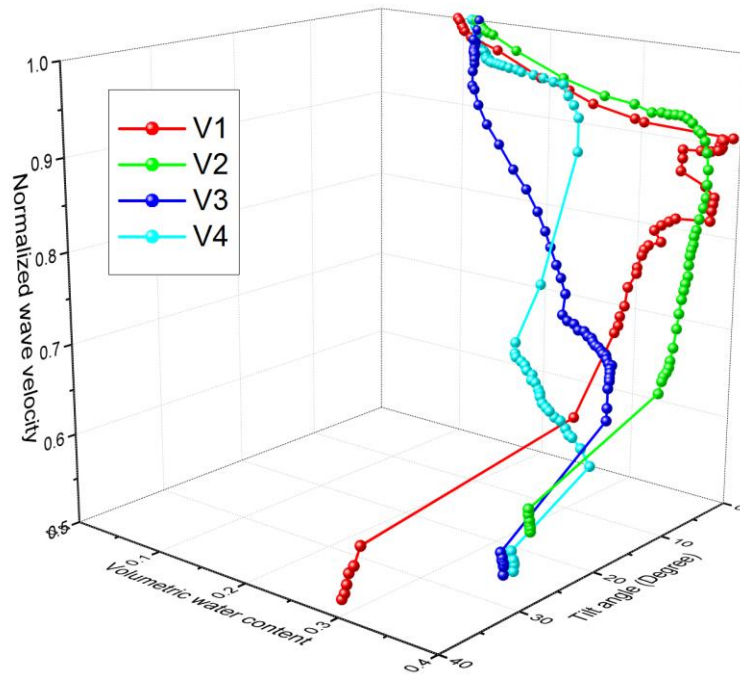
(i) 2-45-15-1.4

Figure 6.4 (continued): Relationship between normalized elastic wave velocity against volumetric water content and tilt angle, presented through a 3-D plot
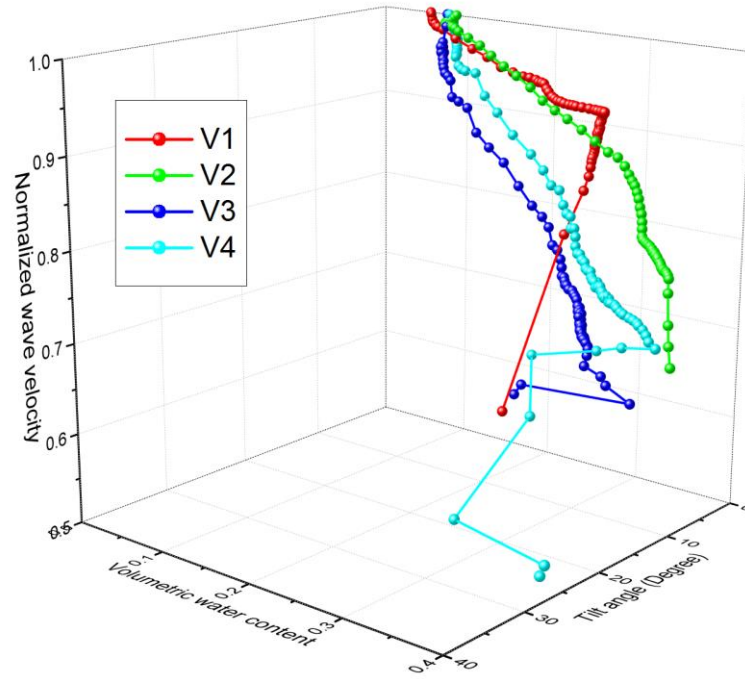
(j) 2-40-10-1.2
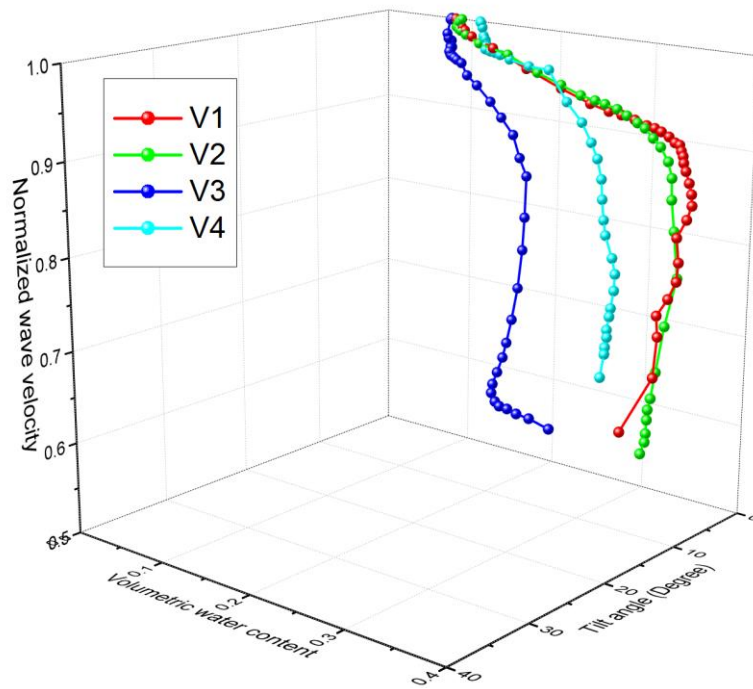
(k) 2-40-10-1.3

Figure 6.4 (continued): Relationship between normalized elastic wave velocity against volumetric water content and tilt angle, presented through a 3-D plot
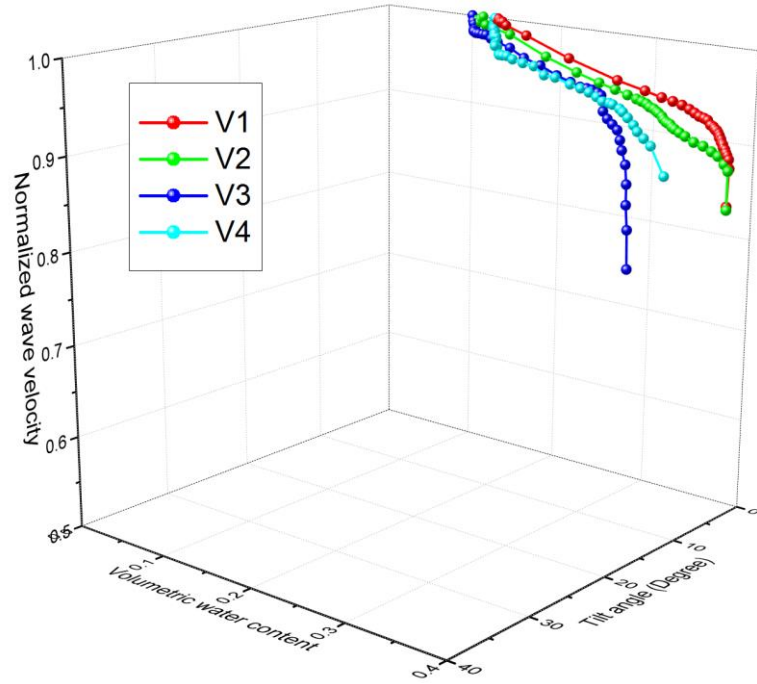
(l) 2-40-10-1.4
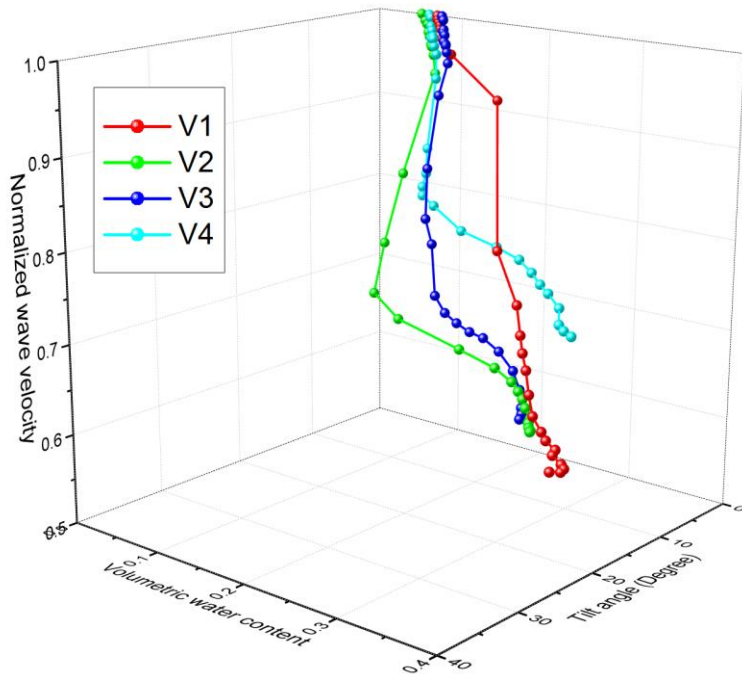
(m) 2-50-10-1.2

Figure 6.4 (continued): Relationship between normalized elastic wave velocity against volumetric water content and tilt angle, presented through a 3-D plot
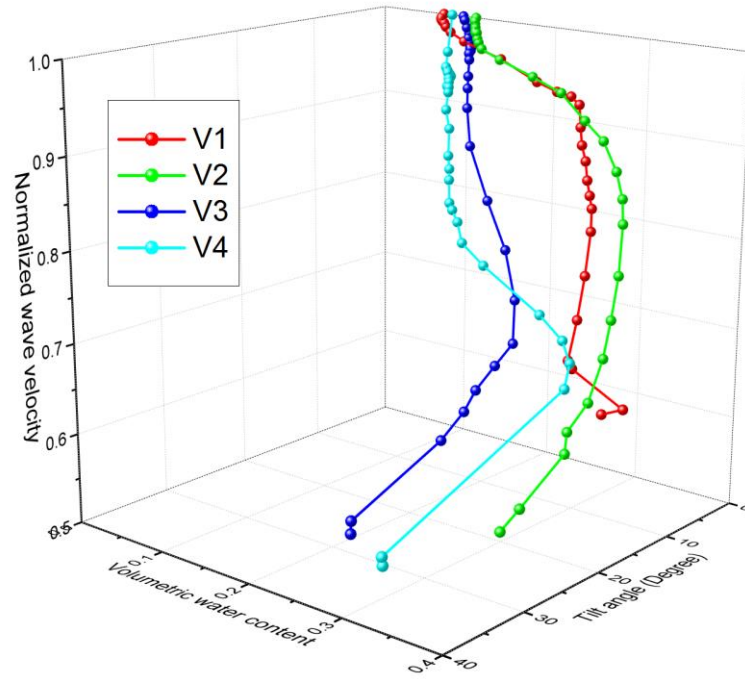
(n) 2-50-10-1.3
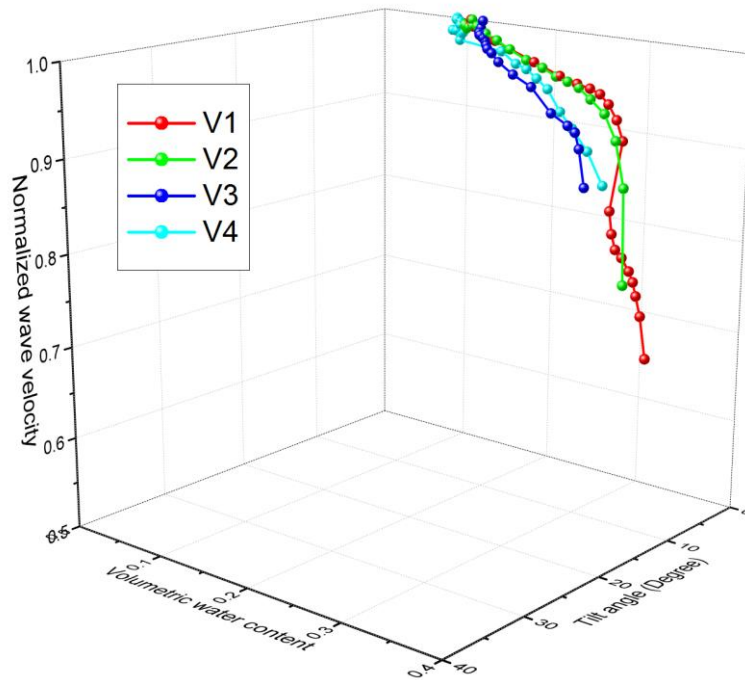

(o) 2-50-10-1.4

Figure 6.4 (continued): Relationship between normalized elastic wave velocity against volumetric water content and tilt angle, presented through a 3-D plot

6.3.2. Effect of Soil Density

Figure 6.5 shows the variation of normalized elastic wave velocity with volumetric water content and tilt angle with different dry densities. From the curves of normalized elastic wave velocity versus volumetric water, the general trend of normalized elastic wave velocity with higher density was located above the curves with lower density, regardless of the slope angle and surface layer thickness. This is because, for the same volumetric water content, the high-density soils have the greater the suction value than the low-density specimens (Gallage & Uchimura, 2010; Jiang et al., 2016; Zhou et al., 2014; Li & Chen, 2016), causing higher wave velocity as a result of higher density. However, a clear difference cannot be observed between these curves of normalized elastic wave velocity with tilt angle for soils having various densities. It meant that the decrease rate of normalized elastic wave velocity with tilt angle seemed to be independent of density.

Figure 6.6 shows the effect of density of soil on failure average volumetric water content and failure time. Failure average volumetric water content and failure time are defined as the average volumetric water content and elapsed time, respectively, when the elastic wave velocity accelerates to decrease. It can be seen that the failure average volumetric water content and failure time increased as the density increased. In other words, slope with loose deposit initiated failure earlier than that with dense deposit. Low initial matric suction of loose specimens can dissipate very quickly on water injection. Hence, loose soils tend to lose their strength much rapidly and initiate failure earlier than dense soils (Irfan 2014).
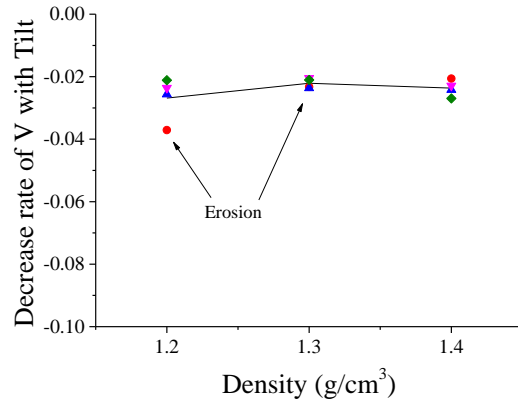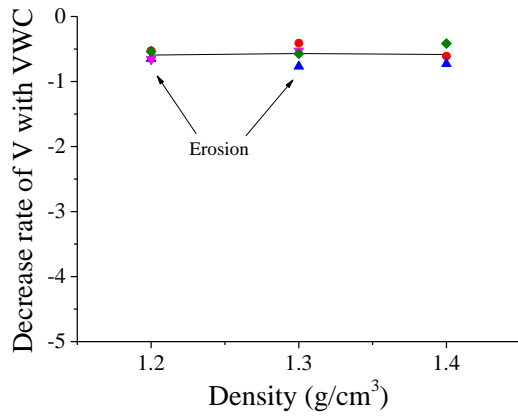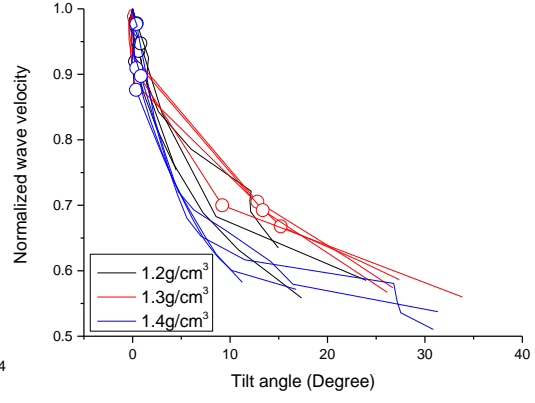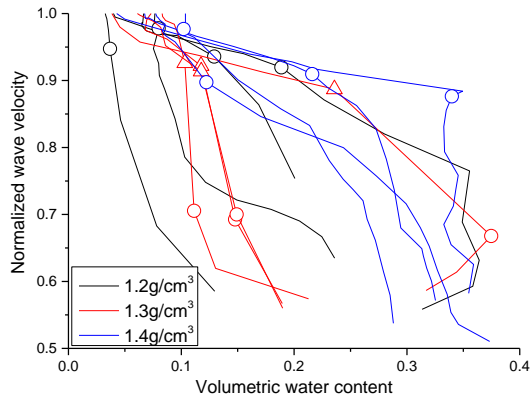
(a)45°-5cm
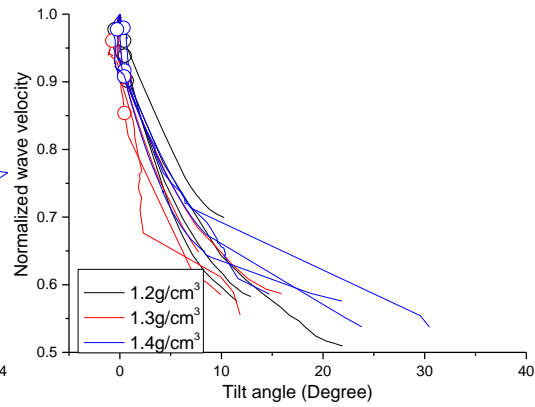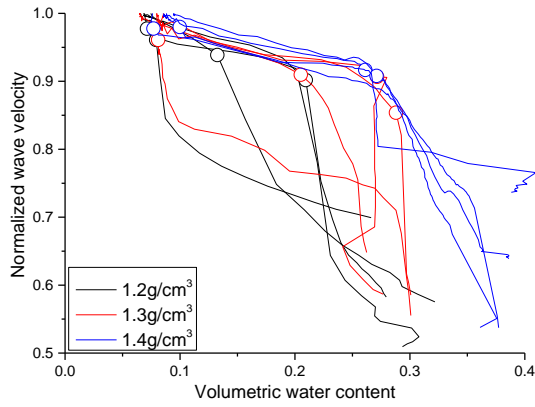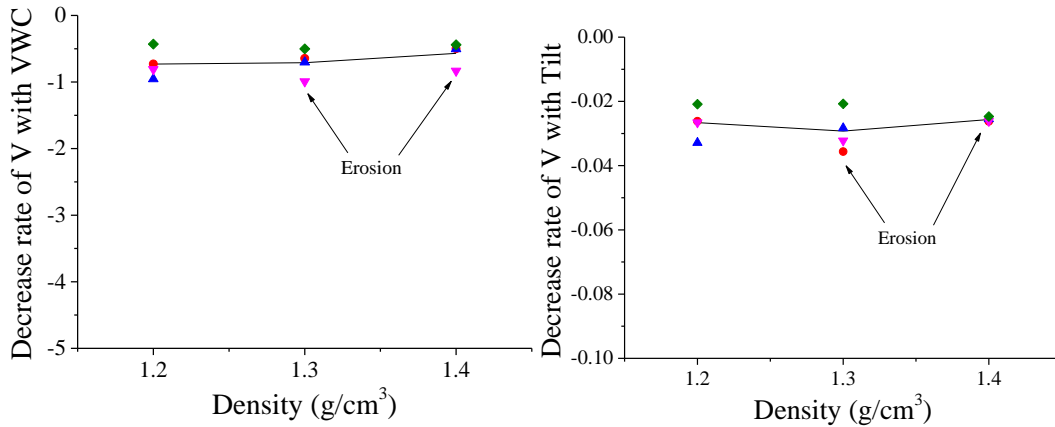
(b)45°-10cm
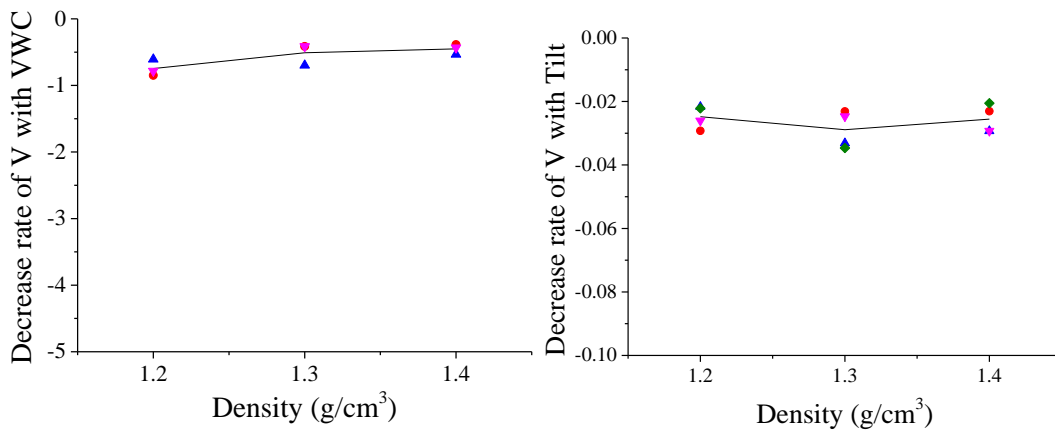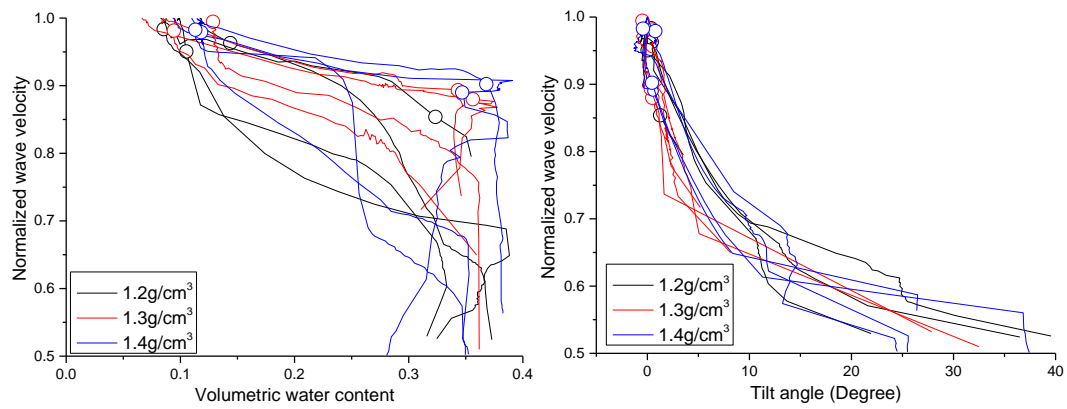
(c)45°-15cm

Figure 6.5: Effect of density of soil on change trend of elastic wave velocity with volumetric water content and tilt angle.
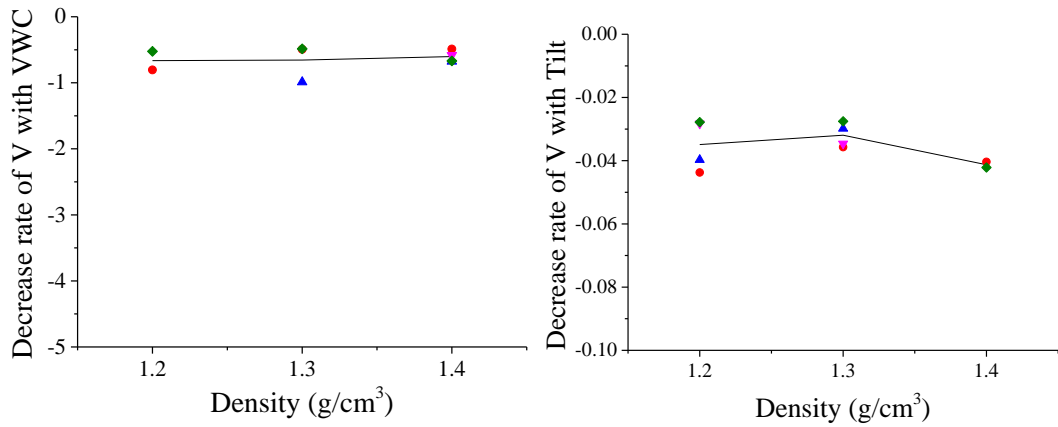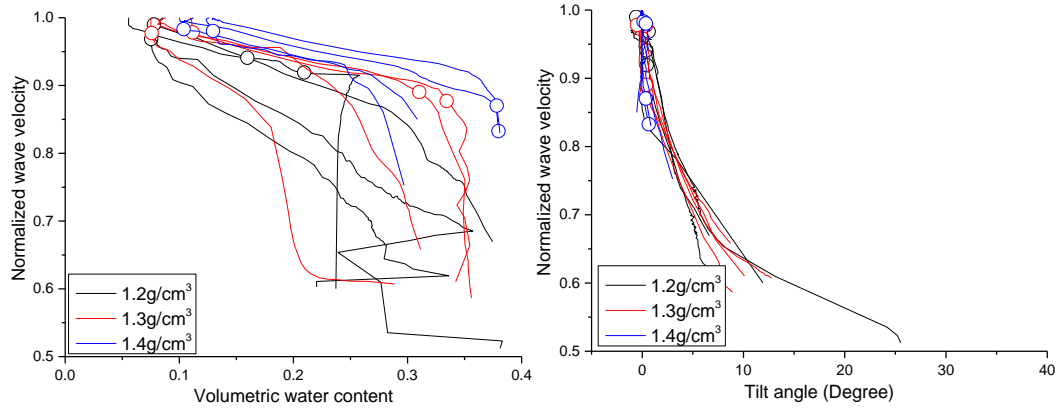
(d)40°-10cm
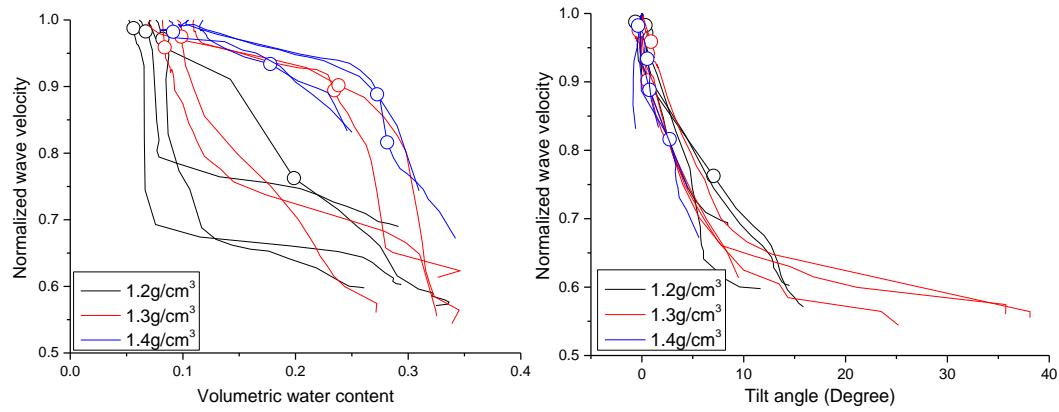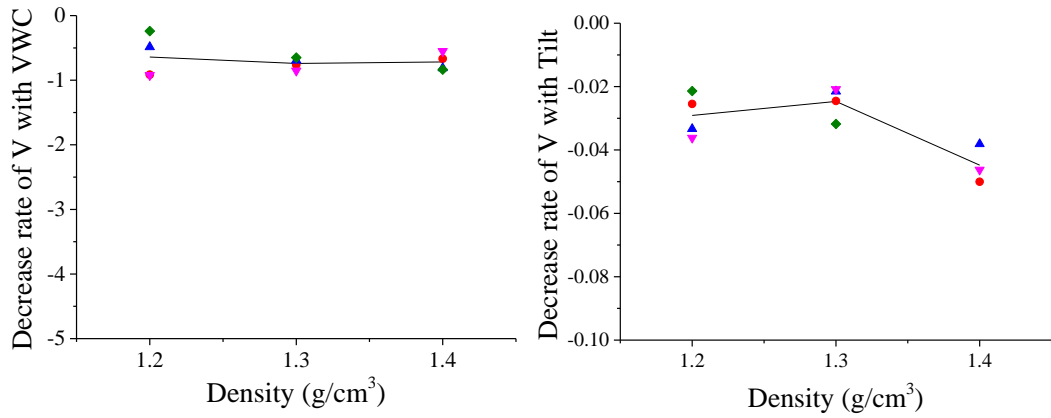
(d)50°-10cm

Figure 6.5(continued): Effect of density of soil on change trend of elastic wave velocity with volumetric water content and tilt angle.
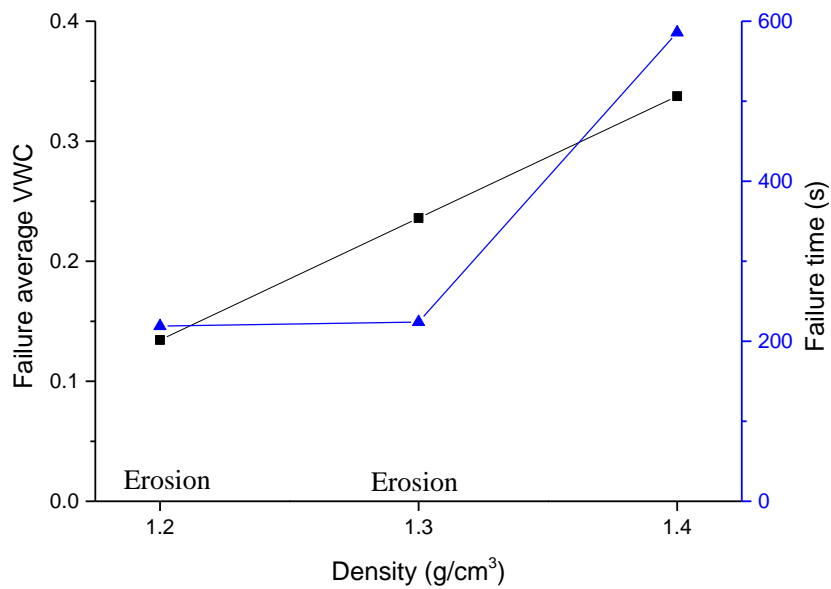
(a)45°-5cm
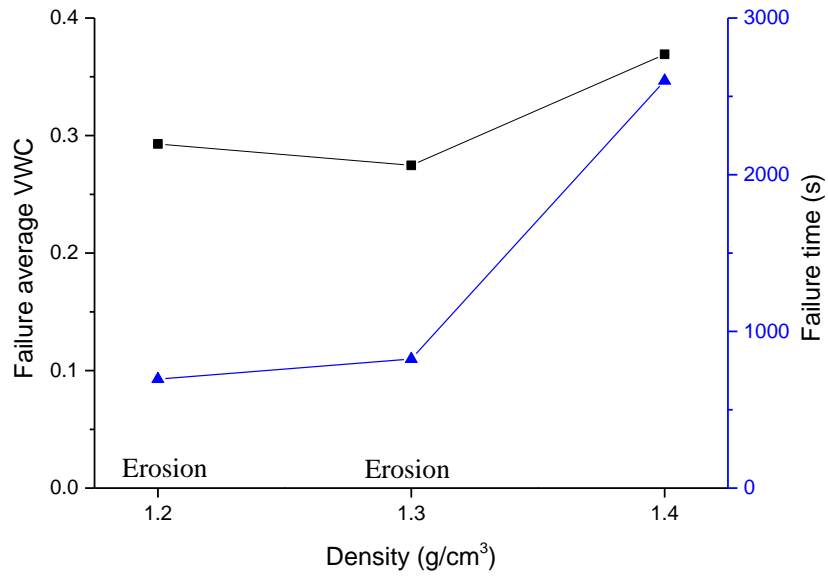
(b)45°-10cm

Figure 6.6: Effect of density of soil on failure average volumetric water content and
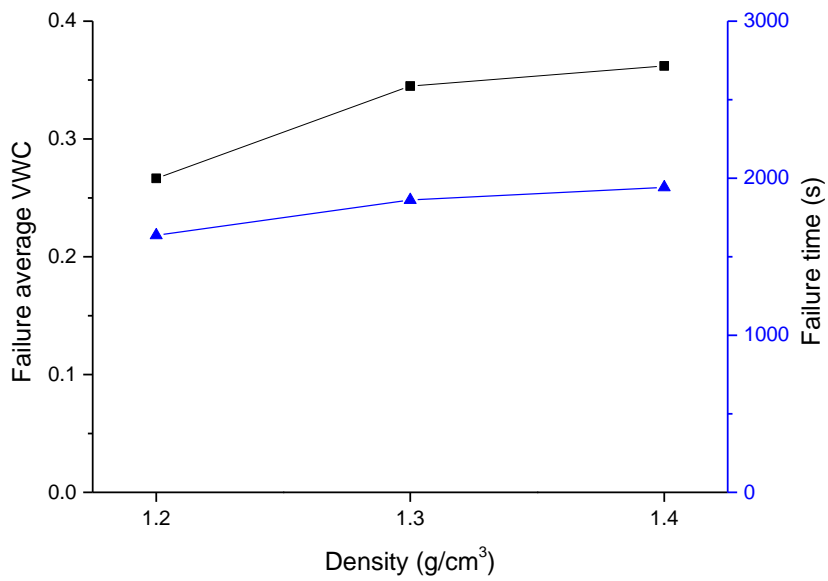
failure time.

(c)45°-15cm
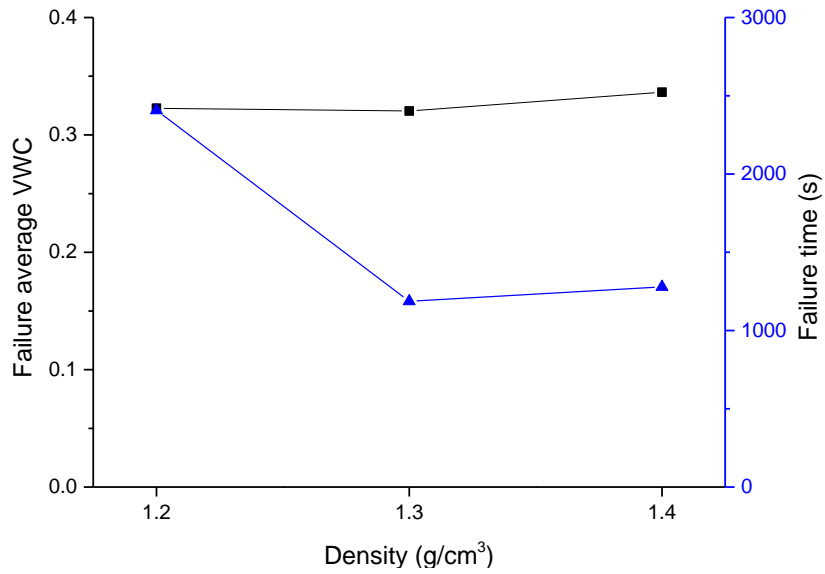
(d)40°-10cm

Figure 6.6(continued): Effect of density of soil on failure average volumetric water content and failure time.
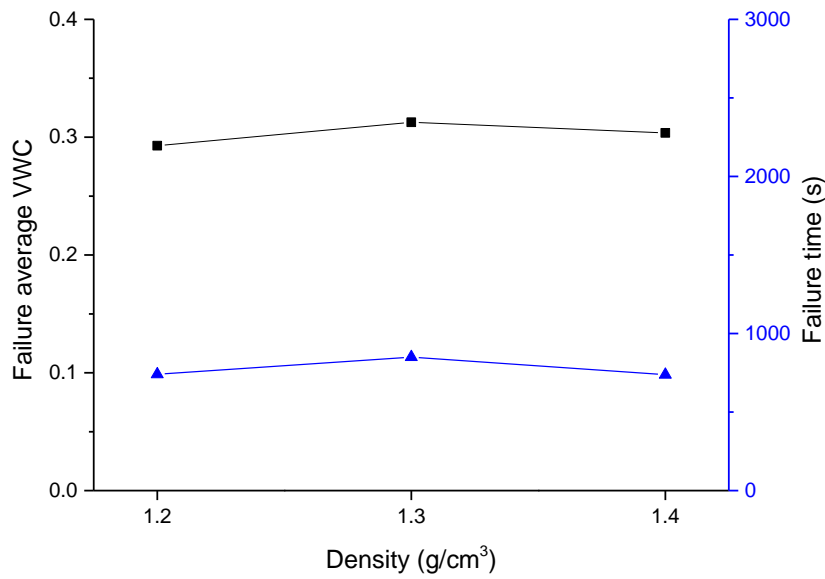
(e)50°-10cm

Figure 6.6(continued): Effect of density of soil on failure average volumetric water content and failure time.

6.3.3. Effect of Surface layer thickness

Figure 6.7 shows the variation of normalized elastic wave velocity with volumetric water content and tilt angle under different surface layer thicknesses of slope. From the curves of normalized elastic wave velocity versus volumetric water, the general trend of normalized elastic wave velocity with larger surface layer thickness was located above the curves with smaller surface layer thickness, regardless of the slope angle and density.

When it rains and the rainfall begins to infiltrate the ground, the volumetric moisture content of the upper soil layer rises to a certain value from the surface layer. The rainwater that infiltrates the ground forms a high moisture content belt and descends from the surface toward the layer underneath. With the elapse of time, and thereafter the water table begins to develop from the lowly permeable base layer. The water table rises with time as the rainwater infiltrates the ground and flows downward due to gravity.

The larger surface layer thickness led to longer time for water table to be formed and rise. Hence, the suction decreased at a smaller rate. As a result, the wave velocity decrease was lower for slope having larger surface layer thickness.

However, a clear difference cannot be observed between these curves of normalized elastic wave velocity with tilt angle for slope having different surface layer thicknesses. The decrease rate of normalized elastic wave velocity with tilt angle was found to be independent of surface layer thickness.

Figure 6.8 shows the effect of surface layer thickness of slope on failure average volumetric water content and failure time. It can be seen that the failure average volumetric water content and failure time increased as the surface layer thickness increased. In other words, slope with thin deposit initiated failure earlier than that with thick deposit. That is because the time for the water table to be formed and rise reduces under larger surface layer thickness.
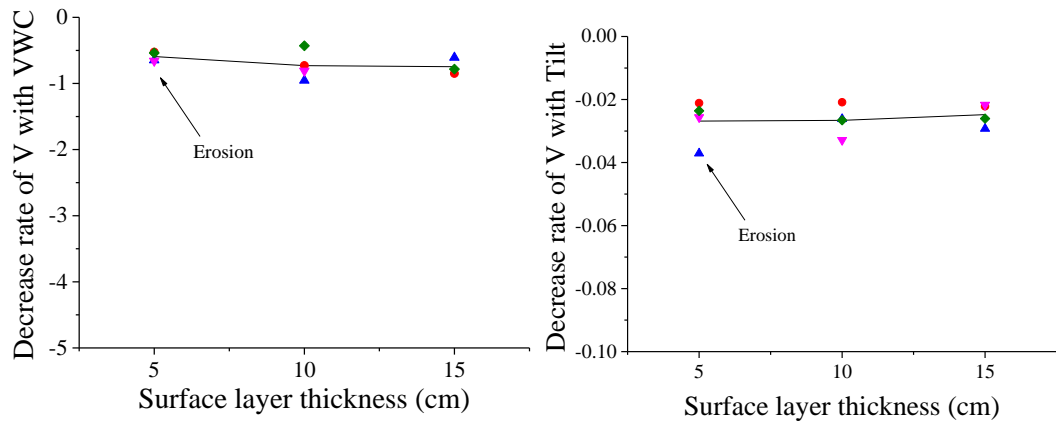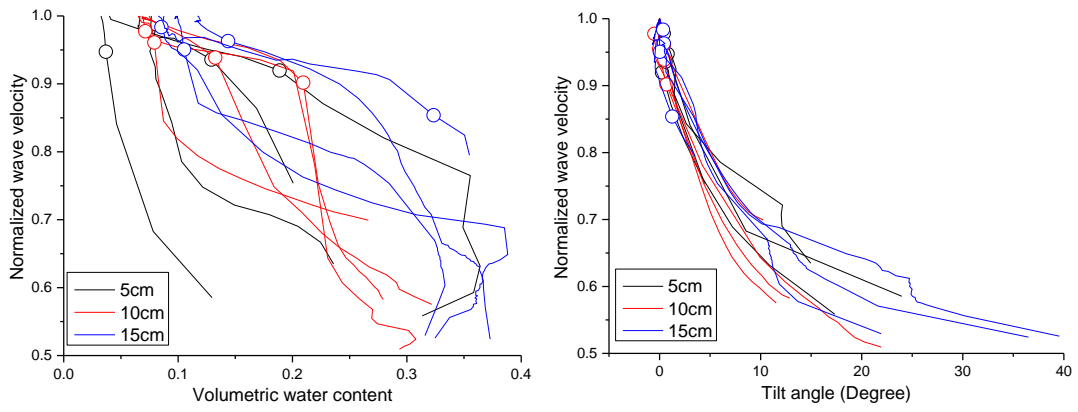
(a)45°-1.2g/cm^3
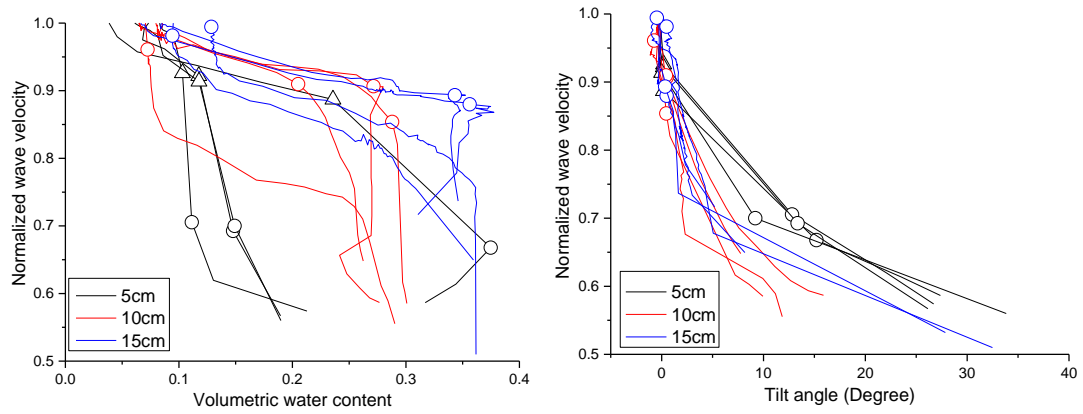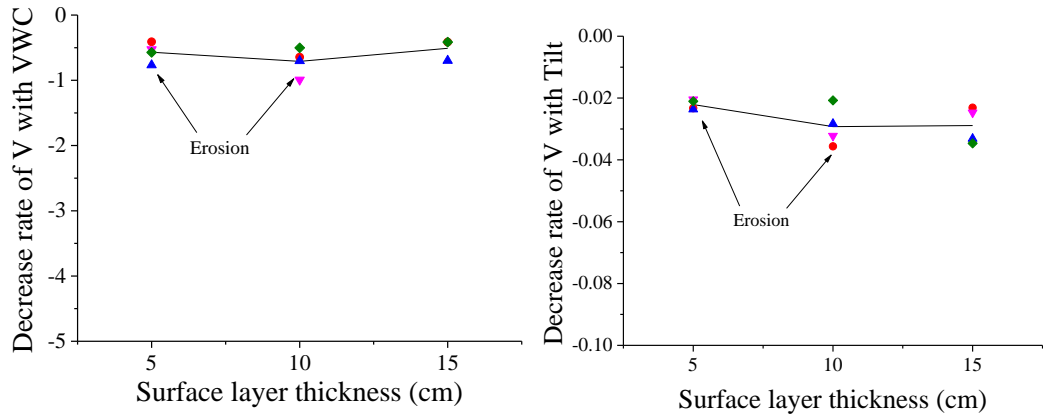
(b)45°-1.3g/cm^3
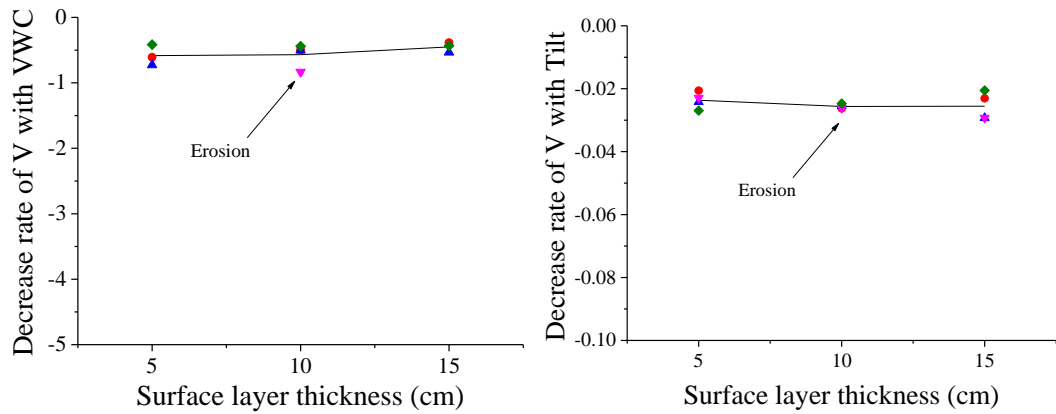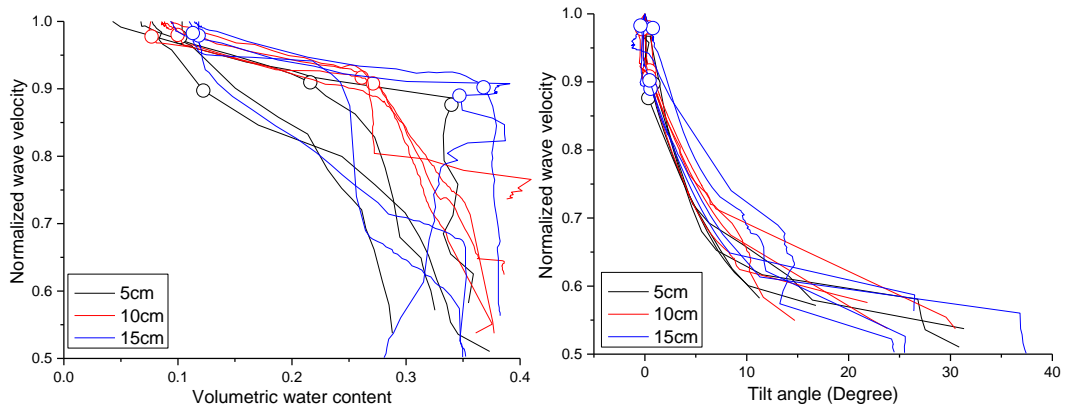
(c)45°-1.4g/cm^3

Figure 6.7: Effect of surface layer thickness of soil on change trend of elastic wave velocity with volumetric water content and tilt angle.
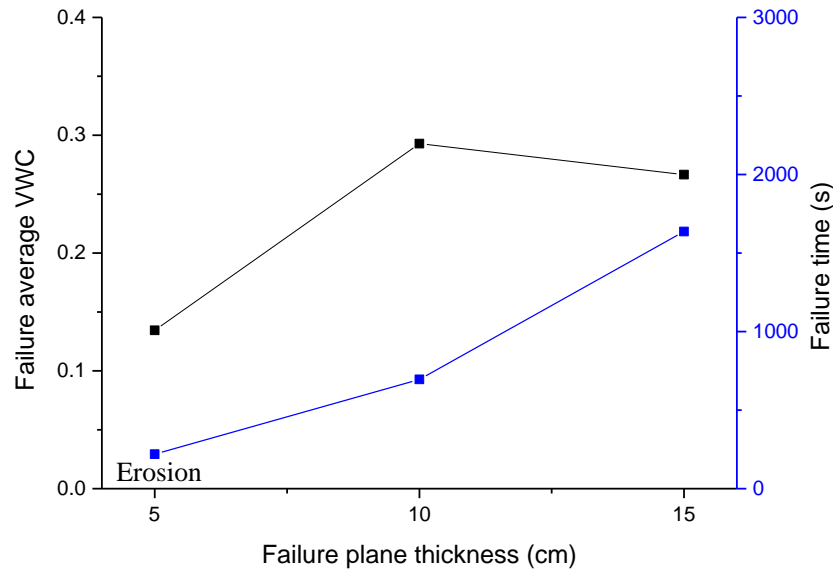
(a)45°-1.2g/cm^3

Figure 6.8: Effect of surface layer thickness of soil on failure average volumetric

water content and failure time.
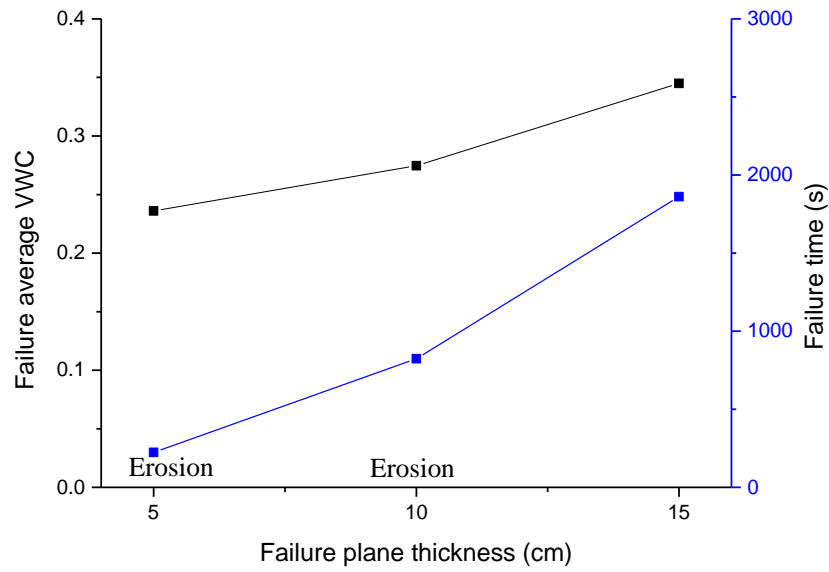
(b)45°-1.3g/cm^3

(continued)
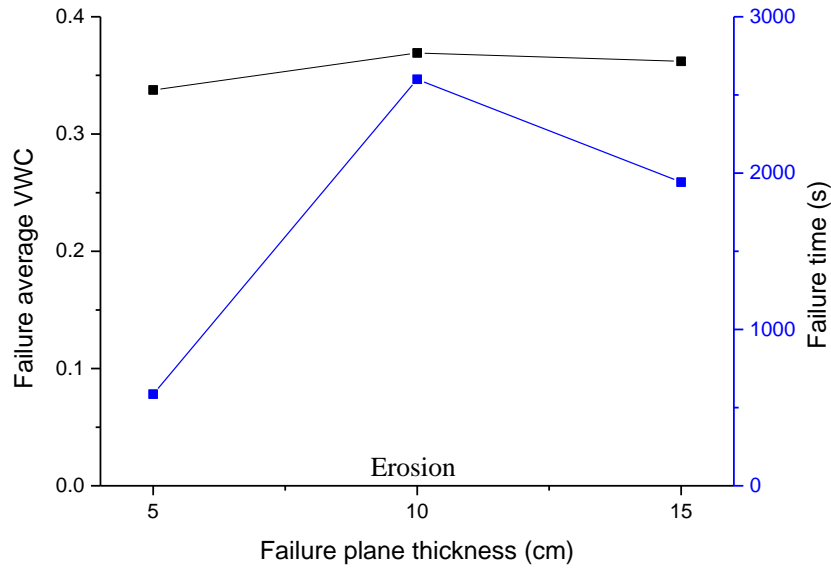
(c)$45°$-$1.4g/cm^3$

(continued)

6.3.4. Effect of Slope Angle

Figure 6.9 shows the variation of normalized elastic wave velocity with volumetric water content and tilt angle under different slope angles. From the curves of normalized elastic wave velocity versus volumetric water, the general trend of normalized elastic wave velocity with lower slope angle was located above the curves with larger slope angle, regardless of the surface layer thickness and density.

It is well known that larger slope angle results in larger shear stress on the failure plane that is unfavorable for the slope stability. This decrease rate of normalized elastic wave velocity with volumetric water content demonstrated that the elastic wave velocity was consistent with the ground stress status.

However, a clear difference cannot be observed between these curves of normalized elastic wave velocity with tilt angle for slope having different slope angles. The decrease rate of normalized elastic wave velocity with tilt angle was found to be independent of slope angles.

Figure 6.10 shows the effect of slope angle of slope on failure average volumetric water content and failure time. It can be seen that the failure average volumetric water content and failure time decreased as the slope angle increased. In other words, steep slope initiated failure earlier than gentle one.
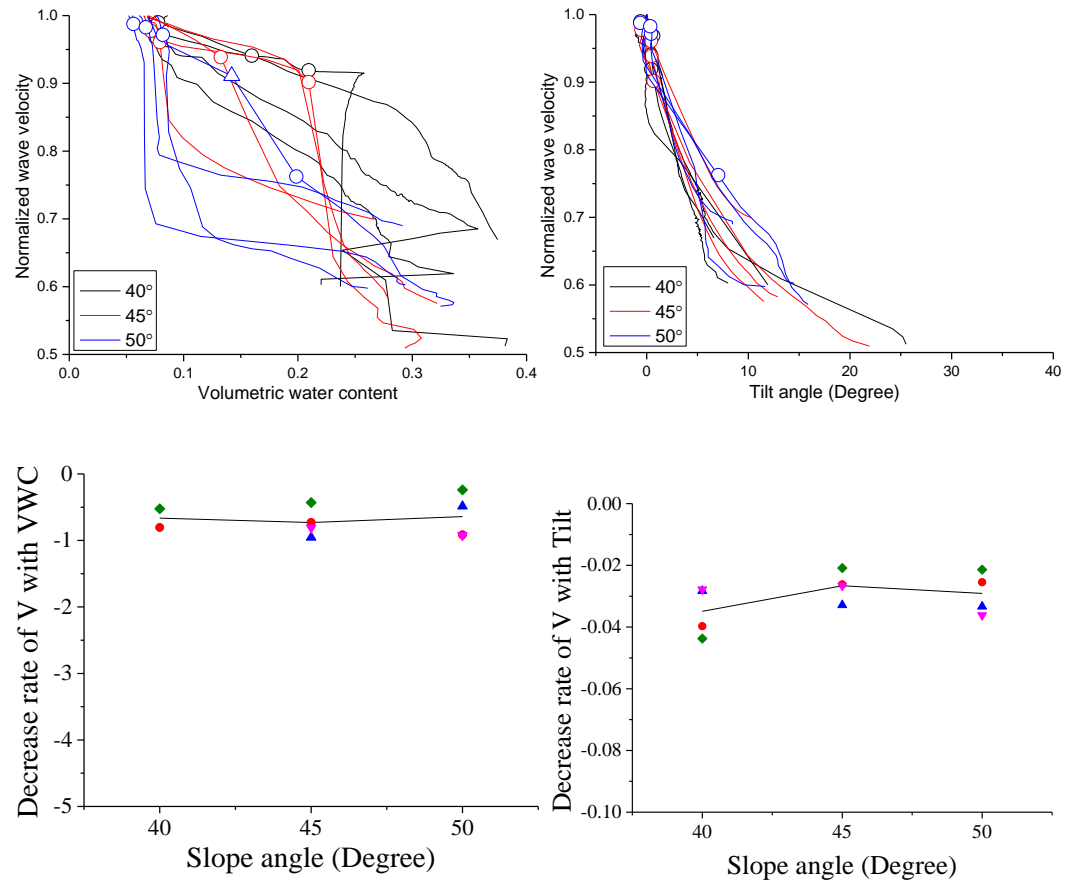
(a) 10cm-1.2g/cm^3
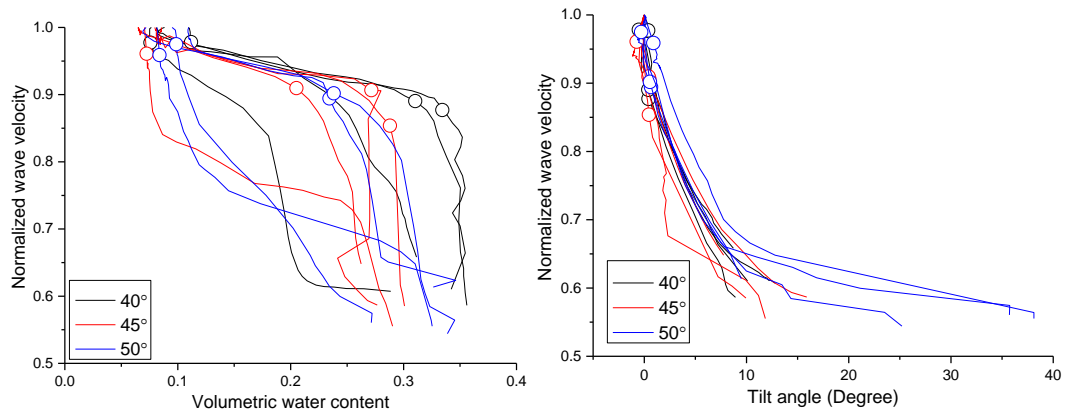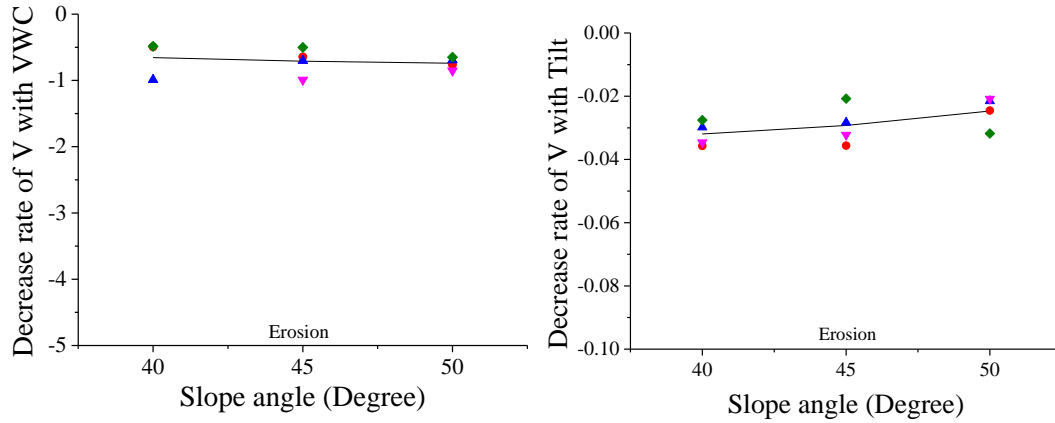
(b) 10cm-1.3g/cm^3

Figure 6.9: Effect of slope angle on change trend of elastic wave velocity with volumetric water content and tilt angle.
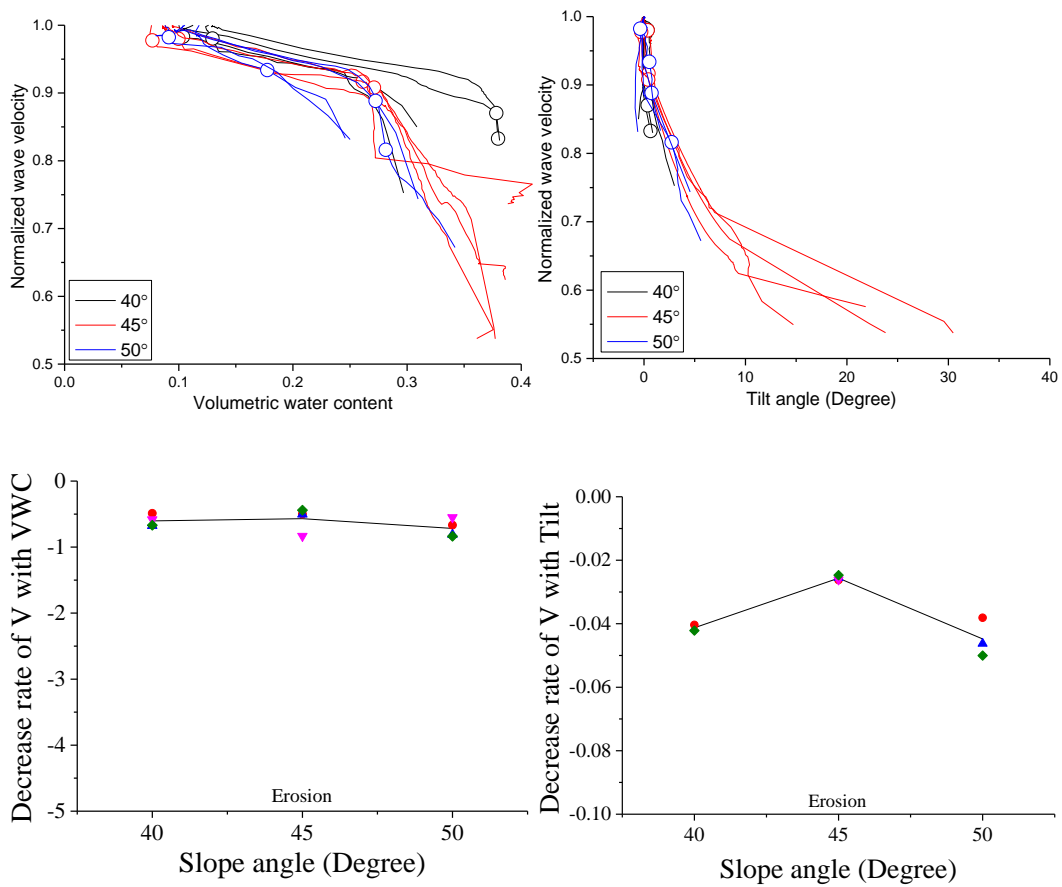
(c) 10cm-1.4g/cm^3

Figure 6.9: Effect of slope angle on change trend of elastic wave velocity with volumetric water content and tilt angle.
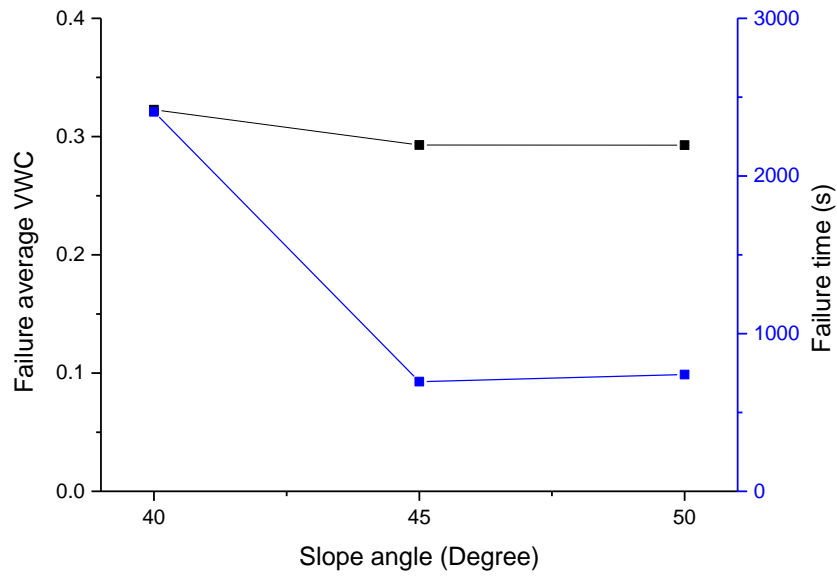
(a) 10cm-1.2g/cm^3

Figure 6.10: Effect of slope angle on failure average volumetric water content and failure time.
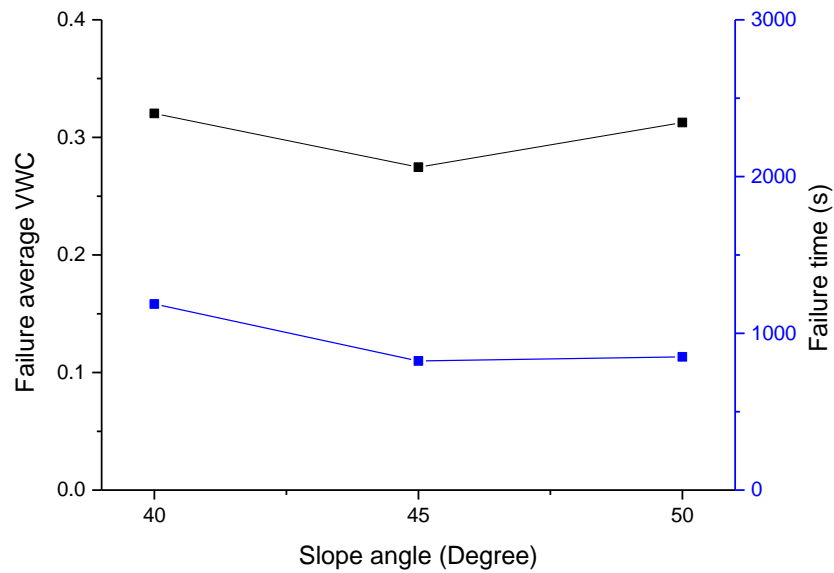
(b) 10cm-1.3g/cm^3

Figure 6.10: Effect of slope angle on failure average volumetric water content and
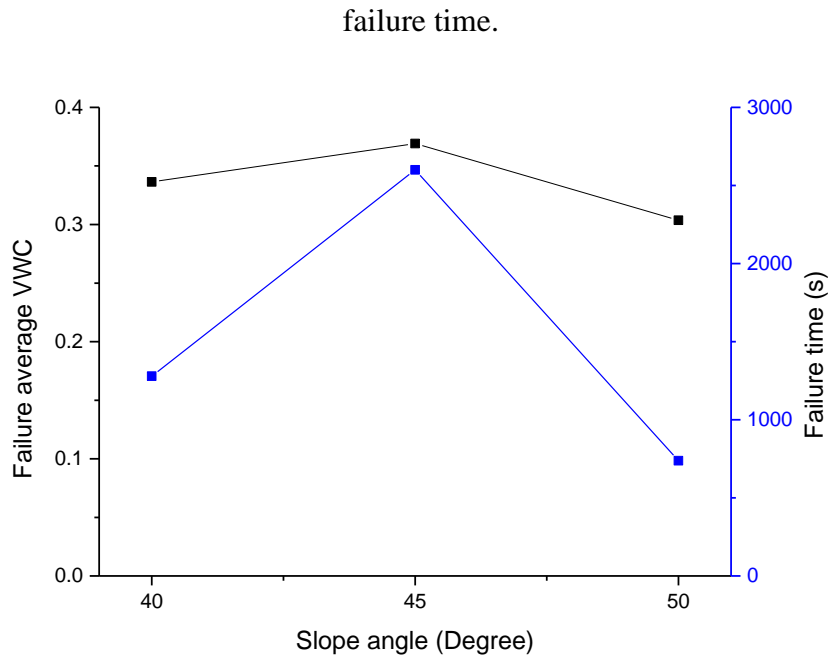
failure time.

(c) 10cm-1.4g/cm^3

Figure 6.10(continued): Effect of slope angle on failure average volumetric water content and failure time.

6.3.5. Slope Failure Mode

Figure 6.11 summarizes the modes of failure observed in all of the experiments. In general, model slopes in all the experiments failed by shallow sliding, involving a large portion of soil mass or localized soil mass near the slope surface. Most slides occurred on a single sliding surface. Still several cases were featured by multiple sliding surfaces.

This implies that rainfall-induced slope failures do not always initiate at the lower part of hillslopes, but rather at the seepage area developed anywhere on the hillslope surface. Field reports on rainfall-induced slope failures indicate that the failures also initiate at middle and upper portions of the hillslope (e.g., Shlemon et al. 1987;Wiezoreck 1987).

This general failure mode is consistent with that which characterizes the rainfall-induced failures of natural or manmade slopes (e.g., Harp 1996; Baum and Chleborad 1999; Rahardjo 1999). Other contributing factors included the mode of water level rise and, to a considerable extent, the hydraulic conductivity of the soils controlled failure modes and the extent of failures.

Cracks appeared during tests, as shown in Figure 6.12. Cracks have a significant effect on the rainfall-induced failure behavior of the slope. The crack has a vital influence on the deformation of the slope near the crack, inferring that the deformation was induced by the rainfall infiltration due to the crack (Zhang et al. 2012).

(a) Single sliding surface   (b) Multiple sliding surfaces
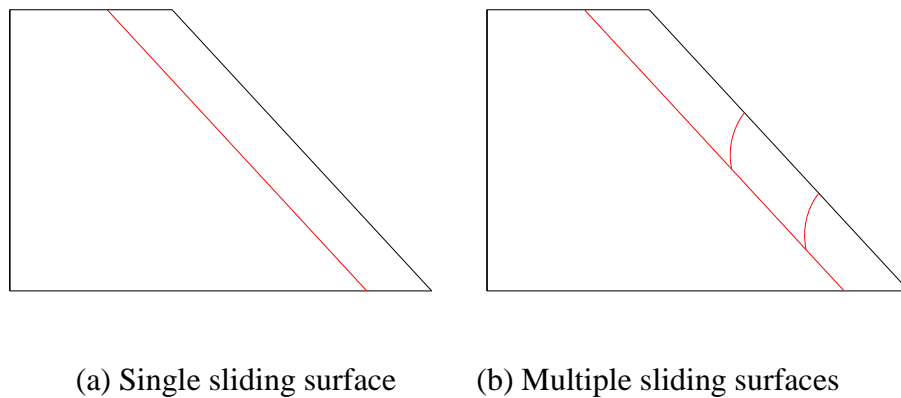
Figure 6.11: Slope failure modes.
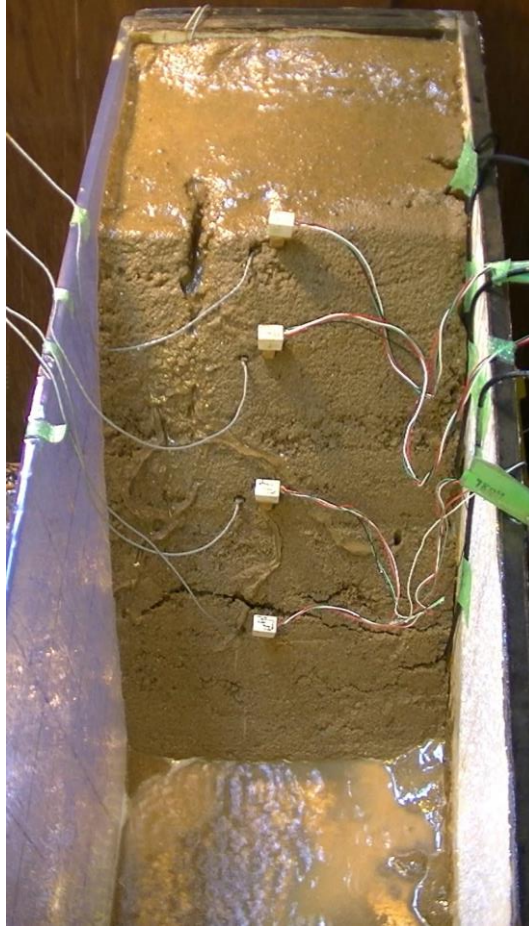
Figure 6.12: Crack and runoff on slope surface (Case 2-50-10-1.4, 480s).

Surface runoff was generated minutes after rainfall began. Simultaneously, the volumetric water content sensors indicated that the soil was not yet completely saturated, indicating that runoff was generated because of excess infiltration. Although the surface runoff discharge was small, its effect on shallow slope failures should not be neglected with the following reasons (Cui et al. 2014).

Firstly, the runoff transported fine particles downslope, leading to a coarsening of the surface soil layers. As a result, some faces of the slope, containing only coarse particles, were left extremely unstable. This instability can contribute to slope failures at or above a critical gradient if rainfall is present.

Secondly, surface runoff is capable of generating shear forces on the surface soil, which may increase its propensity to slide. Based on hydraulics and soil mechanics

theories, this condition can lead to instability in the soil, and potentially, failure.

Thirdly, the surface runoff reached the bottom of the slope with a velocity that was sufficiently high to wash out the entire foot of the slope. This can be exacerbated in high-stress situations when no protective measures have been undertaken. The foot of the slope was easily eroded and destroyed. This phenomenon was also reported in sandy soils, generating retrogressive slope failures (Huang et al, 2008, 2009).

6.3.6. Failure Initiation Location

Figure 6.13 shows the distribution of criteria normalized wave velocity at tilt angle of 0.4 Degree. The number of cases is listed in Table 6.2. The bottom part of slope most frequently gives the lowest response for slope failure. Hence, this recommends installing wave monitor system in the bottom part of slope to monitor the stability of slope.
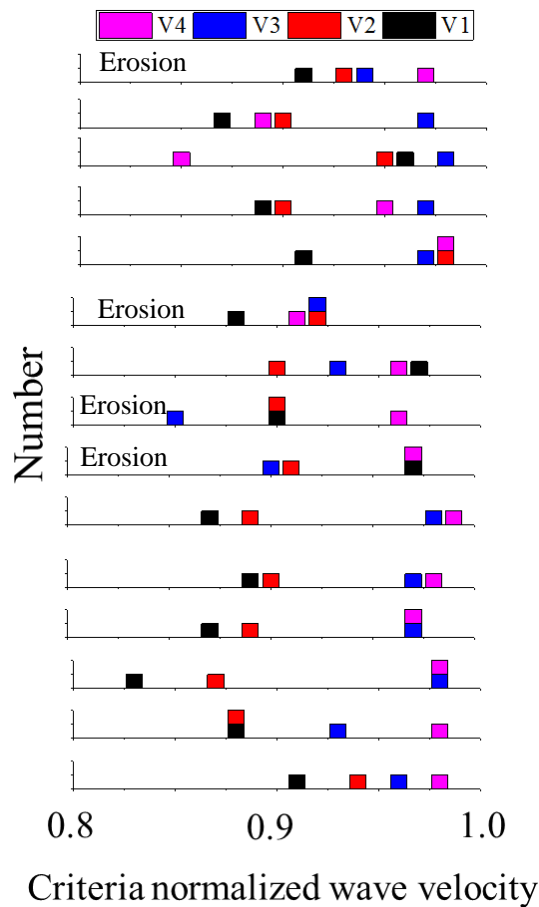
Figure 6.13: distribution of criteria normalized wave velocity at tilt angle of 0.4 Degree.

Table 6.2: Number of case of lowest criteria normalized wave velocity for each location.

Lowest	Number of case
V1	11 (2 erosion)
V2	1
V3	2 (2 erosion)
V4	1

6.3.7. Prediction of normalized wave velocity

From Type 1 tests, the relationship of normalized wave velocity with volumetric water content and tilt angle was obtained:

$$f(w) = -0.2798w + 1.021 \tag{1}$$

$$g(t) = -0.0292t + 1 \tag{2}$$

Where, $f(w)$ and $f(t)$ are the evolution equation for normalized wave velocity with volumetric water content and tilt angle respectively, w and t are volumetric water content and tilt angle respectively. Here, the above two equations were combined as

$$f(w,t) = f(w) \cdot g(t) = (-0.2798w + 1.021) \times (-0.0292t + 1) \tag{3}$$

The combined equation was used to predict the evolution of normalized wave velocity with volumetric water content and tilt angle in Type 2 tests. From Figure 6.14 where points present measured data while curves present predicted value using equation (3), it can be seen that the equation (3) would well describe the wave behavior.
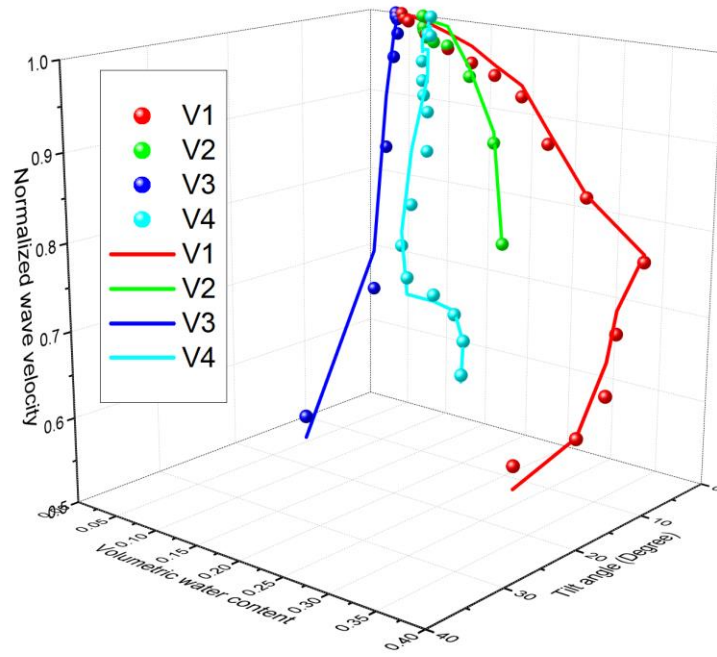
(a)2-45-5-1.2
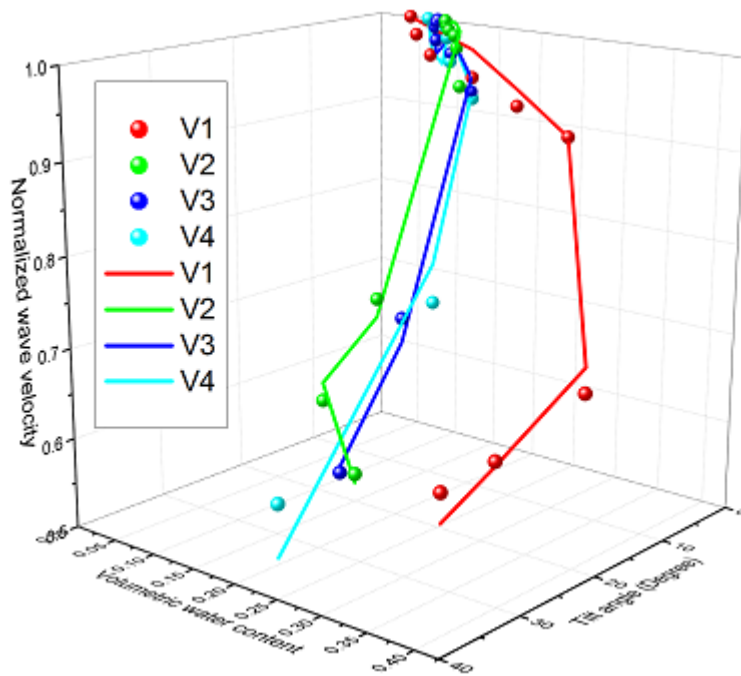
(b)2-45-5-1.3

Figure 6.14: Prediction of normalized wave velocity evolution with volumetric water

content and tilt angle.
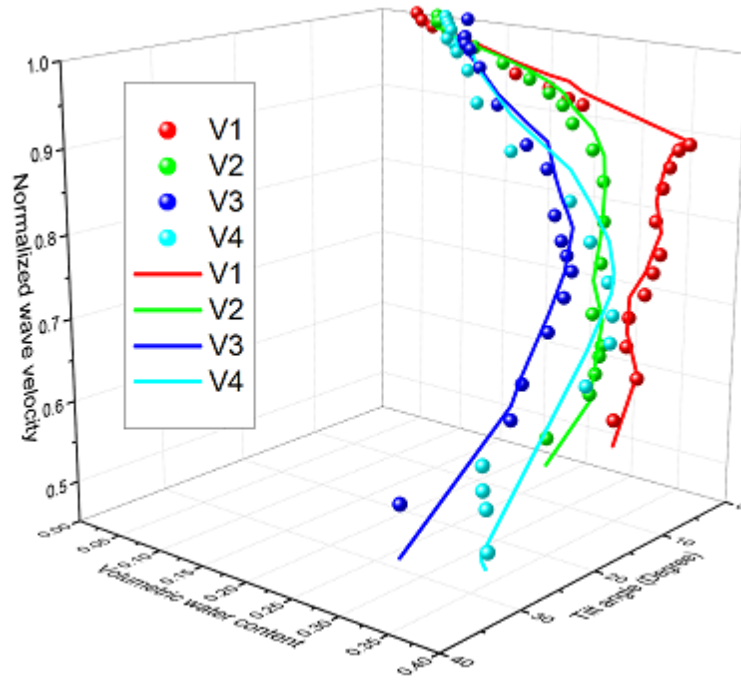
(c)2-45-5-1.4
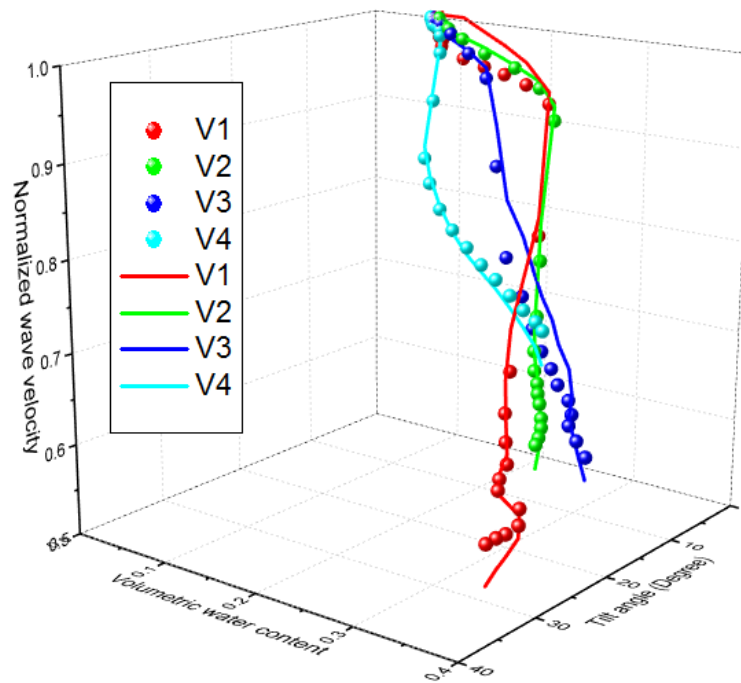
(d)2-45-10-1.2

Figure 6.14(continued): Prediction of normalized wave velocity evolution with

volumetric water content and tilt angle.
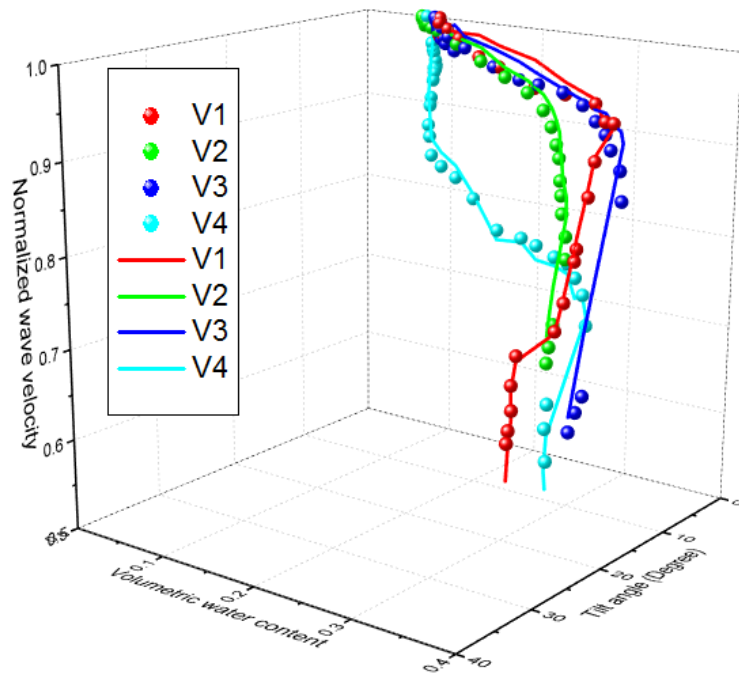
(e)2-45-10-1.3
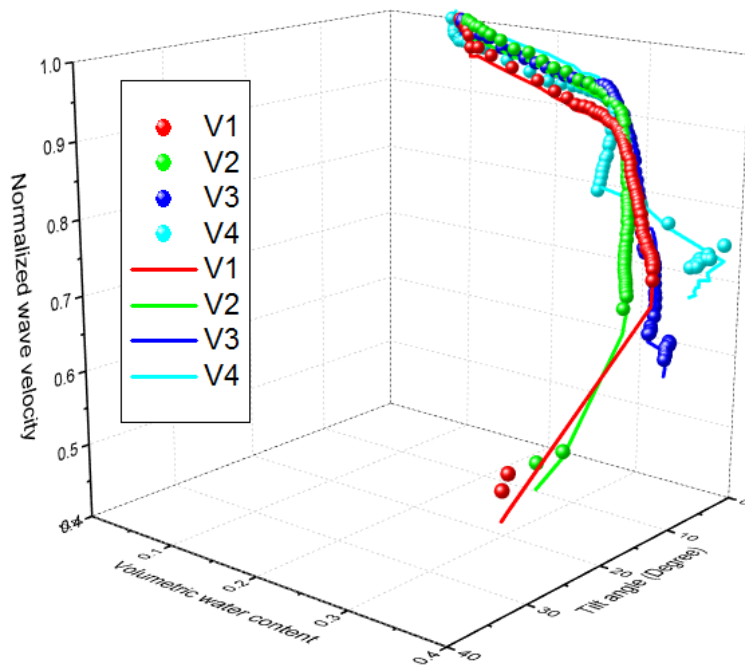
(f)2-45-10-1.4

Figure 6.14(continued): Prediction of normalized wave velocity evolution with

volumetric water content and tilt angle.
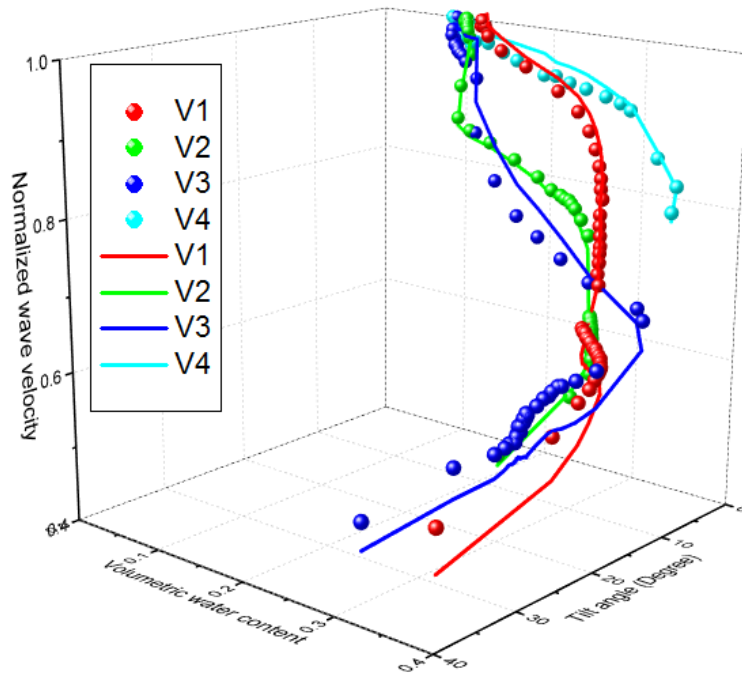
(g) 2-45-15-1.2
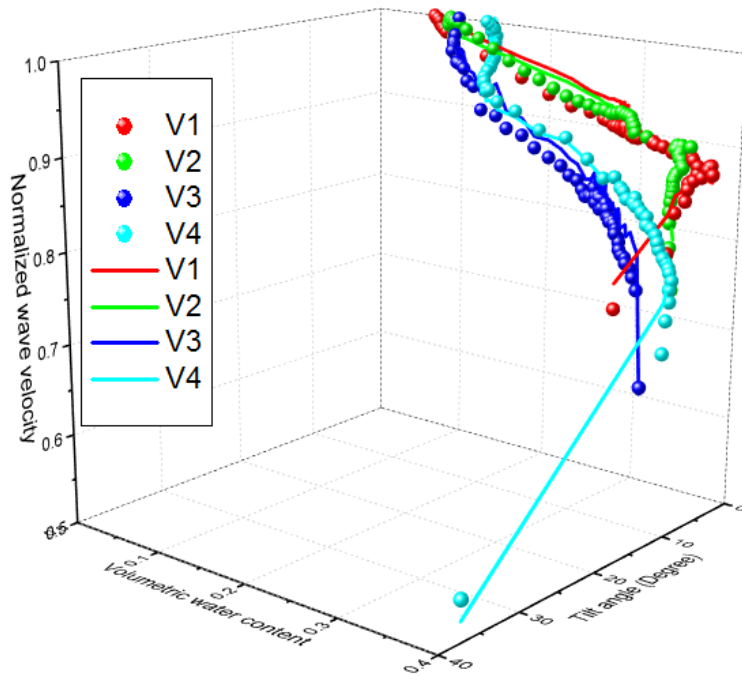
(h) 2-45-15-1.3

Figure 6.14(continued): Prediction of normalized wave velocity evolution with

volumetric water content and tilt angle.
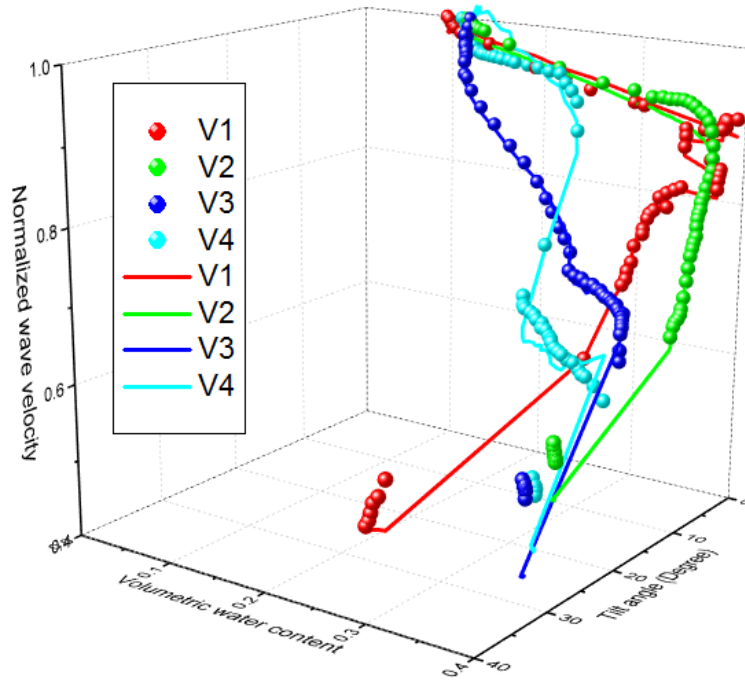
(i) 2-45-15-1.4
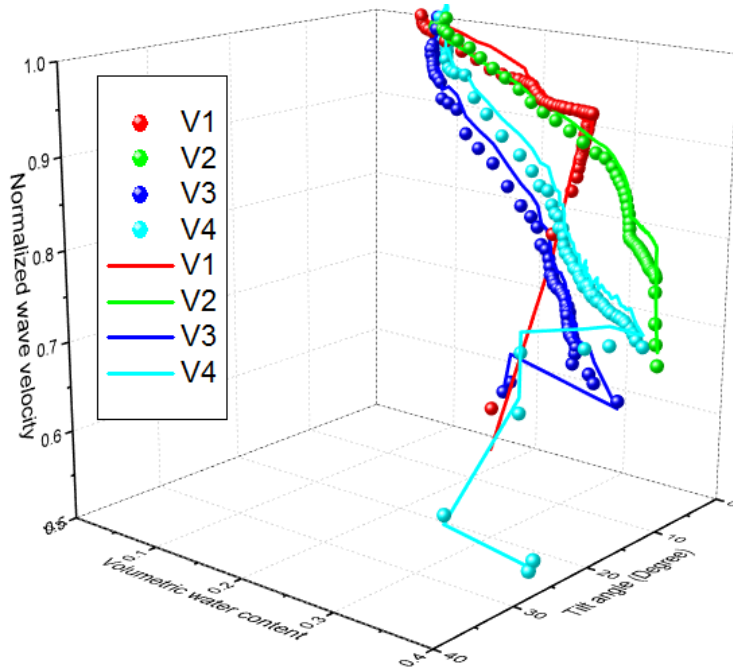
(j) 2-40-10-1.2

Figure 6.14(continued): Prediction of normalized wave velocity evolution with

volumetric water content and tilt angle.
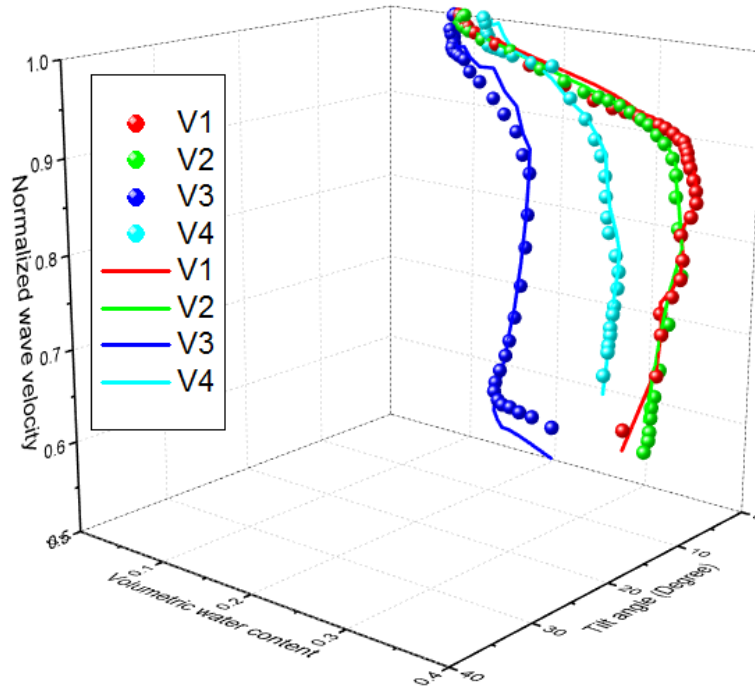
(k) 2-40-10-1.3
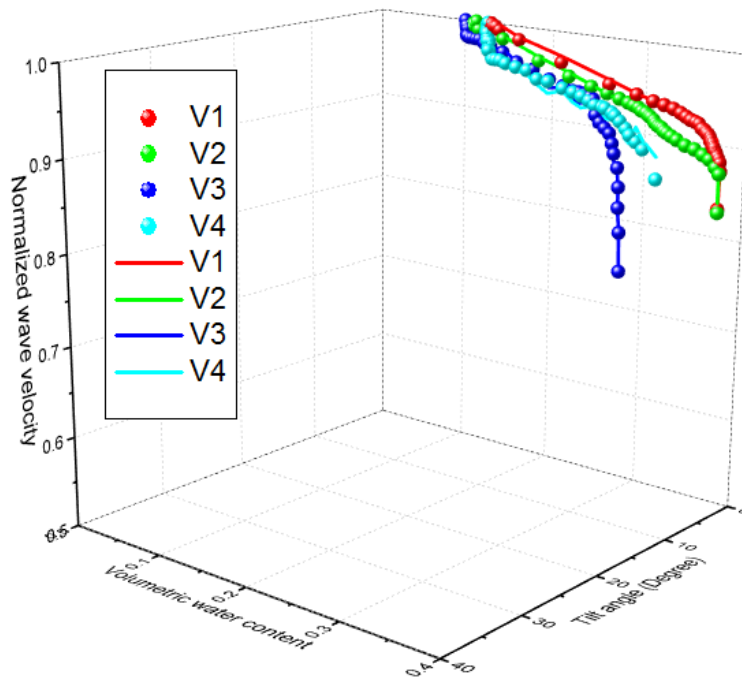
(l) 2-40-10-1.4

Figure 6.14(continued): Prediction of normalized wave velocity evolution with

volumetric water content and tilt angle.
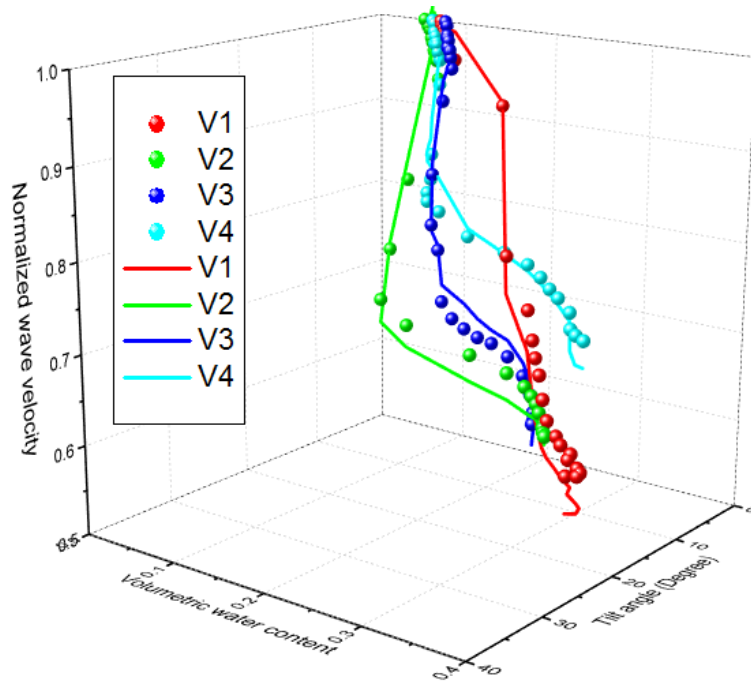
(m) 2-50-10-1.2
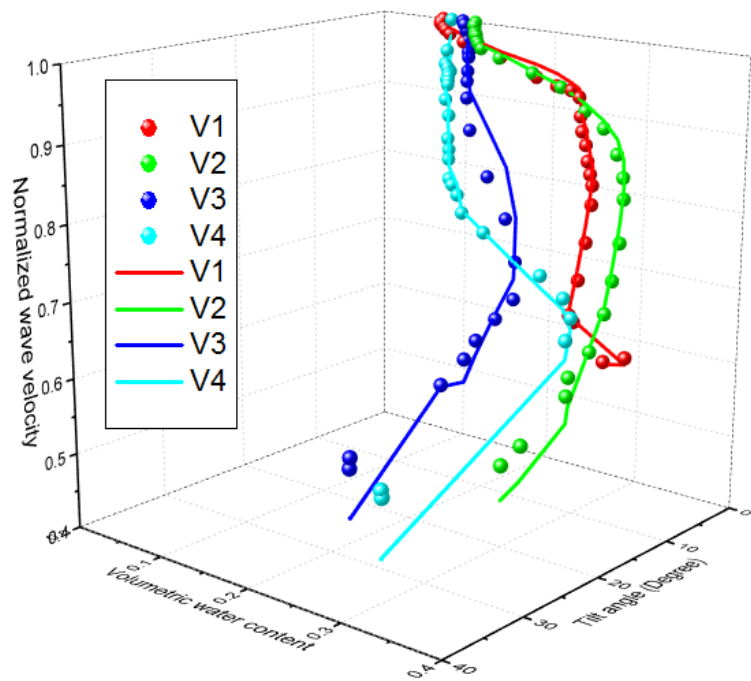
(n) 2-50-10-1.3

Figure 6.14(continued): Prediction of normalized wave velocity evolution with
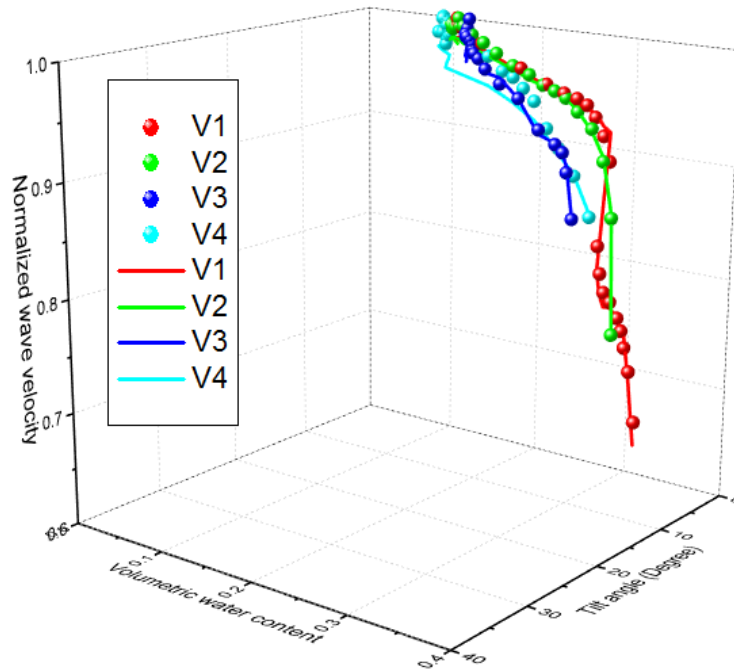
(o) 2-50-10-1.4

Figure 6.14(continued): Prediction of normalized wave velocity evolution with volumetric water content and tilt angle.

6.3.8. Criteria of normalized wave velocity for early warning

To date, there is no any clear standard for selection of criteria of early warning for landslides. Irfan (2014) suggested 0.2% axial strain for yield point. Uchimura et al. (2015) proposed that a precaution be issued at a tilting rate of $0.01\,°$ per hour and a warning be issued at a tilting rate of $0.1\,°$ per hour, to be on the conservative side. Due to different slope scale, their recommendations are not suitable for this study. Herein, the author define the normalized wave velocity based criteria for landslides.

Based on the 0.4 degree of maximum tilt angle defined from type 1 tests, the criteria of normalized wave velocity corresponding to 0.4 degree of tilt angle were regarded

as the threshold for early warning issue. Distribution of Criteria normalized wave velocity from each influence factor is shown in Figure 6.15. The criteria of normalized wave velocity were mainly distributed in a relatively narrow range between 0.9 and 1.

The distribution of criteria normalized wave velocity determined by the bottom sensor is shown in Figure 6.16. The criteria of normalized wave velocity were mainly distributed in a relatively narrow range between 0.87 and 0.92. The criteria normalized wave velocity could be set as 0.92 for early warning. It is proposed that a warning be issued when normalized wave velocity decreases to 0.92.
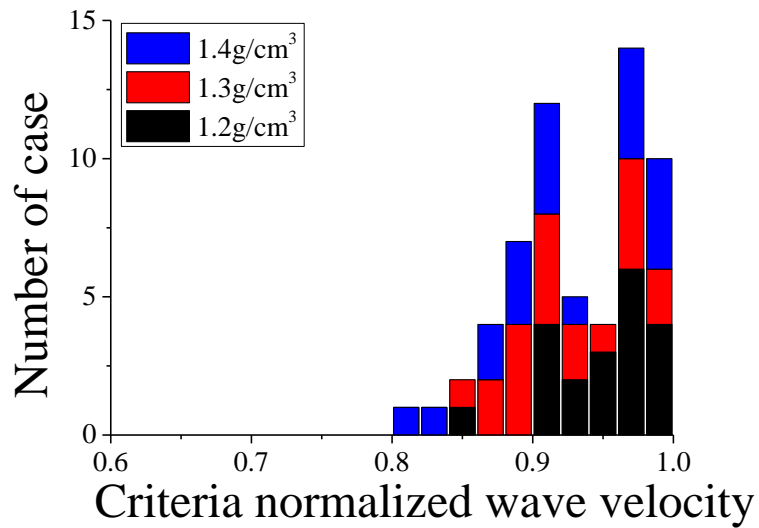
(a)density based
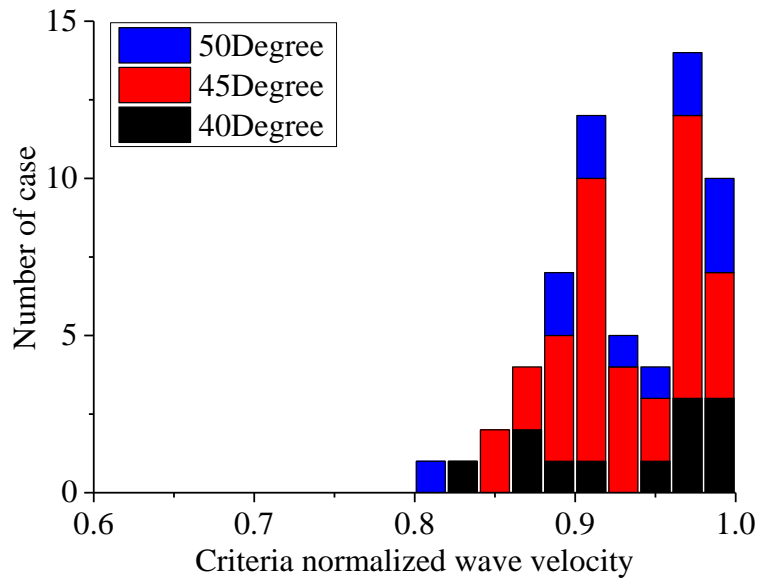
(b) slope angle based
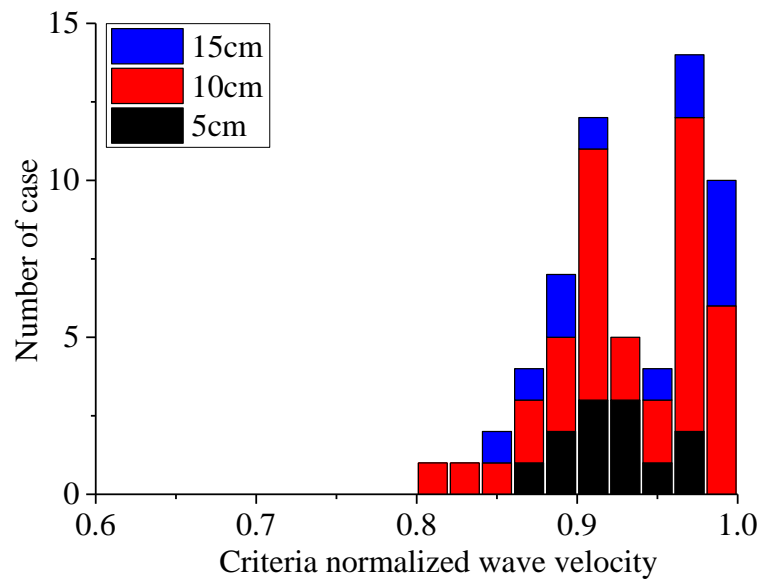
(c) surface layer thickness based

Figure 6.15: Distribution of criteria normalized wave velocity corresponding to 0.4

degree for early warning.
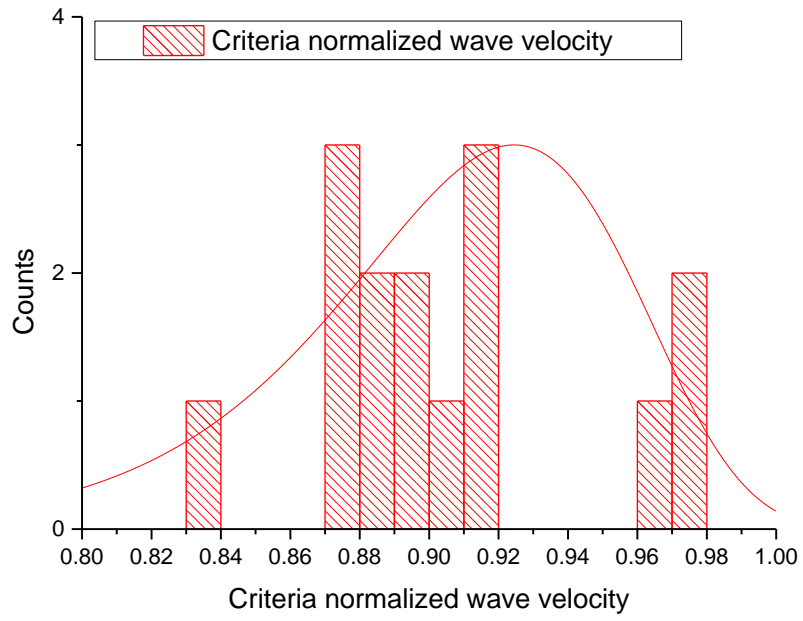
(a) Including erosion
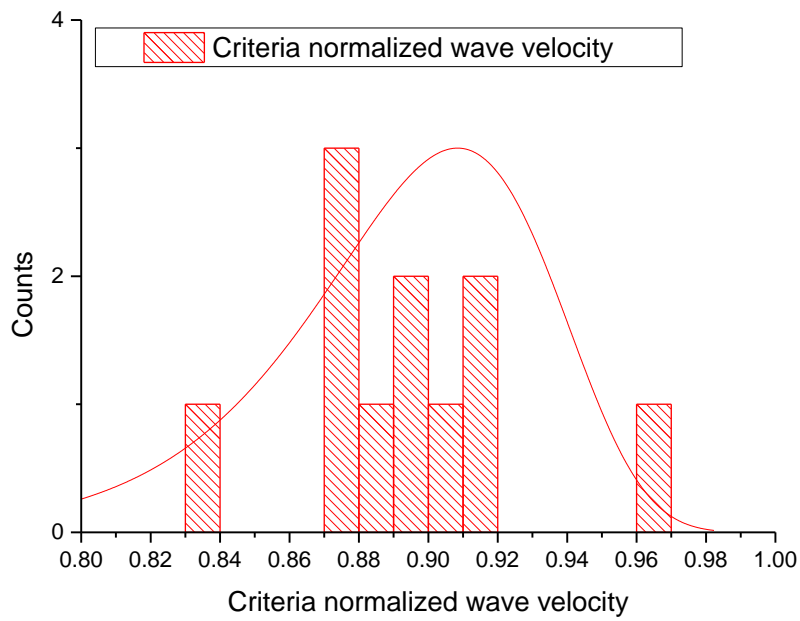
(b) Excluding erosion

Figure 6.16: Distribution of criteria normalized wave velocity determined by the

bottom sensor.

6.3.9. Selection of initial wave velocity for normalization

The selection of initial wave velocity is essential for normalization. From previous study, we found the wave velocity is a function of water content and deformation. The interaction of water content and deformation should be investigated in advance.

Uchimura et al. (2013) developed a scaled model test apparatus to reproduce mechanical conditions in a slope during a process of slope failure (Figure 6.17), and found that the deformation developed corresponding to increment in the volumetric water content in the first wetting stage. But, it does not develop or restore during the consequent drying stage. In the second wetting stage, the deformation stayed constant at the beginning, but it restarted to develop when the volumetric water content exceeded its peak value in the first wetting (see the dotted marker lines in Figure 6.18). Afterward, the shear deformation of the soil mass developed only when the water content exceeded its highest value in the past.

For a wave velocity monitored in a slope, it is expected to decrease with rainfall, and decrease more by deformation. Rainfall stopping, water content decreases by drainage. Hence wave velocity increases to some extent. But deformation cannot recover (Uchimura et al. 2013). As a result, the wave velocity cannot recover to the initial value (Figure 6.19). It is always lower than the initial wave velocity. Therefore, the initial wave velocity could be selected as the first recorded value after installing the wave measurement system.
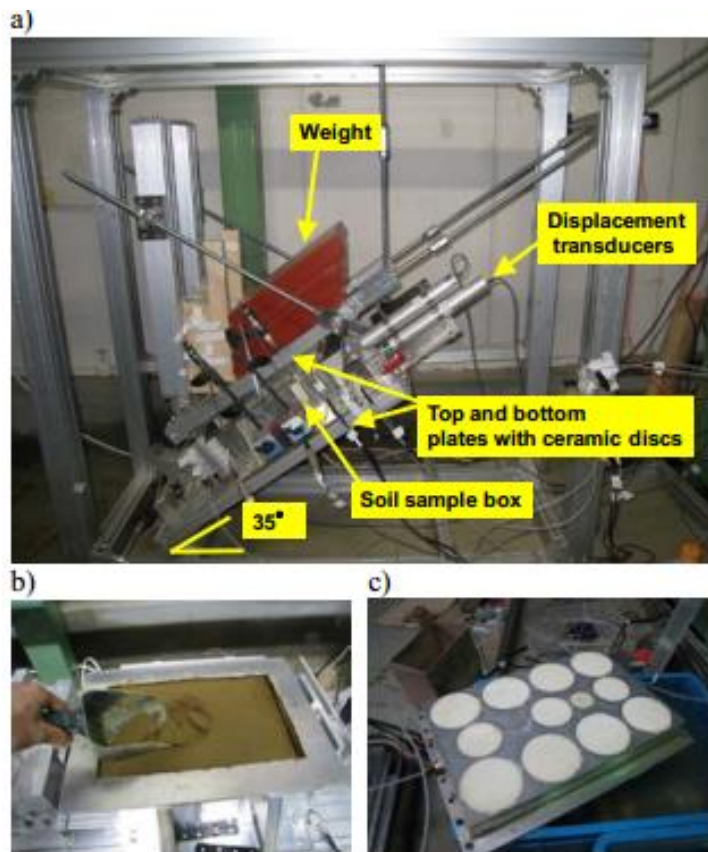
Figure 6.17: Photos of model test apparatus: a) whole view; b) modeled soil mass surrounded by confining plates; c) top/bottom plate with ceramic discs.
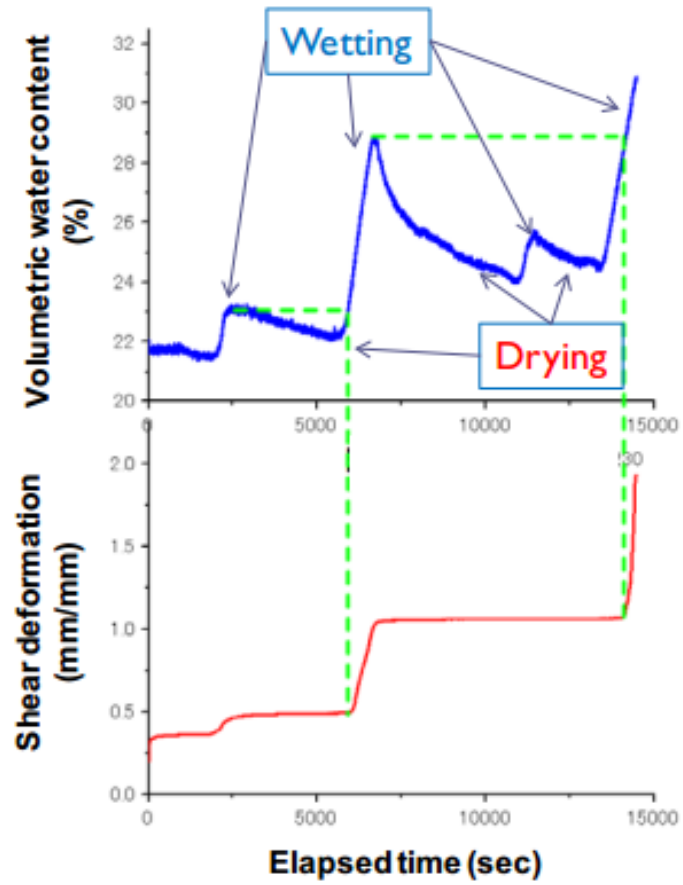
Figure 6.18: Volumetric water content and shear deformation in the deformable zone of soil mass versus time.
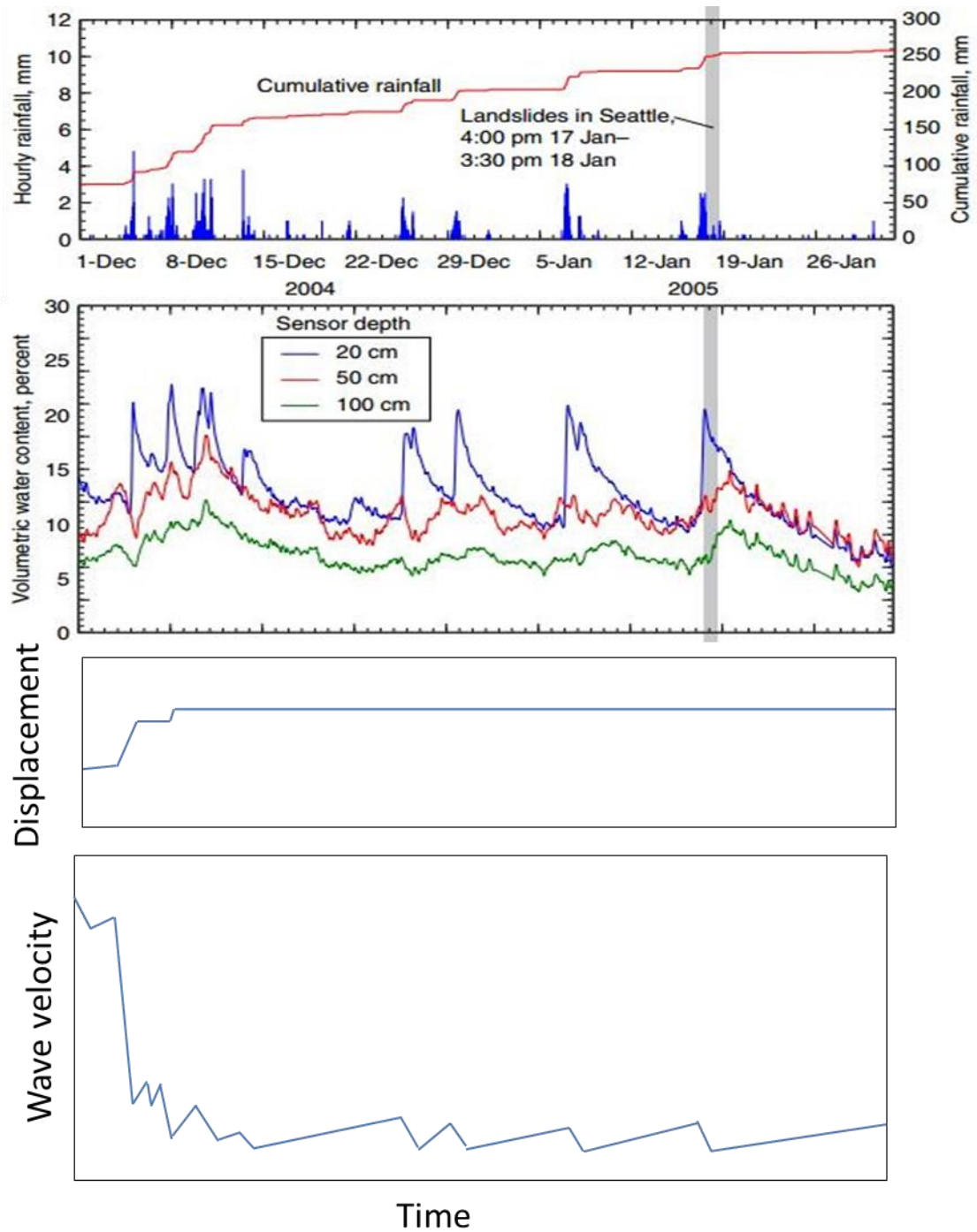
Figure 6.19: Rainfall history VWC, predicted displacement and wave velocity.

6.4. SUMMARY

This chapter summarizes experimental studies reproducing rainfall-induced slope failure, and the corresponding behavior of elastic wave velocities during slope failure. Behavior of elastic wave velocities was found to decrease with water content as well soil deformations. With changes in soil moisture due to water infiltration, elastic wave velocities gradually kept on decreasing. As soon as slope initiated failure, wave velocities decreased at an accelerated rate. Such sharp decrease after a threshold about 0.92 of normalized elastic wave velocity can be useful for predicting failure initiation in actual landslide conditions.

The general trend of normalized elastic wave velocity with volumetric water content for soil with higher density was located above the curves for soil with lower density, regardless of the slope angle and surface layer thickness. The failure average volumetric water content and failure time increased as the density increased.

The general trend of normalized elastic wave velocity with volumetric water content for slope with larger surface layer thickness was located above the curves with smaller surface layer thickness, regardless of the slope angle and density. The failure average volumetric water content and failure time increased as the surface layer thickness increased.

The general trend of normalized elastic wave velocity with volumetric water content for slope with lower slope angle was located above the curves for slope with larger slope angle, regardless of the surface layer thickness and density. The failure average volumetric water content and failure time decreased as the slope angle increased.

The decrease rate of normalized elastic wave velocity with volumetric water content and tilt angle was found to be independent of density, slope angle, and surface layer thickness. The changes of normalized elastic wave velocity with volumetric water content and tilt angle were simulated by the relationship functions obtained from flat

model tests. It showed that the simulated curves agreed well with measured data.

6.6. REFERENCE

Baum, R. L., and Chleborad, A. F. (1999). Landslides triggered by Pacific Northwest storms, November and December 1998. *Information Reports*, U.S. Geological Survey, Washington D.C..

Baum, R. L., & Godt, J. W. (2010). Early warning of rainfall-induced shallow landslides and debris flows in the USA. Landslides, 7(3), 259-272.

Cui, P., Guo, C. X., Zhou, J. W., Hao, M. H., & Xu, F. G. (2014). The mechanisms behind shallow failures in slopes comprised of landslide deposits. *Engineering Geology*, *180*, 34-44.

Gallage, C. P. K., & Uchimura, T. (2010). Effects of dry density and grain size distribution on soil-water characteristic curves of sandy soils. *Soils and Foundations*, *50*(1), 162-172.

Harp, E. L., et al. (1996). Landslides and landslide hazards in Washing ton State due to February 5–9, 1996 storm. *U.S. Geological Administrative Rep.*, U.S. Geological Survey, Washington D.C..

Huang, C. C., Lo, C. L., Jang, J. S., & Hwu, L. K. (2008). Internal soil moisture response to rainfall-induced slope failures and debris discharge. *Engineering Geology*, *101*(3), 134-145.

Huang, C.C., Ju, Y.J., Hwu, L.K., Lee, J.L. (2009). Internal soil moisture and piezometric responses to rainfall-induced shallow slope failures. *Journal of Hydrology*, *370*(1), 39-51.

Irfan, M. (2014). Elastic wave propagation through unsaturated soils concerning early warning of rain-induced landslides. PhD Thesis, Univeristy of Tokyo, Japan.

Jiang, Y., Chen, W., Wang, G., Sun, G., & Zhang, F. Influence of initial dry density and water content on the soil–water characteristic curve and suction stress of a reconstituted loess soil. *Bulletin of Engineering Geology and the Environment*, 2-11.

Li, B., & Chen, Y. (2016). Influence of dry density on soil-water retention curve of unsaturated soils and its mechanism based on mercury intrusion porosimetry. *Transactions of Tianjin University*, *22*, 268-272.

Rahardjo, H. (1999). The effect of rainfall on the slope stability of residual soil in Singapore. *Report Research Project*, Nanyang Technological University, Jurong, Singapore.

Sharma, R. H., & Nakagawa, H. (2010). Numerical model and flume experiments of single-and two-layered hillslope flow related to slope failure. *Landslides*, 7(4), 425-432.

Shlemon, R. J., Wright, R. H., and Montgomery, D. R. (1987). Anatomy of a debris flow, Pacifica, California. *Review in engineering geology*, Vol. VII—Debris flows/avalanches: Process, recognition, and mitigation, J. E. Costa and G. F. Wieczorek, eds., Geological Society of America, Boulder, Colo., 181–199.

Uchimura, T. (2011). Wave velocity in unsaturated slopes in relation to moisture and stability. *Proceedings of the 14th Asian Regional Conference on Soil Mechanics and Geotechnical Engineering*, Hong Kong,466-471.

Uchimura, T., Suzuki, D., Getie, G., Yamada, S., Towhata, I., & Wang, L., et al. (2013). Evaluation of instability of slopes under heavy rainfall based on realtime monitoring of deformation and water contents. Ckcnet Cn.

Uchimura T, Towhata I, Wang L, et al. (2015). Effects of dry density and grain size distribution on soil-water characteristic curves of sandy soils. *Soils and Foundations*, *55*(6), 1086-1099.

Wieczorek, G. F. (1987). Effect of rainfall intensity and duration on debris flows in Central Santa Cruz Mountains, California. *Review in engineering geology, Vol. VII-Debris flows/avalanches: Process, recognition, and mitigation*, J. E. Costa and G. F. Wieczorek, eds., Geological Society of America, Boulder, Colo., 93–104.

Zhang, G., Wang, R., Qian, J., Zhang, J. M., & Qian, J. (2012). Effect study of cracks on behavior of soil slope under rainfall conditions. *Soils and Foundations*, *52*(4), 634-643.

Zhou, W. H., Yuen, K. V., & Tan, F. (2014). Estimation of soil–water characteristic curve and relative permeability for granular soils with different initial dry densities. *Engineering Geology*, *179*, 2-9.

CHAPTER 7

DISTINGUISH OF Vp AND Vs BY THE BENDER ELEMENT TEST

7.1. GENERAL

In chapter 5 and chapter 6, the wave signal was recorded. But the wave type was not recognized. The wave is generated by the vibration of the solenoid. Wave signal came in mixture of S-wave and P-wave. It is difficult to say the wave travel time was determined by whether S-wave or P-wave. For bender element test, the wave source is clean. The wave could be generated only in S-wave and P-wave. An ordinary triaxial apparatus which is capable of measuring SWCC is modified in this study to enable the measurement of elastic wave velocities (S-wave and P-wave velocities). The elastic wave velocity is determined at different volumetric water content. Determination of SWCC is typically carried out in a pressure plate apparatus or a tempe pressure cell. In present study, a typical triaxial apparatus has been modified to serve as an SWCC measurement apparatus. The designed apparatus could not only determine SWCC under different magnitudes of K_o stress, but was also able to measure elastic wave velocities (shear wave velocity and compression wave velocity) in due course.

7.2. EQUIPMENT DESIGN

A triaxial apparatus equipped with elastic wave measurement system, was modified to enable the measurement of SWCC under constant total stress conditions. The apparatus comprised of base pedestal embedded with a donut shaped ceramic disk (*AEV*=100 kPa), and piezoelectric disk transducer at its center (Figure 7.1).

In this study, a disc type piezo-ceramic element was employed. P-type as well as S-type piezoceramic element is manufactured by Fuji ceramics corporation (Model: P-type: Z2T20D-SYX (C-6); S-type: SZ5T20D-LLYX (C-6)). This can employ P-wave and S-wave measurement individually. This study applied the single piezoelectric transducer which can measure p-wave as well as S-wave on a single specimen. P-type and S-type piezoelectric elements were merged as a single element (PS-type) with good bond of Araldite. Details of assemble are shown in Figure 7.2.The PS-type piezo-ceramic transduce was applied on this study. Figure 7.3 shows schematic representation of disk transducer used for this study.

Figure 7.1: Modified pedestal and top cap of triaxial apparatus. Disk type piezoelectric transducers are fitted at their respective centers.
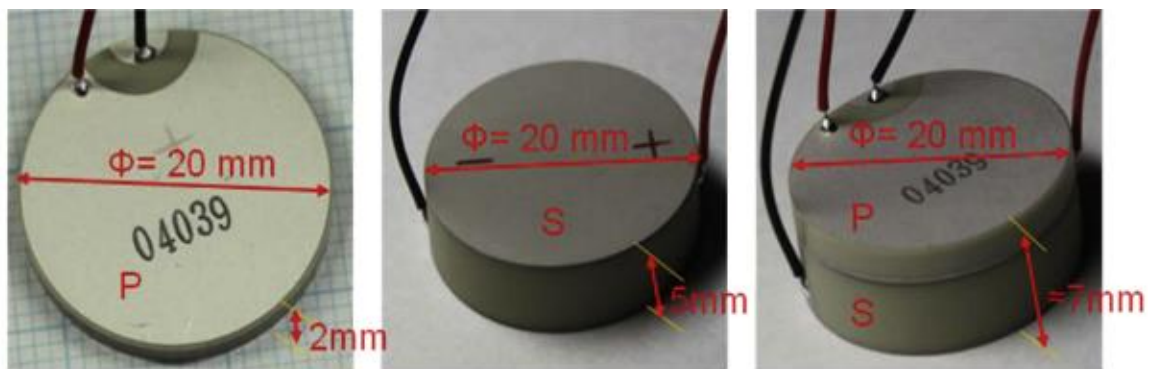
Figure 7.2: Pictures of piezo-ceramic elements used in this study (Suwal & Kuwano, 2013).
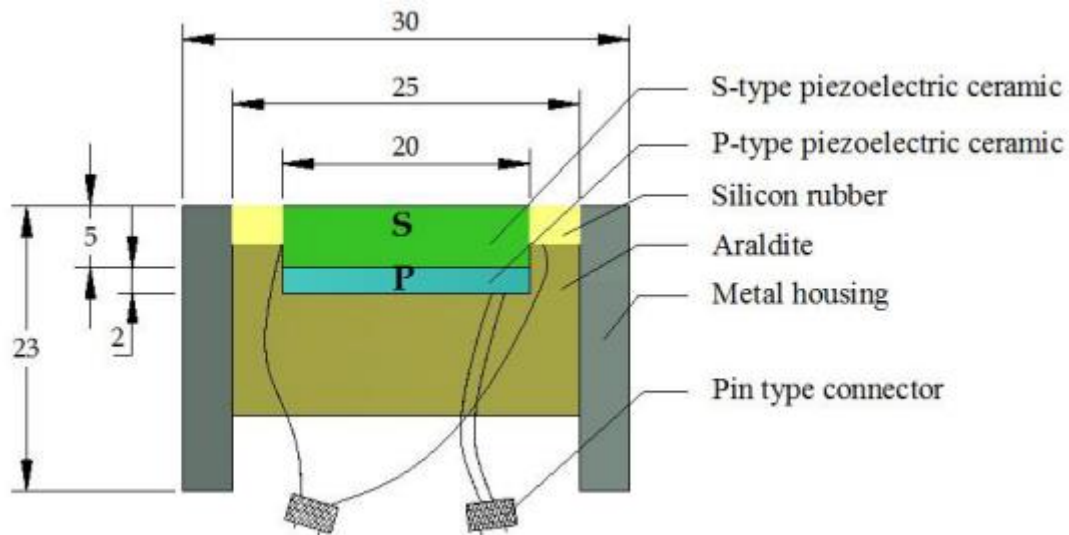
Figure 7.3: Schematic diagram of piezoelectric disk transducer.

Specimens (75 mm in diameter and 41 mm in height) were prepared inside a latex membrane which was supported by a brass split mold. To avoid radial expansion/contraction, split mold was kept in place throughout the length of experiments. Vertical movement of top cap was however, not restricted; and the specimens were effectively under K_o stress conditions. Vertical movement of top cap was recorded by an *LVDT* attached to a vertical rod connecting the top cap. Any changes in vertical stress were countered by adding/removing dead loads on top of a platform connected with top cap.

Saturation state of specimen was established by monitoring the amount of water sucked in or drained out of the specimen. Water flowing in or out of the specimen was established by monitoring the weight of a water bottle connected to saturated ceramic disk. Water in this bottle was kept at atmospheric pressure by making a small hole in the top portion of bottle. Evaporation losses through this hole were determined by means of a similar water bottle which served as a reference. Weight of water bottle connected to soil sample was thus adjusted for evaporation losses. Rate of water flowing in or out of the specimen was observed by continuously recording the weight of water bottle. For this, water bottle was placed on a weighing balance and a camera took photos of its readings at regular time intervals.

For elastic wave measurement, disk type piezoelectric transducers (Irfan & Uchimura, 2013; Suwal & Kuwano, 2013) were used. Other components of wave measurement

setup consisted of function generator (*Tektronix, AFG3022B*, as shown in Figure 7.4), power amplifier (*NF Corp. model HSA4012*, as shown in Figure 7.5) and digital oscilloscope (*HIOKI model 8860 with Hioki 8957 high resolution input module*, as shown in Figure 7.6). The exciter disk transducer in the top cap was triggered by a pulse generated by function generator, and amplified by the power amplifier. The generated pulse travelled through the soil specimen and was received by the receiving disk transducer in the base pedestal. The received signal was transmitted to the oscilloscope to be digitally displayed. Schematic illustration of the test setup is shown in Figure 7.7.
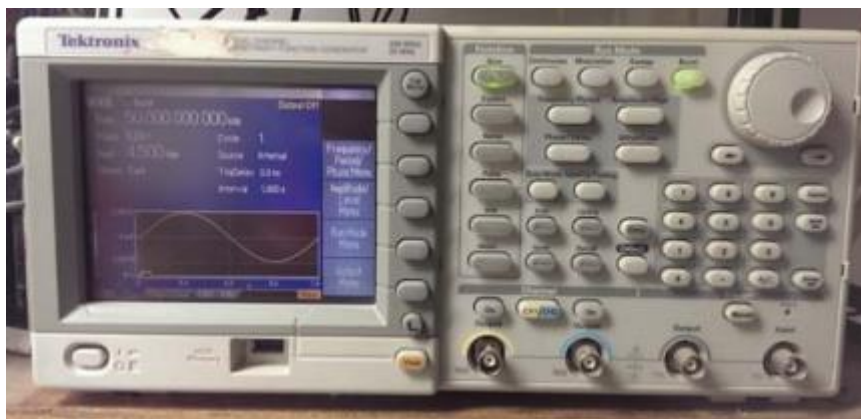
Figure 7.4: Tektronix AFG-3022C function generator used in this study

Figure 7.5: Power amplifiers used in this study.
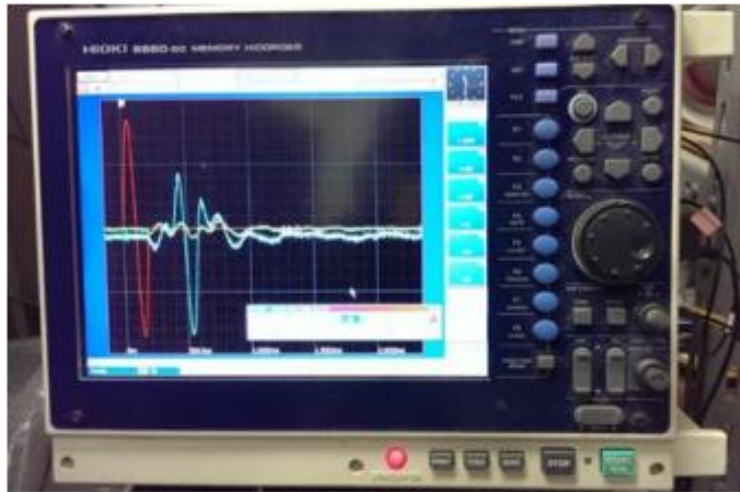
Figure 7.6: Wave recording devices used in this study.
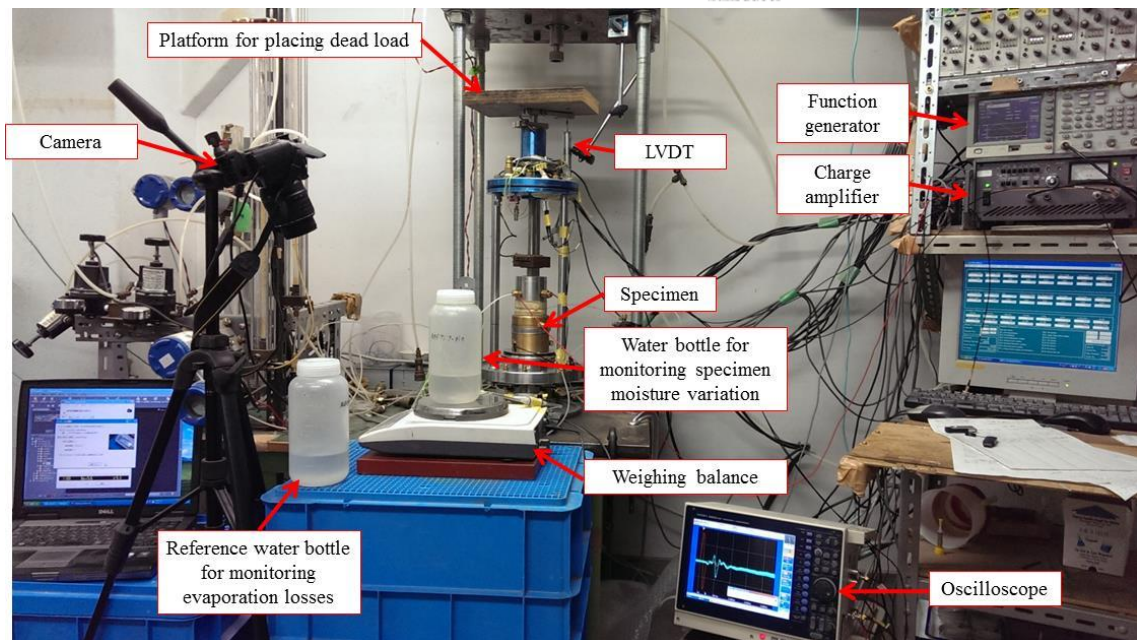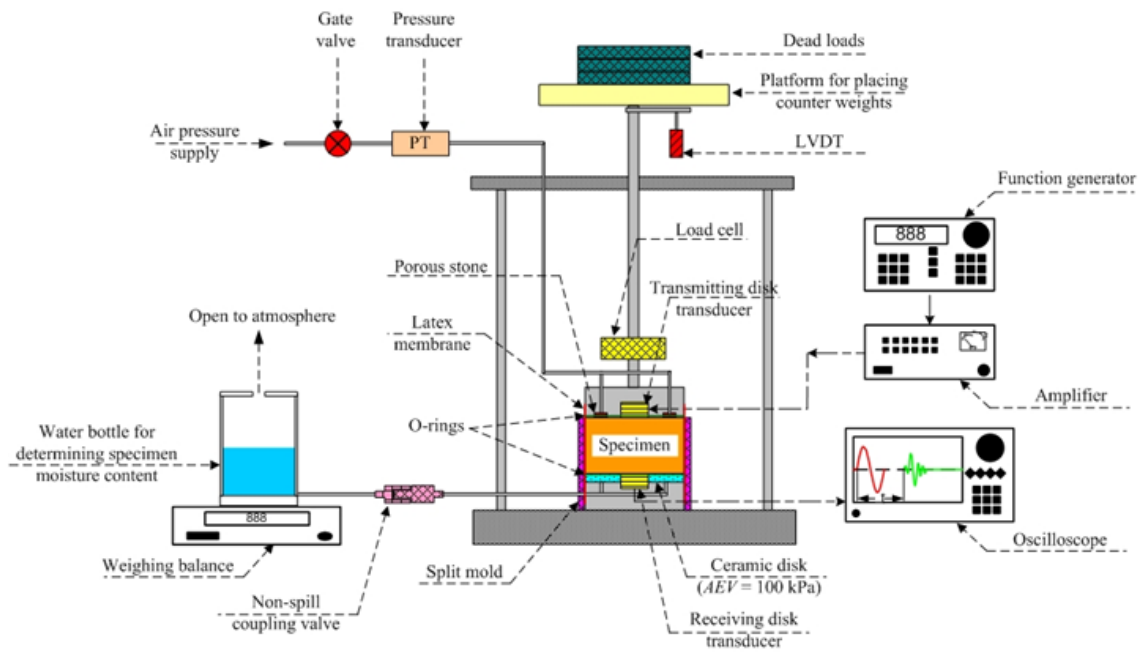
Figure 7.7: Schematic layout of modified SWCC-wave velocity apparatus.

7.3. TEST PROCEDURES

7.3.1. Specimen Preparation and Saturation

The experimental procedures broadly involved ceramic disk saturation, sample preparation, and obtaining drying and wetting SWCC with elastic wave measurements. The test started by saturating the ceramic disk. For saturation, the ceramic disk base

pedestal was immersed in water and subjected to negative pressure of -101.78 kPa. After 24 hours, it was removed from the saturation tank, installed in the triaxial apparatus and connected to a water bottle in order to avoid de-saturation of ceramic disk. Rubber membrane (0.3 mm thick) was fastened to the circumference of base pedestal and split mold was set up. Weight of oven-dried Edosaki sand, required to achieve target density was computed. Soil was mixed with water to attain gravimetric water content of 10% for all experiments. Water connection to ceramic disk was closed and its surface was wiped with a tissue paper. Specimen was then directly prepared on top of the saturated ceramic disk by tamping moist sand into four equal layers (wet tamping technique).

The prepared specimen was then saturated by flowing water through the ceramic disk. Very small water head (1~2 kPa) was used to avoid any possibility of piping inside the specimen. Soil specimen (along with base pedestal and mould) was disconnected from water bottle and weighed at regular intervals. Specimen was considered to be saturated when it attained a constant weight. Saturation of specimen was generally completed in 3~4 days. Steps involved in specimen preparation and saturation are described in Figure 7.8.
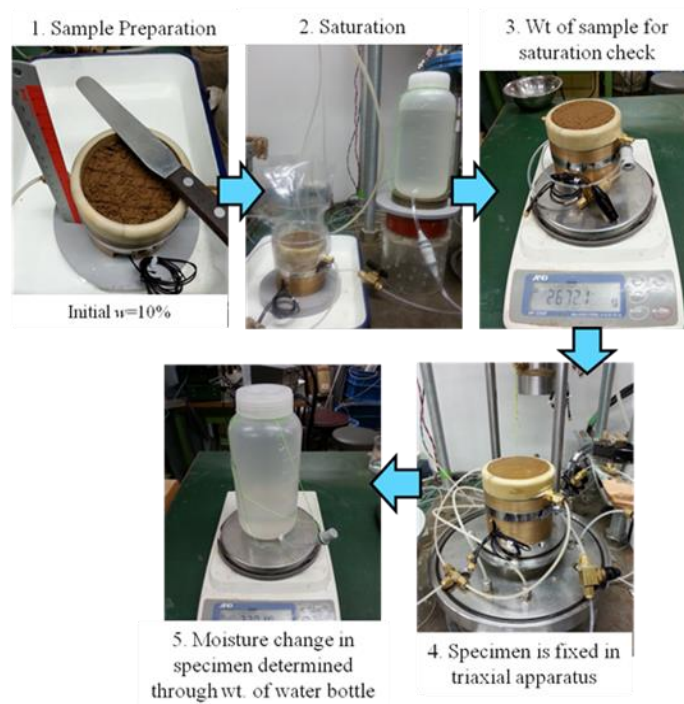
Figure 7.8: Specimen preparation and saturation.

7.3.2. Determining Drying and Wetting SWCC

For the determination of SWCC during drying and wetting, the saturated soil specimen was subjected to various magnitudes of matric suction and the corresponding change in specimen moisture was recorded. Once the specimen set up was complete, water level in the bottle was brought to the center of specimen and pore air pressure was vented to atmosphere (i.e., air pressure inside the specimen (u_a) is zero) (Figure 7.9). This condition represented zero matric suction ($u_a-u_w=0$), and it was maintained until constant weight of water bottle was attained. From this point, the specimen was subjected to drying path by increasing matric suction to 0.5 kPa, 1.0 kPa, 2.0 kPa, 4.0 kPa, 7.0 kPa, 10.0 kPa, 15.0 kPa, 30.0 kPa, and 50.0 kPa. For matric suction between 0 kPa to 4.0 kPa, pore air pressure was not changed ($u_a=0$), and the desired magnitude of matric suction was obtained by lowering the level of water bottle. For example, level of water was lowered to 40 cm below the center of specimen in order to apply suction of 4.0 kPa. However for matric suction greater than 4.0 kPa, water level was brought back to the center of specimen ($u_w=0$) and pore air pressure by an air compressor, through the top cap, was increased. The magnitude of applied suction was thus equivalent to the applied pore air pressure. In order to maintain the axial stress constant throughout the experiment, a counter weight, equivalent in magnitude to the applied pore air pressure, was placed on the top cap.
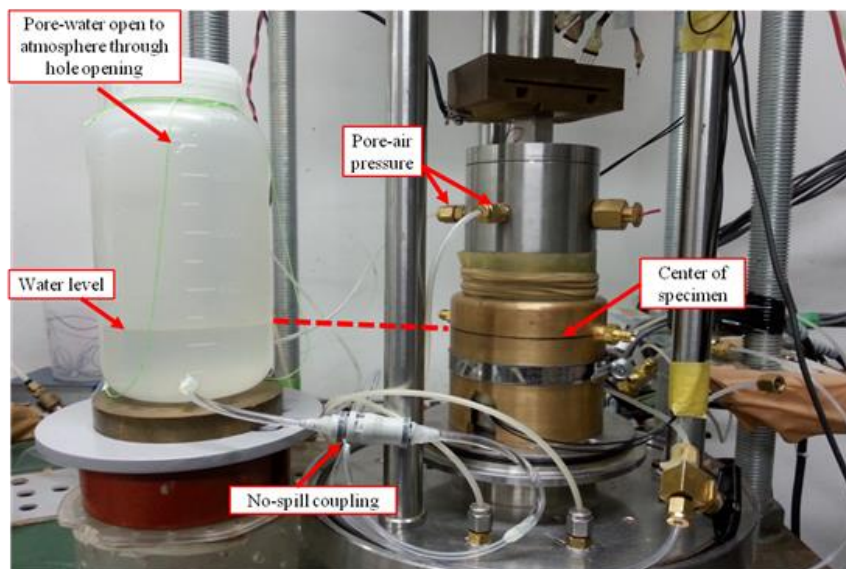
Figure 7.9: Water injection/drainage setup.

On each increment of matric suction, water flowed out from the specimen until equilibrium was reached. Equilibrium condition was generally reached in 24~48 hours and it was established when the weight of water bottle connected to the specimen became constant. Once the equilibrium was reached, shear and compression wave velocities through the soil were determined. For determining the amount of water drained out from the specimen, non-spill coupling valve linking the water bottle and soil specimen was disconnected, and water bottle was weighed carefully. Reference water bottle for determining evaporation water losses was also weighed and the corresponding corrections were applied. Maximum matric suction that can be applied to the specimen is limited by the air entry value of the ceramic disk, which was equal to 100 kPa for present apparatus. In this study, maximum matric suction applied to the specimen was 50 kPa, because it was extremely difficult to keep the specimen air-tight beyond this level.

To simulate the wetting path, pore air pressure was reduced from 50 kPa while maintaining the water level at the center of specimen. On decreasing the pore air pressure, water flowed into the soil specimen through the ceramic disk until equilibrium was reached. Water bottle was disconnected from the specimen and its weight was recorded to determine the amount of water sucked by the specimen. The same procedure was repeated for lower matric suction values greater than 4.0 kPa. Matric suction values of 4.0 kPa and lower were applied by venting pore air to atmosphere (u_a=0), and lowering the water level from the center of specimen. Similar to the drying path, elastic wave velocities (Vs and Vp) were determined after equalization of matric suction at each level.

When the specimen reached zero matric suction during the wetting process (i.e., pore air vented to atmosphere, and water level maintained at center of specimen), the assembly was disconnected and the corresponding moisture content was determined by oven-drying the soil specimen. Final moisture content, along with the previous readings of water bottle at various suction levels, was used to back calculate the actual water content of soil specimen at various suction levels.

7.4. TYPICAL TEST RESULTS

7.4.1. Signal Interpretation

By monitoring the input and output signals in the BE tests, wave velocity V, either Vs or Vp, can be calculated as follows:

$$V = L/t \qquad (1)$$

Where L the length of specimen, t is the travel time of the wave.

Figure 7.10 shows the received P-waves by one cycle of sinusoidal input at different frequencies.
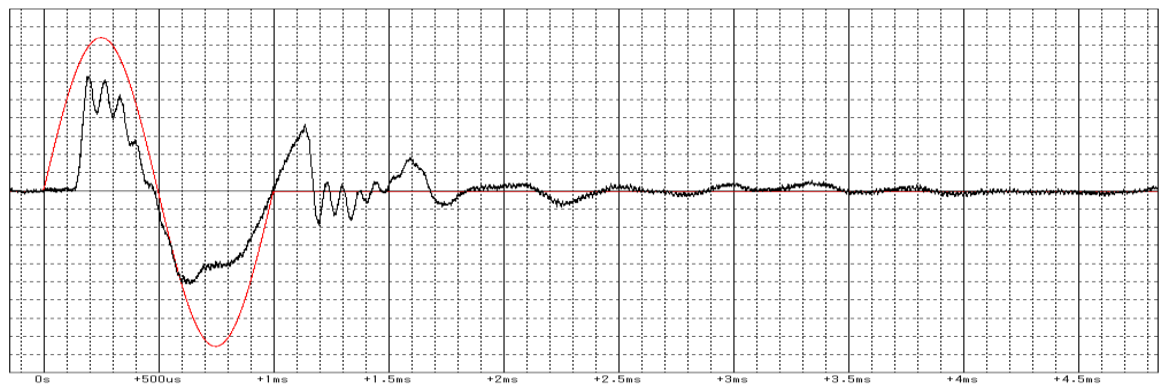
(a) 1kHz
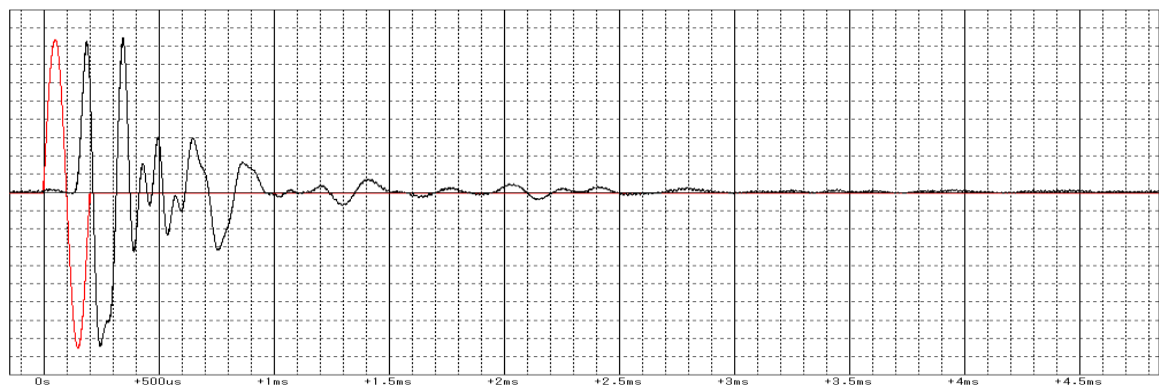
(b) 5kHz
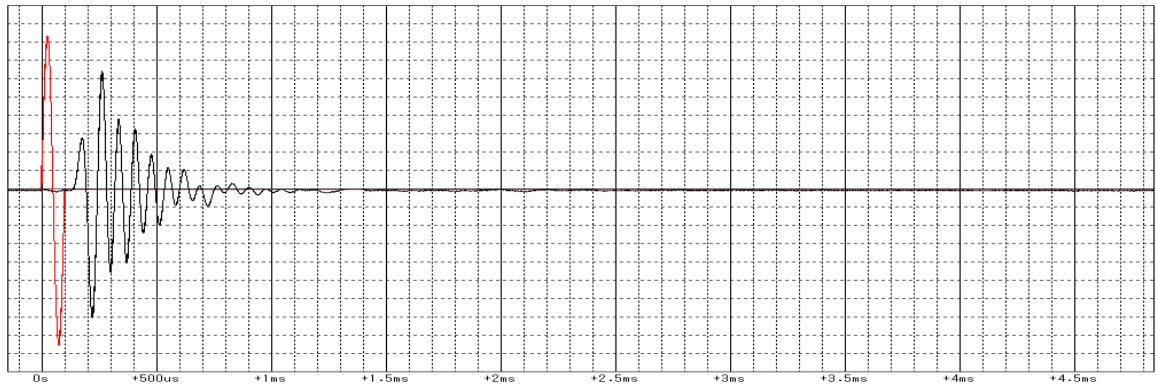
(c) 10kHz
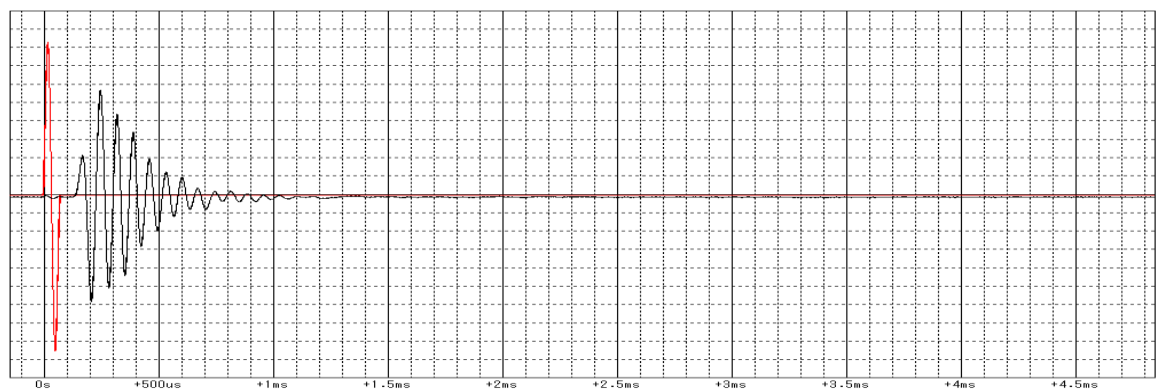
(d) 15kHz
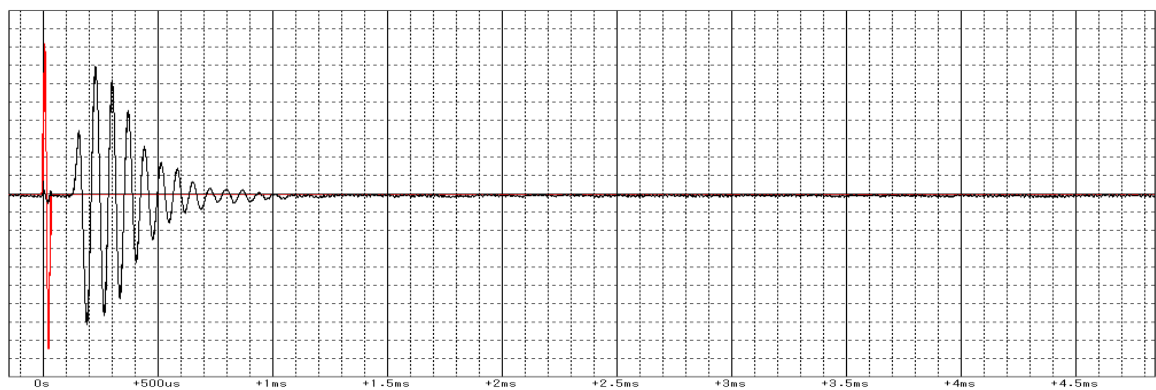
(e) 20kHz

Figure 7.10: Received P-wave wave.

Figure 7.11 shows the received S-waves by one cycle of sinusoidal input at different frequencies. The first part of the received signal is confirmed to be the near field

component, as its polarization is opposite to the input, and the corresponding arrival time is near the value of the P-wave propagation.
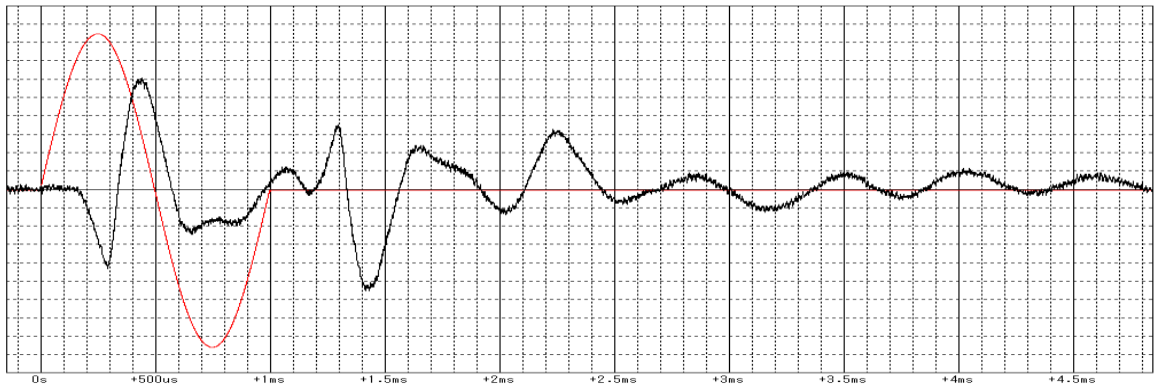
(a) 1kHz
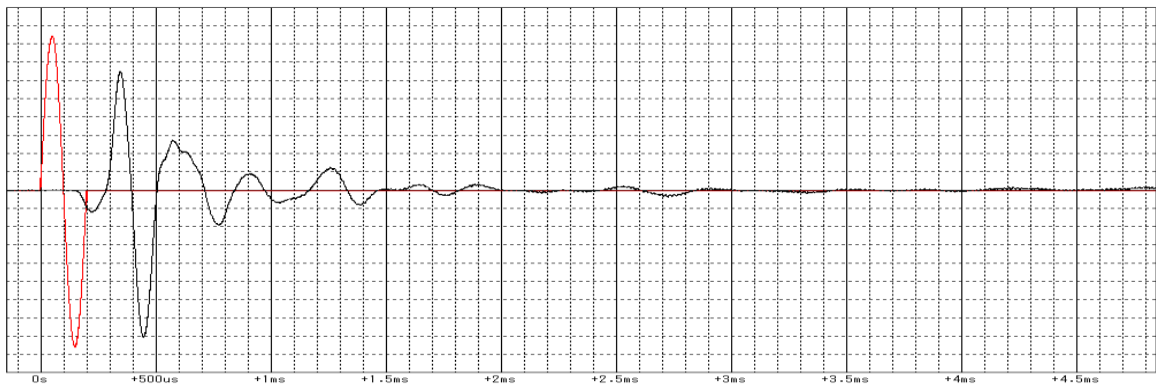
(b) 5kHz
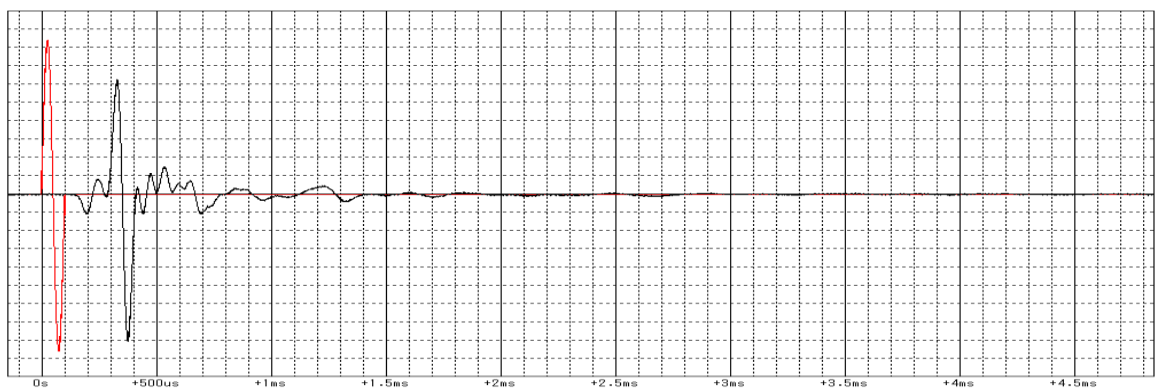
(c) 10kHz
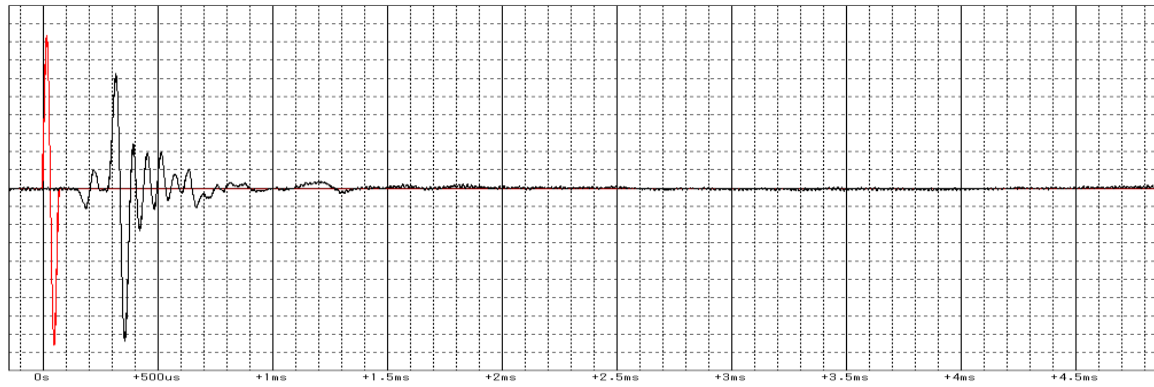
(d) 15kHz
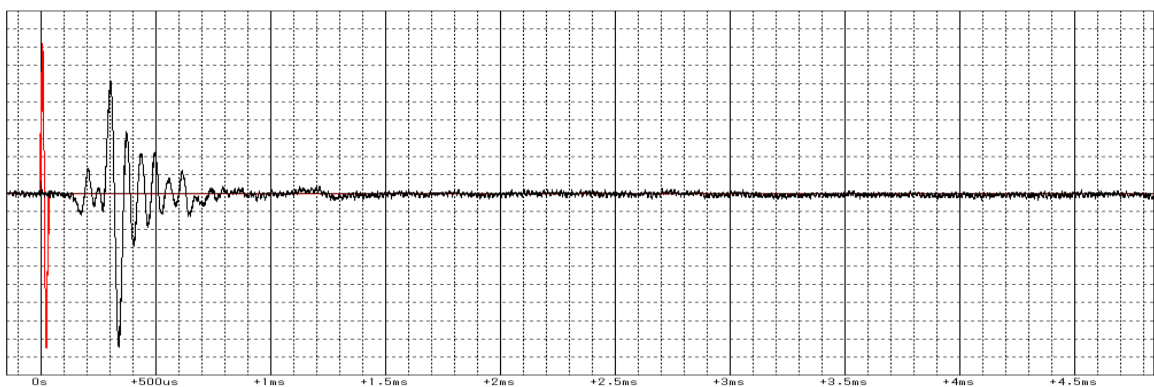
(e) 20kHz

Figure 7.11: Received S-wave wave.

It is well agreed that the tip-to-tip distance between the source and the receiver elements can be taken as the travel distance (Dyvik and Madshus, 1985; Viggiani and Atkinson, 1995; Lee and Santamarina, 2005; Yamashita et al., 2009; Irfan, 2014).

7.4.2. SWCC and Wave Velocity

Figure 7.12 to Figure 7.14 show test results of a preliminary test conducted on Edosaki sand with density of 1.2, 1.3 and 1.4g/cm. The test was conducted under net normal stress (σ-u_a) of 10 kPa. Unlike a typical SWCC test conducted in tempe pressure cell, small magnitude of net stress was required in order to maintain good contact between disk transducer and soil. Elastic waves would not be able to transmit from the sensor to the soil without proper contact. SWCC presented was found consistent with the results of Gallage and Uchimura (2010). S-wave and P-wave

velocities increased with matric suction (see Figure 7.12 to Figure 7.14). The behavior appears to be bi-linear, with a clear hysteresis between the drying and wetting curves. Increase in wave velocities with matric suction may be attributed to the increasing soil stiffness. Figure 7.15 represents the behavior of S-wave and P-wave velocities with volumetric water content and comparison between model tests was made. Decrease in wave velocities with volumetric water content may be because of gradual decrease of suction and effective stress of soil. Magnitudes of S-wave and P-wave velocities were compared with those obtained through model tests. Results were found to be reasonable and consistent with S-wave. P-wave was masked during the wave propagation. A possible reason could be the weak near field component which travels with the velocity of P-wave, which cannot be clearly detected in the wave signal.
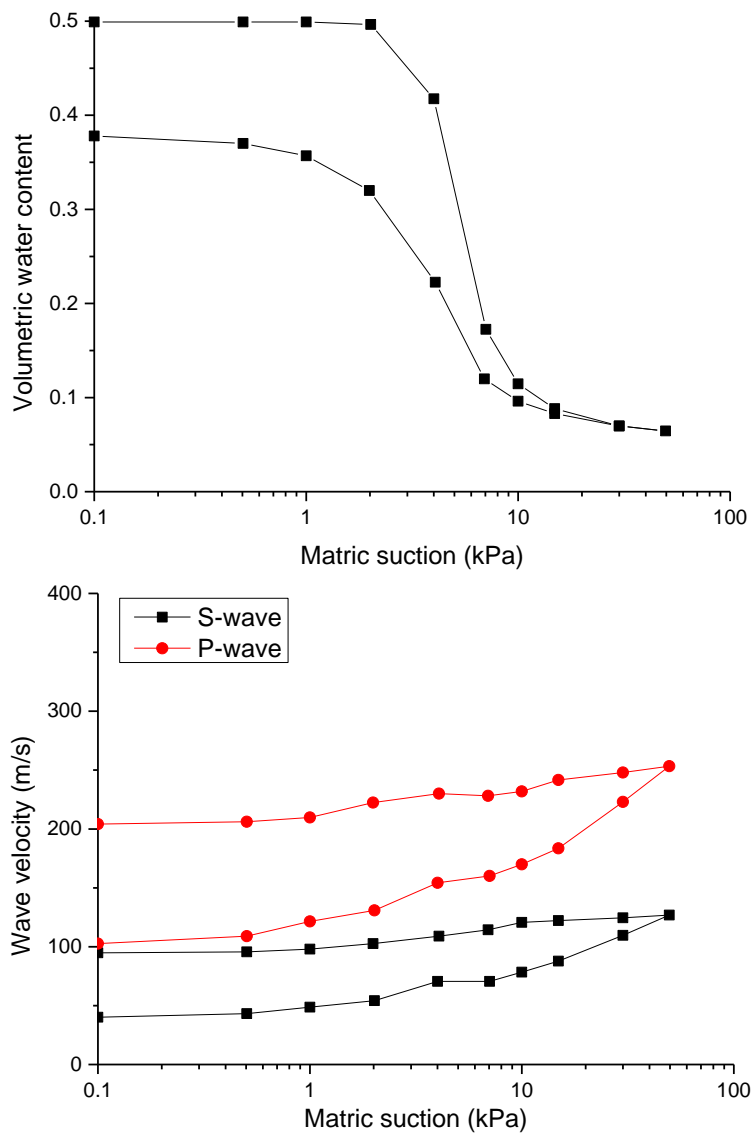
Figure 7.12: SWCC and wave velocity for soil with density of 1.2g/cm^3.
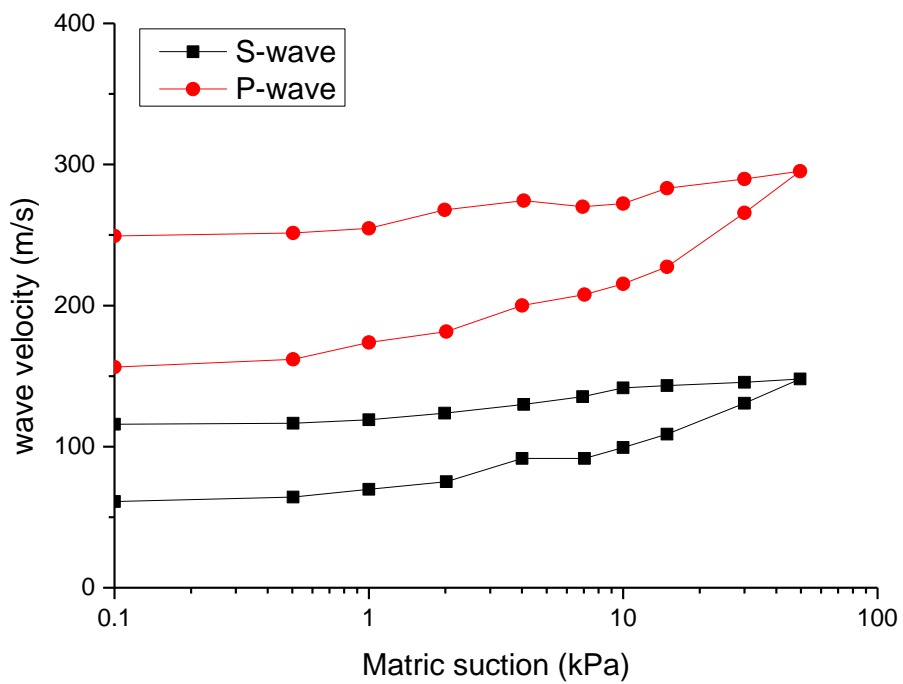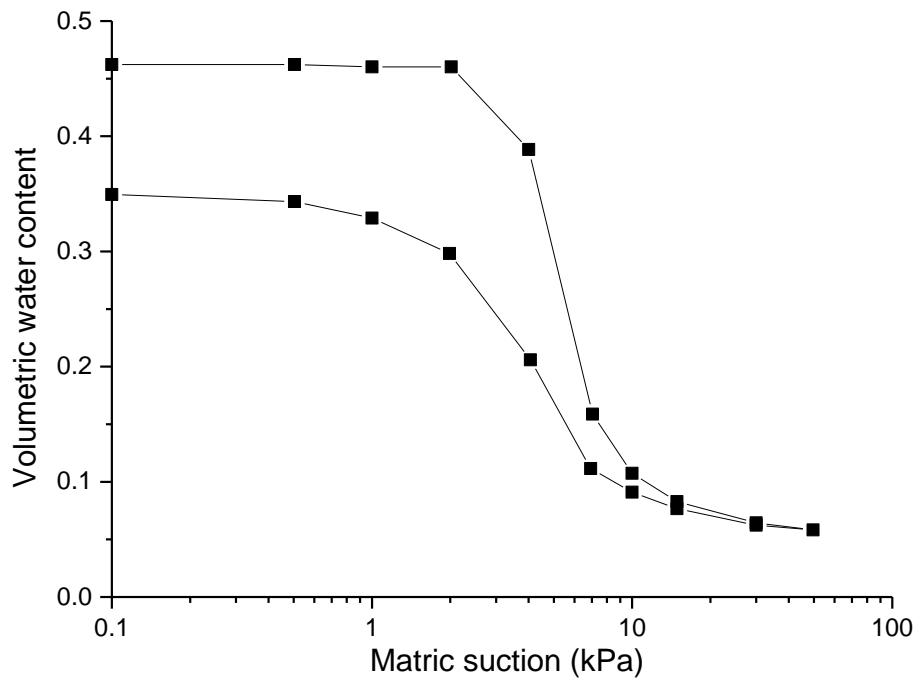
Figure 7.13: SWCC and wave velocity for soil with density of 1.3g/cm^3.
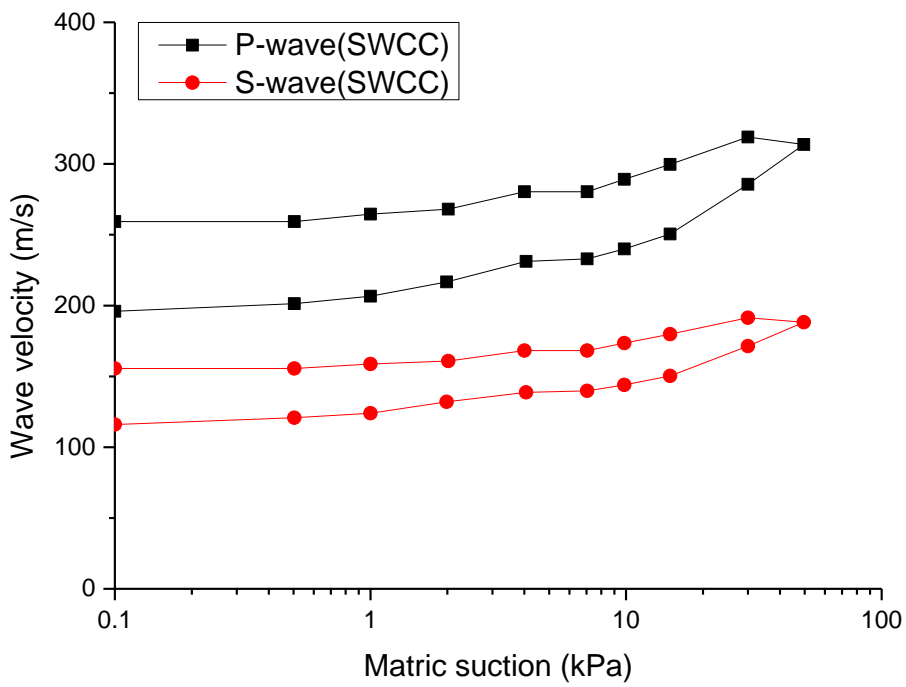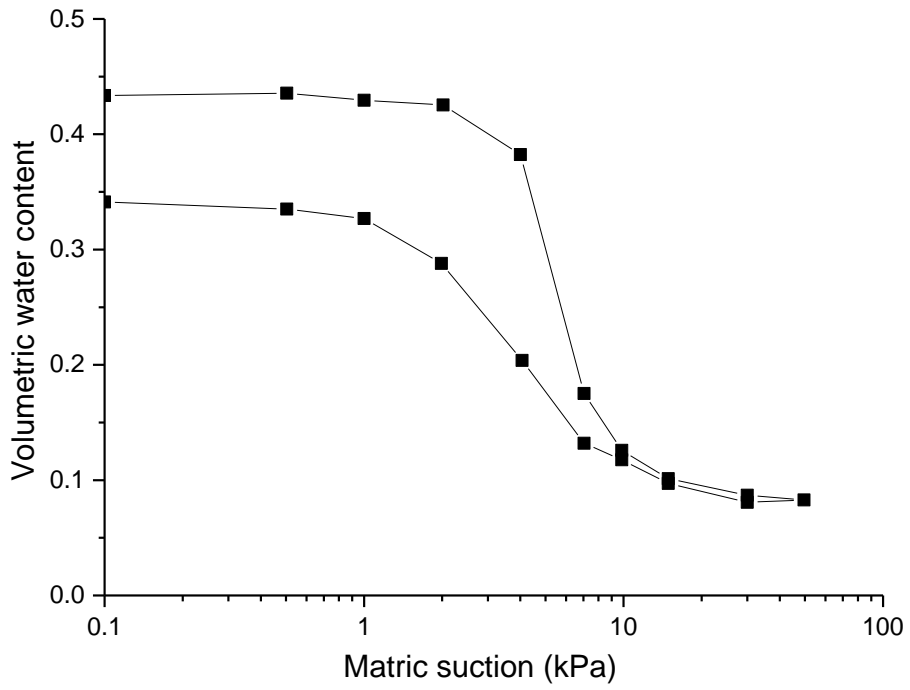
Figure 7.14: SWCC and wave velocity for soil with density of 1.4g/cm^3.
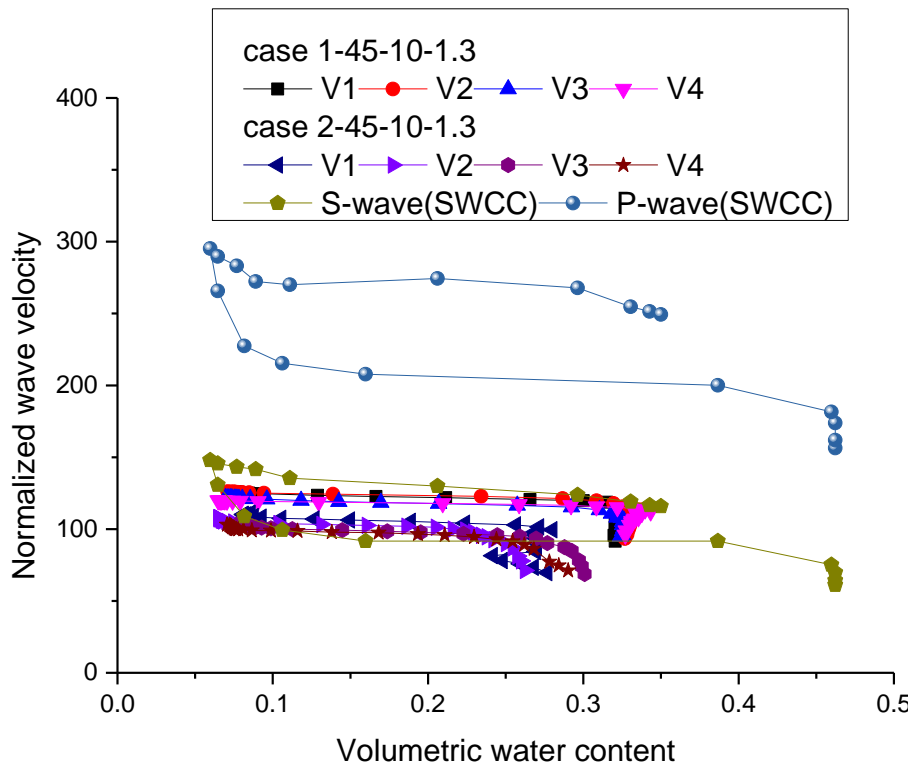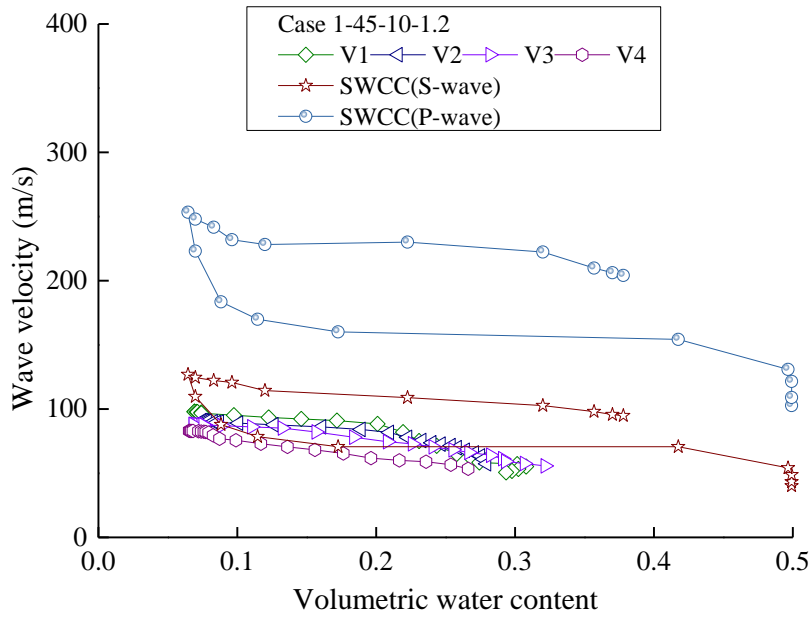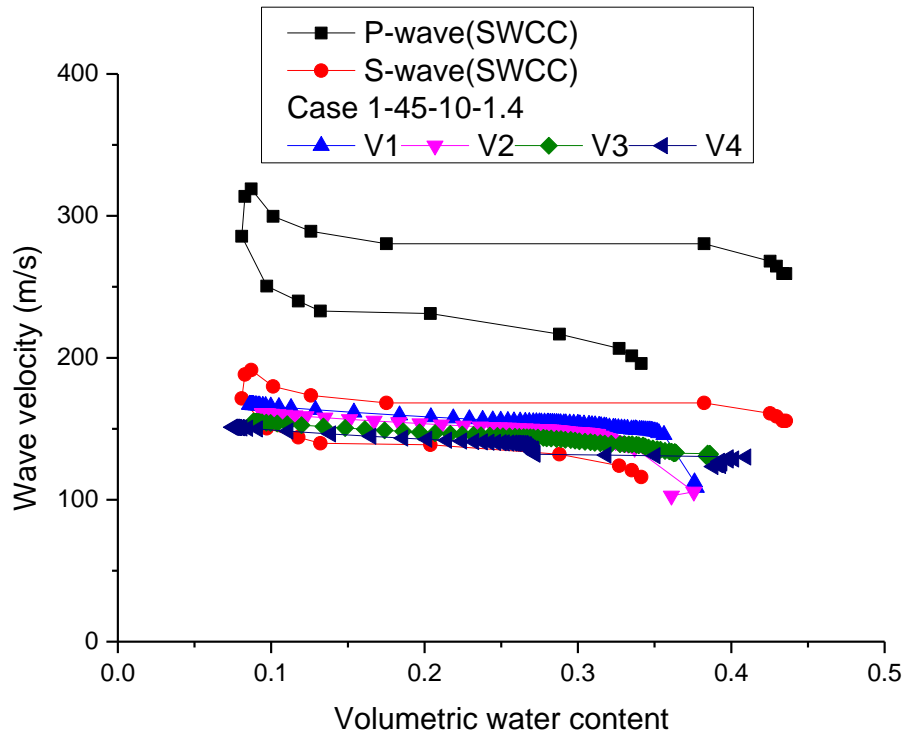
Figure 7.15: comparison of S-wave and P-wave velocities with volumetric water content obtained through SWCC tests and model tests.

7.5. CONCLUDING REMARKS

An apparatus to study the variation of elastic wave velocities (shear wave and compression wave velocities) during drying and wetting path of SWCC is devised in this paper. The apparatus finds itself quite unique, as no standard apparatus is available for the said purpose. Basic working principle and limitations of the apparatus are discussed.

S-wave and P-wave velocities increased with matric suction. The behavior appears to be bi-linear, with a clear hysteresis between the drying and wetting curves. Increase in wave velocities with matric suction may be attributed to the increasing soil stiffness.

Magnitudes of S-wave and P-wave velocities were compared with those obtained from model tests. Results were found to be reasonable and consistent with S-wave.

7.6. REFERENCES

Gallage, C., & Uchimura, T. (2010). Effects of dry density and grain size distribution on soil-water characteristic curves of sandy soils. *Soils and foundations, 50*(1), 161-172.

Irfan, M., & Uchimura, T. (2013). Measuring shear and compression wave velocities in laboratory triaxial tests using disk shaped composite P/S piezoelectric transducer. *IACGE 2013: Challenges and Recent Advances in Geotechnical and Seismic Research and Practices ASCE GSP # 232*, 414-421.

Suwal, L. P., & Kuwano, R. (2013). Disk shaped piezo-ceramic transducer for P and S wave measurement in a laboratory soil specimen. *Soils and foundations, 53*(4), 510-524.

Dyvik, R., Madshus, C. (1978). Lab measurements of Gmax using bender elements. In: Khosla V (ed) Advances in the art of testing soils under cyclic conditions. ASCE, New York, 186–196.

Viggiani, G., Atkinson, J.H. (1995). Interpretation of bender element tests. Géotechnique 45 (1), 149–154.

Lee, J. S., & Santamarina, J. C. (2005). Bender elements: performance and signal interpretation. Journal of Geotechnical and Geoenvironmental Engineering, 131(9), 1063-1070.

Yamashita, S., Kawaguchi, T., Nakata, Y., Mikami, T., Fujiwara, T., & Shibuya, S. (2009). Interpretation of international parallel test on the measurement of Gmax using bender elements. Soils and foundations, 49(4), 631-650.

Irfan, M. (2014). *Elastic Wave Propagation through Unsaturated Soils Concerning Early Warning of Rain-induced Landslides.* PhD Thesis, Univeristy of Tokyo, Tokyo.

CHAPTER 8

FIELD APPLICATION OF ELASTIC WAVE VELOCITIES FOR LANDSLIDE PREDICTION

8.1. GENERAL

The challenge in this study is to predict the stability of soil slope using elastic wave velocities. Rain-induced landslides usually occur at shallow layer (Anderson & Sitar, 1995; Ng & Pang, 2000; Farooq et al., 2004). During the rainfall event, water infiltrates into the slope causing higher pore water pressure. As a result, the matrix suction in soil decreases leading to lower shear strength. Due to the loss of shear strength, the soil slope surface begins to become increasingly unstable and this destabilization continues to a point where equilibrium cannot be sustained any more, thus this slope finally fails. The following section discusses the potential of applying the idea of elastic wave velocities to predict such rain induced landslides by a medium scale model test and a large scale model test.

8.2. MEDIUM SCALE MODEL TEST

8.2.1. Material and Methods

The soil samples used were obtained from a landslide site in Izu-Oshima. The soil contains fines content of 6% and the fines are non-plastic. Physical properties and grain size distribution curve are given in Figure 8.1.
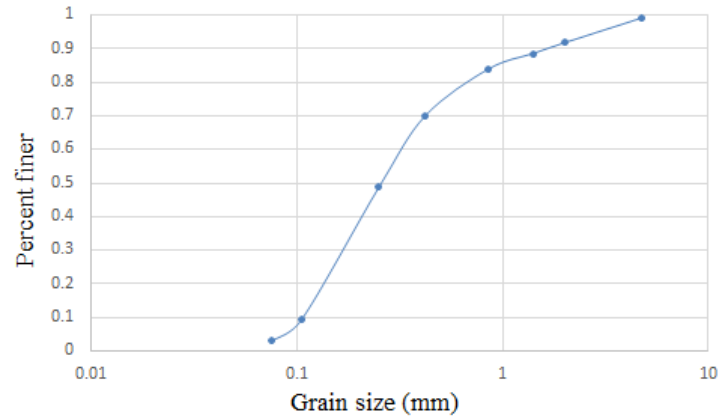
Figure 8.1: Grain size distribution of Oshima soil.

The tank used in the model tests is shown schematically in Figure 8.2. It is 220cm long, 80cm wide and 100cm high. Its walls are made of steel plates, except for the front one which is made of acryl glass for easy observation of the deformation process.
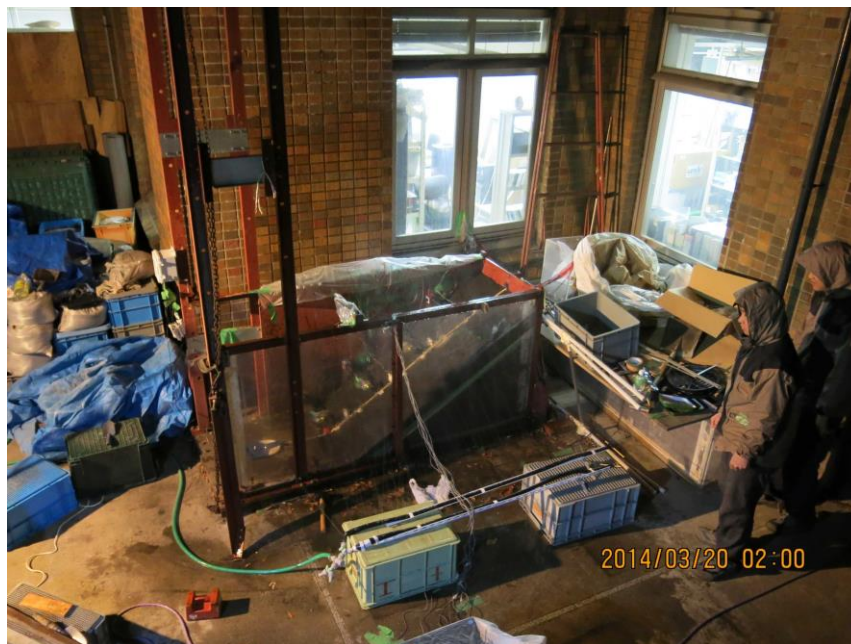
Figure 8.2: Photo of the experimental soil tank.

Various sensors, such as self-made pore-water pressure transducers, soil moisture content transducers, wave transducers, and displacement marker and laser

displacement transducers, were installed in the model slope, as shown schematically in Figure 8.3. Wave sensors were connected to Keyence data logger and others were connected to HOBO data logger.

The soil moisture content transducers and wave transducers as well as data logger were introduced in Chapter 3. In order to measure pore to give a comprehensive view of unsaturated soil behavior, a small sized pore-water pressure sensor was made (Figure 8.4). This sensor employs micro porous membrane as it gives shorter time to reach equilibrium when measuring pore-water pressure compared to ceramic disk (Nishiumura et al., 2012).

Surface displacement was measured by placing targets on the slope surface and monitoring their movement with a laser displacement transducer fixed in support adjacent to the target (see Figure 8.5). This sensor uses a high precision laser beam which can detect infinitesimal displacements within 10μm, thereby providing extremely accurate measurements of minute displacements of the slope surface. The readings are fairly straight-forward, showing a linear relationship between the analog output and detected distance. Moreover, it detects objects with very low surface reflection characteristics, such as black rubber. Because the beam is easy to aim, precise positioning and alignment are possible. In addition to the displacement transducers, pin markers were placed on the slope surface.

Excitation source in the form of a steel rod and pipe with steel endpiece (Figure 8.6) was buried into the slope surface. The endpiece was struck by rod to generate excitations. Waves from the point of excitation would travel towards the receivers which can be interpreted to monitor any variations in the travel time. The wave form is shown in Figure 8.7.
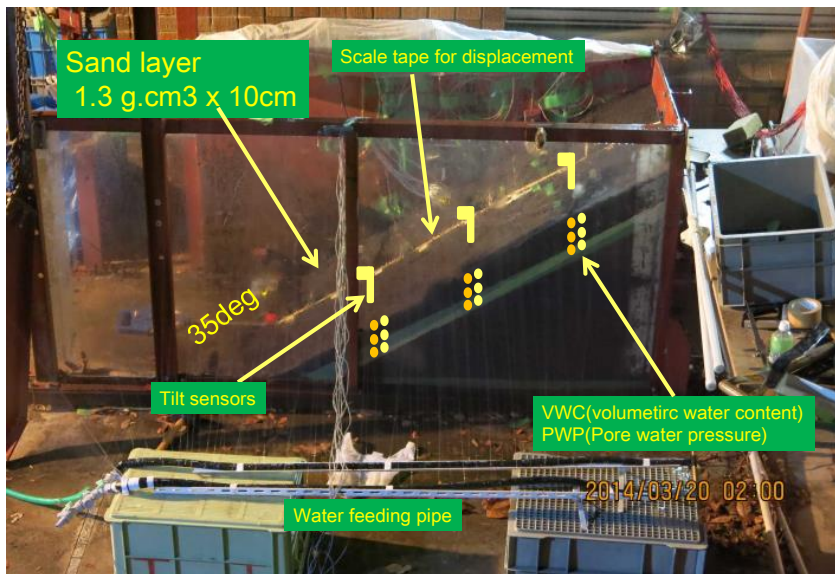
Figure 8.3: Schematic plan of the tank and transducers.

Figure 8.4: Pore water pressure sensor.

Figure 8.5: Laser displacement transducer and target.

Figure 8.6: Excitation generation.

Figure 8.7: Wave form.

Slope model with slope angle of 35° was constructed by compacting Oshima soil. The compaction was performed in order to achieve the maximum dry density for base bed and 1.3 g/cm^3 for surface layer which is of 10cm.

Evaflow side spray irrigation tube system used in this experiment was able to provide a relatively uniform constant rainfall between 20 mm/hr and 50 mm/hr. It was able to control the rainfall intensity by regulating the pressure of the water supplied to the system.

8.2.2. Results

The tilt angle, displacement, volumetric water content, pore water pressure, and wave velocity monitored at differing locations are shown in Figure 8.8 to Figure 8.13. With the infiltration of water, the water content and pore water pressure increases, leading to a decrease of the suction. As a result, the slope surface started to move at an accelerating rate. The failure of the slope was triggered by the decrease in suction leading to a loss of cohesive strength within the saturated part of the soil mass. The wave velocity was found to decrease gradually by wetting and sharply when the displacement increased.
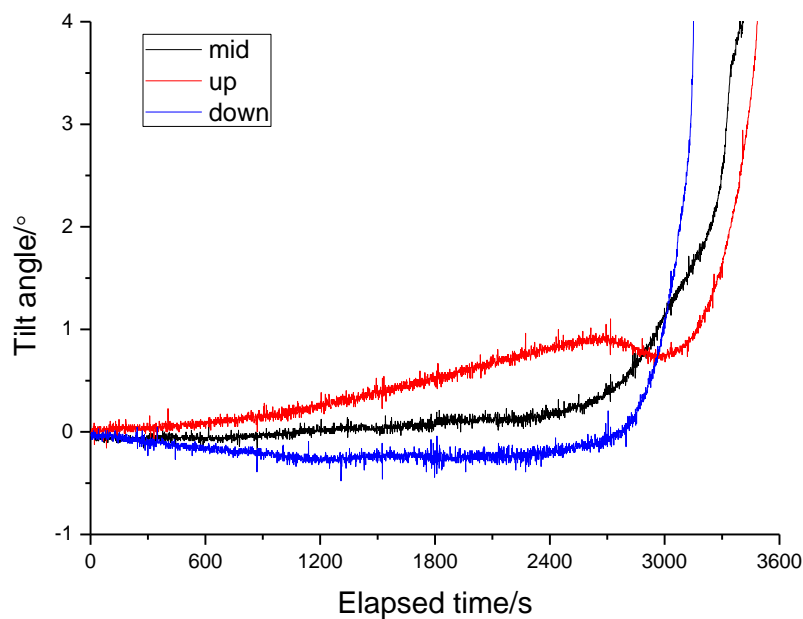
Figure 8.8: Time series data of tilt angle.
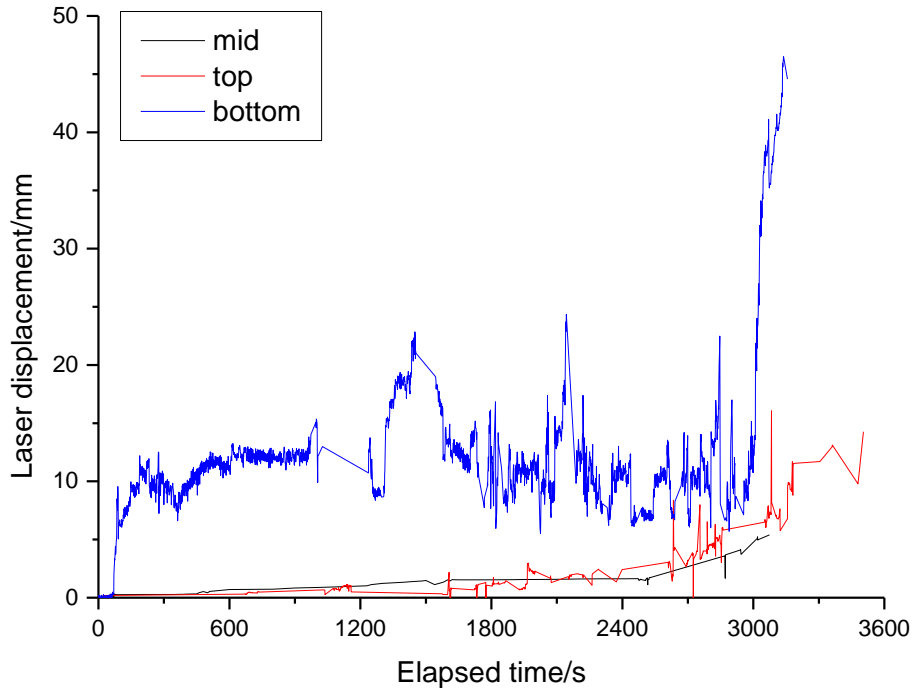
Figure 8.9: Time series data of displacement monitored by laser sensors.
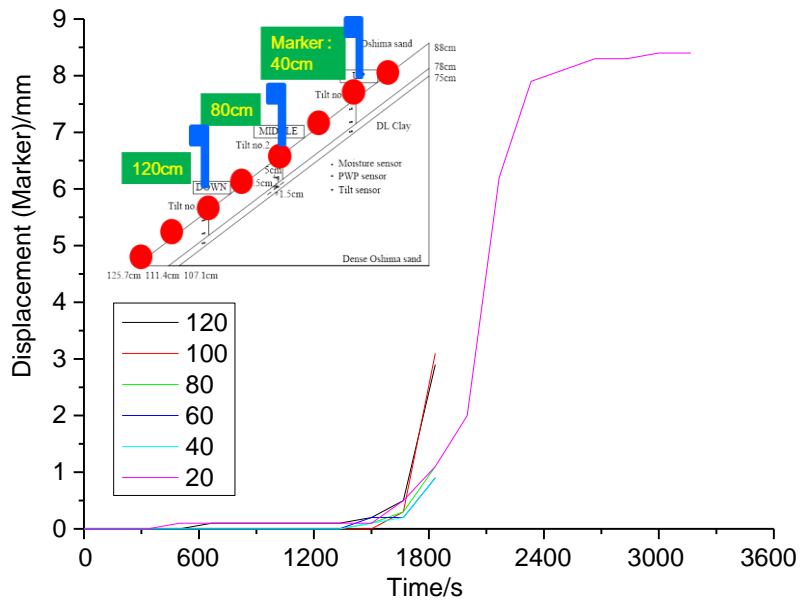
Figure 8.10: Time series data of displacement monitored by markers.
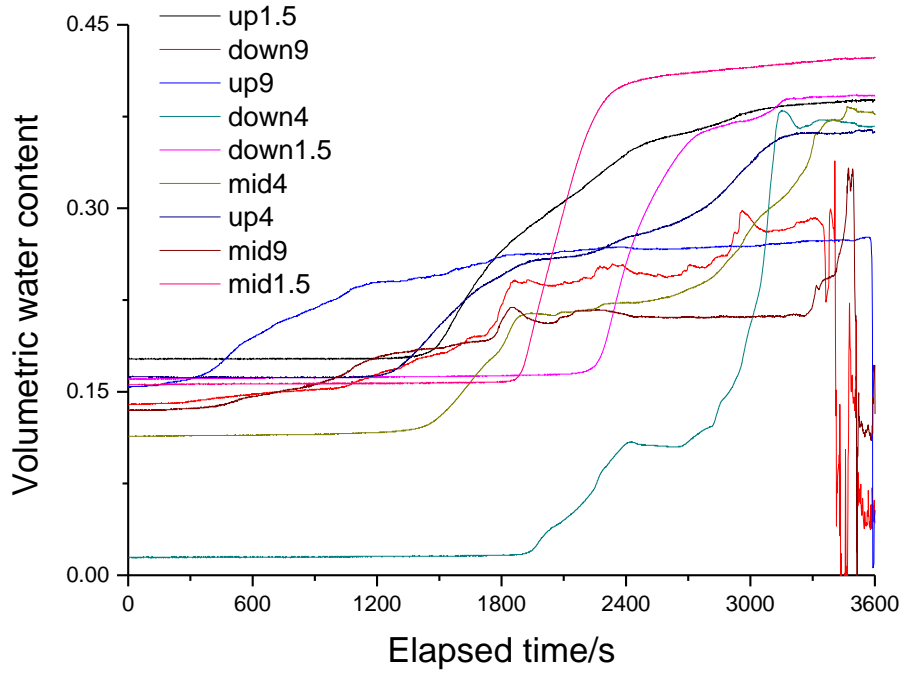
Figure 8.11: Time series data of volumetric water content.
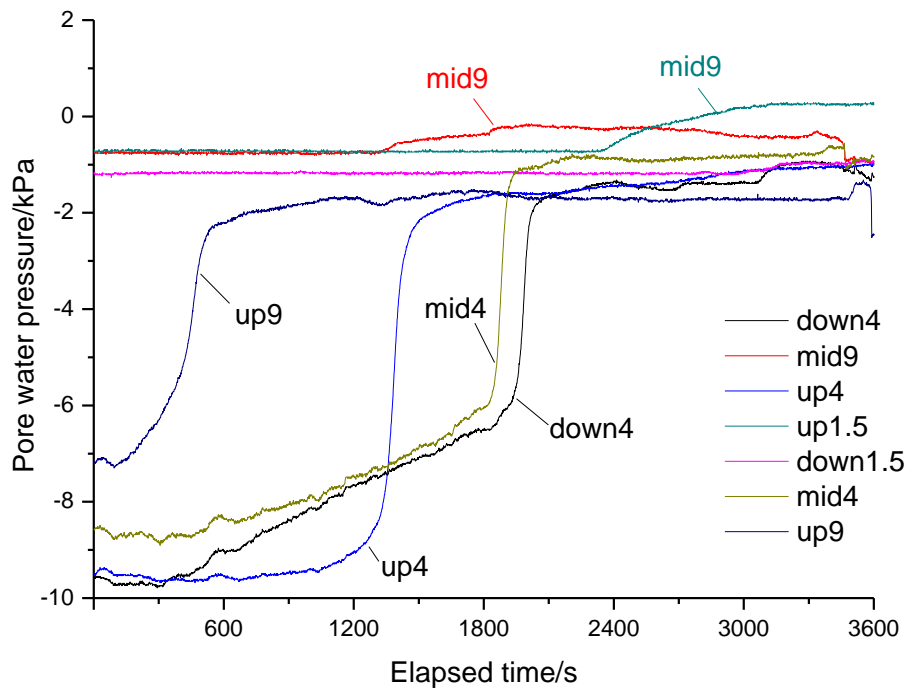
Figure 8.12: Time series data of pore water pressure.
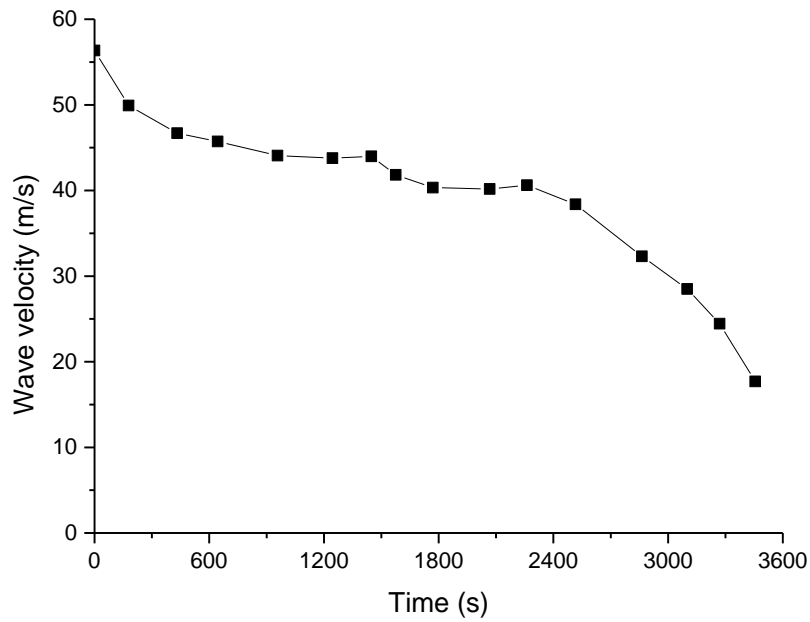
Figure 8.13: Time series data of wave velocity.

Wave velocity was correlated to the monitored volumetric water content (Figure 8.14), displacement monitored by laser sensor (Figure 8.15) and by marker (Figure 8.16), and tilt angle (Figure 8.17). The wave velocity decreased with volumetric water content and deformation. The trend of change in wave velocity with these parameters is consistent with the findings described in Chapter 5.
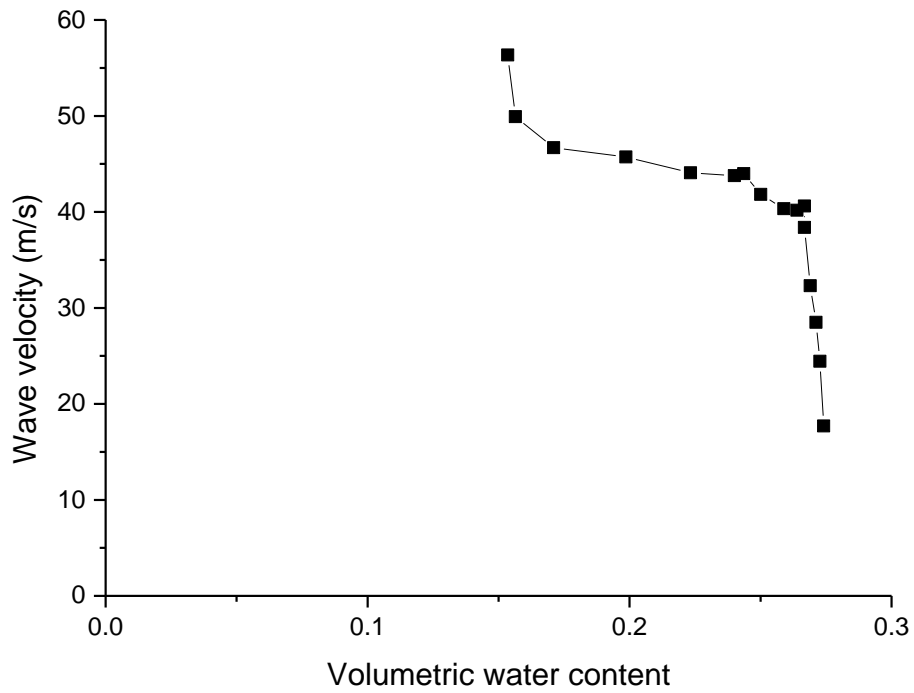
Figure 8.14: variation of wave velocity with volumetric water content.
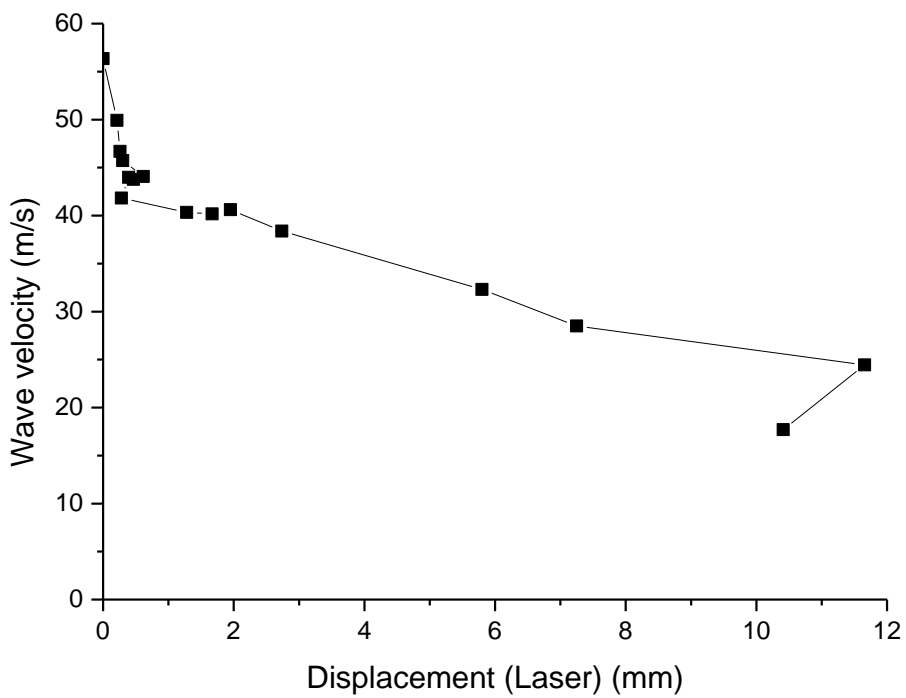
Figure 8.15: Variation of wave velocity with displacement monitored by laser sensors.
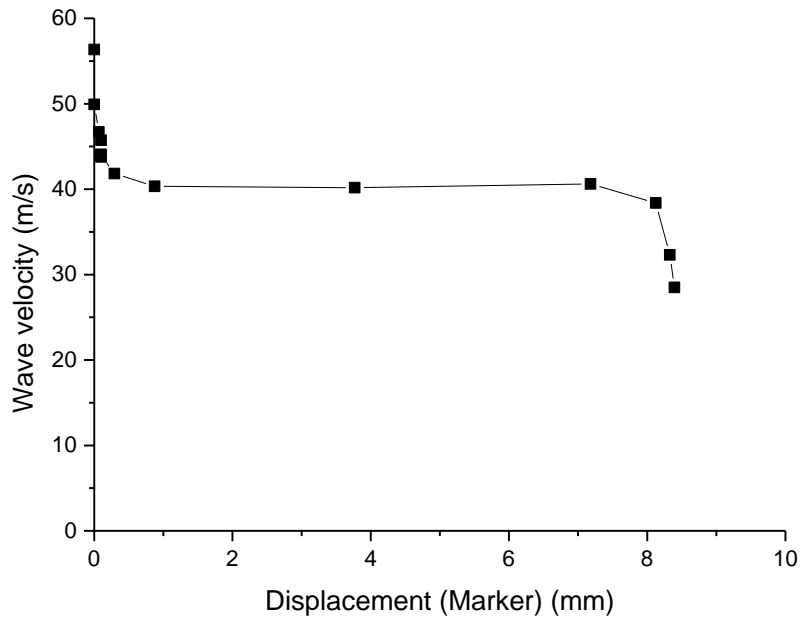
Figure 8.16: Variation of wave velocity with displacement monitored by markers.
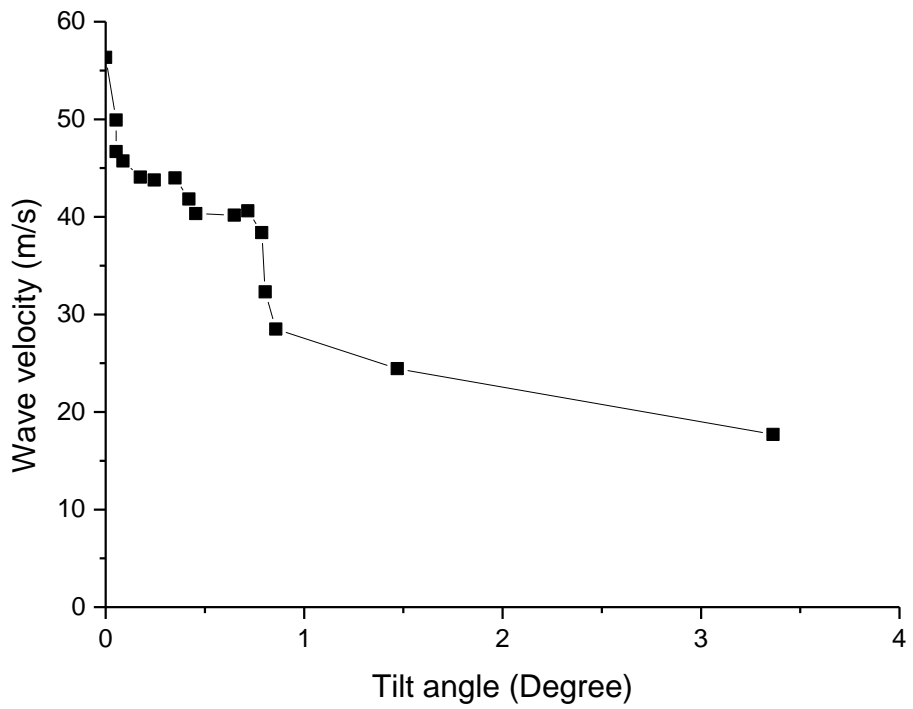
Figure 8.17: Variation of wave velocity with tilt angle.

8.3. LARGE SCALE MODEL TEST

8.3.1. Material and Methods

The large scale model test was conducted in National Research Institute for Earth Science and Disaster Prevention (NIED) in Tsukuba.

Soil used is strongly weathered granite. Its grain size distribution curve and soil-water characteristic curve are shown in Figure 8.18 and Figure 8.19 respectively. The compaction was performed in order to achieve the dry density of 1.6 g/cm^3. The model had a thickness of 1 m, width of 9 m, and a height of 5 m, as shown in Figure 8.20. The slope angle was found to be 40°. Three tilt sensors (Figure 8.21) and four wave sensors (Figure 8.22) were arranged on the deposit slope to monitor the tilt angle and wave velocity. A big solenoid was used as the excitation source, as shown in Figure 8.23.The solenoid attracted the iron nut to hit itself so that the elastic wave could be generated. Figure 8.24 shows the location of the monitoring devices. The rainfall simulator suspended in roof has a rainfall area of 44×72m and a rainfall intensity of 15-300mm/h, and conducts actual size model experiment.
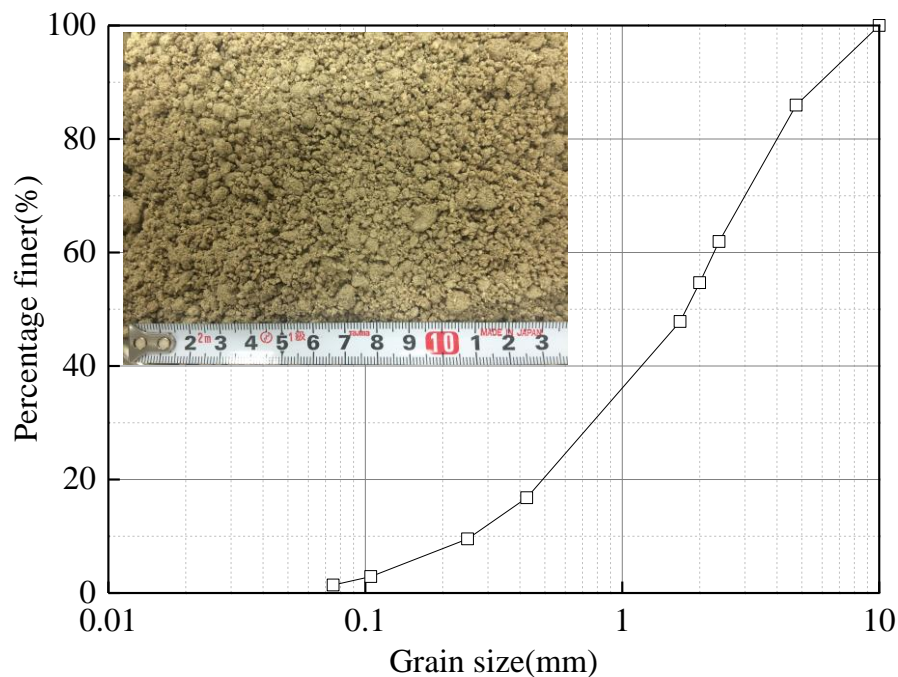
Figure 8.18: grain size distribution curve of used soil.
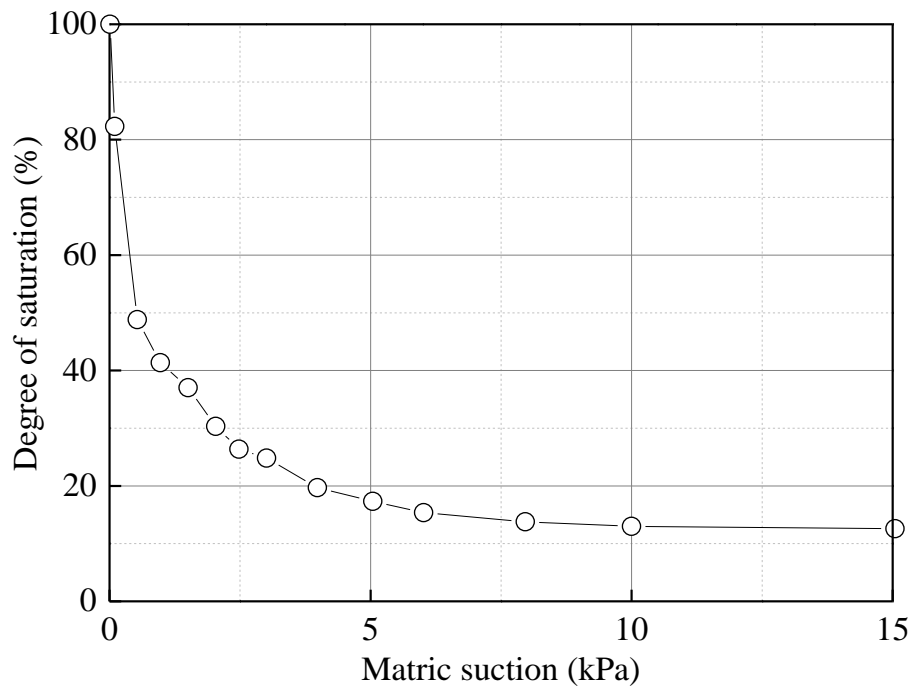
Figure 8.19: soil-water characteristic curve of used soil.

Figure 8.20: Slope model.

Figure 8.21: Tilt sensor.

Figure 8.22: Geophone acting as wave sensor.

Figure 8.23: solenoid used for large scale model test.
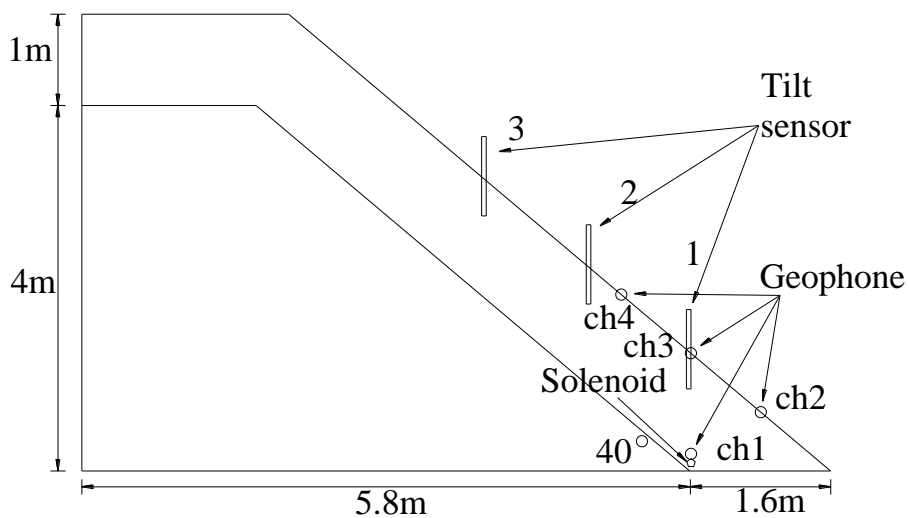
Figure 8.24: Location of the tilt and wave sensors.

Figure 8.25 shows the received wave signal before rainfall was given. It is easy to determine the wave travel time prior to rainfall. However it became difficult when rainfall was given, because the geophone was exposed to rainfall which made much higher noise than signal. So the author attempted to remove the noise resulting from rainfall based on the difference in the frequency of wave signal and rainfall noise with help from a communication company. The denoised signal is shown in Figure 8.26.
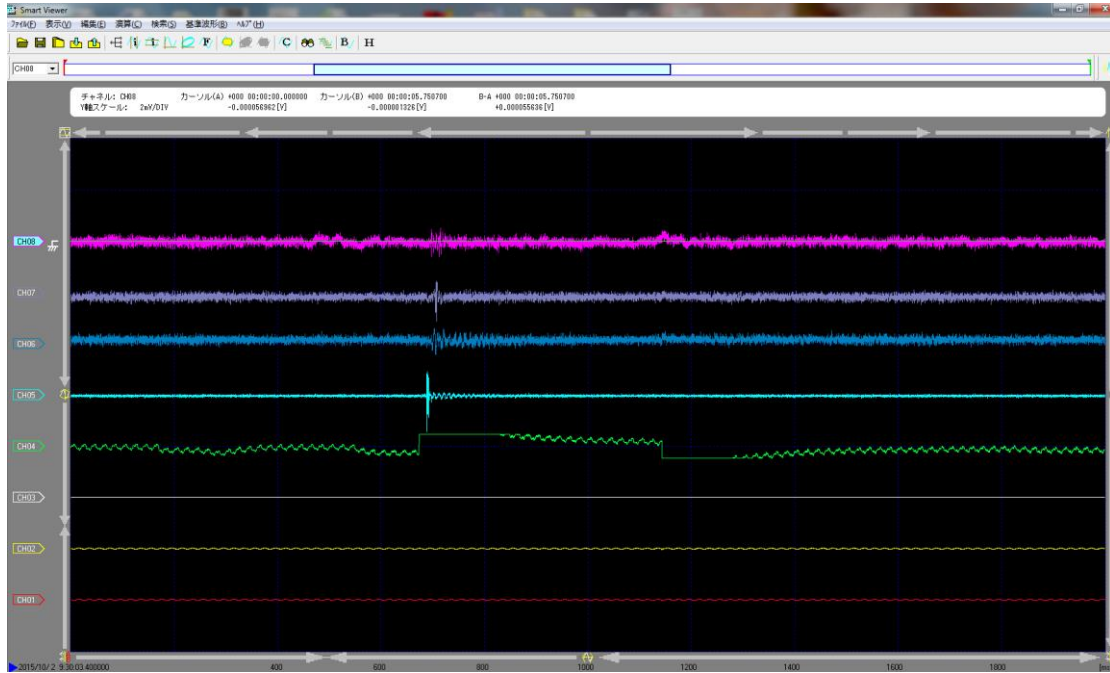
Figure 8.25: Wave form prior to rainfall.
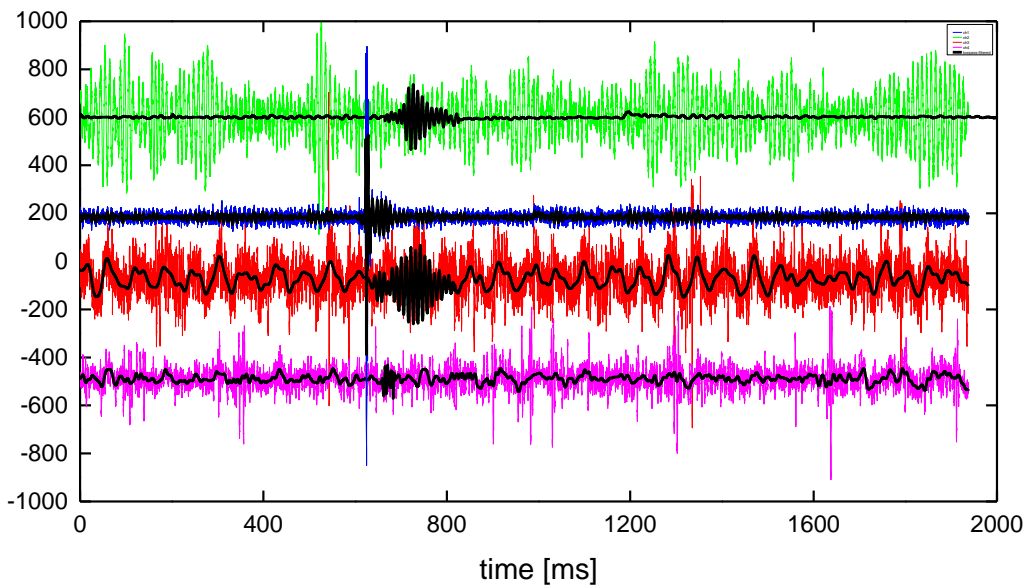
Figure 8.26: Wave single denoised.

8.3.2. Results

As shown in Figure 8.27, rainfall was given increasingly to further the slope failure

and shorten the experimental period. Tilt angle for sensors at different location exhibited constant before slope failed, as shown in Figure 8.28. The tilt angle started to increase just minutes before failure.

Figure 8.29 shows the time series data of normalized wave velocity. The normalized wave velocity decreased with time, which demonstrates the potential of the system to provide alternative stability information to detect and provide an early warning of slope failure.

Unfortunately, the wave data ended at 240~280min because the wave receivers were removed due to collapse of slope surface caused by runoff erosion (Figure 8.30), and so the final failure information of the deformation event was not monitored. Continuous wave velocity measurement was not available. However, interpretation of inclinometer measurements made during the completed test confirmed that no deformation occurred during this period, the small decrease by 5~8% in wave velocity was attributed to increase of water content. Therefore, in field test, the receivers should be placed in a certain of depth in case of removal caused by runoff erosion and noise from circumstance.
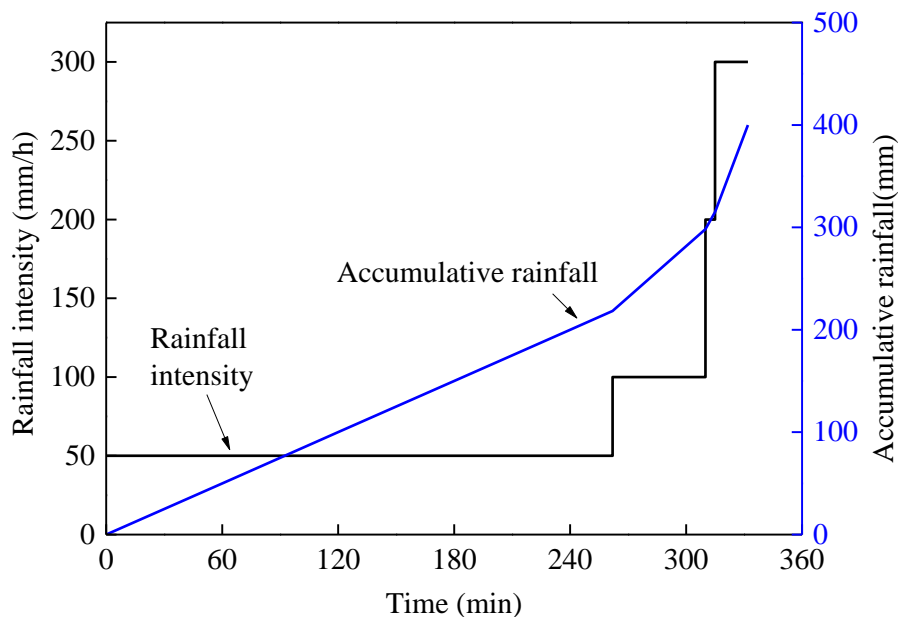
Figure 8.27: Time history of rainfall.
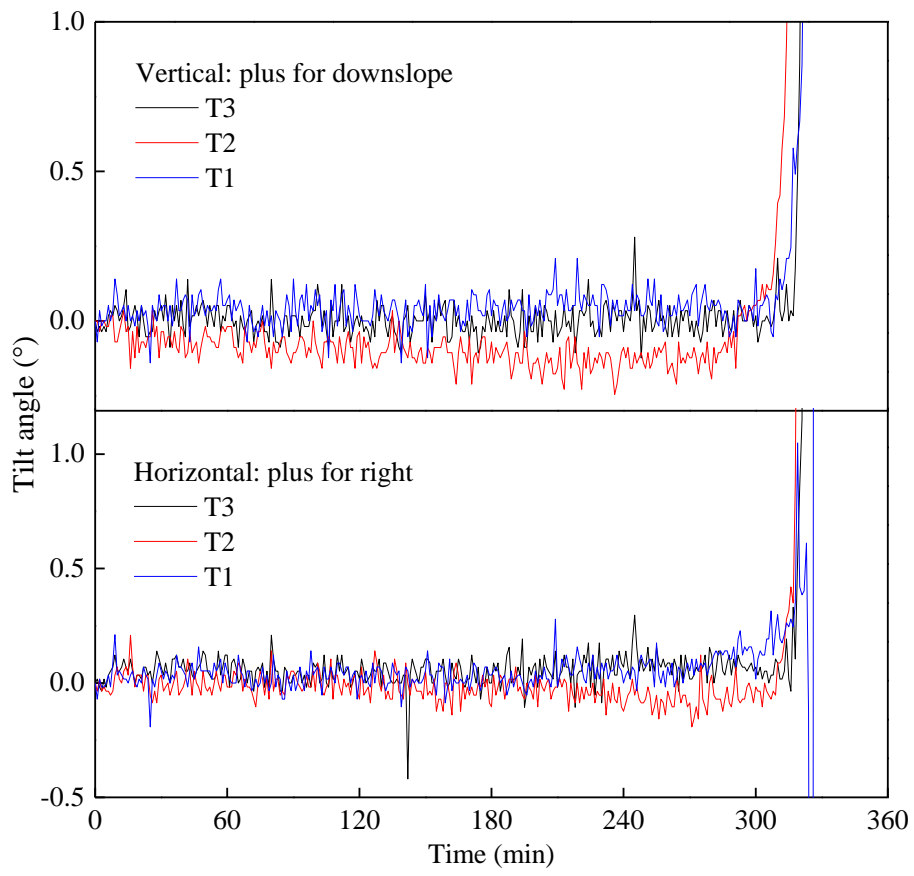
Figure 8.28: Time history of tilt angle.
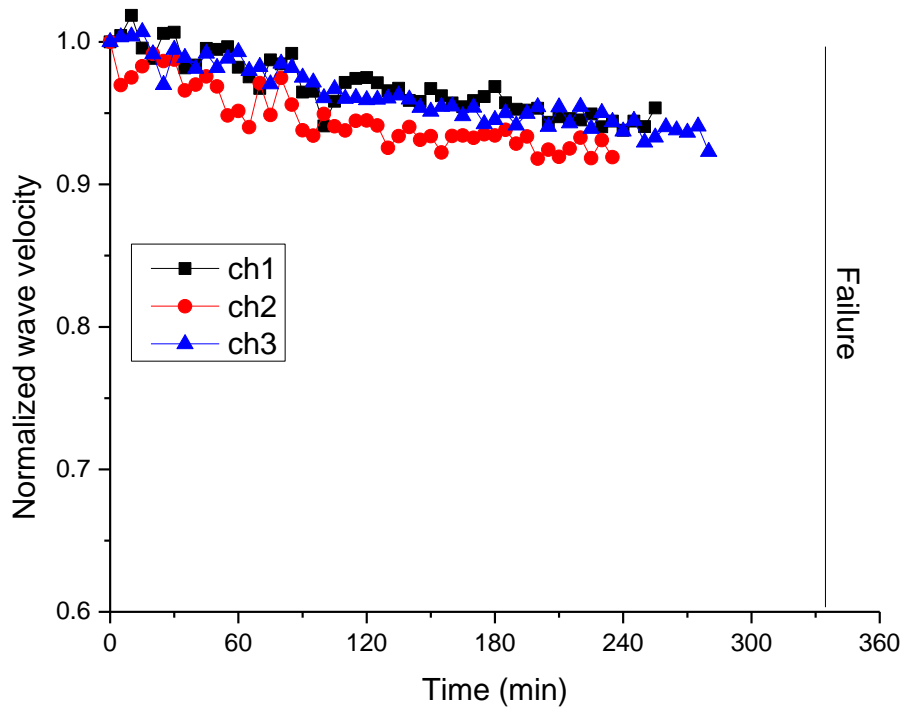
Figure 8.29: Time series data of normalized wave velocity.

Figure 8.30: Wave receivers removed due to collapse of slope surface caused by runoff erosion.

8.4. FIELD APPLICATION

The wave velocity based early warning system of slope failure composes of wave exciter/transmitter and receiver devices.

A variety of receiving devices like electromagnets, piezoelectric ceramics, accelerometers, microphones, geophones, etc. are already available commercially.

In general context, transmitters can be divided into two broad categories; (i) without any mechanical moving parts, e.g., piezoelectric or electromagnetic type transmitters, etc, and (ii) excitation by means of mechanical movements, e.g., drop hammer, etc. Transmitters of the former category may require less driving voltage but are generally capable of generating excitations which are low in amplitude. These low amplitude excitations may not be able to be transmitted to receivers, a few meters from the exciter. On the other hand, transmitters of the latter category can generate high amplitude excitations which may be received several meters away.

However, a continuous source of large driving voltage may be required for them; which may be a concern for landslide monitoring in remote areas. In any case, a more cost-efficient approach for landslide monitoring based on elastic waves may be to install several receiving units on the slope surface which are made to receive excitations from a single excitation device.

As for the power supply, the author tried to calculate the amount of energy the system required. As shown in Figure 8.31, a SPT test was conduct. The excitation could be generated by falling a 5kg drop hammer from a certain of height to hit the ground. Even 5cm height could generate enough energy to transmit elastic wave to the sensor located eight meters away, as shown in Figure 8.32. the energy corresponding to height of 5cm for drop hammer (5kg) is E=mgh=2.5J. A conventional AA battery could have capacity of over 6000J. It means that an AA battery could work 2400 times. If 5min once, an AA battery could keep working for 200h which is long enough to

cover several rainfall events.

Figure 8.31: SPT test for energy calculation.
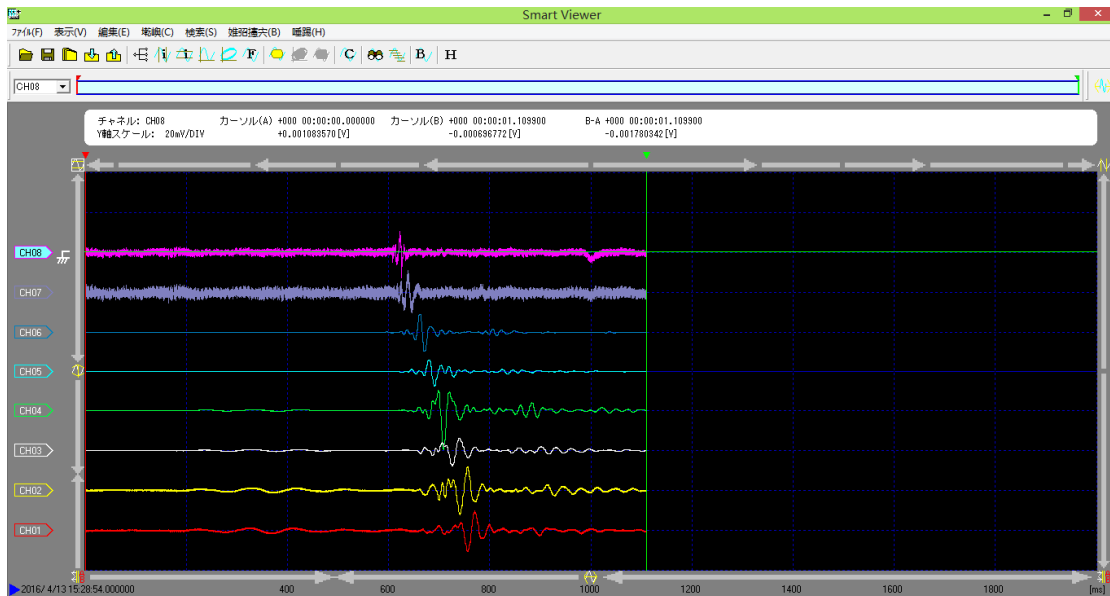
Figure 8.32: Wave form for SPT test.

8.4. SUMMARY

This chapter discusses the potential of applying the idea of elastic wave velocities to predict such rain induced landslides by a medium scale model test and a large scale model test. Also, this chapter presents future avenues for its practical use in the field.

8.5. REFERENCES

Anderson, S. A., & Sitar, N. (1995). Analysis of rainfall-induced debris flows. *Journal of Geotechnical Engineering*, 121(7), 544-552.

Farooq, K., Orense, R., & Towhata, I. (2004). Response of unsaturated sandy soils under constant shear stress drained condition. *Soils and foundations*, 44(2), 1-13.

Ng, C. W., & Pang, Y. (2000). Influence of stress state on soil-water characteristics and slope stability. *Journal of Geotechnical and Geoenvironmental Engineering*, 126(2), 157-166.

Nishiumura, T., Koseki, J., Fredlund, D. G., & Rahardjo, H. (2012). Microporous membrane technology for measurement of soil-water characteristic curve. *Geotechnical Testing Journal*, *35*(1), 1–9.

CHAPTER 9

CONCLUSIONS & RECOMMENDATIONS

9.1. GENERAL

To reduce the damage caused by landslides, an early warning system is necessary to enable the early detection of landslide indicators and timely evacuation of residents from landslide-prone areas. The underlying concept is to watch the variation of different slope parameters during rainfall, and issue a landslide warning when these parameters approach their respective critical values. One of the key questions in doing so is "Which parameters to watch?". A new idea to predict slope failure by using elastic wave propagation in soil has been presented in this study. A thorough laboratory investigation by means of slope model test was conducted to explore the validity of this idea. Early detection of slope failure indicator over large areas of slope model can be accomplished by monitoring elastic wave velocity in real time or near-real time. Effects of soil density, failure plane thickness, and slope angle on the wave behavior were examined. The evolution of wave velocity is driven by the coupled effect of increasing water content and deformation that appeared to be interrelated.

Furthermore, an attempt was made to investigate the elastic wave variation respectively with either water content or deformation by means of a "flat" model test.

In addition, a typical triaxial apparatus has been modified to serve as an SWCC measurement apparatus. The designed apparatus could not only determine SWCC under different magnitudes of K_o stress, but was also able to measure elastic wave

velocities (shear wave velocity and compression wave velocity) in due course. On this basis, that the received wave type from model tests was either P-wave or S-wave was identified.

The potential of applying the idea of elastic wave velocities to predict such rain induced slope failure was discussed by a medium scale model test and a large scale model test.

Major conclusions derived from these studies are summarized in the following section.

9.2. CONCLUSIONS

9.2.1. Flat Model Test

Flat model tests were performed to separately investigate the influences of water content and shear deformation on elastic wave propagation. The influence of water content on elastic wave velocity is investigated with no shear deformation conditions. Similarly, the influence of shear deformation on elastic wave velocity is investigated at the constant water content condition. Conclusions drawn from these experiments are summarized in the following points;

● The influence of water content is found to be limited. At most 10% decrease in normalized wave velocity is caused by increase of water content in the range of dry condition to saturated condition.

● Whereas, the influence of deformation was much more significant compared to water content. The decrease rate of normalized wave velocity with tilt angle is independent of volumetric water content. This finding could be used to monitor the excavation slope stability.

- The relationship functions of normalized elastic wave velocity with either volumetric water content or tilt angle were obtained.

9.2.1. Conventional Slope Model Test

Model tests reproducing rainfall-induced slope failure were performed and the corresponding behaviors of elastic wave velocities during slope failure were recorded. Conclusions drawn from these experiments are summarized in the following points;

- Behavior of elastic wave velocities was found to decrease with water content as well soil deformations. With changes in soil moisture due to water infiltration, elastic wave velocities gradually kept on decreasing. As soon as slope initiated failure, wave velocities decreased at an accelerated rate. Such sharp decrease after a threshold at 0.92 of normalized elastic wave velocity can be useful for predicting failure initiation in actual landslide conditions.

- The general trend of normalized elastic wave velocity with volumetric water content for soil with higher density was located above the curves for soil with lower density, regardless of the slope angle and failure plane thickness. The failure average volumetric water content and failure time increased as the density increased.

- The general trend of normalized elastic wave velocity with volumetric water content for slope with larger failure plane thickness was located above the curves with smaller failure plane thickness, regardless of the slope angle and density. The failure average volumetric water content and failure time increased as the failure plane thickness increased.

- The general trend of normalized elastic wave velocity with volumetric water content for slope with lower slope angle was located above the curves for slope with larger slope angle, regardless of the failure plane thickness and density. The

failure average volumetric water content and failure time decreased as the slope angle increased.

- The decrease rate of normalized elastic wave velocity with volumetric water content and tilt angle was found to be independent of density, slope angle, and surface layer thickness. The changes of normalized elastic wave velocity with volumetric water content and tilt angle were simulated by the relationship functions obtained from flat model tests. It showed that the simulated curves agreed well with measured data.

9.2.3. Bender Element Test

An apparatus to study the variation of elastic wave velocities (shear wave and compression wave velocities) during drying and wetting path of SWCC was devised. Basic working principle and limitations of the apparatus were discussed. Conclusions drawn from these experiments are summarized in the following points;

- S-wave and P-wave velocities increased with matric suction. The behavior appears to be bi-linear, with a clear hysteresis between the drying and wetting curves. Increase in wave velocities with matric suction may be attributed to the increasing soil stiffness.

- Magnitudes of S-wave and P-wave velocities were compared with those obtained from model tests. Results were found to be reasonable and consistent with S-wave.

9.2.4. Field Application of Elastic Wave Velocities for Landslide Prediction

A medium scale model test and a large scale model test were conducted to confirm the potential of applying the idea of elastic wave velocities to predict such rain induced landslides. The evolution of elastic wave velocity showed

consistent observation from small scale model tests. This demonstrates that monitoring elastic wave velocity could be utilized in actual slopes for identification of failure initiation.

9.3. RECOMMENDATIONS FOR FUTURE RESEARCH

Due to the limitation of time, equipment and the scope of the current study, the finding of this study may be further extended in several aspects. Some recommendations for future researches are summarized below;

- The scope of present study was limited to Edosaki sand only. Validity of these findings on other soil types is required to be confirmed. This observation is of real significance with respect to clayey soils and colluvial deposits.

- In present study, the change of elastic wave velocities to water content as well as deformations was well explored in controlled laboratory environment. However, practical application of these concepts for actual landslide early warning requires similar confirmations in actual field conditions where several unforeseen parameters may also play their part. Field study is indispensable in establishing a more realistic and practical approach for landslide early warning.

- Measurement of elastic wave velocities in the field would require sophisticated transmitter and receiver devices. Cross-disciplinary research together with knowledge of electrical engineering and geotechnical engineering, is therefore required to develop efficient, low energy, low noise transmitter and receiver devices for landslide early warning systems.